UNIVERSIDAD PONTIFICIA COMILLAS

ESCUELA TÉCNICA SUPERIOR DE INGENIERIA (ICAI)

Instituto de Investigación Tecnológica (IIT)

Optimising the electrical infrastructure of mass transit systems to improve the use of regenerative braking

Tesis para la obtención del grado de Doctor

Directores: Prof. Dr. D. Ramón Rodríguez Pecharromán

Prof. Dr. D. Antonio Fernández Cardador

Autor: Ing. D. Álvaro Jesús López López

Madrid 2016

CONSTANCIA REGISTRAL DEL TRIBUNAL DEL ACTO

DE LA DEFENSA DE TESIS DOCTORAL

TÍTULO: Optimising the electrical infrastructure of mass transit systems to improve the use of regenerative braking.

AUTOR: Álvaro Jesús López López.

DIRECTORES: Ramón Rodríguez Pecharromán y Antonio Fernández Cardador.

TUTOR-PONENTE: Ramón Rodríguez Pecharromán.

DEPARTAMENTO: Instituto de Investigación Tecnológica.

FACULTAD O ESCUELA: Escuela Técnica Superior de Ingeniería.

Miembros del Tribunal Calificador:

PRESIDENTE: Dr. D. José Germán Giménez Ortiz **Firma**:

VOCAL: Dr. D. Masafumi Miyatake **Firma**:

VOCAL: Dr. D. Pablo Arboleya Arboleya **Firma**:

VOCAL: Dr. D. Luis Rouco Rodríguez **Firma**:

SECRETARIO: Dr. D. José Antonio Rodríguez Mondéjar **Firma**:

Fecha de lectura:

Calificación:

Extended Abstract

The aim of this abstract is to present a brief summary of the thesis "Optimisation of the electrical infrastructure of mass transit systems in order to take full advantage of regenerative braking".

Introduction

Mass Transit Systems (MTSs) play a pivotal role in the transport system of large cities, both in developed and developing countries. Shifting the urban transport system from light duty vehicles (cars and commercial vans) to MTSs would be beneficial both in terms of greenhouse gas emissions and pollution. To make this change possible, it is important to improve MTSs to make them fast and efficient systems.

Although MTSs are highly efficient nowadays, there is still room to improve them. From the energy-efficiency standpoint, the introduction of regenerative-braking trains leads to energy consumption reduction that may approach 40 %. However, the electrical characteristics of most MTSs (they are DC-electrified systems) make it difficult to take full advantage of regenerative braking energy. It has been observed in several studies that the receptivity of MTSs to regenerative-braking energy varies from system to system, and between operation headways.

Among the different approaches to increase receptivity, this thesis focuses on the improvement of the electrical infrastructure. These improvements usually consist in the installation of expensive devices that must be properly justified. As a result, the studies devoted to MTS electrical infrastructure improvement usually present optimisers which obtain the results by means of electrical railway simulators.

In this context, the main objective of this thesis is to improve the electrical infrastructure of a railway DC-electrified MTS in order to take full advantage of the train regenerative braking energy.

To achieve this objective, the thesis tackles from the electrical multi-train simulator problem to the MTS electrical infrastructure problem. In addition, this thesis includes a detailed analysis of the effects of the MTS traffic model used in optimisation studies. From the conclusions of these studies, the thesis aims to include actual traffic operation conditions in order to obtain more accurate results for the system global energy efficiency.

MTS simulation

Chapter 2 in this thesis tackles the electrical multi-train simulator problem. As a result of the works in the frame of this thesis, a detailed electric railway simulator has been implemented. Its details are given in this chapter.

It first performs a review of the most important elements in this kind of simulator, making especial emphasis on the energy consumption concerns. Detailed models are proposed for trains, the electrical network, traction substations (SSs), including reversible substations (RSs), and Energy Storage Systems (ESSs).

Then, these models are integrated into an electrical railway simulation tool which generates the electrical-circuit snapshots that must be studied, and solves the mixed AC-DC load flow problem implementing a unified approach.

Provided this simulator is the key tool for all the studies in this thesis, the thesis includes detailed explanations of the measures implemented to optimise the simulator in term of robustness and computation time. Regarding the former, a novel set of heuristic rules devoted to finding the electrical topology of the circuits to be solved has proven to make the simulator extremely robust to the train load-regeneration profiles and the infrastructure topology. Regarding computation time, the main time-consuming tasks in the simulator have been identified and refined.

Case-study and preliminary analysis

Chapter 3 presents the case-study MTS line which will be used to apply the studies in the thesis. This is a double-track line with two terminal stations. From the electrification perspective, it consists in a 600-V line featuring 11 traction substations and 23 passenger stations distributed along 19 km.

In addition, this chapter performs some preliminary studies to identify the most relevant energy losses from the electrical infrastructure perspective. These studies make it possible to detect the main weaknesses of the case-study line and so to define the main targets to improve MTSs from the energy-efficiency standpoint. In particular, the reduction of rheostat losses arises as the main goal to attain the objective of the thesis: the system receptivity exhibits a clear decrease trend for long headways, which suggests that it is possible to achieve relative energy savings close to 20 % by improving this factor.

The thesis reviews the main rheostat reduction mechanisms, and it identifies the limitations to increase receptivity by installing RSs or ESSs at a given location in the line (mainly electrical interferences provoked by active SSs).

The main current trends in MTS infrastructure improvement have been reviewed as well in the thesis, classifying them into low- and high-investment techniques. Among the low-investment techniques, the thesis includes a detailed study of the implications of the SS no-load voltage tuning in the system energy consumption. A novel variable no-load voltage scheme which adapts to the variable headway in MTSs has been proposed.

Regarding the expensive infrastructure-improvement techniques, the thesis makes especial emphasis on RSs, which are currently regarded as the most effective technique when power flows from the railway system back to the utility grid are remunerated. Nevertheless, ESSs are comprehensively analysed. The reason is that they are expected to be improved in the medium-term future, which could make them attractive from the investment feasibility standpoint.

The traffic in MTSs

Chapter 4 is devoted to the study of the effects of traffic on MTS energy consumption. This thesis has proven that the habitual traffic approach in infrastructure design and optimisation studies is too simplified to obtain accurate energy-saving results. This usual approach includes a single traffic scenario per headway. It has been observed to be unable to represent the complex and variant energy interactions between trains in MTSs, especially from the energy-saving perspective.

To overcome this problem, this thesis proposes a traffic model which includes variations in the most relevant traffic variables. A large number of system operation samples, or traffic scenarios, are generated to compose a traffic space which includes the complex energy exchanges between trains and their relative frequencies.

Provided the use of a large set of traffic scenarios as the input to MTS optimisation studies could lead to unmanageable computation times, this thesis has explored the possibility of taking into account the train energy interactions by means of a reduced set of representative traffic scenarios. To attain this objective, this thesis proposes a characterisation of the traffic scenarios based on the location and amount of rheostat losses. This characterisation is inspired in the rheostat reduction mechanisms. The thesis proves that using this traffic space characterisation to select the representative scenarios makes it possible to obtain energy-saving results which relative error with respect to the mean energy-saving results of the whole traffic space are lower than 5 %. The energy-saving error results obtained with the single-scenario traffic approach – the usual approach in the literature– is far worse than those obtained with the proposed method. For some particular infrastructure improvement configurations, energy-saving error figures close to 70 % have been obtained with the single-traffic method.

As a result of these studies, three sets of representative scenarios for three operation headways have been generated. These headways are used to take into account the different operation modes of the line during working and ferial days. Specifically, 4-, 7- and 15-minute headways have been included in the studies in the thesis.

Traffic scenario compression

Even though a few representative scenarios for each operation headway have been selected, the simulation time to obtain the energy figures of the case-study line have been increased with respect to the usual traffic approach in the literature. This simulation-time increase is however essential to obtain accurate results. Nevertheless, it will limit the possible complexity of the method to search for optimal infrastructure configurations.

To tackle this concern, Chapter 5 has proposed a novel method to reduce the number of snapshots that must be simulated to obtain the MTS energy figures. It is based on the idea of grouping similar snapshots in a smart way in order to simulate similar load-regeneration profiles just once.

Specifically, the compression method is performed in two steps: 1) a clustering stage where the snapshots in the uncompressed traffic scenario are grouped following rheostat-loss amount, train positions and SS voltages; and 2) a stage devoted to search for an optimised equivalent load-regeneration profile to be fed into the electrical railway simulator.

The energy-saving error obtained with the compression method have been proven to be lower than 5 % with a number of snapshots accounting for just 20 % of the total number of snapshots in the uncompressed traffic scenario. Therefore, 80 % computation-time reduction may be obtained by the application of this novel compression method. The method has been proven to be clearly better than the simulation time subsampling approach.

MTS infrastructure optimisation

Chapter 6 collects all the know-how generated along the thesis on energy concerns in MTSs to present an electrical infrastructure optimiser.

The classical optimisation approaches have been discarded due to their limitations to tackle problems as complex as the MTS infrastructure optimisation. A swarm-intelligence computation method has been used instead: the Particle Swarm Optimisation.

The optimisation method in the thesis composes the representative scenarios for the traffic headways into a weekly operation plan to obtain annual energy consumption figures for the case-study line. The method is not only concerned about energy savings. It applies the Net Present Value (NPV) of the required investment to assess its economic feasibility. Thus, it makes it possible to assist the MTS operator to take investment decisions oriented to reduce energy consumption.

The optimum location and size of RSs are included in the optimisation problem. Two infrastructure optimisation approaches have been proposed to prove the versatility of the optimiser. The first one is defined to search for the optimum RS locations and sizes without any restrictions. A second approach is carried out in two stages: a first one where the size of the RSs installed is imposed to be homogeneous, and a second stage where this restriction is relaxed, to find the unconstrained global optimum.

The optimiser proposed has proven to be able to find the global optimum or a very similar sub-optimum in highly complex search spaces. Specifically, it has made it possible to find the maximum energy-consumption reduction subject to having positive NPV.

Although the optimisation times have been thoroughly reduced with respect to a careless approach as a result of the different measures taken along the thesis, distributed computation has been applied to boost the computational efficiency of the optimisation method proposed.

List of symbols

Symbol	Description
MTS	Mass Transit System.
SS	Substation.
RS	Reversible Substation.
ESS	Energy Storage System.
A	Davis formula (running resistance) independent term. [N].
B	Davis formula term dependent of speed. [N-h/m].
C	Davis formula term dependent of the square of speed. [N-h^2/km^2].
K_{tunnel}	Tunnel coefficient. Dimensionless.
v_{train}	Train Speed. [m/s].
μ_M	Efficiency coefficient in the train model. Dimensionless.
U_{NOM}	Nominal voltage at train pantograph. [V].
F_M	Maximum equivalent train effort, dependent on speed. [N].
I_M	Pantograph current for maximum traction. [A].
P_{pant}	Pantograph power. [W].
F	Actual equivalent effort at wheels. [N].
pf	Penalty factor. Dimensionless.
V_d	Voltage in the DC side of the rectifier. [V].
k_1	Rectifier constant, dependent on its topology. Dimensionless.
k_2	Rectifier constant, dependent on the per unit system selected. Dimensionless.
a	Transformer tap ratio. Dimensionless.
V_{term}	Voltage in the AC side of the rectifier. [V].
α	Rectifier ignition angle. [rad].
X_c	Reactance seen by the rectifier. [Ω].
I_d	Rectifier DC side current. [A].
μ	Rectifier overlap angle. [rad].
R_c	Rectifier commutation resistance. [Ω].
$V1_{chrg}$	ESS charge-process voltage threshold. [V].
$V2_{chrg}$	ESS charge-process maximum-allowed-current voltage. [V]
$IMAX_{chrg}$	ESS maximum allowed charge current. [A].
$V1_{dis}$	ESS discharge-process voltage threshold. [V].

Symbol	Description
$V2_{dis}$	ESS discharge-process maximum-allowed-current voltage. [V]
$IMAX_{dis}$	ESS maximum allowed discharge current. [A].
G_{sys}	Nodal conductance matrix of the electrical system. [S].
V_{sys}	Nodal voltage vector of the electrical system. [V].
I_{sys}	Nodal current vector of the electrical system. [A].
Y_{ij}	Admittance-matrix element. [S]
θ_{ij}	Angle of the admittance-matrix element. [rad]
Vac_i	Voltage of an AC node. [p.u.]
δ_i	Angle of an AC node. [rad].
P_AC_i	AC-node active power. [p.u.].
Q_AC_i	AC-node reactive power. [p.u.].
N	Number of AC nodes in the system.
P_ACterm_i	Active power of a rectifier AC terminal. [p.u.].
Q_ACterm_i	Reactive power of a rectifier AC terminal. [p.u.].
X_C, r	Reactance seen by the AC terminal of rectifier r.
λ_r	Rectifier resistance to reactance ratio. Dimensionless.
ξ_r	$\tan^{-1}\lambda_r$. Dimensionless.
α_r	Rectifier ignition angle. [rad].
μ_r	Rectifier commutation overlap angle. [rad].
Idc_r	Current in the DC side of the rectifier. [p.u.].
A_{REC}, B_{REC} C_{REC}, D_{REC}	Rectifier coefficients.
P_DCterm_j	Active power of a rectifier DC terminal. [p.u.].
M	Number of DC nodes in the system.
γ_r	*ON-OFF* binary control variable for rectifier r. Dimensionless.
P_Rh_j	Power sent to rheostats by train at node j. [p.u.].
λ_j	Rheostat binary control variable for train at node j. Dimensionless.
$\boldsymbol{X}^{(a)}$	System state variable initial guess vector.
$\Delta\boldsymbol{X}^{(a)}$	System state variable increase vector.
$J^{(a)}$	Jacobian matrix.
$\boldsymbol{Mm}^{(a)}$	State variable mismatch vector.
$nRect$	Number of rectifiers in the system.
$\boldsymbol{\Gamma}$	Diagonal matrix for rectifier-state control
$\boldsymbol{\Lambda}$	Diagonal matrix for train-state control
$nDCnodes$	Number of pure DC nodes in the system.
Wr_Snp	Number of snapshots where the simulator fails to converge in the robustness test.
N_Snp	Total number of snapshots in the robustness test.
E_SAVING_i	Energy saving value. [W·s].
$E\_CONSUMED_{Raw}$	Energy consumed in the raw. [W·s].
$E\_CONSUMED_{RS,i}$	Energy consumed when a reversible substation is installed. [W·s].
$E\_RETURNED_{RS,i}$	Energy returned to the utility grid. [W·s].
E_{saving}^{REF}	Reference energy savings. [W·s].
E_{saving}^{COMP}	Energy savings with the modelling approach. [W·s].
ε_{COMP}	Absolute energy-saving error. [W·s].
$P_{CONDUCTION}$	Conduction power losses. [W].
$P_{RHEOSTAT}$	Rheostat losses. [W].
$E_{RECTIFIED}$	Rectified energy. [W·s].
$E_{REGENERATED}$	Regenerated energy. [W·s].

Symbol	Description
$E_{TRACTION}$	Energy consumed by train with traction purposes. [W·s].
$E_{AUXILIARY}$	Energy consumed by trains to feed the auxiliary equipments. [W·s].
$E_{CONDUCTION}$	Conduction losses. [W·s].
$E_{RHEOSTAT}$	Rheostat losses. [W·s].
E_{LOSS_ESS}	Losses in ESS converters. [W·s].
E_{STORED_ESS}	Energy stored in ESSs. [W·s].
$SizeVector$	Vector with the different traffic-scenario-set sizes for traffic-input size concerns.
$PrRh$	Function devoted to process the rheostat losses. Defined for each scenario and RS location [W]
$scen$	Traffic scenario under analysis.
loc	RS location under analysis.
R	Number of rheostat-loss events in the scenario under analysis.
Erh_i	Amount of rheostat losses in the rheostat-loss event i. [W·s].
F_{RH}	Filter function defined to process the rheostat losses. Dimensionless.
drh_i	Distance between the train which exhibits rheostat losses and the RS location. [m].
SFR	Space-filtered rheostat function. Dimensionless.
Df	SFR distance factor. [m].
Wf	SFR modulation factor. Dimensionless.
HDf	SFR high-distance factor. [m].
$EBFR$	Experience-based filter function. Dimensionless.
$EBFR\_case$	EBFR function applied to each rheostat-loss reduction case. Dimensionless.
V_{Rh}	EBFR rheostat-braking voltage threshold. [V].
V_{RS}	EBFR RS location voltage. [V].
R_l	EBFR supply-system impedance. [Ω/m]
Δt	EBFR sampling time. [s].
$Vraw_{loc}$	EBFR RS location voltage in the raw system. [V].
V_{BTr}	EBFR braking train voltage. [V].
f_{ON_SS}	EBFR binary factor to represent electric interferences. Dimensionless.
$nCOMB_{TS}$	Total number of possible combinations of a selection within the traffic space.
$nSAMP_{TS}$	Number of samples in the traffic space.
n_SAMP_{TINP}	Number of samples included in the traffic-input.
CR	Compression ratio. Dimensionless.
CR_{vec}	Vector including several CR factors.
$PtyT_t^c$	Purity factor for the equivalent train t in cluster c. Dimensionless.
$nRht_t^c$	Number of samples in cluster c where the equivalent train t exhibits rheostat losses.
$nNRh_t^c$	Number of samples in cluster c where the equivalent train t does not exhibit rheostat losses.
C	Number of samples (snapshots) in cluster c.
$PtySS_a^c$	Purity factor for the SS a in cluster c. Dimensionless.
$nSS\_ON_a^c$	Number of samples in cluster *c* where the SS *a* is in *ON* mode.
$nSS\_OFF_a^c$	Number of samples in cluster *c* where the SS *a* is in *OFF* mode.
$\overline{Pty_c}$	Average purity factor associated to cluster *c.* Dimensionless.
NT	Number of equivalent trains in cluster c.
NSS	Number of SSs in the system.
ELP	Equivalent Load/Regeneration Profile.
PSO	Particle Swarm Optimisation.
F_{ELP}	Fitness function in the ELP search problem. Dimensionless.
P_i	Power consumed or regenerated by the ith train in the ELP. [W].

Symbol	Description
P_i^{MAX}	Higher bound for P_i. [W].
P_i^{MIN}	Lower bound for P_i. [W].
T	Number of trains in the cluster expressed by the ELP.
ω_i	Weighting factors used in F_{ELP}.
M	Large number used in the ELP search process. Dimensionless.
WRh	Wrong rheostats. Dimensionless.
SS_{OFF}	Subset containing *OFF* SSs.
SS_{ON}	Subset containing *ON* SSs.
ω_1	*OFF*-SS voltage weighting factor. [1/V].
ω_2	*ON*-SS power weighting factor. [1/W].
ω_3	Conduction losses weighting factor. [1/W].
V_{Ref}^j	Reference voltage for SS *j.* [V].
V_{Eq}^j	Equivalent voltage for SS *j.* [V].
Ess_{Ref}^k	Reference SS energy for SS k. [W·s].
Ess_{Eq}^k	Equivalent SS energy for SS k. [W·s].
$Eloss_{Ref}$	Reference conduction losses. [W·s].
$Eloss_{Eq}$	Equivalent conduction losses. [W·s].
P_t^{ELP}	Power for train t in the ELP. [W].
P_t^{PSO}	Power for train t yielded by the PSO. [W].
PRh_t^{PSO}	Rheostat-loss power for train t yielded by the PSO. [W].
PRh_t^{REF}	Mean rheostat-loss power for the trains modelled by train t. [W].
IAE_{COMP}	Relative integral absolute error (IAE). [%]
h	ELPs in the compressed traffic scenario.
$E_{saving,i}^{REF}$	Energy savings for the snapshot i. [W·s].
$E_{saving,h}^{COMP}$	Energy savings for the ELP h. [W·s].
C_{RS}	RS cost. [€].
α_{PWR}	RS cost per installed power unity. [€/W].
P_{RS}	Rs size. [W].
NPV	Net Present Value. [€].
ES_t	Economic savings in the period t. [€].
r	Discount rate. [p.u.].
T	Number of years in the NPV formula. [years].
C_0	Investment costs. [€].
p_k^i	Position for the element *k* at iteration *i*. Different possible dimensions.
v_k^i	Speed for the element *k* at iteration *i*. Different possible dimensions.
imp_k	Impetus factor for the iteration *k*.
$c1_k^i$	Cognitive-speed forget coefficient. Dimensionless.
$c2_k^i$	Social-speed forget coefficient. Dimensionless.
$fcog$	Cognitive factor. Dimensionless.
$fsoc$	Social factor. Dimensionless.
p_k^{best}	Position with the best fitness value for the element k. Different dimensions.
p^{BEST}	Global best fitness value. Different dimensions.
SS_{VEC}	SS location vector. [m].
AoI_{SSi}	Area of influence of each RS location. [m].
$SIZE_{VEC}$	Vector with RS sizes. [W].
$E\_SS_{Raw}^{WEEK}$	Weekly SS energy consumption in the raw system. [W·s].
$E\_SS_{Elem}^{WEEK}$	Weekly SS energy consumption for an element in the swarm. [W·s].
NPV_{Elem}	NPV for an element in the swarm. [€].

Symbol	Description
Hdw	Total number of operation headways.
$E\_SS_{repr}^{h}$	SS energy consumption for the scenario $repr$ and headway h. [W·s].
$RepH_h$	Total number of representative scenarios selected for headway h.
$ScenDur_h$	Duration of the traffic-scenario samples for headway h. [hours].
OpH_h^{WORK}	Weekly number of hours for headway h in working days. [hours].
OpH_h^{FERIAL}	Weekly number of hours for headway h in ferial days. [hours].
NRS	Number of RSs installed.
N_{sizes}	Number of discrete RS sizes selected.

Acknowledgements

Quiero comenzar esta sección agradeciendo el apoyo del Colegio Nacional de Ingenieros del ICAI a esta tesis, apoyo que se ha materializado a través de una Beca de Investigación.

Gracias a los compañeros de Quintana por vuestra acogida. Me hicisteis sentir integrado y querido en un tiempo récord.

Gracias a todos los compañeros del IIT, en especial a los de Ricci, por haberme sostenido en los momentos bajos y por haber soportado estoicamente mis bromas. Pensad que será casi siempre en vosotros en quien piense cuando eche de menos esta etapa de mi vida.

También quería agradecer al IIT como institución el haberme siempre hecho notar el apoyo a mi investigación, incluso en los malos momentos. Es el IIT, sin ningún género de dudas, un buen sitio para emprender esta etapa de evolución intelectual y personal que es el doctorado.

Thanks to my friends in the Electrical Engineering School at KTH for having hosted me in such a charming way. Special thanks to Lars Abrahamsson for having supervised my stay at KTH, supporting me not only in the scientific issues, but also personally.

Remembering my stay at Stockholm, it is impossible not to make a special mention to Amin and Behnaz, who opened the doors of their home and shared tenths of great dinners and chats with me. Thank you, my friends.

Muchas gracias a Antonio y a Paloma, por haber estado siempre ahí dando consejos y complementando mis ideas. Tanto las que han llegado a buen puerto, como las que se quedaron en el camino. En especial a Antonio, que es director de esta tesis y que siempre me ha deslumbrado con su facilidad para comprender mis a veces enrevesados enfoques, ofreciéndome una o varias ideas para mejorarlos.

Muchísimas gracias a mi “Jefe”, Ramón. En definitiva, quien posibilitó esta etapa creyendo en mi. De Ramón he aprendido tantísimas cosas a lo largo de estos seis años. No hay palabras para agradecer la cantidad de tiempo que me ha dedicado, incluso en fases de puntas fuertes de trabajo para él; la cantidad de veces que ha sabido lidiar con mi “cabezonería” (¡y eso que casi siempre acaba teniendo razón él!); los valiosísimos consejos para las actividades de docencia, la cantidad de palabras de apoyo en los momentos bajos, el no haber dejado implícitos los reconocimientos a mi esfuerzo, etc., etc., etc. Gracias de nuevo, Ramón. Esta tesis es también tuya.

Termino con la familia. Primero la política: Millones de gracias a Carmen, José Luís, Ana, y a todos mis Sánchez de Ávila. He sentido vuestro apoyo y cercanía en todo momento. Me habéis hecho sentir uno más.

Millones de gracias a María y a Rose, por estar siempre ahí y por cuidar de mis hermanos, ¡que no es tarea fácil!

No quiero olvidarme de mis sobrinillos: Toni, que está echándome las primeras sonrisas; Dani, que está también empezando a hacer buenas migas conmigo; y especialmente Emma, esa pícara rubiaja que me tiene encandilado. Millones de gracias por hacer que el tiempo se pare con vosotros.

Millones de gracias a Grego y Claudio. No sé qué haría sin vosotros, hermanos. No sería nadie. Esta tesis va especialmente dedicada a vosotros dos.

Millones de gracias a mis padres, Toti y Gregorio. Todos los éxitos que coseche en esta vida, que terminar la tesis es uno, serán gracias a vosotros. Serán gracias a vuestra infinita paciencia, a vuestro amor y al desinteresado apoyo que me dais siempre. Ya te lo recordaré luego por la noche, Mamá.

Millones de gracias y besos a Miry, el amor de mi vida. Sólo tú sabes lo que es aguantar mi día a día “en modo tesis”. Te estaré eternamente agradecido, pues esto no habría sido posible sin tu facilidad para encontrar las palabras exactas en cada momento, para gestionar mis pausas, para alumbrarme con tu experiencia en estas lides, para sacrificar demasiados fines de semana, etc., etc., etc. Si hemos “sobrevivido” a esto… ¡Ya no hay quien nos pare!

CHAPTER 1

INTRODUCTION

1.1. THE IMPORTANCE OF MASS TRANSIT SYSTEMS

From the final decades of the XX century, the Earth regarded as a system is starting to exhibit changes that suggest that it is to some extent sensitive to the effects of the human development. The dimensions of this concern are as large as to make it transcend the scientific community. Indeed, Pope Francis has recently published –assisted by a number of Ecology authorities, among others– an Encyclical Letter (Francis 2015) where he deals with this problem. In this letter, he urges all the actors in the global scene, from individuals to policy makers, to make it possible a change to a new sustainable development paradigm.

From the Science perspective, in the last decades, Earth System scientists are providing evidence that the human development is not likely to be sustainable. As a result of an extent research, (Rockström, Steffen et al. 2009) proposed a frame of planetary boundaries to make it possible to ensure that human activities are not affecting the Earth System in such a way that it changes its state irreversibly. The results in this work suggested that, in the current situation by that time, some of these planetary boundaries (climate change, Nitrogen flow and loss of biodiversity) had been transgressed.

Recently, the same research group has published a review of their previous work in (Steffen, Richardson et al. 2015). Here, the planetary boundary conceptual frame is updated. The results of the new boundary assessment are far from showing an

improvement with respect to the situation in 2009. Actually, four boundaries are transgressed in this new evaluation.

Although it has been proved not to be the only issue to be addressed, the climate change problem arises as one of the most relevant scientific concerns nowadays. Several research works suggest that the anthropogenic emission of certain gasses, mainly those known as greenhouse gasses (GHGs), is provoking an increase in the total amount of energy stored in the climate system. This is clearly reflected in a rise of the temperatures of the sea and the land surfaces. Regarding this, the International Panel for the Climate Change (IPCC) has recently published a thorough review of the climate change problem where it warns that these changes may be irreversible under any of the emission scenarios assessed (IPCC 2014).

The main recommendations after the analysis of the climate change problem consist in a change to decarbonised development paradigms. The IPCC also recommends the development of business models that make this transformation feasible from the economic standpoint.

One of the sectors that must be thoroughly reviewed is the transport sector, responsible for a large share of the global 1) final energy consumption and 2) GHG emissions. Regarding the former, according to (Sims, Schaeffer et al. 2014), the final energy consumption associated with the transport sector represented 28 % of the total energy use, with 40 % of that used in urban transport (11 % with respect to the total final energy consumption figure). This means that urban transport has a significant weight in the global energy consumption.

Regarding GHG emissions, 7 Gt CO_2 eq were attributable to the transport sector in 2010, which represent more than double emissions with respect to the 1970 figures. Around 80 % of this increase is due to road vehicles.

From the urban transport perspective, this represents the fact that mobility has been shifted to the Light Duty Vehicle (LDV, passenger cars and commercial vans) side from the middle of the XX century. This increase in the use of motor vehicles is indeed reflected in a link between development and the number of LDVs (Schafer, Victor 2000).

It is important to note that cities where the mobility scheme is dominated by LDVs are facing another challenge: the effects of air pollutants on human health. The World Health Organisation (WHO) reported that 3.7 million premature deaths were attributable to ambient air pollution in 2012 (WHO 2014). Several fossil-fuel-combustion pollutants like nitrogen dioxide, ozone or particulate matter (PM) have been related with respiratory and cardiovascular diseases through a number of observational studies (Miller 2007, Brunekreef, Forsberg 2005, Pope CA 2004, Brunekreef, Holgate 2002). In addition, the mechanisms for air pollutants to induce diseases also seem to be identified (Mills, Donaldson et al. 2009).

Taking these facts into account, the task to change the urban mobility concept to a new paradigm less dependent on LDVs appears as an important concern for transport

scientists and policymakers. In this line, a recent study by (Kenworthy 2013) has observed that the use of LDVs and the Gross Domestic Product is starting to decouple. Furthermore, in twelve over the forty-two cities worldwide included in the analysis, the average use of cars has declined. The author points the improvement in the relative speed of public transit systems as one of the likely reasons for this tendency. This phenomenon has been in turn induced by the strong global trend towards urban rail.

Consequently, the promotion of a shift from LDVs to Mass Rapid Transit Systems (or simply Mass Transit Systems, MTSs) arises as a key factor to improve urban transport systems both in developed and developing countries. And it is clear that fast and efficient MTSs will ease this change process.

In urban environments, underground and commuter railway systems should be conceived to play a pivotal role in order to achieve clean and energy-efficient transport systems. First, because trains' energy efficiency is higher than that of LDVs. Then, because the shift towards an MTS-based mobility concept would move GHG emissions to power generation centres which are often far away from over-polluted urban environments. In addition, the amount of CO_2 emissions depends on the energy generation mix and so it is expected to be minimised in a few decades (Peterson, Schleich et al. 2011), especially after the recent agreement resulting from the Paris Climate Change Conference (UNFCCC 2015).

1.2. THESIS MOTIVATION

One of the key factors for the high energy efficiency figures of rail systems is the low train running resistance with respect to that of road vehicles. This is due to the low deformability of both train wheels and rails.

Then, electric railway systems, where trains are electrically connected between them or to an electrical network in general, present a further advantage from the energy-efficiency standpoint. The reason is that many trains are nowadays equipped with regenerative braking systems. This kind of rolling stock is able to convert kinetic energy back into electrical energy during braking. Several studies have proved that it is possible to obtain consumption reductions greater than 30 % by the application of regenerative braking (González-Gil, Palacin et al. 2014, López-López, Pecharromán et al. 2014, Gunselmann 2005).

To illustrate the regenerative braking potential, Figure 1-1 presents the power and speed profiles of a train running on a flat stretch between two passenger stations. These profiles have been broken down into three phases: 1) acceleration, 2) cruising and 3) braking.

The energy consumed or regenerated in each phase has been included in the top-side graph of the figure. It is important to note that the energy regenerated represents around 36 % of the total energy consumed by the train during the acceleration and cruising phases. Of course, as the length of the inter-station stretch increases, this percent figure would decrease consequently. Nevertheless, it is in line with the usual distances between stations in MTSs.

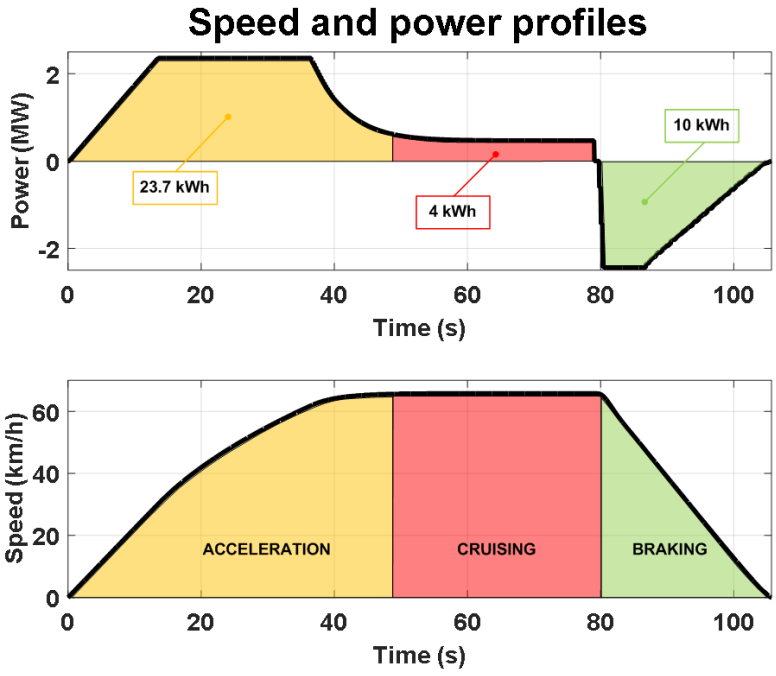

Figure 1-1. Energy figures in a typical train power and speed profile.

This means that, disregarding transmission losses, another train which was able to use the energy regenerated by the one in Figure 1-1 would only absorb 64 % of its accelerating and cruising energy from other sources. Consequently, SS consumption would drop, boosting the system energy efficiency.

However, reusing regenerative braking energy is not always possible. The main reason is that most MTSs are direct-current (DC) electrified systems (Profillidis 2006, Östlund 2012). For historical reasons (DC motors were easier to control), this kind of electrification spread in urban systems like tramway or underground. Currently, some other advantages of DC power transmission still make railway infrastructure designers to use DC electrifications in new MTSs. Examples of these advantages are: the reduced electro-magnetic emissions (avoiding interferences with the signalling system), the lower number of conductors required for the supply systems, the fact that from the utility grid perspective DC railways are balance loads, etc.

In comparison with alternating current (AC) systems, DC-electrified railway systems exhibit three main drawbacks:

- It is much more difficult to manufacture high-voltage DC circuit breakers than AC breakers for eliminating large short-circuit currents.
- It is not possible to step down a DC voltage by means of a transformer, and when the state-of-the-art of power electronics did not make easy to implement DC-DC conversion, the electrification voltage had to be that of the motors. Then, even in recent times, the maximum reverse voltage of semiconductors has traditionally limited the maximum electrification voltage. As a result, in DC systems, feeder (overhead conductor or third rail) voltage is usually lower than that in AC-electrified systems. Thus, DC railway systems present in general lower energy efficiency than AC railway systems. A good overview of energy issues in both kinds of electrifications is presented in (Koseki 2010).
- The DC-system substation (SS) electrical topology is disadvantageous. Electrical railway systems are connected to the utility grid by means of a set of SSs, which make it possible to feed the trains with the required level of power quality (in-range voltages, etc.). SSs in DC-electrified systems are made up of a transformer, used to step the utility grid voltage down to the railway system one, and an AC-DC converter (rectifier). Provided its robustness and simplicity, in the overwhelming majority of the DC-electrified railway systems, SS rectifiers are diode rectifiers, i.e. they are one-quadrant converters which only allow power to flow from the utility network to the railway system.

This latter drawback of DC system is responsible for the problems to absorb regenerative braking. The reason is that, without amendments, the one-quadrant SS scheme makes it necessary to consume regenerative braking power instantaneously. If the intensity of the traffic in a given line is high (peak-hour), power regenerated by a braking train is likely to be absorbed by a powering one. However, if the traffic density is low, the probability of no train drawing power from the feeder line when a certain train brakes rises up.

When this situation takes place, provided rectifiers do not allow power to flow from the railway system to the utility grid; regenerated power must be burnt in dedicated on-board resistors (rheostats). This is made in order to prevent voltage in the feeder line from reaching hazardous levels. Thus, there are situations where the DC network will be receptive to regenerated power and situations where it will not accept this energy.

This fact implies a practical limitation of the regenerative-braking potential which may spoil the system energy-efficiency figures with respect to an ideal situation where the system is fully receptive to this source of energy.

Consequently, it may be stated that although MTSs are characterised by high energy-efficiency figures, there is still room for optimising them from an energy consumption point of view. This is, indeed, one of the main targets of this thesis: **to assess the specific ability of current MTSs to absorb regenerative braking energy, and to review and analyse possible techniques or strategies to improve these systems.**

In general, there are several approaches to improve MTSs from an energy efficiency perspective. It is possible to: 1) optimise the design of the trains, 2) optimise the operation of the system, and 3) optimise the infrastructure.

With respect to the train design, it must be noted that it has been continuously subject to improvements from the electrical standpoint. Hence, modern electric trains are highly efficient, and it is not easy to achieve qualitative improvements in their electrical performance. Nevertheless, a comprehensive study on the different factors affecting rolling stock efficiency and the way they may be changed to improve the train energy figures is presented in (Kondo 2010).

However, there is still room to improve the design of the trains from other perspective. E.g.: there are several research efforts devoted to reduce the total mass of the trains in order to reduce consumption (Bombardier 2009), increase the capacity of the trains by augmenting the number of seats, bi-level trains; use of innovative fuels, hybridisation, etc.

Then, regarding the system operation, there is a first concern in the planning stage when MTS operators try to optimise the capacity of the system. The main target in this stage is to satisfy the passenger demand with the minimum number of trains in order not to have low train occupation rates.

Then, once the operation plan is set, there are two main approaches in the literature to reduce energy consumption:

- Optimising the energy consumption of each single train in the line. The most relevant trend in this approach is eco-driving. This designation collects strategies which are oriented to minimise train energy consumption in a given service. Studies in this field try to determine the speed and power profiles (driving strategy) which yield the minimum energy consumption for a given trip time. As a result, a pareto front gathering the best driving strategies for a set of trip times is obtained. Good examples of research on railway energy efficiency by optimising

the driving strategy may be found in the studies by (Domínguez, Fernández-Cardador et al. 2014a, Carvajal-Carreño, Cucala et al. 2014, Sheu, Lin 2012, Lin, Sheu 2011, Sicre, Cucala et al. 2010, Fernández-Cardador, Cucala 2010, Domínguez, Fernández-Cardador et al. 2010, Miyatake, Ko 2010, Miyatake, Haga et al. 2009, Domínguez, Fernández-Cardador et al. 2008, Ko, Koseki et al. 2005).

- Designing the operation timetables to synchronise the accelerating and braking phases of trains, thus reducing rheostat loss events (Yang, Chen et al. 2015, Pena-Alcaraz, Fernández-Cardador et al. 2012, Nasri, Moghadam et al. 2010, Miyatake, Ko 2007). This approach is thus oriented to improve the receptivity to regenerative braking energy.

Finally, from the infrastructure standpoint, it is possible to make a distinction between the rail infrastructure itself and the electrical infrastructure. Regarding the former, an example of measurement to make MTS more energy efficient is to design longer platforms, so allowing each train to transport more passengers. It is also commonplace nowadays to set passenger stations in high positions to use the potential energy in the braking and motoring phases of the trains, or to maximise the radius of the curves to avoid speed limitations, etc.

Regarding the electrical infrastructure, it is possible to design it in such a way that it is able to absorb braking power even when there are not enough trains consuming power in the line (Xia, Chen et al. 2015, Wang, Yang et al. 2014, Bae 2009, Chuang 2005, Hui-Jen, Chao-Shun et al. 2005). **This thesis focuses on the latter research interest**.

Figure 1-2 shows a scheme of the electrical infrastructure of a typical MTS. Trains are fed by a system which connects them to the utility grid (usually to medium-voltage bars) via SSs. The return current is usually collected by rails, which are isolated from the terrain.

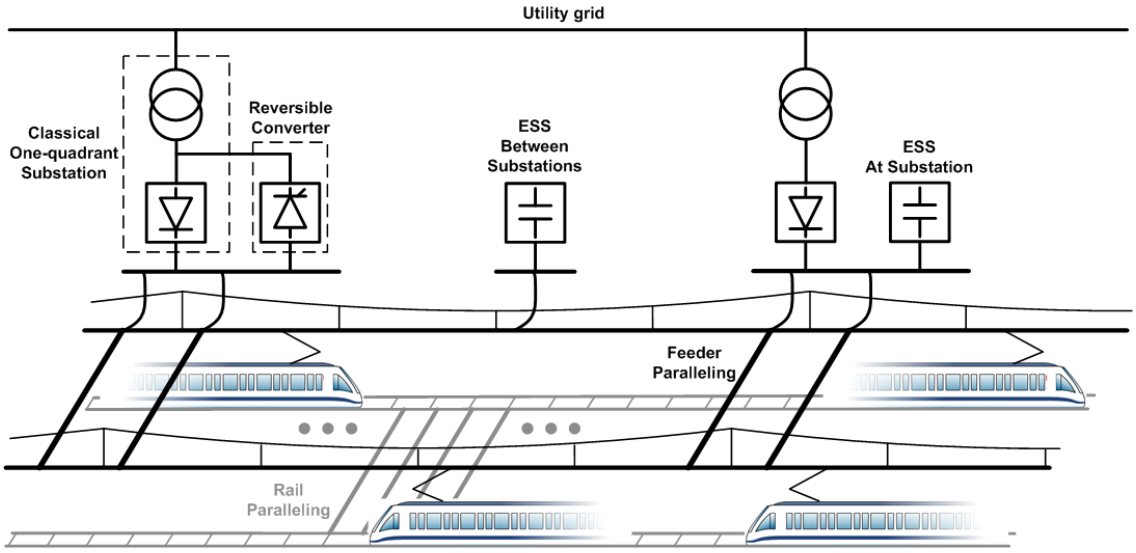

Figure 1-2. MTS electrical infrastructure scheme.

The electrical infrastructure of an MTS may be improved by installing certain devices and subsystems which help increase receptivity. These devices can make this parameter fairly insensitive to the traffic characteristics. The most common among them are reversible substations (RSs) and Energy Storage Systems (ESSs).

The former increase receptivity by allowing power flows from the railway system to the utility grid. The latter store energy surpluses temporarily and feed this energy back to the railway system afterwards, when there are motoring trains nearby.

ESSs present several advantageous characteristics like voltage stabilisation or the possibility to be installed between SSs. However, for several reasons, the current trend when power flowing from the railway system to the utility grid is remunerated consists of using RSs (Gelman 2013). These reasons will be thoroughly presented in Chapter 3.

In any case, the inclusion of devices to increase receptivity leads to large investments, so their necessity must be properly motivated. Several issues, such as the total number of devices installed, their size, location or control parameters must be properly determined. Indeed, the literature provides a number of studies dealing with the optimal location of RSs or ESSs in a given system (the literature review regarding this topic is included in Sections 4.1 and 6.1).

However, the list of available references is not extensive, and it does not cover all the aspects to be tackled in MTS infrastructure optimisation. For instance, these references usually implement metaheuristic strategies to search for the optimum electrical infrastructure configuration. However, it has not been clarified to what extent it is possible to trivially find the number and location of the devices to be installed by simply analysing the topography of the line, or based on the experience of the MTS operator.

Consequently, **advancing in the study of the optimal improvement of MTS electrical infrastructure has been identified as other of the main reasons to develop this thesis**.

A general concern in the MTS design studies is related to the tools used to obtain the results. Provided the high complexity and time variability of the electrical railway systems, these studies are in the majority of cases performed with simulation tools. Thus, there are several examples of electrical multi-train simulators in the literature (the literature review regarding this topic is included in Chapter 2).

When the MTS studies cope with the optimisation of the electrical infrastructure, it is extremely important to have optimised simulation times in order to make it possible to implement complex search processes. In addition, it is of course important that the electrical multi-train simulator exhibits high accuracy figures for the results to be reliable.

To tackle this concern, **this thesis will study the models of the most important elements in MTSs, and will integrate them into an electrical multi-train simulator.**

The main approaches to optimise the computational behaviour of the simulator will be studied in the thesis.

There is a final concern to be covered by this thesis. Figure 1-3 shows a simple double-track line with three stations and two trains. Then, Figure 1-4 shows two possible traffic situations. Specifically, Figure 1-4.a presents the disadvantageous case where the acceleration, cruising and braking phases are synchronised. It may be observed in the bottom-side graph that the net power is high during the accelerating phases, and then it is negative during the braking ones. Consequently, first the electrical system will have to supply high powers, and then it will not be possible to reuse regenerative braking energy, which will necessarily be sent to rheostats.

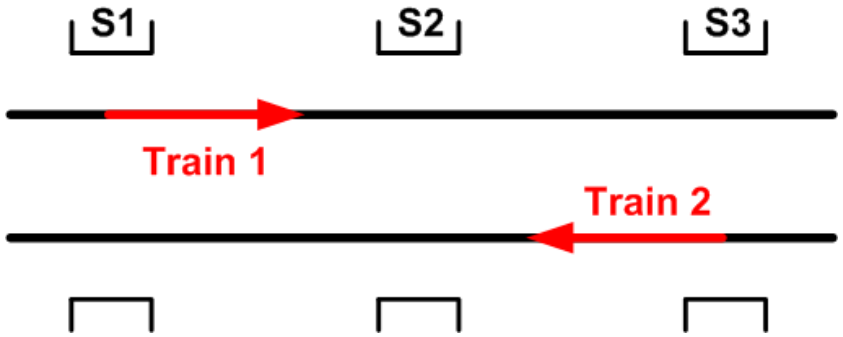

Figure 1-3. Line example to illustrate the influence of the traffic.

Figure 1-4.b presents the opposite extreme, where accelerating and braking phases are optimally synchronised to take advantage of regenerative braking. This has a further advantageous side effect: in addition to reuse the regenerative braking energy, the maximum power demanded to the electrical system will decrease.

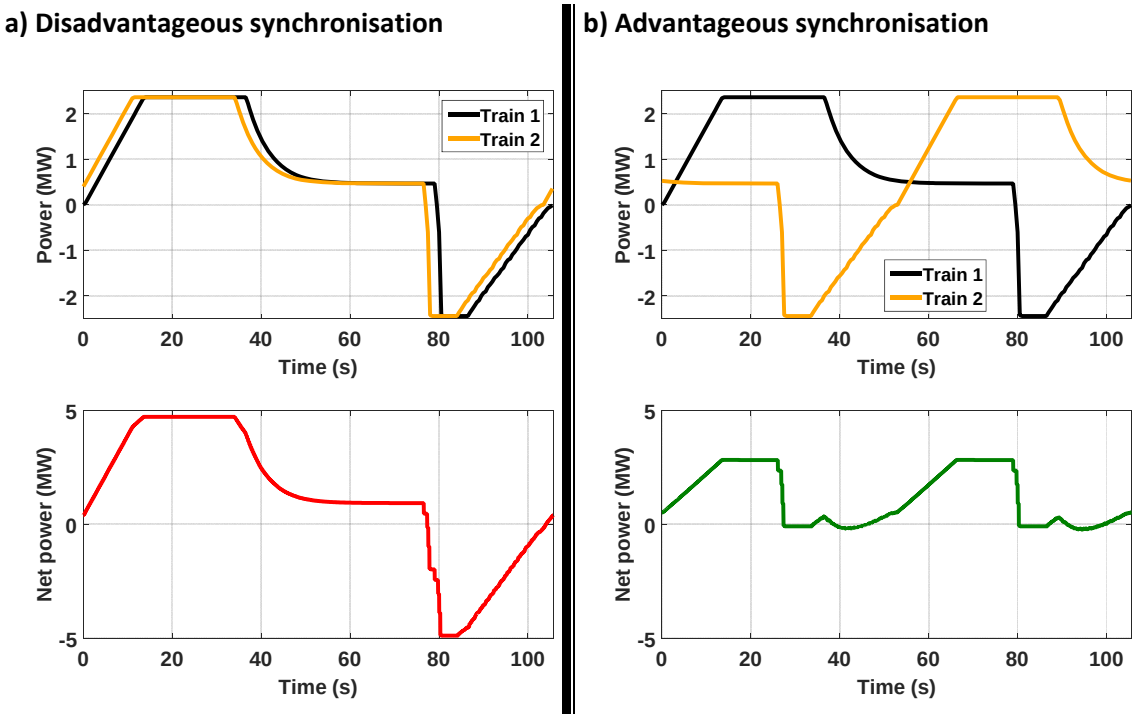

Figure 1-4. Examples of train power synchronisations.

After the analysis of these two situations, it is clear that the global-system energy figures will be strongly influenced by the way the accelerating, cruising and braking phases of all the trains are combined. In other words, the system energy figures will be seriously influenced by the characteristics of the traffic.

In the actual operation of a given system, there will be a variety of traffic situations which range between the situations depicted in Figure 1-4.a, and those in Figure 1-4.b. If situations analogous to the former are recurrent, the application of techniques to increase receptivity will likely be useful. If they most recurrent patterns are similar to those in Figure 1-4.b, these techniques will not make much sense.

Consequently, it is important that the traffic model used in a study to improve the electrical infrastructure of an MTS is able to properly represent the actual interactions between the trains in the system. If this is not the case, the conclusions of the study are subject to be inaccurate, or even erroneous.

However, most of the MTS infrastructure optimisation studies in the literature include strongly simplified traffic models (see Section 4.1). These models have not been proved to properly represent the actual interactions between trains. To tackle this concern, **this thesis aims to study the effects of the traffic on the most relevant energy and energy-saving MTS figures, and to propose an extended traffic modelling approach**.

1.3. THESIS OBJECTIVES

1.3.1. MAIN OBJECTIVE

The main objective of this thesis is to improve the electrical infrastructure of a railway DC-electrified Mass Transit System in order to take full advantage of the train regenerative braking energy. This thesis aims to include actual traffic operation conditions in order to obtain more accurate results for the system global energy efficiency.

Although several different options to improve Mass Transit Systems will be analysed, this thesis focuses on the main current trend to improve their energy efficiency: Reversible Substations. Specifically, the studies in this thesis aim to determine optimal infrastructure improvement configurations derived from the installation of reversible substations (layout, size, control parameters, etc.). These optimal infrastructure configurations will be supported by the required economic criteria in order to assist the Mass Transit System operator in the investment decision-making process.

1.3.2. SPECIFIC OBJECTIVES

The development of tools and conceptual frames to make it possible to attain the main objective of this thesis yields the following list of particular objectives:

1. **Development of accurate models of the most important electric elements in MTSs**

This objective covers the necessity to review the available models of the different elements in the electrical infrastructure and the trains. The implementation of accurate models for these elements is required to obtain valid and general results in the thesis.

The main elements to be reviewed are:

- The train model. It is important to use a detailed model of the train from the perspective of the type of electrical load that it represents. In addition, it is required to model the train regenerative braking energy management, i.e., which fraction of regenerative power will be used to supply the train auxiliary consumption, which one will be injected into the system for other loads to use it, and finally which fraction will be sent to rheostats.
- The supply and return circuit model.
- The substation model. It is important for DC-railway energy studies to implement an accurate model of the AC-DC interface. It is important to note that usual rectifiers exhibit different behavioural modes depending on the rest of the elements in the system. Therefore, an accurate representation of these devices is important to prevent the studies in the thesis to obtain erroneous results. It is also required to have accurate representation of the bidirectional substation (reversible substation), which is currently the key element to improve MTS energy efficiency.
- The Energy Storage System model. As will be explained, the current state-of-the-art of these devices does not make them competitive with respect to RSs unless train voltage support is required or reverse power flows are not remunerated. However, the notable amount of research which is being conducted to improve these devices makes them a potential good candidate for a medium-term future. Consequently, it arises as an interesting concern to study ESS and to implement accurate models to represent them.

2. **Integration of the MTS-element models into an electrical railway simulator. Improvement of the simulator performance**

Due to the high complexity of MTSs, the majority of the references in the literature devoted to their study make use of simulators. Thus, the development of this electrical railway simulator will make it possible to evaluate the energy efficiency of the MTS.

The simulator must be able to solve the electric railway system load flows in a certain time interval. It must be noted that the heterogeneity of the load-regeneration situations to be tackled, together with the presence of non-linear and time-variant elements, tends to make it a difficult task to solve the load flows. Actually, it is possible to have situations where the simulator could not find the electrical topology

of the system. Therefore, the simulator must be implemented in a robust way which is able to solve these highly complex situations.

In addition, the computation time performance of the simulator will influence the characteristics of a simulation-based optimisation algorithm. Specifically, for the same modelling accuracy, a fast simulator will make it possible to properly carry out searches in complex search spaces; whereas a slow simulator will probably lead to a relaxation of the optimiser goals. Consequently, the computation time of the simulator must be reviewed with the aim to set it to low time figures.

3. Development of a representative traffic scenario generator

In a railway system, a rigorous evaluation of the feasibility of an infrastructure improvement must be supported by the use of realistic traffic scenarios. This implies that the traffic used in MTS studies must accomplish the system capacity rules.

However, this is not strictly enough. In addition, the traffic scenarios used must be representative of the actual interactions between substations, braking trains and motoring trains. Thus, provided in the actual operation of MTSs the traffic is subject to variations, an accurate study should include several traffic scenarios which are able to represent the diverse traffic situations.

Unfortunately, as the number of traffic scenarios included in the system is increased, the simulation time to obtain energy consumption figures for the system increases consequently. This computation-time increase, as already stated in the previous specific objective, punishes the behaviour of simulation-based infrastructure optimisers.

To tackle this concern, this thesis aims to analyse the minimum number of traffic scenarios required to obtain accurate energy-saving results in MTS energy efficiency studies.

4. Assessment of the possibility to reduce the computational burden of MTS infrastructure optimisation studies by compressing the traffic scenarios.

This thesis is aimed at minimising the simulation based MTS optimisers computational times. The reason behind this objective is the same presented in the 2nd specific objective: if the computational burden associated with the obtainment of the MTS energy figures is reduced without a significant effect on accuracy, it will be possible to have more ambitious MTS infrastructure optimisers.

It must be noted that the extension of the traffic model derived from the 3rd specific objective will in general lead to an increased number of traffic scenarios, thus decreasing the computation-time performance of the optimiser. Therefore, after the selection of the representative scenarios, it could be useful to minimise the time required to simulate each of these scenarios.

Consequently, in the frame of this specific objective, this thesis will explore the possibilities to compress the traffic scenarios, making use of less train load profiles to express approximately the same information they include.

5. **Development of an optimisation algorithm which makes it possible to find optimal MTS infrastructure configurations from the energy-efficiency standpoint.**

Finally, this objective consists of developing an automatic search algorithm that makes it possible to obtain optimum MTS infrastructure improvements from the energy-saving standpoint. This MTS infrastructure optimiser will be able to use the most advantageous improvement technology, and it will determine the number of devices to install and their layout and sizes.

The optimisation method will include the cost assessment information required for the infrastructure improvements proposed to make sense from the investment decision point of view.

1.4. STRUCTURE OF THE DOCUMENT

This thesis is structured into seven chapters:

- This first one has presented an introduction to the thesis followed by its motivation and objectives.
- Chapter 2 presents the electrical multi-train simulator developed in the frame of this thesis, which has been used as the key tool to obtain its results.
- In Chapter 3, the main characteristics of MTSs from the energy-efficiency standpoint are given. Several approaches and techniques to reduce MTS energy consumption are reviewed and proposed.
- Chapter 4 is devoted to the study of the effect of the traffic variations on the energy-saving figures. The limitations of the usual traffic modelling approach are explored and a novel method to select a reduced-size set of representative traffic scenarios is proposed.
- Chapter 5 tackles the traffic scenario compression, which is applied to the representative scenarios selected. This is a novel method presented in this thesis to reduce the computation time required by MTS infrastructure optimisers to obtain general and accurate results.
- Chapter 6 presents the MTS infrastructure optimisation method proposed in this thesis. This optimiser makes it possible to determine the number, location and size of the devices that must be installed in a given MTS to optimise its energy efficiency.
- Finally, Chapter 7 gathers the main conclusions drawn from the studies in the thesis. In addition, it highlights its most relevant contributions and proposes some future works.

CHAPTER 2

MASS TRANSIT SYSTEM SIMULATION

2.1. INTRODUCTION

This chapter presents the details of the electrical multi-train simulator developed in the frame of this thesis. The simulator is the key tool to perform the different studies presented along the thesis. However, readers more interested in MTS energy efficiency studies than in the characteristics and implementation details of the simulator may skip this chapter and start from Chapter 3.

Provided the high complexity of the electrical interactions in railway systems, they are quite often analysed by means of electrical multi-train simulators. These simulators make it possible to represent the complex traffic situations that take place in those systems, as well as their time variance. Consequently, realistic results of variables such as catenary voltages, energy consumption, etc. may be obtained by means of this kind of simulators.

There are plenty of instances of this kind of simulators, being (Mellitt et al., 1978) one of the firsts to be presented, which has been intensively referenced in the literature on this topic. In (Goodman et al., 1998), an interesting review of the state-of-the-art of railway simulators is carried out, but there are plenty of newer references.

Figure 2-1 shows the general structure of an electrical railway simulator. Two parts can be distinguished in the system: the train movement simulator and the power network simulator.

The former is named 'Train movement simulator'. It is in charge of calculating the position and power demand of one train in the system. To calculate them, it makes use of the topographic information of the tracks, the characteristics of the train and the operation data. The latter, named 'Network simulator', calculates the voltages, currents and powers in every node of the power network. This electrical network simulator is essential for the purposes of this thesis. Therefore, although the movement simulator is also depicted, this chapter makes a special emphasis on the presentation of its characteristics.

Although there are substantial differences between AC and DC railway systems, the scheme in Figure 2-1 can be applied to both types of electrification. Furthermore, the train movement simulator block will hardly change from one system to another, despite the differences in the rolling stock traction equipment characteristics, etc. However, the power network simulator used in an AC system is relatively simple since there are few nonlinear constraints involved, whereas in a DC system the complexity of the model may be much higher.

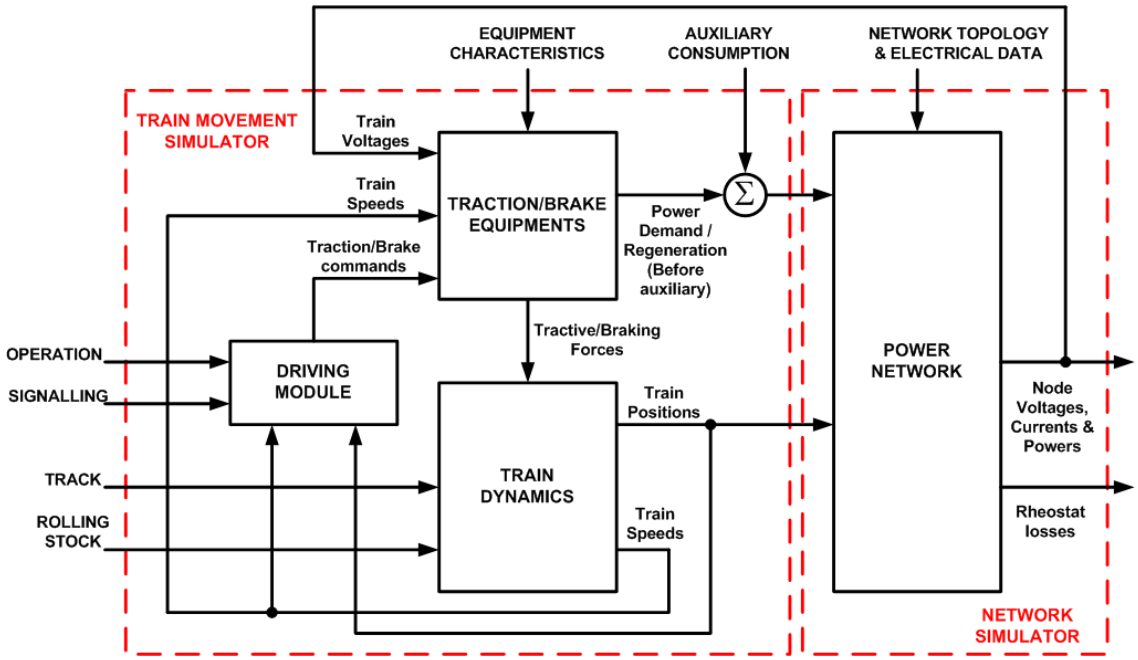

Figure 2-1. General structure of an electrical multi-train simulator.

It is important to note that the structure in Figure 2-1 exhibits three loops. First, there are two inner train speed and position feedbacks. Both signals are used in the driving module, together with operation and the current signalling information to decide the control actions to take (traction command). Then, the actual traction forces are dependent on the train speed. These first loops may be regarded as internal loops in the train movement simulator.

Then, there is a feedback of the trains' pantograph voltages. This loop is devoted to reflect a loss of traction effort that may arise when the voltage seen by the train drops. This third loop couples the movement and the network blocks in the simulator. However, it will be explained later that this effect may be neglected, especially in non inter-operable systems as MTSs if they are operated with inverter-driven three-phase-

motor trains. Under this assumption, the outer loop can be eliminated, effectively decoupling both parts of the simulator.

It is important to note that the signalling system is not represented in the thesis. The reason is that the studies in this thesis do not include traffic situations where trains disturb each others. Instead, the electrical studies in this thesis make use of a nominal traffic approach where trains are separated by the headway. Then, this is complemented by introducing variations in some traffic variables (e.g., the dwell times) that, however, do not lead to disturbed traffic conditions. This approach is supported by the fact that trains in MTSs, which are usually operated with Automatic Train Operation (ATO), exhibit fairly stable and robust running times.

Once the general lines of an electrical multi-train simulator have been presented, it is time to analyse the different blocks in the diagram. It is clear that a simulator requires models for all the elements that take place in a typical railway system. Then, once all the elements have been modelled, there is a further task to integrate them in order to characterise their interactions in the actual system. By doing this, the resulting simulator may be able to represent the reality to be simulated to a certain extent.

This chapter is devoted to this topic, and will be split into three sections. First, the models for the most important elements in an electric railway system are presented, with the required literature support to justify modelling decisions. The elements which take place in all the electric railway systems will be complemented with the two more common elements to improve DC-electrified systems: RSs and ESSs. Although this thesis focuses on DC-electrified systems, provided the simulator developed is able to represent both AC and DC railway, this chapter presents the main models for both types of system.

Second, the process to integrate the models into an electrical railway simulator is thoroughly explained. Third, there is a section devoted to the measurement of the computational performance of the resulting simulator, both in terms of time performance and robustness.

Regarding the contributions of this chapter, it presents a set of heuristic rules to obtain the electrical topology of the elements in MTSs. This part of the simulator, which is essential for its correct functioning and convergence characteristics, is often omitted in the related literature.

2.2. MODELS AND METHODS FOR THE MTS ELECTRICAL SIMULATION

This section reviews the modelling approaches that may be found in the literature for the most relevant elements in an electric railway system. The different sub sections give some relevant references to support the models presented.

2.2.1. TRAIN MODEL

It is commonly accepted that, from the railway electrical system standpoint, modern trains behave as voltage-independent power loads; i.e., the power consumed by a train does not depend on the voltage at the pantograph or collector shoe (Goodman, Siu et al. 1998). The main reason for this may be found in the input converters that modern trains feature. Both if the input voltage of the inverters that feed the motors is pre-conditioned or not, the power electronic devices control makes it possible to modulate the input current in order to have an appropriate input power to the motors.

Then, there are railway networks that may be used by several different types of train. These networks are regulated in Europe by (EN 50388 2012), and they are usually referred to as inter-operable railway networks. When this normative applies, the maximum traction current must be reduced as the pantograph voltage drops. Trains running on these rails must feature this traction current reduction curve, which therefore changes their electrical model to a power load which depends on the pantograph voltage. It must be noted that both the constant power load and this alternative load model are non linear models.

Once known the type of load to be assigned to the train model, it must be completed by representing the train efficiency; i.e., the power losses in the elements that may be found in the train's power path. Figure 2-2 depicts the principal power losses in a typical train. Although there are several topologies to convert the electrical power in the pantograph into mechanical power in the wheels (or vice-versa), the main losses in the train power chain are: losses in electrical conductors, losses in power electronics devices and motors, and running-resistance losses, explained by the Davis formula (2.1), (Lukaszewicz 2001).

$$P_{running} = A + B \cdot v_{train} + C \cdot K_{tunnel} \cdot v_{train}^2 \quad (2.1)$$

Where,

- A, B and C are coefficients depending on the train design which express the relation between the running resistance and the train speed.
- K_{tunnel} is a coefficient to express the effects of a tunnel on the running resistance. It is greater than 1, and values around 1.3 are common.
- v_{train} is the train speed.

Regarding the braking phase, it must be noted that in general, the braking power is used to supply the auxiliary equipment consumption. Then, if there is a regenerative power surplus, the train would try to inject this power into the catenary system. It will

be explained in Chapter 3 that the use of regenerative braking energy is a key factor to improve the MTS energy efficiency.

Actually, the portion of the kinetic energy stored in the train in the beginning of the braking phase which is not fed back into the catenary system may be regarded as a further source of losses. Regarding this, two additional loss sources arise: 1) the power dissipated in the non-electrical braking systems, like pneumatic braking, as a result of the blend of braking systems; and 2) the portion of the electrical braking power that is not accepted by the system, and is hence dissipated in on-board rheostats.

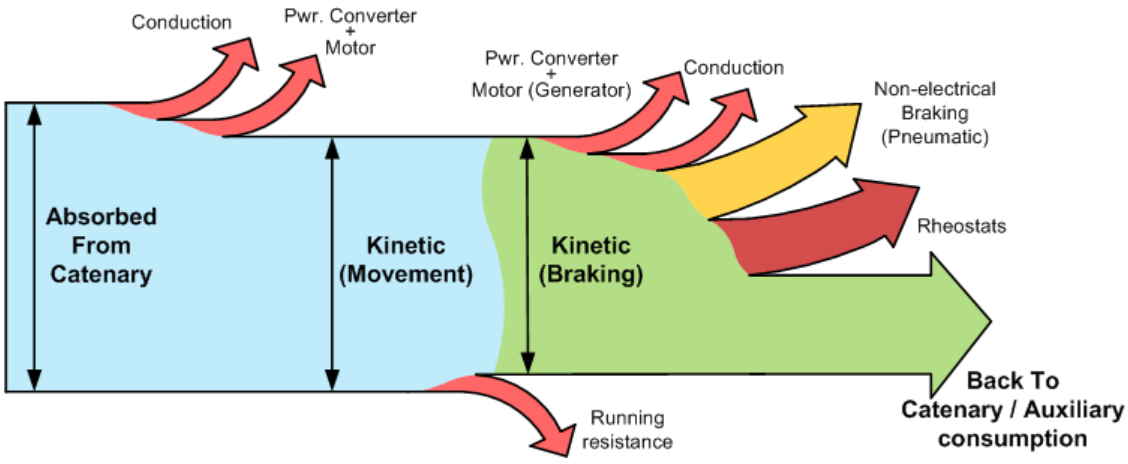

Figure 2-2. Energy flows inside the train.

Taking this into account, there are two main approaches in the related literature to determine the train pantograph power from the requested wheel power: a detailed and a simplified approach. The former is based on detailed models of all the elements in the train power path (Chymera, Renfrew et al. 2010). The application of this modelling approach requires a large amount of information about constructive details of the train such as impedances of motor windings, power electronics characteristics, etc. Thus, in the majority of cases it is difficult to properly apply this kind of modelling. The latter approach (simplified) consists of determining the train efficiency from real measurements by applying fitting techniques. If these measurements are available, the simplified approach may be regarded as a simple and powerful means to obtain the train efficiency model (Sicre, Cucala et al. 2012, Dominguez, Fernandez et al. 2011, Pilo, Rouco et al. 2000, Mellitt, Goodman et al. 1978).

The train model in the thesis

From the type-of-load standpoint, it must be taken into account that this thesis is focused on the study of MTSs, which are closed systems that are not subject to the inter-operable network normative. Consequently, the voltage-independent power load has been the choice for the type of load model.

However, as it happens in any railway system, trains are banned to induce pantograph voltages greater than the 20 % of the infrastructure nominal voltage. Rheostat losses are due to this norm. To represent this behaviour, the simulator in the thesis switches

the train model from voltage-independent power to voltage source when the maximum allowed voltage is reached.

Regarding train efficiency, in the acceleration phase, the model in the electrical multi-train simulator makes use of the maximum force and current curves provided by the manufacturer to obtain the electrical power at the pantograph from the mechanical power at wheels. Figure 2-3 presents an example of these curves.

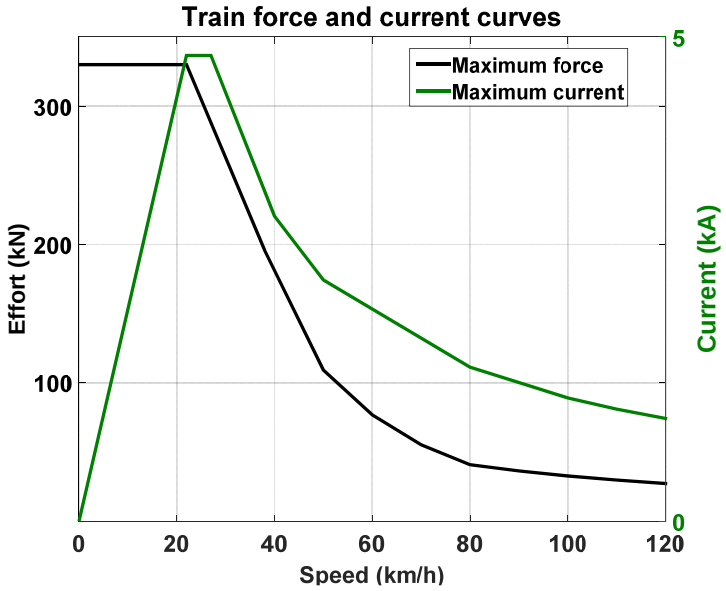

Figure 2-3. Example of maximum effort and current curves.

The relation between the maximum mechanical and electrical power as a function of the train speed yields a variable efficiency coefficient for maximum traction, as expressed in (2.2).

$$\mu_M(v_{train}) = \frac{F_M(v_{train}) \cdot v_{train}}{U_{NOM} \cdot I_M(v_{train})} \tag{2.2}$$

Where,

- $\mu_M(v_{train})$ is the efficiency coefficient, which depends on the train speed.
- U_{NOM} represents the nominal voltage at train pantograph.
- $F_M(v_{train})$ is the maximum effort for speed v_{train}.
- $I_M(v_{train})$ is the current absorbed at the pantograph when the motors apply the maximum effort at speed v_{train}.

It is important to note that the model makes use of the nominal pantograph voltage to obtain the efficiency coefficient. The reason is that this is the electrical condition in the curve-measurement tests. Then, in the actual operation of the system, the electrical power absorbed by modern trains will not be affected by pantograph voltage variations due to their input conditioning converter (Goodman, Siu et al. 1998).

Usual values for μ_M are around 0.87. With this efficiency coefficient, it would be possible to obtain the electrical power from the mechanical one when the train is applying maximum traction effort.

However, for traction efforts lower than the maximum one, train manufacturers do not supply the effort-current curves. Though, it is knoun that the efficiency exhibits a certain decrease when the train converters drive powers lower than the maximum one. One of the reasons for this efficiency decrease is that when the power delivered by the train is low, the fairly constant switching losses in its power converters may become a significant fraction of the total energy figures, leading to low efficiency values.

To refine the efficiency model, this thesis includes the approach presented by (Dominguez, Fernandez et al. 2011), where an empirical penalty factor which depends on the actual-maximum effort ratio was proposed. The expression of the resulting pantograph power is given in (2.3).

$$P_{pant}(F, v_{train}) = \mu_M(v_{train}) \cdot F \cdot v_{train} \cdot pf\left({}^{F}/_{F_M(v_{train})}\right) \quad (2.3)$$

Where,

- $P_{pant}(F, v_{train})$ is the power at the train pantograph.
- F is the actual effort applied at train wheels.
- $pf\left({}^{F}/_{F_M(v_{train})}\right)$ represents the penalty factor

pf is adjusted from real measurements, and it represents a linear penalisation on the train energy efficiency as a function of the ratio between the maximum available and the requested traction. It takes values between 0.57 and 1 for the train model included in this thesis. Although the lowest bound may be regarded as an extremely poor efficiency figure, it must be noted that it is line with the operation of the train at low power.

The results of the speed profile simulator have proved to predict, with very low error figures, the energy consumption and running times of trains in real operation. Further details of the speed profile simulation may be found in (Dominguez 2013).

With respect to the braking phase, the efficiency model used to calculate the regenerative braking power is analogous to the one for the accelerating phase. However, the electrical braking curve is complemented by the rest of braking systems (blending), mainly the pneumatic one. The braking strategy implemented consists of using all the available electrical braking effort and then to add pneumatic braking if the train is requested to apply higher braking efforts. Figure 2-4 shows an example of the braking curves, together with an example of the braking blend strategy.

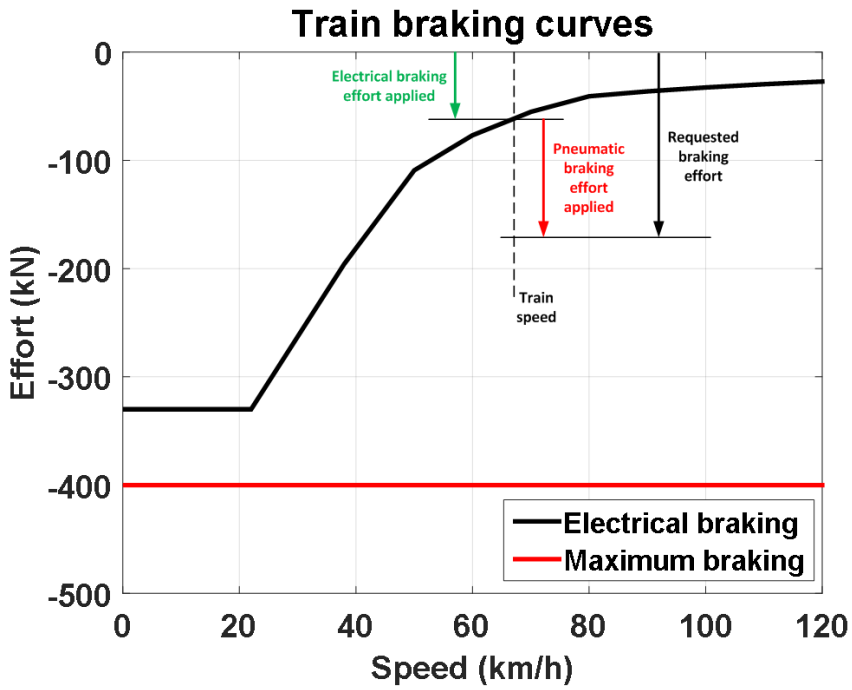

Figure 2-4. Example of braking curves.

Just to conclude the presentation of the train model, it is necessary to define the braking power management strategy. Regarding this, the braking power obtained from the braking curves and the efficiency model is first used to supply the auxiliary equipment consumption.

Then, if the braking power is greater than the auxiliary consumption, the power surplus is injected into the catenary system. As already stated, this mechanism is subject to having pantograph voltages lower than the rheostat threshold. If this limit is hit, the train switches to constant voltage mode. This represents the activation of the braking chopper on-board the train, which is in charge of clamping this voltage by sending the excessive braking power to rheostats.

2.2.2. ELECTRIC SUPPLY NETWORK MODEL

2.2.2.1. FEEDER SYSTEM

In AC-electrified systems, traction SSs are made up of transformers, which are linear elements (disregarding saturation effects). Therefore, the main modelling difficulties consist of properly representing the inductive coupling between wires, distributed capacitors, etc. The complexity of these models is especially high in auto transformer (AT) systems (e.g.: 2x25 kV) due to the increased number of electrical conductors. For this reason, there is a number of articles aimed at obtaining simplified models for the 2x25 kV systems.

In this line, (Pilo, Rouco et al. 2012) present a reduced-size model for 2x25 kV systems. Its structure is that of a 1x25 kV system, which leads to a reduction in the complexity and computer memory use of the simulator. This simplification is made by defining equivalent impedances to group the effects of the ‘negative’ feeder. The result is an

accurate model for low frequencies that suits load flow and stability analyses. For the same kind of analyses, (Mariscotti, Pozzobon et al. 2007) present a low frequency model for 2x25 kV systems where the number of conductors is reduced from 14 to 3.

On the other hand, in the case of (Brenna, Foiadelli 2010), no relevant simplifications are performed. This work presents a detailed model designed to carry out sensitivity analyses that assist the decision taking in the design stage of 2x25 kV systems.

In DC-electrified networks, the movement of the train is not fast enough to induce relevant high frequency transients in the system. Thus, it is appropriate to represent them as systems where changes take place slowly from one state to the following one as the trains' positions vary (Talukdar, Koo 1977). Consequently, inductive effects are neglected in all the DC railway simulators found in the literature.

There are two main feeder system structures in DC-electrified systems: 1) the catenary system and 2) the third rail system. In the former, trains are equipped with pantograph systems to collect the supply currents, whereas in the latter, they perform this task by means of collector shoes.

2.2.2.2. RETURN CIRCUIT SYSTEM

In railway systems, the current return from trains to SSs is a very relevant concern. This current usually flows through the rails and, in case they are not isolated, also through the terrain. As a result, there are points where the type of electrical conduction changes from electronic (metal conductors) to ionic (terrain). If the current flow in these points is not avoided or at least controlled, the corrosion phenomena associated with this change of conductor type could cause severe structural damages.

To tackle this issue, some systems feature dedicated return feeders. In others, rails are isolated to limit the amount of current flowing through the structure. However, the isolation is usually far from being perfect, and a careful design of the return system including collector mats is required (Pires, Nabeta et al. 2009).

Consequently, in studies where it is important to get details on rail voltages or leakage currents, the rail and terrain distributed impedance must be carefully modelled. In this line, (Yu, Goodman 1990) present a mathematical model of the return circuit that has been intensively referenced in the related literature. (Mariscotti 2003) performs a study on the leakage current distribution which aims to assess the interferences with the signalling systems. It is both valid for AC and DC systems. Then, with regard to the rail voltage studies in DC systems, (Pires, Nabeta et al. 2007) present a very detailed model of the return circuit. This study introduces different models to represent the current return paths in surface and underground systems. For the latter, two approaches with increasing complexity (two-earth and three-earth models) are derived to model the collector mats used to avoid or to dramatically reduce the current flowing through the structure.

In energy efficiency studies where rail voltages are not relevant information, it is common to lump the rail and the catenary systems into a single equivalent resistance (Chymera, Renfrew et al. 2010).

The electric supply network model in the thesis

The rail voltages and the leakage currents are out of the main scope of this thesis. For this reason, the studies presented in this thesis use the lumped feeder-return model for the electric supply network.

2.2.3. TRACTION ELECTRICAL SUB STATION MODEL

In AC railway systems, as stated in Section 2.2.2.1, the electrical traction SSs are made up of transformers which usually step the utility grid voltage down to the railway network one. Thus, only the well-known transformer model (often a simplified version) is required. In most articles presenting AC railway simulators, the substation model is restricted to the transformer, but no details are given (Pilo, Rouco et al. 2012, Mariscotti, Pozzobon et al. 2007, Pilo, Rouco et al. 2000).

In DC railway systems, the electrical traction SSs consist in AC-DC converters (rectifiers) that transform the alternating current in the utility grid into direct current to feed the trains. In the overwhelming majority of DC-electrified systems, this conversion is carried out by means of uncontrolled (diode) rectifiers.

The most extended diode rectifier model may be found in a number of power electronics books, as (Seguier, Labrique 1993), or in more specific books as (Arrillaga, Watson 2001). The latter, although derived for mixed AC-DC power transportation systems as HVDC or FACTS, presents an interesting approach oriented to the solution of mixed AC-DC load flows.

In the model by (Arrillaga, Watson 2001), the voltage in the DC side of the rectifier, in per unit (p.u.) magnitudes, is obtained from (2.4).

$$V_d = k_1 \cdot a \cdot V_{term} \cdot cos\alpha - k_2 \cdot X_c \cdot I_d \quad (2.4)$$

Where,

- V_d represents the voltage in the DC side of the rectifier.
- k_1 is a constant which depends on the rectifier topology and the selected per unit system.
- a is the transformer tap ratio, which is only necessary when the substation transformer features a tap changer.
- V_{term} is the voltage in the AC side of the rectifier.
- α is the ignition angle.
- k_2 is a constant that depends on the selected per unit system.
- X_c is the reactance seen by the rectifier.
- I_d is the DC side current.

Resistive and conduction losses in the semiconductor devices are neglected, since the reactive voltage drop related to the rectifier overlap angle (μ) is considered to be the dominant effect.

Although this model is accurate enough for transportation systems, the work by (Tylavsky, Trutt 1983) points out that in systems with lower power ratings, it may exhibit a certain lack of accuracy. This article derives a refinement of the rectifier model by 1) the inclusion of a non-null resistance in the reactance seen by the converter, which modifies the voltage drop results; and 2) the inclusion of the resistive losses. The new formula proposed by (Tylavsky, Trutt 1983) for the voltage in the DC side of the rectifier, in p.u. magnitudes, is given in (2.5).

$$V_d = V_{term} \cdot \frac{\cos\alpha + \cos(\alpha+\mu)}{2} + \frac{\pi^2}{18} \cdot \left(2 - \frac{3\mu}{2\pi}\right) \cdot R_c \cdot I_d \qquad (2.5)$$

Where the notation in (2.4) is followed, with the addition of

- μ, the overlap angle, and
- R_c, the commutation resistance.

In this model by (Tylavsky, Trutt 1983), the RMS AC line current value is set to be equal to the load current (I_d) in per unit magnitude. However, in the work by (Tzeng, Wu 1995), some discrepancies with real measurements were observed. To overcome this problem, (Tzeng, Wu 1995) develop a more complex model where the AC line current is precisely calculated. To do that, they generate an approximate waveform taking into account the different commutation phases and then obtain its Fourier transform. By including this enhancement, the model provides more accurate values of the active and reactive powers consumed by the rectifier.

Despite the complexity increase in the model by (Tzeng, Wu 1995), this enhanced accuracy in the AC side is important to properly represent the electrical variables in the AC rings that are becoming more and more common in MTSs.

Then, there are a number of studies where the AC side of the system is not analysed. The SS model is simplified to a Thévenin equivalent dipole where a series resistor represents both the active and reactive voltage drop in the traction SS (Chymera, Renfrew et al. 2010, Barrero, Tackoen et al. 2008b, Destraz, Barrade et al. 2007, Cai, Irving et al. 1995b).

Reversible Substation

The model for the RS may be obtained by applying the substation model for power flows from the DC-side to the AC-side. Actually, RSs are often implemented as an additional converter in parallel with the existing rectifier. The additional converters are usually made up of thyristors or IGBTs, and unlike the diode rectifiers, they are controlled converters.

For the case of the detailed substation model, the work in (Tzeng, Wu et al. 1998) explains the particularities of the application to the reversible converter. Since this converter is controlled, the main difference with respect to the uncontrolled rectifier

is that now, it is required to define a control strategy. The constant ignition angle (α) and the constant voltage are the most common ones.

The substation model in the thesis

The detailed rectifier model presented by (Tzeng, Wu 1995) is the one included in the SS model of the simulator. Section 2.3.2.1, which presents the DC railway load flow solver, gives a detailed presentation of the converter equations.

Regarding the RS model, the simulator of this thesis features two alternative models:

- The detailed model presented in (Tzeng, Wu et al. 1998), which suits these studies where the AC side of the railway system plays an important role.
- A simplified model with a voltage-current control curve plus an average efficiency coefficient, which may be used for systems without internal AC rings. This simplified approach allows the simulator to represent any control strategy implemented in the reversible converter. The voltage-current control curve is presented in Section 2.2.4.

In the case of the latter modelling approach, it must be noted that under this model simplification, the RS model coincides with the model of the charge process in the ESS model, as will be explained in Section 2.2.4.

2.2.4. ENERGY STORAGE SYSTEM MODEL

The Energy Storage Systems (ESSs) have become a hot topic for researchers in MTS electrification. They have three main uses: 1) they may increase the ability of the system to absorb regenerative braking, thus increasing the MTS energy efficiency; 2) they may be used to stabilise the catenary voltage in weak networks, avoiding hazardous (low) voltage levels; and 3) they may be used to reduce the peak power consumption in SSs, which under certain billing schemes can reduce the excessive power economic penalties.

A good survey from ESS historical uses to their current state-of-the-art in Japan may be found in (Konishi, Morimoto et al. 2010). This interesting study analyses the physical characteristics of the different technologies that may be used to store energy. The selection of the type of energy storage depends on the required power and energy densities for the particular application of the ESS. Figure 2-5 [Source: (Konishi, Morimoto et al. 2010)] shows the main applications of the current energy storage trends regarding their energy density (J/kg) and power density (W/kg).

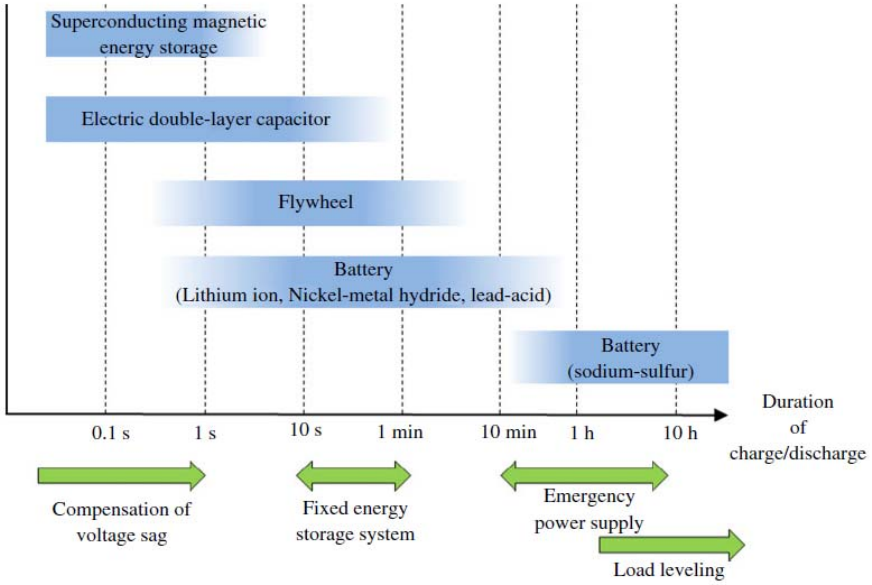

Figure 2-5. Main uses for the different storage technologies. Source: (Konishi, Morimoto et al. 2010)

Elements like the Electric Double Layer Capacitors (EDLCs), with high power density, have been used in important MTSs as Madrid Metro to stabilise the catenary voltage and to save energy (Siemens 2009). Other relevant studies as (Lee, Oh et al. 2008, Rufer, Hotellier et al. 2004) confirm the good performance of ESS for this application. Again their high power density, added to the easiness to determine their state of charge makes them suitable for on-board applications in light systems (tramways), as presented in studies like (Barrero, Mierlo et al. 2008, Barrero, Tackoen et al. 2008a). In this line, the work by (Arboleya, Coto et al. 2014) presents a detailed EDLC model for on-board applications. It must be noted that in tramway systems in certain cities, the application of on-board energy storage is fundamental to make it possible to remove the catenary system in historical zones (CAF 2016).

Regarding energy saving in fixed posts (trackside ESSs), the energy density requirements are higher. For this application, the EDLC energy density is slightly low. Other technologies as flywheels or batteries arise as good solutions. However, due to some practical problems, the former has just been applied a few times, and in experimental projects (Lafoz, Ugena et al. 2005).

Battery ESSs are the most extended for fixed-post energy saving applications. Specifically, the Li-Ion technology exhibits the best properties for its high energy density and life cycle (Umeda, Nobuhara et al. 2011, Nagaoka, Oue et al. 2006).

In most cases, the topology of ESSs follows the concept depicted in Figure 2-6. The conditioning converter is a bidirectional PWM converter devoted to the charge and discharge control. For storage technologies as EDLCs or batteries, the conditioning converter consists of an input filter and one or some cascaded DC-DC converters aimed at stepping the catenary voltage down to the storage element ratings. In both cases, this conditioning converter is also in charge of preventing the storage element from operating in hazardous conditions.

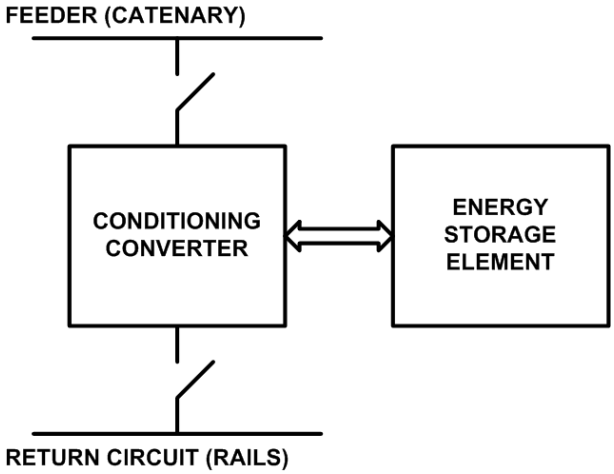

Figure 2-6. General structure of an ESS.

Once the general structure of ESSs is known, it is necessary to model the system efficiency and its control curve. With regard to the former, which is essential for energy saving studies, there are three main approaches in the related literature:

- First, there are studies which model efficiency in a simplified way by simply setting it to a constant value around the mean efficiency (Barrero, Tackoen et al. 2008a). Although simplified, this model may be enough when the number of scenarios analysed rises up.
- Second, there is a detailed modelling approach for ESS based on EDLCs. In this model, the internal resistance of EDLCs is used to derive the system efficiency (Domínguez, Fernandez-Cardador et al. 2012). Other studies also include the variable capacity effect that EDLC exhibit (Funaki 2010, del Toro Garcia, Roncero-Sanchez et al. 2010).
- Third, in battery based ESSs, detailed models include a law to determine the state of charge and the equivalent series resistance. This will limit the charge and discharge of the device under certain circumstances (Nagaoka, Oue et al. 2006).

With regard to the ESS control, the strategies to charge and discharge the storage device will depend on the type of use that the ESS is given: energy saving, voltage support or peak shaving. Again, the study by (Konishi, Morimoto et al. 2010) presents several options for the control curve of ESS, although it is pointed out that this is one of the important concerns to be improved in the close future.

Figure 2-7 presents the general structure used in for the ESS control curve. It may be represented by six parameters divided into two groups of three parameters for the charge and discharge process respectively. They are given in (2.6).

$$ESS_{PARAMS} = [V1_{chrg} \quad V2_{chrg} \quad IMAX_{chrg} \quad V1_{dis} \quad V2_{dis} \quad IMAX_{dis}] \tag{2.6}$$

Where

- $V1_{chrg}$ and $V2_{chrg}$ represent, respectively, the voltage threshold for the charge process and the voltage for the maximum allowed charge current.

- $IMAX_{chrg}$ is the maximum allowed current for the charge process.
- $V1_{dis}$ and $V2_{dis}$ represent, respectively, the voltage threshold for the discharge process and the voltage for the maximum allowed discharge current.
- $IMAX_{dis}$ is the maximum allowed current for the discharge process.

The values for the charge and discharge processes are not necessarily linked. In addition, these values are neither required to be constant, especially in the case of the voltage parameters. Regarding this, it is important to note that this flexible structure, with six degrees of freedom, allows the MTS operator to implement almost any control strategy. If the ESS main application is to save energy, it will be important to have enough room in the storage device for the energy generated by a braking event. This may be promoted by fixing high values to $V1_{dis}$, easing the discharge process. In the case of voltage stabilisation, it will be important to have enough energy stored in the ESS for supplying the traction power to neighbour trains. To prevent the system from being empty when these events take place, the ESS may be allowed to absorb energy in the standby voltage gap. The case of peak shaving is between voltage stabilisation and energy saving, and it is not as intensively studied as these cases.

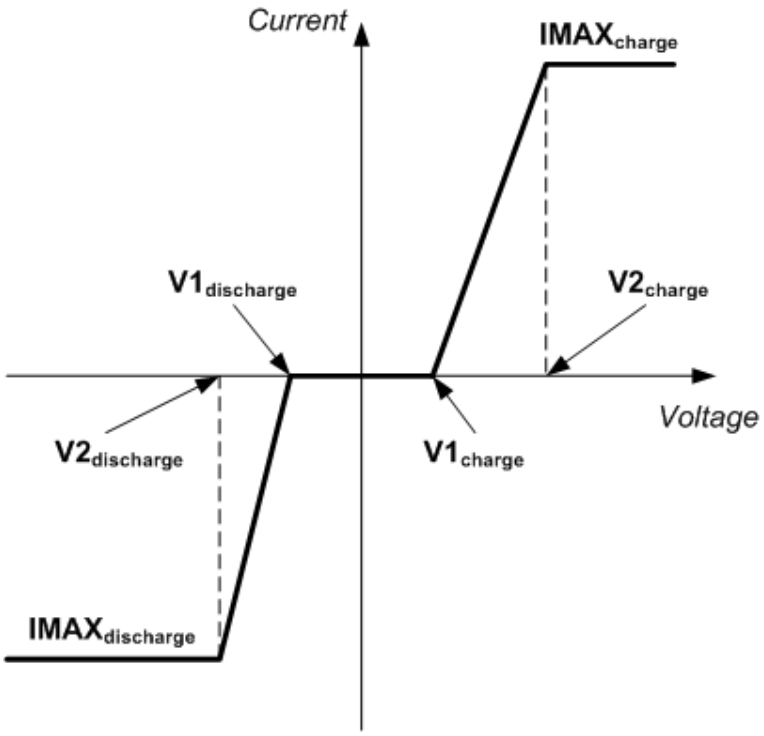

Figure 2-7. General ESS control curve.

Finally, it must be remarked that there may be other set of control rules –which are usually higher in the control hierarchy– devoted to prevent the storage device from being operated in ways that might shorten its life (Barrero, Tackoen et al. 2008a, Nagaoka, Oue et al. 2006).

The ESS model in the thesis

The ESS model in the simulator includes the six-parameter control curve in Figure 2-7. Regarding the ESS power efficiency, there are two options:

- A complex approach where the charge and discharge processes have variable efficiency. The values of this efficiency coefficient depend on the state of charge of the storage element and the power at the connection to catenary. This efficiency surface suits the EDLC ESS, where the currents in the storage element side of the system soar when the state of charge is low and the input (or output) power is high. The reason is that these elements exhibit a quasi linear relation between the state of charge and its terminal voltage. Figure 2-8 presents an example of this power efficiency surface for the charge process of a 2.5 kWh, 1 MW ESS.
- A simplified approach where the power efficiency of the converter is a fixed parameter with an average value (e.g.: 0.95). Although simplified, this is a good approach for strategic energy saving studies. In addition, the surface power efficiency approach is not likely to be a good ESS model for energy storage technologies which electrical behaviour differ from that of the EDLC.

As stated in Section 2.2.3, this latter modelling approach may be applied to RSs by simply disabling the discharge process. In energy saving studies for systems which do not present internal AC rings, this is a good-enough RS model.

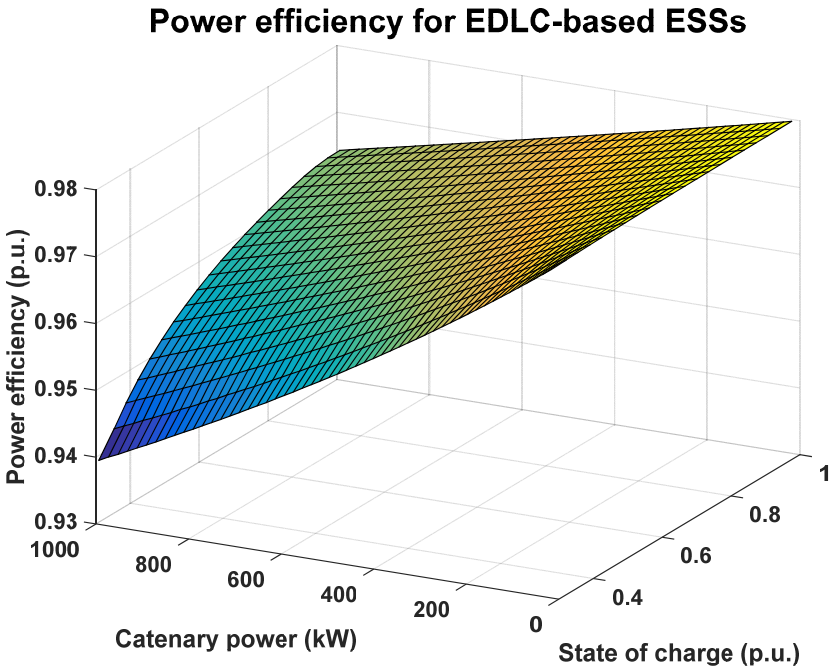

Figure 2-8. ESS power efficiency surface example. Charge process.

2.2.5. LOAD FLOW SOLUTION APPROACHES

To complete the electrical multi-train simulator, it is necessary to implement an algorithm which, integrating all the models already defined, is able to obtain the solutions for the electrical variables in the system, i.e., to solve the so called load flow

problem. This section performs a review of the literature related to the load-flow solution in traction systems.

It was stated in Section 2.2.1 that trains behave as non linear loads from an electrical standpoint. That applies both to the constant power model and to the voltage-dependent power model. That implies that the load flow solution is non linear as well (Cai, Irving et al. 1995a). Consequently, the solution of this problem must be obtained by the application of iterative methods.

The load flow problem in AC railway systems is completely analogous to that in power transportation and distribution networks. In this field, power engineers have thoroughly studied the possible solution methods for over a century, establishing the Newton-Raphson algorithm as the reference solution method (Grainger, Stevenson 1994).

In any case, it is possible to find alternative approaches for the solution of AC railway system load flows. A good example may be found in (Abrahamsson, Söder 2011), which analyses the heaviest achievable traffic densities in the Swedish rail system by means of a neural network based tool.

The load flow problem in DC railway systems is more complex. There are qualitative similarities with HVDC links in AC power systems, which have been a research concern since decades. However, as derived in Section 2.2.3, in systems like DC railways, where voltage and power ratings are low with respect to HVDC links, some of the modelling approaches for these systems are not applicable. The studies devoted to research on the solution of the load flow in DC traction systems are more recent. In addition, many authors set the focus on the DC side of the system (misrepresenting the AC side), which is solved with iterative methods based on linear approximations of the system (Chymera, Renfrew et al. 2010, Cai, Irving et al. 1995b, Mellitt, Goodman et al. 1978).

This approach is accurate for the DC side of the system. However, in the typical DC systems (MTSs), operators usually find several restrictions to connect the railway system to the utility grid. For this reason, it is becoming more and more common to install dedicated medium voltage AC rings (15-20 kV) to feed traction SSs when it is not possible to connect the MTS to the utility grid. The analysis of this kind of systems requires representing both sides of the railway system, and there are several examples of studies tackling this mixed AC-DC load flow in the literature.

In this context, it is possible to make a distinction between mixed AC-DC methods and iterative methods based on linear approximations of the system.

Mixed AC-DC methods

Within the mixed AD-DC methods, there are two clearly different approaches: sequential and unified strategies (Tzeng, Wu 1995):

- In the sequential methods, AC and DC systems equations are solved separately. These methods iterate until the terminal conditions of the interface elements between the AC and the DC sides (diode rectifiers, reversible substations, or both)

are satisfied. They are generally simple to implement and several control specifications can be easily adopted. (Pires, Nabeta et al. 2009) make use of a sequential method to solve the mixed AC-DC load flow problem. In this paper, it is argued that unified methods can suffer from slow convergence problems when introducing a detailed model of the return circuit in the DC traction network. This is due to the fact that the number of buses in the system becomes huge and the impedances between these buses span to a wide range of magnitudes. In the adopted solution, AC and DC side load flows are solved separately until the power in both sides of the interfaces are coherent. The power factor in converters is modelled as a constant value, which is likely to be a source of error regarding rectifier's reactive power consumption.

- In the unified methods, the AC and DC systems equations are combined together with the residual equations, describing the rectifier terminal behaviour. The result is a set of equations to be solved simultaneously. Unified methods present better computer efficiency and convergence features than the sequential methods, and so they seem more suitable for the use in industrial AC-DC systems. The work in (Tzeng, Wu 1995) performs a rigorous comparison between the three main methods that could be utilized to solve the unified AC-DC load flow problem. These are: the Gauss-Seidel (G-S), the Newton-Raphson (N-R), and the fast decoupled N-R methods. The G-S method presents a slow rate of convergence, especially when approaching the solution. Several hundreds of iterations are common for 1 % accuracy in 50-100 bus systems. The fast decoupled N-R method is based on the general relationships between 1) active power and angles, and 2) reactive power and voltage module. However, these relations do not totally exist in AC-DC power systems. In addition, the Jacobian matrix with the residual equations cannot be completely pre-inverted. Hence, the N-R method, with its powerful convergence features appears as the most suitable technique for solving mixed AC-DC load flows. (Arboleya, Diaz et al. 2012) is another good example of application of unified methods to solve the DC railway load flow. Apart from a rigorous and compact expression of the power equations, the main contribution of this study is the use of graph theory to model train movement, assisting the result interpretation stage.

In the electrical railway simulator developed in this thesis, the unified AC-DC approach has been adopted to solve mixed AC-DC load flows.

Iterative methods based on linear approximations

In this type of solutions, the AC network is tackled in a simplified way, usually as an infinite network; and rectifiers at electrical SSs are also modelled in a simplified way. The DC side of the system is solved by the application of the nodal admittance matrix, given in (2.7).

$$[G_{sys}] \cdot [V_{sys}] = [I_{sys}] \tag{2.7}$$

Where,

- G_{sys} is the nodal conductance matrix of the system. This is an *[n x n]* square matrix, being *n* the number of nodes in the system.
- V_{sys} is an *[n x 1]* vector containing the voltages of the nodes in the system.
- I_{sys} is an *[n x 1]* vector containing the currents of the nodes in the system.

(2.7) is a linear equation, and hence its simple inversion yields the voltage results for the nodes in the system. However, these results will make no sense until the nodal powers match the trains' power consumptions. Thus, these methods are implemented in an iterative fashion starting from a certain initial guess, and the stopping criteria are based on the train power mismatches.

(Cai, Irving et al. 1995a) proposes two methods for the solution of this problem:

- The matrix conductance method: the trains' conductance is adjusted by combining their power demands and their voltages in the previous iteration. Convergence is attained when the train power mismatch goes below the specified tolerance.
- The current vector method: these positions in I that represent a train are modified by combining trains' power demands and the voltages in the previous iteration.

The current vector method exhibits better convergence characteristics, but still not as powerful as the convergence characteristics of the N-R method. Nevertheless, there are recent studies that implement this type of techniques (Chymera, Renfrew et al. 2010, Barrero, Tackoen et al. 2008b, Destraz, Barrade et al. 2007).

Computer memory management

In most power systems, since they are not highly meshed, when the number of nodes grows, the admittance matrix exhibits a huge number of elements which are zero, i.e., it is a sparse matrix.

When such sparse matrices must be inverted, several problems may arise: memory consumption, accuracy or CPU time consumption. This is why many papers have dealt with this topic, developing or applying several different techniques for the sparse matrix management. In this review, the results shown are restricted to applications to traction systems.

(Cai, Irving et al. 1995b) applied three different techniques for solving a multi-ladder two-track DC railway study case. After the comparison of these three methods, it proposed the target Gauss elimination plus Zollenkopf's bi-factorization method as a powerful tool to manage the sparse matrix problem.

Then, in a more recent study, (Pires, Nabeta et al. 2007) studied the application of the Incomplete Cholesky Conjugate Method (ICCG) to solve the DC traction load flow including earthing models. This method is used to dramatically reduce the number of iterations for solving the problem.

Search for the system electrical topology

In the presentation of the rectifier and the train models, it was stated that these elements switch between two electrical models depending on certain variables. In the case of the rectifier, this element is only active when the voltage at the DC side is lower than a certain threshold. When it is higher, the rectifier becomes inactive, since it is not able to drive negative currents. In the case of the train, when its pantograph voltage reaches the rheostat voltage, it behaves as a voltage source.

Regarding this, it must be noted that in MTSs with several SSs, it is not straightforward to determine the electrical mode of every element subject to change. The exhaustive checkout of all the possible topologies is unmanageable. Therefore, this task is usually performed by means of a set of heuristic rules devoted to iteratively change the system topology until the correct one is found. Unfortunately, these rules are usually omitted in the presentation of the simulator in the literature.

The load flow solution method in this thesis

The simulator developed in this thesis implements a unified AC-DC load flow approach. The N-R method has been selected to iterate from an initial guess to the load flow solution.

The load flow solver has not presented remarkable memory problems in the range of system nodes managed in the energy saving studies developed in the frame of this thesis. Actually, the use of specialised sparse matrix management functions in Matlab has not shown to be effective in the habitual range of system nodes handled in this thesis (50 - 500).

Consequently, apart from a careful development and revision of the code, no special memory management measures have been taken. It must be noted that the current machines where simulations are carried out are more powerful than those used in (Pires, Nabeta et al. 2007, Cai, Irving et al. 1995a).

Finally, the heuristic rules to find the system topology are presented in Sections 2.3.2.2 and 2.4.1.1.

2.3. IMPLEMENTATION DETAILS OF THE SIMULATOR

This section presents the details of the electrical multi-train simulator developed in the frame of this thesis, i.e., the integration of the models of the different elements in a DC railway system into an electrical multi-train simulator.

It must be noted that the simulator developed in this thesis is mainly aimed at energy efficiency studies. Therefore, all the modelling decisions have been made to properly represent energy issues. As a result, the electrical multi-train simulator developed makes it possible to obtain valid results, similar to other simulators independently developed. Indeed, its results have been compared to those obtained with another electrical railway simulator developed in the Sapienza University, Rome, Italy (Falvo, Sbordone et al. 2014).

The simulator has been designed to make it possible to analyze AC-, DC-electrified and mixed railway systems regardless their topological complexity (branches, isolated zones, etc.). Regarding this, although the simulator is able to process AC electrified railway systems, due to the special interest of DC electrified MTS from the thesis objective standpoint, the simulator details given will be restricted to this latter kind of system.

Figure 2-9 represents the Gane and Sarson data flow diagram of the simulator (Gane, Sarson 1979). In this kind of diagrams, shaded boxes represent interfaces with the user, normal boxes stand for active processes which may retrieve, process and save data; and open boxes represent passive blocks in which data may be permanently or temporarily stored.

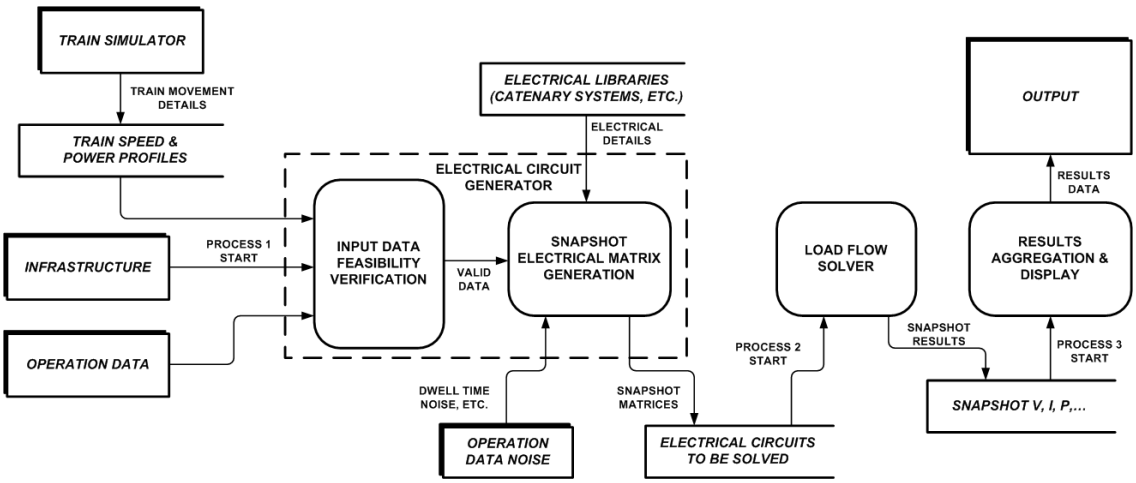

Figure 2-9. Electric railway simulator Gane & Sarson data flow diagram

The simulator consists of three cascaded processes: 1) the electrical circuit generator, 2) the load flow solver, and 3) the result aggregator.

2.3.1. THE ELECTRICAL CIRCUIT GENERATOR

As trains in the electric railway system move, therefore changing their positions and power consumptions, the electrical circuit to be solved for the system analysis changes accordingly. This first block of the simulator is in charge of the generation of these time-variant electrical circuits to represent the railway system. To do that, it makes use of the dwell time information included in the operation data to compose the movement and power consumption of each single train. Then, the headway information is used to generate the train circulation schedule and its associated power demands. It must be noted that the simulator allows the user to include variations (noise) in the operation data.

The result of this process is a set of 'snapshots' representing the evolution of the system in the period of time to be simulated. The electrical circuit generator block has been implemented in Visual Basic for Applications (VBA) and Excel. The core of this part of the simulator was already developed at the beginning of this thesis. However, several developments have been included in this code in the frame of this thesis, being the most important: the inclusion of ESSs, the generalisation of the timetable generation to include the possibility of representing stochastic dwell times; and, of course, the refinement and debugging of the VBA code.

2.3.1.1. DATA ACQUISITION

The electrical circuit generator collects the information about the system to be simulated, which must be introduced by the user in a set of Excel sheets. This information may be broken down into: 1) infrastructure data, 2) train movement and power profiles and 3) traffic operation data (timetable).

Figure 2-10 presents the main infrastructure elements included in the simulator's representation of MTSs:

- **Utility grid**: There are several approaches to represent the utility grid, depending on the degree of detail of this network. Generally, from the MTS standpoint, it could be enough to represent it by a simple infinite network which feeds all the SSs with connection to this grid. Nevertheless, the simulator allows the representation of different utility grid voltages, which could be an interesting object of study.
- **Medium-voltage AC rings**: Internal grids laid by the MTS operator may be introduced in the model.
- **Connection topology**: The simulator allows the definition of switches which states may be modified for the simulation of different system topologies. This may be especially useful for degraded condition operation studies.
- **Substation transformer**: Different types of substation transformers for 6 or 12 pulse rectifiers are available.
- **Diode rectifiers**: They are the most common type of SS rectifier in actual systems. Different types of rectifiers may be included in the model (6, 12 pulse rectifiers, etc.)

- **Substation feeder**: The number and position of the connections between the substation bus bars and the catenary system may be easily introduced to accurately represent the system's topology.
- **Catenary system**: Regarding this, the simulator allows the user to introduce any kind of catenary topology, including paralleling bonds between track catenaries, branches, rigid or conventional catenary, etc.
- **Reversible converters and ESS**: The simulator allows introducing any kind of RS and ESS configuration. The latter are not restricted to SS locations, but they can be placed at any point in the tracks, as happens in actual systems.

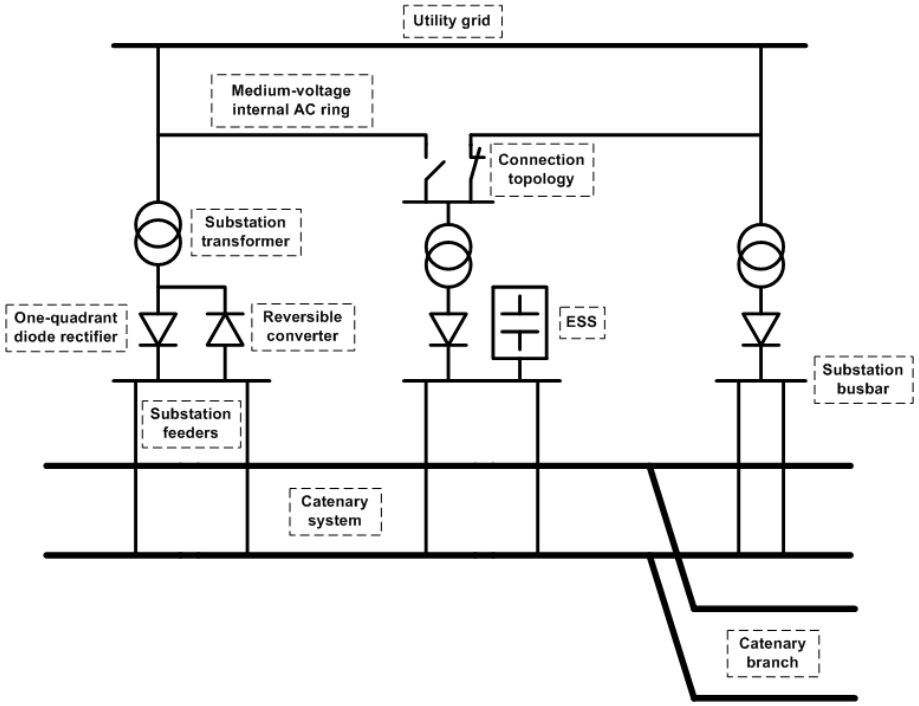

Figure 2-10. Infrastructure elements included in the electrical multi-train simulator.

The user of the simulator is in charge of properly determining the connections between the different elements in the infrastructure, the nominal voltages of the different electrical zones, the characteristics of the devices in the substations, etc.

Once the infrastructure details are available, it is required to know the speed and power consumption details of the trains' movements between passenger stations. For the studies in this thesis, these data are generated off-line by means of an IIT-built train simulator. This simulator has proved to generate different kinds of speed profiles with a high degree of accuracy (Dominguez, Fernandez et al. 2011).

The input to the electrical multi-train simulator is a matrix which columns represent train's position, time, power and speed. Motoring trains are expressed by powers greater than zero, whereas negative powers represent the maximum power to be injected in the catenary system. These powers already include the auxiliary power consumption. The rows represent movement samples, which must be given at a fixed sampling time.

Once known the infrastructure and train movement details, these data must be combined to generate the traffic in the system. Thus, the only information left is the operation information. Regarding these operation details, the simulator allows representing any kind of traffic timetable. To do this, the simulator's interface provides a timetable sheet where the speed profiles between stations are combined. Figure 2-11 shows an example of this timetable interface for one of the tracks in a six-station line. For the case of a double-track line, the interface for the other track would be analogous. The interface allows setting the headway and the departure time of the first train in the track as independent variables. The latter makes it possible to freely shift the trains in this track with others in different tracks of the system. The dwell times at stations are also independent variables. This allows representing the traffic in a line under uncertain conditions.

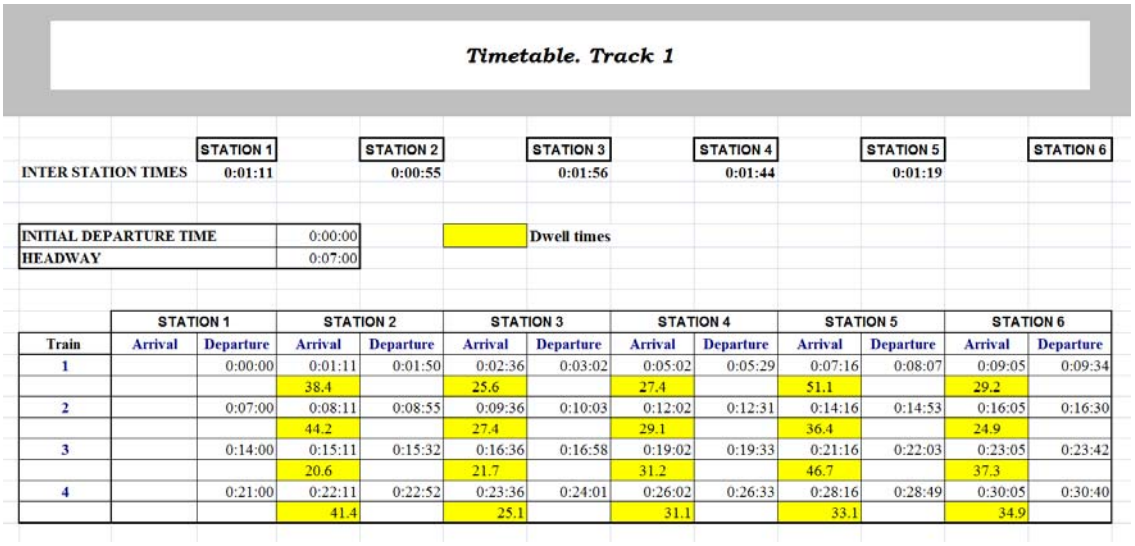

Timetable. Track 1

	STATION 1	STATION 2	STATION 3	STATION 4	STATION 5	STATION 6
INTER STATION TIMES	0:01:11	0:00:55	0:01:56	0:01:44	0:01:19	

INITIAL DEPARTURE TIME	0:00:00
HEADWAY	0:07:00

Dwell times

	STATION 1		STATION 2		STATION 3		STATION 4		STATION 5		STATION 6	
Train	Arrival	Departure	Arrival	Departure	Arrival	Departure	Arrival	Departure	Arrival	Departure	Arrival	Departure
1		0:00:00	0:01:11	0:01:50	0:02:36	0:03:02	0:05:02	0:05:29	0:07:16	0:08:07	0:09:05	0:09:34
			38.4		25.6		27.4		51.1		29.2	
2		0:07:00	0:08:11	0:08:55	0:09:36	0:10:03	0:12:02	0:12:31	0:14:16	0:14:53	0:16:05	0:16:30
			44.2		27.4		29.1		36.4		24.9	
3		0:14:00	0:15:11	0:15:32	0:16:36	0:16:58	0:19:02	0:19:33	0:21:16	0:22:03	0:23:05	0:23:42
			20.6		21.7		31.2		46.7		37.3	
4		0:21:00	0:22:11	0:22:52	0:23:36	0:24:01	0:26:02	0:26:33	0:28:16	0:28:49	0:30:05	0:30:40
			41.4		25.1		31.1		33.1		34.9	

Figure 2-11. Simulator's timetable interface.

The input data are finally completed by a set of simulation options, being the simulation start and final times and the time sampling rate the most relevant ones.

2.3.1.2. GENERATION OF THE SNAPSHOT FILES

Figure 2-12 presents the workflow of the electrical circuit generator. Prior to the snapshot generation, there is a process in charge of verifying that the data introduced by the simulator user are valid. If the proposed infrastructure and operation are electrically feasible (no sections are electrically isolated, trains are inside the system, etc.), the electrical circuit generation process is started.

The circuit generation process starts by acquiring all the data entered in the dedicated interface sheets. These data are arranged into *train service* objects which are contained by a *schedule* object that also contains the infrastructure connection details, operation details, start and final times, sampling time, etc.

This information is used to calculate the evolution of the trains' positions and power consumption or regeneration along time, at the specified sampling rate. The result is also stored in this *schedule* object.

Then, a *circuit* object is used to generate the electrical circuits that will be output for the load flow solver stage. Prior to entering the time-instant simulation-loop, the circuit containing the fixed infrastructure connections is generated. This circuit is common to all the snapshots.

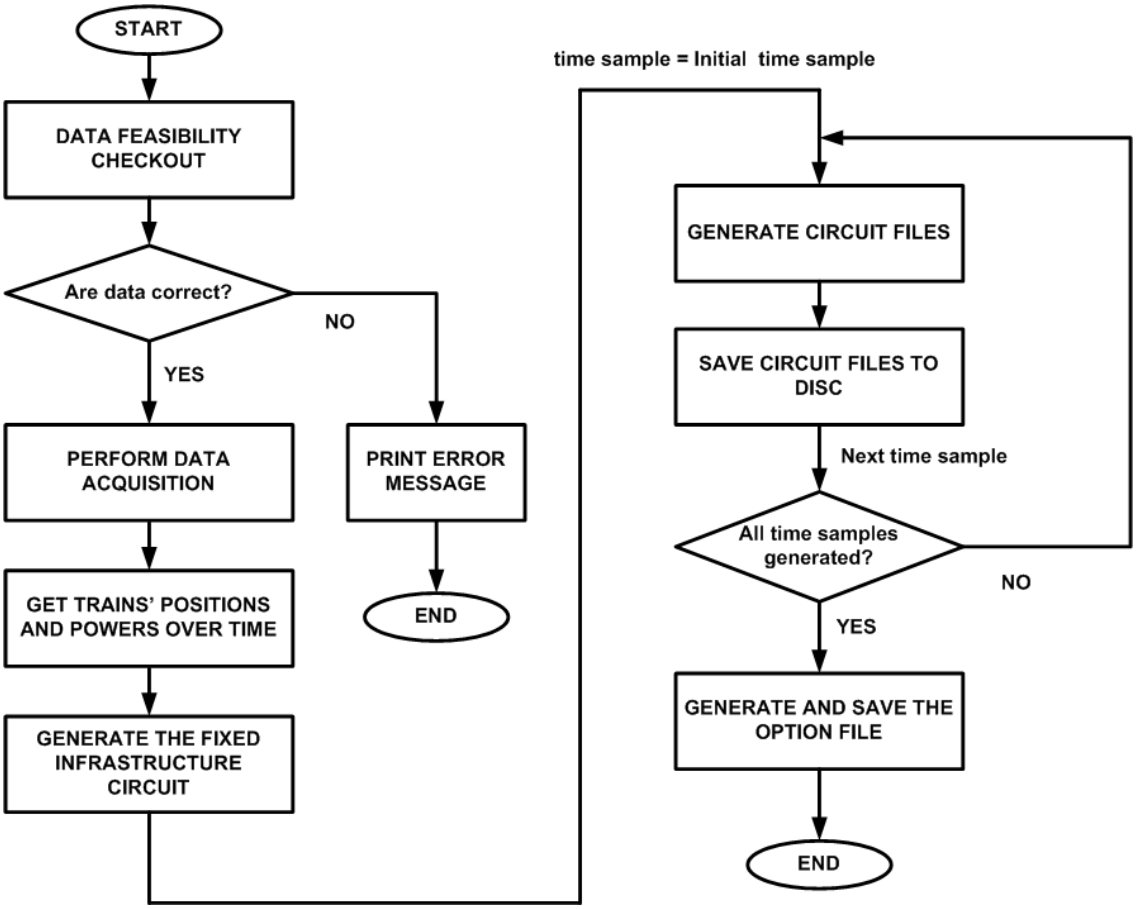

Figure 2-12. Snapshot generation workflow.

After this, the generation process enters a loop where the trains for each particular time instant are added to the fixed infrastructure circuit. When this task is performed, three files are saved in a folder specified by the user: 'AC_XXXX.m', 'DC_XXXX.m', 'RECT_XXXX.m'. These files contain the information about the AC and DC sides of the system and the rectifier stations, respectively. They are generated in m-file format, compatible with Matlab. The loop is repeated until the final simulation time sample is reached.

When this happens, the process generates a further file named 'Options.m' with additional information to guide the load flow solve process, and it is terminated.

2.3.2. THE LOAD FLOW SOLVER

The load flow solver represents the core of the electrical multi-train simulator developed in this thesis. This process solves the non linear load flow problem for all the circuits generated by the electrical circuit generator. At the beginning of this thesis, the load flow solver was in an early stage. It was able to solve both AC and DC

circuits, but its robustness and time performance characteristics were still subject to be improved. The current version of the load flow solver is an improved version of that one.

2.3.2.1. THE LOAD FLOW PROBLEM IN DC-ELECTRIFIED MTSS.

As stated in Section 2.2.1, trains behave as non linear loads. Thus, the obtainment of the node voltages in a railway system consists in a non linear problem, which must be solved by applying iterative methods. This is usually referred to as the load flow problem, and it represents an intensively studied topic in power-system analysis (Grainger, Stevenson 1994).

Although the positions and magnitudes of the load in a railway system are time-variant, it is accepted that these changes are slow enough to neglect the electrical transients in the system (see Section 2.2.2.1). Therefore, the analysis of the power system in MTS is always performed by the concatenation of a series of static load flows.

The application of the load flow solving techniques to DC-electrified railway lines must take into account the particularities of these systems. Figure 2-13 shows the electrical model used to represent a given load configuration, already in per unit magnitudes. The rectifiers separate the AC and the DC sides in the system. There are four qualitatively different kinds of node. Following the node number reference in the right side graph in Figure 2-13:

- Pure AC nodes: 1 – 3.
- Terminal AC nodes (AC nodes in rectifiers): 4 and 5.
- Terminal DC nodes (DC nodes in rectifiers): 6 and 7.
- Pure DC nodes: 8 – 11.

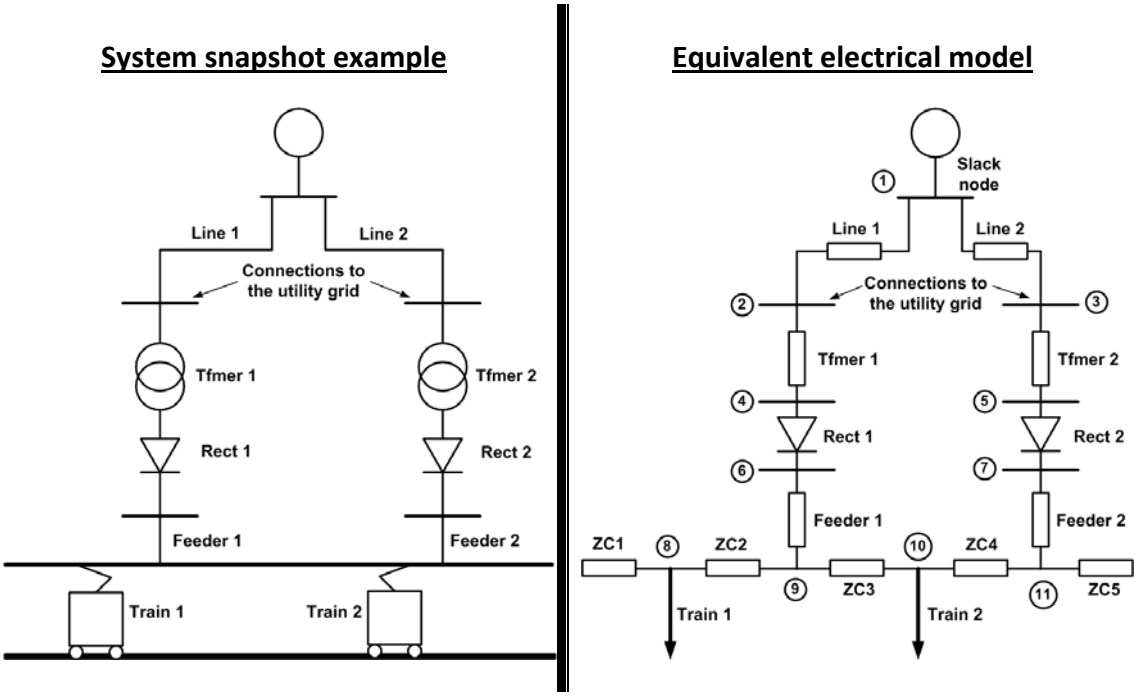

Figure 2-13. Example of train loads in a DC railway system and equivalent electrical model.

AC nodes, including the terminal ones, are characterised by two state variables: their voltage module and angle. Within the pure AC nodes, one of them must be defined as the slack node, used as the reference voltage value. In the per unit magnitude system, its voltage value is generally set to 1 and its angle to 0. Then, the state variables of the rest of pure AC nodes must be obtained from their power equations.

The power equations of the AC nodes in the system may be obtained from Y –the admittance matrix of the system– and the node voltages. Y represents the connections between the nodes in the system. The expressions for a typical element in Y (Y_{ij}) and the node voltage (Vac_i) are given in (2.8) and (2.9). All the equations in this section are expressed in p.u. magnitudes.

$$Y_{ij} = |Y_{ij}| \measuredangle \theta_{ij} = Gac_{ij} + jBac_{ij} \tag{2.8}$$

$$Vac_i = |Vac_i| \measuredangle \delta_i \tag{2.9}$$

The expressions of the AC node active and reactive power equations for the i^{th} node in the system are presented in (2.10) and (2.11).

$$P\_AC_i = \sum_{n=1}^{N} |Y_{in} Vac_i Vac_n| \cos(\theta_{in} + \delta_n - \delta_i) \tag{2.10}$$

$$Q\_AC_i = -\sum_{n=1}^{N} |Y_{in} Vac_i Vac_n| \sin(\theta_{in} + \delta_n - \delta_i) \tag{2.11}$$

Where,

- P_AC_i is the scheduled active power in node *i*.
- Q_AC_i is the scheduled reactive power in node *i*.
- N is the number of AC nodes in the system, including the terminal ones.

In the example in Figure 2-13, there are no power demands in the AC side of the system, so the active and reactive power demand in nodes 2 and 3 is consequently 0.

The power equations of both AC and DC terminal nodes are affected by the rectifier AC-DC conversion. As stated in Section 2.2.3, the detailed rectifier model presented by (Tzeng, Wu 1995) has been implemented in the simulator. For the sake of clarity, some details of the model are omitted. For further information about this rectifier model, the reader is invited to visit the original article by (Tzeng, Wu 1995).

The rectifier link between the AC and DC terminal nodes modifies their power equations. The AC terminal node power equations for the rectifier *r*, connecting the AC node *i* and the DC node *j*, are given in (2.12) and (2.13).

$$P\_ACterm_i = \left(\sum_{n=1}^{N} |Y_{rn} Vac\_term_i Vac_n| \cos(\theta_{rn} + \delta_n - \delta term_i)\right) + \frac{3|Vac\_term_i|^2}{4\pi X_{C,r}} \cos\xi_r \, A_{REC}(\alpha_r, \mu_r, \lambda_r) + \frac{|Vac\_term_i| Idc_r}{2} B_{REC}(\alpha_r, \mu_r, \lambda_r) \quad (2.12)$$

$$Q\_ACterm_i = -\left(\sum_{n=1}^{N} |Y_{rn} Vac\_term_i Vac_n| \sin(\theta_{rn} + \delta_n - \delta term_i)\right) + \frac{3|Vac\_term_i|^2}{4\pi X_{C,r}} \cos\xi_r \, C_{REC}(\alpha_r, \mu_r, \lambda_r) + \frac{|Vac\_term_i| Idc_r}{2} D_{REC}(\alpha_r, \mu_r, \lambda_r) \quad (2.13)$$

Where,

- P_ACterm_i is the active power demanded in the terminal node *i*.
- Q_ACterm_i is the reactive power demanded in the terminal node *i*.
- $X_{C,r}$ is the reactance seen by the AC terminal of the rectifier *r*.
- $\lambda_r = \frac{R_{C,r}}{X_{C,r}}$ is the resistance to reactance ratio of the impedance seen by the AC terminal of the rectifier *r*, which is mainly the SS transformer impedance.
- $\xi_r = \tan^{-1}\lambda_r$
- Idc_r is the current in the DC terminal of the rectifier.
- α_r, μ_r are the ignition and the commutation overlap angles of the rectifier *r*. In the diode rectifier case, they are uncontrolled variables.
- $A_{REC}, B_{REC}, C_{REC}, D_{REC}$ are four coefficients which depend on the ignition and overlap angles and the resistance to reactance ratio seen by the transformer. They are obtained from the Fourier expansion of the AC line current waveform used in the model by (Tzeng, Wu 1995). Their expressions, for the rectifier *r*, are given in (2.14) – (2.17).

$$A_{REC}(\alpha_r, \mu_r, \lambda_r) = 2\mu_r \sin\xi_r + \cos(\xi_r + 2\alpha_r + 2\mu_r) - \cos(\xi_r + 2\alpha_r) - 4\cos\xi_r \cos(\xi_r + \alpha_r)\left[e^{-\lambda_r\mu_r}\cos(\xi_r - \alpha_r - \mu_r) - \cos(\xi_r - \alpha_r)\right] \quad (2.14)$$

$$B_{REC}(\alpha_r, \mu_r, \lambda_r) = \cos\xi_r\left[e^{-\lambda_r\mu_r}\cos(\xi_r - \alpha_r - \mu_r) - \cos(\xi_r - \alpha_r)\right] + \cos(\alpha_r + \mu_r) + \cos\alpha_r \quad (2.15)$$

$$C_{REC}(\alpha_r, \mu_r, \lambda_r) = 2\mu_r \cos\xi_r + \sin(\xi_r + 2\alpha_r + 2\mu_r) - \sin(\xi_r + 2\alpha_r) + 4\cos\xi_r \cos(\xi_r + \alpha_r)\left[e^{-\lambda_r\mu_r}\sin(\xi_r - \alpha_r - \mu_r) - \sin(\xi_r - \alpha_r)\right] \quad (2.16)$$

$$D_{REC}(\alpha_r, \mu_r, \lambda_r) = -\cos\xi_r\left[e^{-\lambda_r\mu_r}\sin(\xi_r - \alpha_r - \mu_r) - \sin(\xi_r - \alpha_r)\right] + \sin(\alpha_r + \mu_r) + \sin\alpha_r \quad (2.17)$$

Then, the power equation for the DC terminal of the rectifier *r* is presented in (2.18). The only state variable for a DC node is its voltage.

$$P\_DCterm_j = -Vdc\_term_j Idc_r + \sum_{m=1}^{M} Gdc_{jm} Vdc\_term_j Vdc_m \tag{2.18}$$

Where,

- P_DCterm_j is the scheduled active power in the terminal node *j*.
- M is the number of DC nodes in the system, including the terminal ones

In addition to the terminal-node state variables, each rectifier is defined by three state variables: α_r, μ_r and Idc_r, as can be observed in equations (2.12), (2.13) and (2.18). Therefore, three additional equations representing the rectifier model are required to obtain the solution of the system load flow. These are not explicitly forced to be a specific set of equations. Again, the ones proposed by (Tzeng, Wu 1995) have been adopted in this thesis. They are presented in (2.19), (2.21) and (2.22).

$$\gamma_r \cdot \left(Vdc_j - \frac{|Vac_i|}{2} [\cos \alpha_r + \cos(\alpha_r + \mu_r)] + \frac{\pi^2}{18} \left(2 - \frac{3\mu_r}{2\pi}\right) R_{C,r} Idc_r \right) = 0 \tag{2.19}$$

$$\gamma_r = \begin{cases} 1 & if \quad Idc_r > 0 \\ 0 & if \quad Idc_r = 0 \end{cases} \tag{2.20}$$

$$Idc_r - \frac{6|Vac_i|}{\pi X_{C,r}(1 + e^{-\lambda_r \mu_r})} \cos \xi_r \left[e^{-\lambda_r \mu_r} \cos(\xi_r + \alpha_r) - \cos(\xi_r + \alpha_r + \mu_r) \right] = 0 \tag{2.21}$$

$$\alpha_r + \sin^{-1}\left(\frac{\pi R_{C,r} Idc_r}{6|Vac_i|}\right) = 0 \tag{2.22}$$

$$Idc_r, \alpha_r, \mu_r \geq 0 \tag{2.23}$$

Where γ_r is a binary variable for diode rectifiers that becomes 0 when the rectifier is inactive. It represents that in the *OFF* mode, there is not an effective link between the AC- and the DC-bar voltages, and therefore, equation (2.19) must not be fulfilled. When the SS includes a reversible converter, γ_r may also become -1 to control the reversible power flow case. It must be noted that, taking (2.23) into account, equations (2.21) and (2.22) are both applicable to rectifier *ON* and *OFF* modes.

Finally, the power equations required to obtain the voltages of the pure DC nodes, including trains, is given in (2.24).

$$P\_DC_j - P\_Rh_j = \sum_{m=1}^{M} Gdc_{jm} Vdc_j Vdc_m \tag{2.24}$$

$$P\_Rh_j \leq P\_DC_j \cdot (1 - \lambda_j) \tag{2.25}$$

$$P_{Rh_j} \geq 0 \tag{2.26}$$

$$\lambda_j = \begin{cases} 1 & if \quad Vdc_j < V\_Rh \\ 0 & if \quad Vdc_j = V\_Rh \end{cases} \tag{2.27}$$

$$Vdc_j \leq V\_Rh \tag{2.28}$$

Where,

- P_DC_j is the scheduled power in the DC node *j*. It will be non null in the nodes that represent trains. Specifically, positive values correspond to a net regeneration in trains (braking) and negative values to a net demand (motoring trains or braking trains regenerating less than their auxiliary consumption).
- λ_j is a binary variable that becomes 0 when the voltage in node *j* hits the maximum voltage allowed, i.e. the rheostat voltage level. In other words, λ_j becomes 0 when the train at node *j* enters rheostat-braking mode.
- P_Rh_j is the power sent to rheostats. It will only be non null at braking trains, and in case pantograph voltage reaches the rheostat voltage level. When this event takes place, the node *j* becomes a voltage source to represent the effect of the train's on-board chopper. This converter clamps the pantograph voltage to prevent the train from unfulfilling the system maximum-voltage rules. In this case, P_Rh_j plays the role of a slack variable that makes it possible to fulfil the system power-balance equations. When this variable is allowed to be non-null ($\lambda_j = 0$), it must be lower than the power regenerated at node j.
- V_Rh is the rheostat voltage level.

The addition of RSs to the system is carried out by implementing the model in (Tzeng, Wu et al. 1998). In this case, the reversible converter which links the DC side of the system to the AC one, allowing reverse current flows, must be a controlled device. These devices present the same AC and DC terminal equations, but the converter state variables and residual equations are changed. The constant advance angle control ($\pi - \alpha$) strategy presented in (Tzeng, Wu et al. 1998) has been included in the thesis simulator.

In the case of ESSs, the DC terminal voltage equation is modified by introducing the power consumption or generation correspondent to the ESS voltage-power curve (see Figure 2-7). It must be noted that this power is not an independent variable, but it is influenced by the DC terminal voltage.

The power-balance and rectifier equations presented so far define a system of equations that makes it possible to obtain the solution for the electrical variables of the system. However, as already stated, this is a non linear set of equations that requires to be solved with iterative methods. In this thesis, provided its optimum convergence properties, the N-R method has been selected to solve the system's state equations.

The Newton-Raphson method

The N-R is the reference method in the load flow analysis of AC power systems. It is a general solution method for non linear systems of equations, which is based on the Taylor series expansion of multi-variable functions. The presentation of the N-R method in this section does not aim to be intensive. The reader is invited to visit any power system analysis reference as (Grainger, Stevenson 1994) for further details on the method.

The N-R method obtains the solution of the system equations from an initial guess of the state variables. In general, this initial guess will not fulfil the system equations. The mismatch between the actual scheduled powers in the nodes and the values obtained with the guess is used, together with the Jacobian matrix of the system equations, to obtain a new guess for the state variables. This process is applied iteratively until the mismatch values fall below a predetermined tolerance threshold. The mathematical expression of this process for the iteration a, is given in (2.29) – (2.30).

$$J^{(a)} \cdot \Delta \boldsymbol{X}^{(a)} = \boldsymbol{Mm}^{(a)} \Rightarrow \Delta \boldsymbol{X}^{(a)} = \left[J^{(a)}\right]^{-\mathbf{1}} \cdot \boldsymbol{Mm}^{(a)} \tag{2.29}$$

$$\boldsymbol{X}^{(a+1)} = \boldsymbol{X}^{(a)} + \Delta \boldsymbol{X}^{(a)} \tag{2.30}$$

Where,

- $\boldsymbol{X}^{(a)}$ and $\Delta \boldsymbol{X}^{(a)}$ are the vector containing the guess for the system state variables in iteration *a* and the state variable increase, respectively.
- $J^{(a)}$ is the Jacobian matrix, particularised for the guess of the state variables in iteration *a*.
- $\boldsymbol{Mm}^{(a)}$ is a vector which contains the mismatches of the system equations for the guess of the state variables in iteration *a*.

In the application to the mixed AC - DC railway system problem, the vector $\boldsymbol{X}$ must be particularised to the state variables already presented in this section, and listed in (2.31) – (2.32).

$$\boldsymbol{X} = [\boldsymbol{\delta} \quad |\boldsymbol{Vac}| \quad \boldsymbol{\delta term} \quad |\boldsymbol{Vac\_term}| \quad \boldsymbol{Rect} \cdot \boldsymbol{\Gamma} \quad \boldsymbol{Vdc\_term} \quad \boldsymbol{Vdc} \cdot \boldsymbol{\Lambda}]^{T} \tag{2.31}$$

$$\boldsymbol{Rect} = [\boldsymbol{Rect_1} \quad \dots \quad \boldsymbol{Rect_{nRect}}] \; ; \; \boldsymbol{Rect_r} = [\alpha_r \quad \mu_r \quad Idc_r] \tag{2.32}$$

$$\boldsymbol{\Gamma} = \begin{bmatrix} \overline{\boldsymbol{\gamma}}_{\mathbf{1}} & \dots & 0 \\ \vdots & \ddots & \vdots \\ 0 & \dots & \overline{\boldsymbol{\gamma}}_{\boldsymbol{nRect}} \end{bmatrix} \tag{2.33}$$

$$\overline{\boldsymbol{\gamma}}_{\mathbf{1}} = \begin{bmatrix} \gamma_1 & 0 & 0 \\ 0 & \gamma_1 & 0 \\ 0 & 0 & \gamma_1 \end{bmatrix}, \dots, \overline{\boldsymbol{\gamma}}_{\boldsymbol{nRect}} = \begin{bmatrix} \gamma_{nRect} & 0 & 0 \\ 0 & \gamma_{nRect} & 0 \\ 0 & 0 & \gamma_{nRect} \end{bmatrix} \tag{2.34}$$

$$\boldsymbol{\Lambda} = \begin{bmatrix} \lambda_1 & \dots & 0 \\ \vdots & \ddots & \vdots \\ 0 & \dots & \lambda_{nDCNodes} \end{bmatrix} \tag{2.35}$$

Where,

- $\boldsymbol{X}$ is the state vector, containing the state variables in the system. As it will be explained, the number of state variables is not fixed, and it depends on the states of the controlled and uncontrolled active elements in the system.
- $\boldsymbol{Rect}$ contains the rectifier state variables. The example for rectifier *r* is given.
- $nRect$ is the number of rectifiers in the system.
- $\boldsymbol{\Gamma}$ is a diagonal control matrix containing the states of the rectifiers, defined in (2.20). It may be observed in (2.31) that the null elements in this matrix remove the state variables of the *OFF* rectifiers from the state vector.
- $\boldsymbol{\Lambda}$ is a diagonal control matrix containing the states of the trains, defined in (2.27). The elements in this matrix may only be 0 for braking trains, when they enter rheostat-braking mode. The voltage in rheostat trains is known, and it equals the rheostat voltage level. It may be observed in (2.31) that the voltages of rheostat trains are removed from the state vector by the null elements in $\boldsymbol{\Lambda}$.
- $nDCNodes$ is the number of pure DC nodes in the system. Obviously, the values of λ for these nodes which do not represent trains will be 1.

Other exceptions in the state vector are:

- The slack node, which is used as the reference node. Its voltage module is set to 1 p.u. and its angle to 0°. In the example of Figure 2-13, the node 1 would be the slack bus.
- Any node in the AC side that behaves as a voltage controlled bar must be removed from $|\boldsymbol{Vac}|$. In addition, its reactive power is determined by the rest of the circuit, and therefore this equation must be removed from the system equations. In the simulation of DC electrified railway systems, this kind of nodes is not usual.

Then, the Jacobian matrix is obtained by calculating the partial derivatives of the system equations [(2.10) – (2.11), (2.19) – (2.24)] with respect to the state variables. Although there are techniques to skip updating the Jacobian matrix in certain iterations, in general, the values of the elements in this matrix must be calculated iteration by iteration by particularising the partial derivative expressions to the values of the state variable guess.

The system equations have been arranged in a vector in (2.36). The general expression of the Jacobian matrix and some examples of its elements are given in (2.37) and (2.38).

$$\boldsymbol{Eqs} = [\boldsymbol{Pac} \quad \boldsymbol{Qac} \quad \boldsymbol{Pacterm} \quad \boldsymbol{Qacterm} \quad \boldsymbol{R}\cdot\boldsymbol{\Gamma} \quad \boldsymbol{Pdcterm} \quad \boldsymbol{Pdc}\cdot\boldsymbol{\Lambda}]^{\mathrm{T}} \tag{2.36}$$

$$J = \begin{bmatrix} J_{11} & \cdots & J_{17} \\ \vdots & \ddots & \vdots \\ J_{71} & \cdots & J_{77} \end{bmatrix} \tag{2.37}$$

$$J_{11} = \frac{\partial Pac}{\partial \delta}; J_{21} = \frac{\partial Pac}{\partial |Vac|}|Vac|; \ldots; J_{43} = \frac{\partial Qterm}{\partial \delta term}; \ldots; J_{77} = \frac{\partial Pdc}{\partial |Vdc|}|Vdc| \tag{2.38}$$

Where,

- $\boldsymbol{Pac}$ represents the vector of active power-balance equations for pure AC nodes, defined in (2.10).
- $\boldsymbol{Qac}$ represents the vector of reactive power-balance equations for pure AC nodes, defined in (2.11).
- $\boldsymbol{Pacterm}$ represents the vector of active power-balance equations for rectifier AC terminal nodes, defined in (2.12).
- $\boldsymbol{Qacterm}$ represents the vector of reactive power-balance equations for rectifier AC terminal nodes, defined in (2.13).
- $\boldsymbol{R}$ represents the vector of residual equations of the rectifiers [(2.19), (2.21) and (2.22)]. This is again modulated by $\boldsymbol{\Gamma}$, which means that the *OFF*-rectifier equations are removed from the system.
- $\boldsymbol{Pdcterm}$ represents the vector of power-balance equations for rectifier DC terminal nodes, defined in (2.18).
- $\boldsymbol{Pdc}$ represents the vector of power-balance equations for pure DC nodes, defined in (2.24). This vector is controlled by $\boldsymbol{\Lambda}$. That means that the equations for rheostat-braking trains, which voltage is known, are removed from the system.

With the equations presented in this section and the N-R algorithm application to mixed AC-DC railway systems, it is possible to simulate the behaviour of MTSs from an electrical point of view. However, there are a number of practical problems in the implementation of the N-R algorithm to these systems.

First, it has been stated that that there are elements in the system which may change their state under certain circumstances (mainly trains in rheostat-braking mode and cut-off rectifiers). This is dealt with by means of the control variables included in $\boldsymbol{\Gamma}$ and $\boldsymbol{\Lambda}$. However, the correct combination of these control variables is not known a priori, and neither straightforward to determine. The number of possible combinations for the control variables is huge, and thus they may not be checked exhaustively. Consequently, the load flow solver must search for the correct combination iteratively. In the practical solution of the load flow, some iterations of the N-R algorithm will obtain results which do not fulfil the physical restrictions of the system. These wrong solutions must be discarded, and the topology of the system changed (e.g.: remove SSs, set trains to node voltages, etc.).

Then, the DC railway equations are far from representing a convex problem. Therefore, a large change in the state variables, or even a wrong initial guess could lead to local minima problems, i.e., the N-R method would converge to a solution with non-null mismatch.

Section 2.3.2.2 presents the way in which these problems have been tackled in the simulator's implementation.

Table 2-1. Example of the equations and state variables for the circuit in Figure 2-13.

Example of application

Let us consider the circuit in the right-side graph in Figure 2-13. Let us then suppose that **Train 2**, in node 10, is a braking train which is in rheostat mode, whereas **Train 1** is a motoring train which power is supplied both from **Rectifier 1** and **Train 2**. Under these conditions, **Rectifier 2** must be in *OFF* mode.

Consequently, the list of values for the binary control variables would be:

- $\gamma_1 = 1,\ \gamma_2 = 0$
- $\lambda_1 = 1,\ \lambda_2 = 1,\ \lambda_3 = 0,\ \lambda_4 = 1$

Where the sub-indices for the λ variables correspond to the pure DC nodes, from 8 to 11 in Figure 2-13 (λ_1 represents node 8, etc.).

With this set of control variables, the state variables of the system would be:

- The voltage modules and angles of AC nodes, both pure and terminal nodes, excluding the slack one, i.e. from node 2 to 5.
- The current, commutation angle and overlap angle of **Rectifier 1**. The variables representing **Rectifier 2** are known, and they all equal 0.
- The voltages in all the DC nodes excluding **Train 2** (node 10), which voltage is known, and it equals the rheostat voltage threshold.

The equations used to obtain the values of the state variables would be:

- The active and reactive power equations of both pure and terminal AC nodes, excluding the slack node. It must be noted that in the equations for node 5 (the AC terminal node of the inactive **Rectifier 2**), the terms representing the linkage with the DC side of the system will be null.
- The residual equations of **Rectifier 1**.
- The power equations of both pure and terminal DC nodes, excluding **Train 2** (node 10). It must be noted that in the equation for node 7 (the AC terminal node of the inactive **Rectifier 2**), the term representing the linkage with the AC side of the system will be null.

2.3.2.2. THE LOAD FLOW SOLVER CODE DETAILS

This section presents the details of the implementation of the load flow solver developed in this thesis. The code has been implemented in Matlab.

Figure 2-14 presents the flow diagram of the general structure of the load flow solver. The flowchart shows that there are two loops in the solver. First, there is an inner loop to perform the N-R method iterations. Then, there is an outer loop to visit all the snapshots generated by the electrical circuit generator.

Before entering the snapshot loop, the main simulation parameters are loaded. This is performed by loading the 'Options.m' file generated by the electrical circuit generator and by initialising other variables that influence the solver behaviour, e.g.: the maximum number of iterations of the N-R method.

Then, the solver enters the snapshot loop, where all the electrical circuits generated by the previous process in the simulator are analysed. The first step in this loop consists of loading the files saved by the electrical circuit generator for the snapshot under analysis. The loaded information contains the initial guess for the state variables of the system, which follows the flat-start approach for node voltages (AC and DC sides) and angles (AC side). Regarding rectifiers, the initial guess is set to α=0, μ=10º and Idc=0.3 p.u.; which have proved to lead to excellent convergence performance. Provided the user of the simulator may impose some operation conditions, the rearrangement flag is set to *ON* after the load process, e.g.: the user imposes a SS to be in off state during the whole simulation.

This rearrangement flag is used by the simulator to warn that there are important qualitative changes in the system nodes. In the DC railway case, the main changes affecting the N-R dynamics are the changes in the states of SSs and trains. It was stated in the presentation of the N-R method in Section 2.3.2.1 that when these events take place, the number of state variables in the system changes. The rearrangement process, which is conditioned by the rearrangement flag to be active, is in charge of changing the structure of the node matrices. Those elements which associated state variables do not take place in the solution process are placed at the last rows, e.g.: the nodes of trains which enter the rheostat braking mode and become therefore voltage sources, the angles and current of a rectifier that enters the cut-off mode, etc.

The following solver task is in charge of calculating the state equation mismatches before changing the values of the state variables. This set of mismatches is used as the reference to assess whether a given change in the state variables is in the right direction.

After this, the Jacobian matrix is generated by particularising, to the current state variable guess, the partial derivatives of the state equations with respect to the state variables.

The following task performed by the solver consists of updating the state variables. This update process is a fundamental part of the N-R method, especially in the DC railway case. The reason is that the directions of change contained in the Jacobian matrix could lead to a worse guess in case the state variable change magnitude is not modulated. To prevent the solver from applying wrong state variable changes, the update process decreases the amplitude of the changes in the state variables in case the norm of the state equation mismatches is not decreased. This is performed by using an initial step size modulator which is halved recursively. Other concerns of the state variable update will be presented in Section 2.4 in the solver robustness discussions.

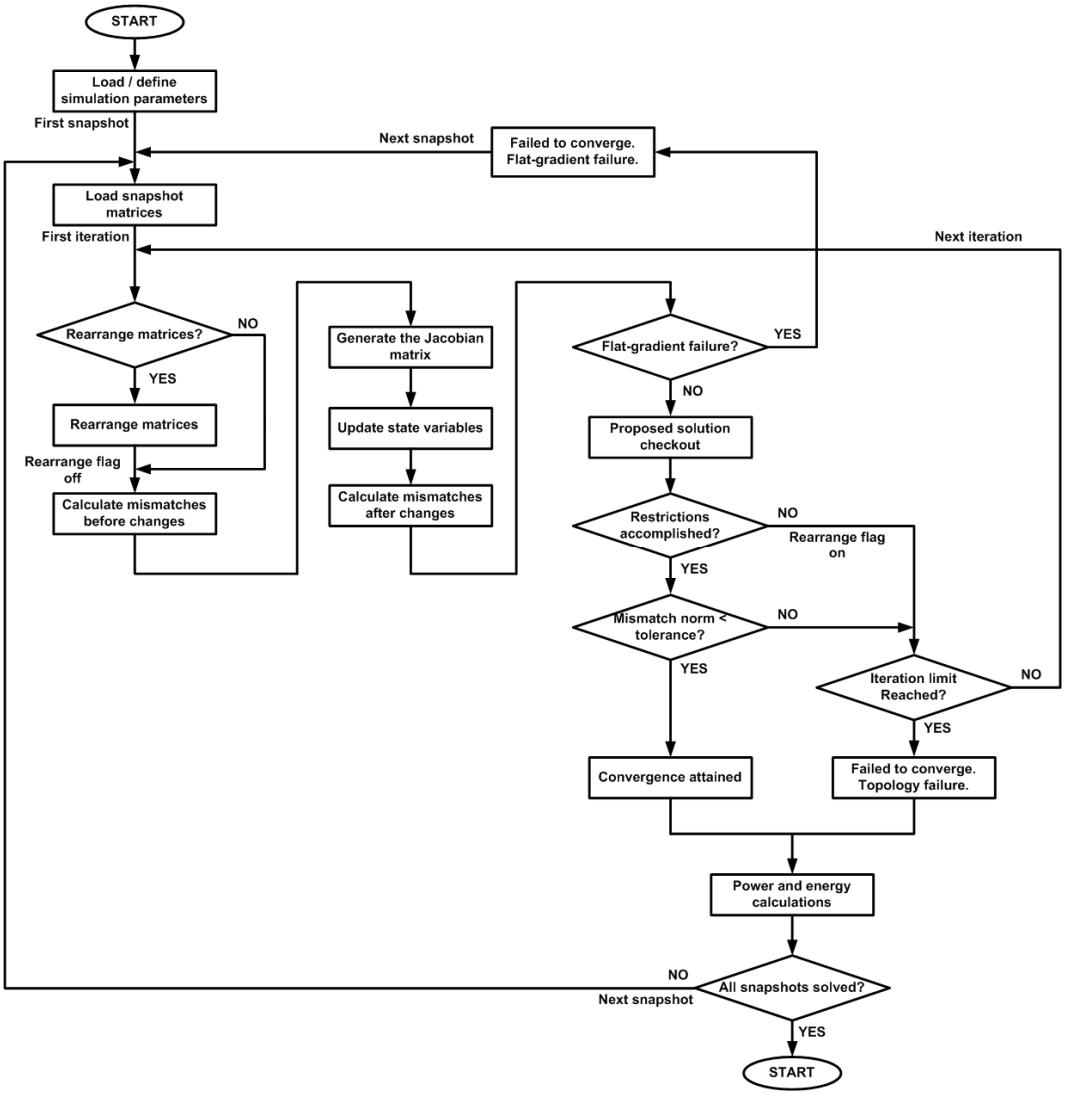

Figure 2-14. Load flow solver flowchart.

After this, in case the norm of the mismatches is not decreased with respect to the reference value, the N-R method is aborted, describing the convergence failure as 'flat-gradient failure'. The reason for this nomenclature is that this event usually takes place when the elements in the Jacobian matrix tend to zero, i.e., the proposed solution is in a minimum of the hyper surface defined by the system equations which does not accomplish the mismatch tolerance. In case the norm of the mismatches is decreased, the N-R iteration process continues.

Then, the values for the state variables in the iteration must be validated. This means to check out whether any of the system constraints has been violated. In a DC railway with regenerative braking trains and diode SSs, the main constraints to regard are:

- Braking trains which are not in rheostat mode cannot reach voltages greater than the rheostat voltage threshold.
- Braking trains which are in rheostat mode cannot supply an amount of power greater than their braking power.
- Active (ON) diode SSs cannot drive negative currents.

- Inactive (OFF) diode SSs cannot exhibit DC voltages lower than the no-load voltage.
- Inactive SSs where there is a reversible converter installed cannot exhibit voltages greater than the RS activation threshold.
- RSs cannot drive reverse currents if their voltage is lower than the RS activation threshold.

Figure 2-15 shows a flowchart which represents the general structure of the checkout routine as it was in the beginning of this thesis. The refinements introduced along the thesis, which have not changed the code structure substantially, will be presented in Section 2.4.1.

This routine is in charge of 1) preventing the solver from validating an erroneous load-flow solution, and 2) obtaining the values of the load flow control variables contained in $\mathbf{\Gamma}$ and $\mathbf{\Lambda}$. It is therefore essential for the load flow solver performance, since a careless implementation of this process may dramatically affect the robustness of the simulator. The checkout strategy determines the ability of the solver to find the correct system topology, defined as the set of states of all the elements in the system. These elements subject to exhibiting different states are: 1) braking trains, which may be in normal or rheostat mode; and 2) SSs, which can be in active, cut-off or reverse mode (when applicable).

The flowchart in Figure 2-15 shows the order in which the constraint violations are reviewed, and the refusal strategy. Regarding the latter, it can be observed that once a violation of the system constraints is found, the routine does not check the rest of conditions. The modes of these elements which are violating a constraint are changed and the change in the state variables proposed by the update routine is discarded. Although this approach could be sub optimum regarding convergence speed, it has proved to be extremely robust. In a greedy approach where the same N-R iteration is used to check all the constraint violations to speed the process up, the bouncing events are more frequent. This leads to a higher rate of hits of the maximum number of N-R iterations allowed (and so to non convergence). Then, when it finds the correct solution, it tends to use a higher average number of N-R iterations.

It is also interesting to note that in the cases when SSs are changed to cut-off mode after a constraint violation, the routine prevents the DC side of the system from being isolated. If this isolation takes place, the Jacobian matrix in the following N-R iteration turns out to be singular, which spoils the solver time performance. This isolation prevention is performed by temporarily activating a SS with a low current value.

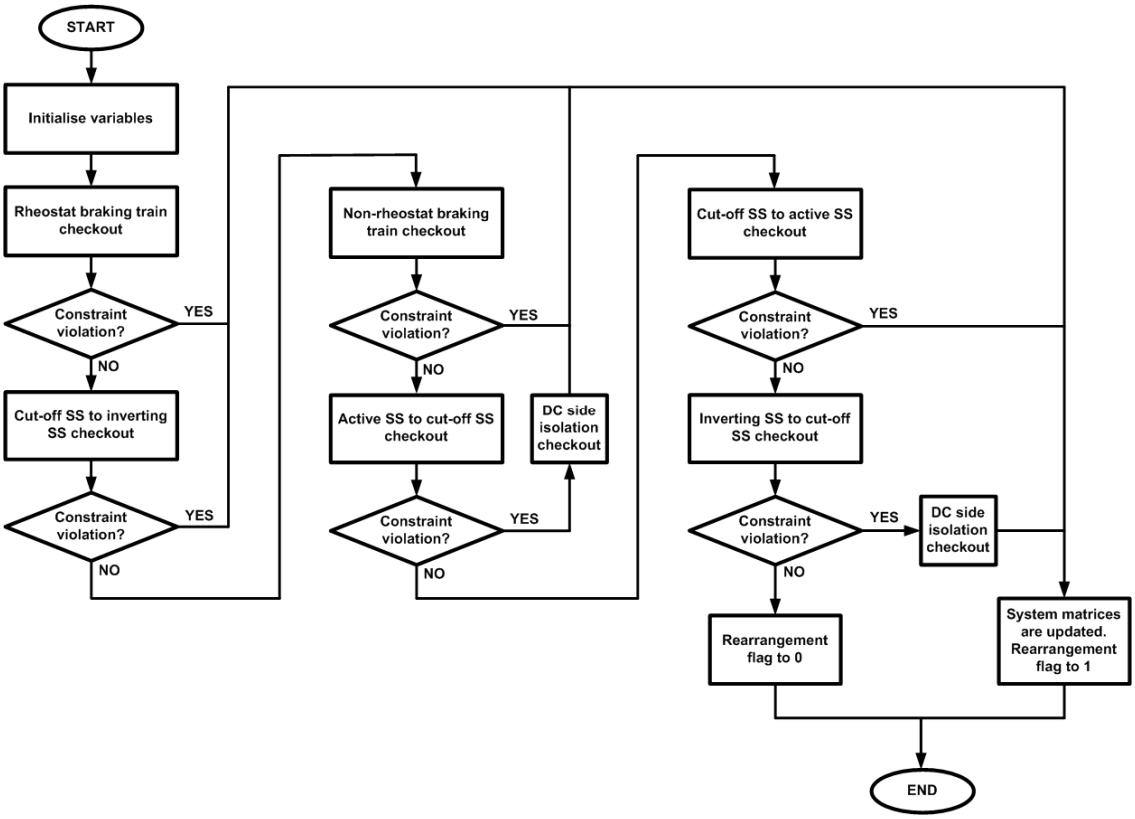

Figure 2-15. Checkout function flowchart.

After the checkout routine, if any system constraint has been violated, the solver goes to a new iteration of the N-R loop. In case the N-R loop iteration limit has been reached, the snapshot analysis is aborted and a flag declaring non convergence for the snapshot due to the impossibility to find the system topology is activated. In case the proposed solution is valid from the system constraint standpoint, the solver checks out whether the norm of the mismatches is lower than the tolerance threshold. In case it is, the solution is validated, convergence is declared, and the solver exits the N-R loop.

Before starting the analysis of the following snapshot, the solver enters a routine in charge of performing the necessary power and energy calculations. The main ones are: 1) for braking trains in rheostat mode, it calculates the portion of the regenerative braking power that was sent to rheostats and it stores the result for the analysis process; 2) the amount of energy in ESSs is updated when applicable. In the version of the solver at the beginning of the thesis, a file containing the results of the load flow for each snapshot was saved to disk for the result aggregator to analyse it.

If the solver detects that it has analysed all the snapshots in the traffic input, it exits the snapshot loop and is terminated.

2.3.3. THE RESULT AGGREGATOR

This last process in the simulator is in charge of concatenating power, voltages and currents along time. After that, results such as energy figures, voltage and current profiles in the lines, etc. are obtained.

The result aggregator performs a snapshot loop to compose all the power and energy figures in the period of time simulated. It will be explained in Section 2.4.2 that unnecessary accesses to disk are rather inefficient regarding time performance. For this reason, in the current version of the code the result aggregation is performed inside the snapshot loop, in the load-flow solving process. Despite of that, the conceptual Gane & Sarson graph in Figure 2-9 is still valid, and it has therefore been conserved in that form.

2.4. SIMULATOR IMPROVEMENT AND PERFORMANCE ASSESSMENT

The simulator performance has been defined to have two dimensions: 1) robustness, and 2) computation-time performance. This section presents the results obtained from these two standpoints.

The performance of the simulator is mostly determined by the performance of the load flow solver. First, regarding robustness, because once the input information is correctly introduced, the electrical circuit generator has no reasons to fail in the generation of the electrical snapshot circuits.

Then, regarding computation time, it must be noted that in the optimiser approach in this thesis, the trains' position and power profiles are generated in a pre-processing stage. This has limited impact on the optimiser times. Therefore, it has not been included in the computation-time performance analyses.

In the case of the result aggregator, first, the process can only succeed in the task it is in charge of; and then, it represents an insignificant fraction of the total computation time of the load flow analysis. For this reason, the study of the code performance has been restricted to the analysis of the performance of the load flow solver.

2.4.1. ROBUSTNESS PERFORMANCE

Robustness is defined as the ability of the solver to find the solution of all the snapshots in the simulated time period. There are two main reasons for the solver not to find the electrical solution of a snapshot. First, due to the fact that the DC railway load flow problem is a non-linear non-convex problem, the solution method may arrive to local minima that do not match the nodal power demands. It is also possible to have power demands which are higher than the maximum power that the catenary system is able to transmit, and are therefore impossible to be satisfied by the system. In this case, the solution obtained by the N-R method is not necessarily a local minimum, but the nodal power demands are not matched either.

When these events take place, the elements in the Jacobian matrix tend to zero with high state equation mismatches. This disables the capacity of the N-R method to change the state variable values from iteration to iteration. For this reason, this kind of convergence failure has been named *flat-gradient failure*.

Second, there are elements like trains and diode SSs which change their behaviour under different circumstances. That introduces a further difficulty to the solution method, since the electrical topology of the system is not determined in the first N-R iteration. It must be noted that the exhaustive test of all the possible mode combinations is unmanageable (for the typical system sizes). Therefore, the search for the system topology (expressed by the particular values of the binary control variables, γ and λ) must be included in the solution method, as described in Section 2.3.2.2. This search for the correct topology is subject to problems like bouncing events, etc. This kind of convergence failure has been named *topology failure*.

It must be noted that a mistake in a single snapshot over hundreds may have important consequences: 1) the power and energy errors in snapshots where convergence was not attained may be huge, so its inclusion in the analysis may lead to wrong results and conclusions, especially for small simulation periods; 2) even for large traffic scenarios, wrong snapshots may make it difficult to perform comparisons between several power system configurations when the decision variable does not exhibit high magnitudes.

Thus, the code robustness has been thoroughly tackled in this thesis. Robustness has been measured by means of an error rate, defined as the ratio between the wrong snapshots and the total number of snapshots included in the simulation (2.39). Since the typical robustness error rate figures tend to be rather low, this error coefficient has been expressed in percent values.

$$Robustness\_\varepsilon = \frac{Wr\_Snp}{N\_Snp} \cdot 100 \tag{2.39}$$

Where,

- Wr_Snp represents the number of snapshots where the simulator failed to converge.
- N_Snp is the total number of snapshots in the simulation.

An early version of the simulator has been used as the reference both for robustness and time performance improvement measurements.

The robustness error rate of this simulator has been measured by means of a robustness test. In order to prevent the results from being affected by particularities of the traffic set selected, the robustness test is made up of three different traffic scenarios. These scenarios have been generated by assigning random dwell times at passenger stations in an MTS with 11 substations and 23 passenger stations. The details on the system characteristics are omitted here for the sake of clarity. Nevertheless, the MTS used for this analysis is the one used as case study system in this thesis, where the headway has been set to 7 minutes (see Section 3.1).

Each of the three scenarios is made up of 420 snapshots, and the number of nodes in the system is: 50 DC nodes and 23 AC nodes including the slack one. In general, a system with only diode substations and trains does not present big difficulties for the solver. However, when the infrastructure includes complex systems like RSs, the reference solver exhibits non null robustness error rates.

To analyse the robustness error rate in a rigorous way, RSs using the simplified control curve-efficiency model have been added to the MTS power system in different configurations. 11 batches containing 10 infrastructure configuration samples each have been generated to define this robustness test. Each RS configuration batch is characterised by the number of installed RSs in the system, which has been increased from 1 to 11. The position and size of the RSs have been selected at random. Table 2-2 shows a selection of samples included in the robustness test.

The application of the robustness test to a version of this or any simulator is performed by the exhaustive simulation of the 110 RS configurations in the 11 10-sample batches.

Table 2-2. Examples of RS configurations in the robustness test.

Batch	Sample	SS1	SS2	SS3	SS4	SS5	SS6	SS7	SS8	SS9	SS10	SS11
1	**6**	-	3MW	-	-	-	-	-	-	-	-	-
2	**3**	-	-	-	-	-	-	-	-	1MW	2MW	-
3	**10**	-	5MW	-	1MW	-	-	2MW	-	-	-	-
7	**1**	1MW	1MW	5MW	1MW	3MW	1MW	-	-	-	-	2MW
11	**10**	3MW	4MW	2MW	4MW	1MW	2MW	1MW	2MW	5MW	2MW	4MW

Figure 2-16 presents the results of the application of the robustness test to the reference simulator for the three traffic scenarios. The difference in the robustness error rates for the traffic scenarios shows that the reference solver is rather sensitive to the set of positions and power demands/regenerations of the trains. There is a steady rising trend in the error rates as the complexity of the RS configurations is increased, especially for the second traffic scenario. In the worst case (traffic scenario 2, batch 11), the simulator fails to converge, in average terms, 11.6 times over the 420 snapshots in each simulation sample. This represents a poor robustness performance. Nevertheless, it must be noted that the RS configurations in the robustness test are rather complex.

On the other hand, the reference simulator performs well for simple RS configurations, especially in the traffic scenarios 1 and 3.

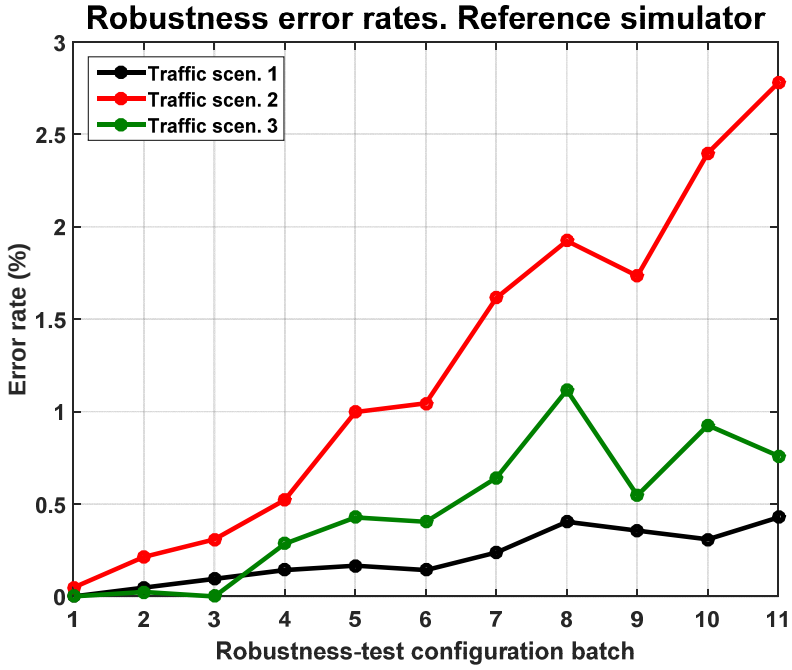

Figure 2-16. Results of the robustness test. Reference simulator.

The simulations included in the robustness test do not include unfeasible power demands. Therefore, all the failures by the reference simulator belong to the topology failure category.

2.4.1.1. CHANGES IN THE LOAD FLOW SOLVER TO IMPROVE ROBUSTNESS

The difficulty to find the correct states of the elements in the system has been proved to be the main solver robustness problem. This is a very important concern regarding the electric railway simulators which has not been thoroughly tackled in the related literature.

One of the few examples which deal with this concern is (Coto, Arboleya et al. 2013). In this study, the authors propose to obtain the electrical topology of the system for each snapshot by explicitly including the multi-modal devices in the constraints of an optimisation problem. The results have been proven to be accurate. However, no details on simulation time and robustness are given. In the works carried out in the frame of this thesis, it has been observed that using a formal optimisation model to simulate MTSs leads to high simulation times. This is especially remarkable when systems which couple the snapshots (ESSs) take place in the system, since they make the size of the optimisation problem soar in terms of number of equations and variables. In addition, the optimisation method may exhibit difficulties to find a point within the feasible region to start searching for the optimum solution in complex electrical topologies (López López, Pecharromán et al. 2012).

For these reasons, the simulator in this thesis deals with this problem by improving the strategy implemented to find the system electrical topology. This strategy is included in the checkout task (Figure 2-15).

Figure 2-17 shows two paradigmatic examples of topology failures in the reference simulator. In both cases, the N-R method enters an infinite loop where it bounces between certain state configurations. In the first example (left), the solver is close to the required mismatch tolerance. However, only one over the three states in this periodic pattern fulfils the system restrictions. The method is not able to find the correct electrical solution. Then, in the second example (right), the N-R loop is locked between two wrong sets of state variable values which are far away from the actual solution of the system equations.

The version of the solver at the end of the works in the frame of this thesis includes two main improvements in the code dealing with this robustness problem: 1) the conditional relaxation of some constraint violation rules; and 2) a mechanism to change the trajectory followed by the N-R method to find the solution.

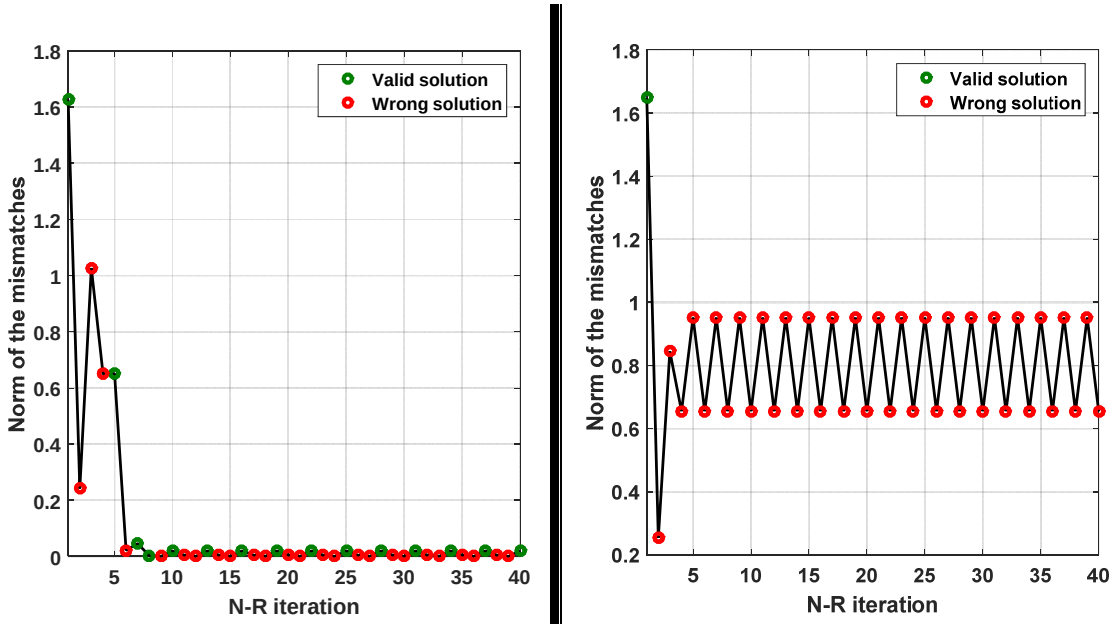

Figure 2-17. Examples of topology failures.

The base for the first code improvement is that the solution yielded by the solver must accomplish the system equations, but it is not forbidden to permit the solver to make use of non valid values of the state equations during the process to find this solution.

Relaxation of the constraint violation rules

This first code enhancement is only activated when the N-R iteration exceeds a tuneable number-of-iteration threshold. The reason for this conditional activation is that for the majority of the snapshots, especially for those where the traction power is much greater than the braking power, the convergence behaviour of the simple checkout strategy is excellent.

However, when the number of iterations of the N-R method exceeds a certain value, the first version of the checkout code is unable to break the bouncing loops. This measure aims to unbalance this bouncing phenomenon to make it possible for the solver to find the system state.

The relaxation mechanism consists of allowing provisional solutions which include:

- Small negative currents in diode rectifiers in active SSs.
- Power generations in rheostat braking trains slightly greater than the regenerated power.
- Inactive SSs which voltage is slightly lower than the activation (no-load) voltage.
- Braking trains which voltage is slightly greater than the rheostat voltage.

Although these solutions are accepted by the checkout routine, the rearrangement flag is set to *ON* to prevent the solver from validating wrong solutions.

The tuning of the magnitudes of the temporarily allowed invalid values is not a straightforward task. It was performed experimentally.

Multiple N-R solution trajectories

This improvement measure attacks the bouncing problem in a different way. In the N-R method, it is required to select an initial set of values for the state variables (the initial guess). Consequently, there is and start point and a solution point to be attained.

In DC railway systems, there is a high variability in the node voltages (especially in the DC side) and the rectifier state variables. Changing the initial guess according to the system load is a difficult task which, in addition, may lead to frequent local minima problems. Therefore, the flat start approach is still the best initial guess option.

However, since the initial guess is usually far from the solution, the initial mismatch tends to be enormous. Under this circumstance, in the first iterations, with high Jacobian values and mismatches, it is easy to improve the mismatch norm. It is hence clear that there are infinite options to change the state variables from iteration to iteration, defining infinite solution trajectories. Therefore, there may be trajectories that lead to bouncing phenomena, which should be skipped.

The key to change the solution trajectories is in the state variable update routine of the N-R method. The change step in the state variable update process is modulated by a factor which is recursively halved until improving the mismatch norm (see 2.3.2.2). Thus, changing the first value that the update function tries for this modulation factor may be used to vary the solution trajectory. In general, the best option is to reduce it, which however slows the N-R convergence characteristics.

To cope with this issue, the multiple N-R trajectory mechanism is only activated if the N-R method is finding difficulties to solve the snapshot. Again, there is an N-R iteration number threshold which activates the mechanism. When this takes place, the state variables are set to the initial guess and the initial modulation factor for the update process is varied. There is a list of 5 deterministic and 2 random values for this modulation factor which are tried before declaring non convergence.

Figure 2-18 shows an example of convergence attainment due to the improved system-state search strategy. It can be observed in the x-axis that the N-R iteration number is high. The solution trajectory is changed every 45 iterations rate in this example. The N-R method is entering bouncing loops until the solution trajectory initialised in iteration 270 is used. This time, a small-step state-variable update and the restriction relaxation rules (iteration 287) make it possible to find the load flow solution in a complex situation.

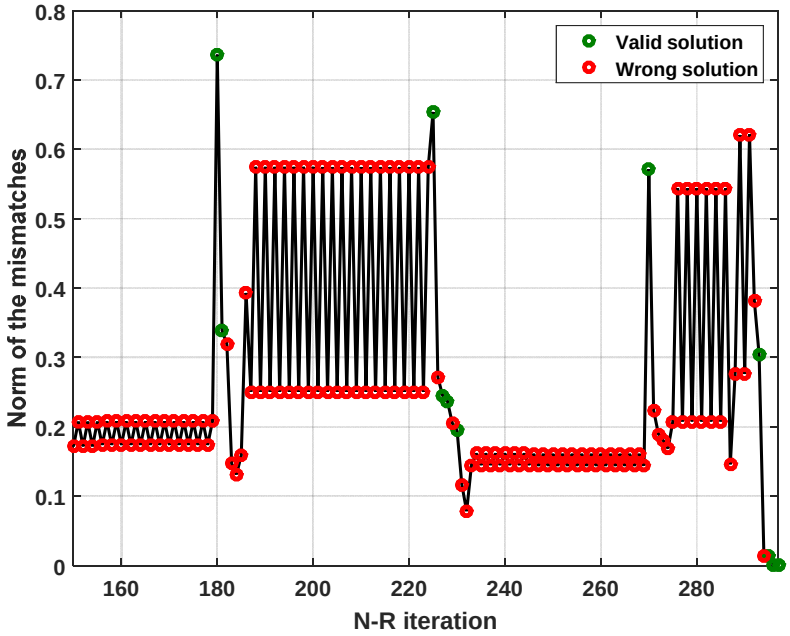

Figure 2-18. Example of convergence attainment due to the improved checkout strategy.

The application of the multiple trajectory mechanism, together with the constraint relaxation measures, boosts the robustness features of the solver. Actually, the current version of the solver, featuring the two robustness improvements, exhibits zero robustness error rate in the robustness test defined in this section. It is important to note that it is the combination of both measures which makes it possible to solve all the snapshots in the robustness test.

2.4.2. COMPUTATION-TIME PERFORMANCE

The computation-time performance of the load flow solver is a key factor in this thesis. The reason is that the optimisation method presented is based on a population search method, which performs a huge number of simulations of the system to find an optimum solution.

As already stated, the load flow solver is implemented in Matlab code. In general, the main issues affecting the time performance of a code implemented in Matlab are:

- The access to or the storage of information. This is common to any programming language, since it is determined by the access times to the hard disk, the RAM memory or the cache.
- The abuse of exhaustive loops (*for*, *while*, etc.) in the code. The Matlab code is an interpreted language that is well known to exhibit poor computation-time performance when these loops are used. The Matlab functions are optimised to work with matrices.
- The use of dynamic memory allocation. Changing the size of a matrix or vector variables dynamically in Matlab (e.g.: inside a loop) spoils the computation times dramatically.

Figure 2-19 shows the share of the total computation time used by the main tasks in the load flow solver for the reference simulator. The computer where the simulations have been carried out runs Windows 7, with an Intel(R) Core(TM) i7-2600 CPU @ 3.4 GHz processor; and 8 GB RAM memory in a 64-bit system. The first sample in the first batch of the robustness test has been used to obtain these results. The time measurements shown in the figure have been obtained by means of the Matlab profiler tool.

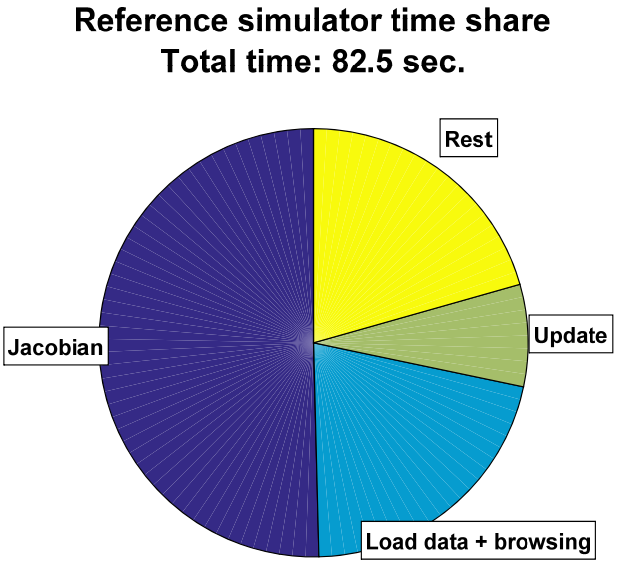

Figure 2-19. Load flow solver computation time share. Reference simulator.

The total computation time for the load flow solver was 82.5 seconds, which represents around 0.2 seconds per snapshot. The generation of the Jacobian matrix consumes around half the computation time (50.4 %, 41.6 s). Then, the second heaviest task is the snapshot information loading, which consumes around the 21.3 % of the total computation time (17.6 s). The time devoted to browse to the electrical circuit files is included in this time item. Then, the update function takes the 7.7 % of the total time (6.4 s). The rest of the time is distributed between the other routines, including the result saving, the mismatch calculation, etc. (20.6 %, 17 s).

Regarding the Jacobian computational burden, it must be noted that in a mixed AC-DC load flow, the regular box pattern in the Jacobian of AC systems is not followed due to the rectifier state equations. That makes it difficult to avoid the use of loops to create the Jacobian matrix. In addition, the Jacobian generator is invoked in every iteration of the N-R method, which makes the number of uses of this routine to soar steadily. Therefore, these results confirm that the use of intensive *for* loops in the interpreted Matlab code is rather inefficient. The translation into C language and the compilation of the code arises as a good possibility to improve the time performance for this function.

Then, the load of information was another a-priori good candidate for decreasing the computation-time performance. A hardware approach like the use of computers featuring solid-state hard disks could dramatically reduce the load time. However, there are also some improvement possibilities from the software standpoint.

Regarding the update function, the main reasons for its time consumption are the loop used to reduce the state variable step size until the mismatch norm is reduced and the inversion of the Jacobian matrix. This matrix inversion is implemented in the way the Matlab's support team recommends to do it, so it is not easy to improve this task.

After the revision of the computation time for the reference simulator, taking into account the Matlab code and hardware limitations, the main improvements to be applied to the load flow solver code are: 1) the refinement of the information loading and result saving processes; and 2) the code translation into C language to make it possible to compile it.

The refinement of the load information and save result processes has been implemented in two ways:

- The way of loading information has been changed. In the reference version of the simulator, the electric information is stored in Matlab m-files. The retrieve of this information must be made by means of an *eval* instruction, which is well known to be time inefficient. This has been improved by storing the electrical circuit results in binary files which information can be retrieved by means of the *fread* function, much more efficient than *eval*. In addition, the way the path with the electric information is input to the simulator has been revisited in order to reduce the browsing time.
- The results are no longer saved to disk snapshot by snapshot. Instead of that, the result aggregation is implemented within the snapshot loop in the load flow solver. By doing this, when the solver exits the snapshot loop, the set of result matrices generated by the last process in the simulator is already available, without the process making frequent accesses to disk.

Figure 2-20 shows the Matlab profiler results after the application of these code refinements. It must be noted that the robustness improvement measures –which tend to make the solver a few slower to boost robustness– are included in this code as well. Actually, these results have been obtained with the current version of the solver without the final code compilation.

The total simulation time, for the same traffic scenario, has decreased to 58.4 s, even after the inclusion of the code robustness improvements. The new simulation time per snapshot has decreased to around 0.14. The time required to *load* the electrical circuits has been reduced to 8.2 s, which means that the refinement of the load process has been a success. The time consumed by the *update* process has been increased to 8.2 s as a result of the robustness improvement measures. With the new lower total simulation time, the Jacobian process (which has taken 40.5 s, a similar figure than the reference one) consumes 68.1 % of the total simulation time. The

Jacobian process is therefore the main reduction target. Its high computational burden associated makes it worthy to implement the code compilation task.

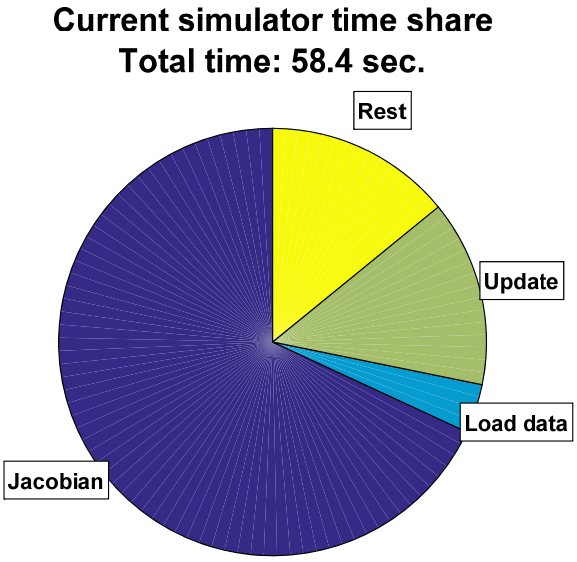

Figure 2-20. Load flow solver computation time share. Current simulator.

The code compilation has been performed by means of the Matlab C Compiler application. This tool features a Matlab-to-C translator assistant that made it possible to obtain the C code version of the simulator without explicitly performing this translation task. However, the Matlab C Compiler translation limitations made it necessary to perform a comprehensive review of the code.

The results of the code compilation are excellent. The computation time for the compiled version of the load flow solver is 1.15 s. This represents a dramatic reduction of the simulation time with respect to the other versions of the code. The Matlab profiler tool does not allow analysing the time share for the different processes of the compiled solver, but after the steep time reduction achieved, this is not of special interest.

After this result, the obtainment of the C version of the code appears as the key factor to boost the simulator's time performance.

Multiple time-measurement analysis

The computation time analysis carried out by means of the Matlab's profiler makes it possible to analyse the main code weaknesses and to address them. However, it is important to perform a more general time-measurement campaign which yields statistically significant computation times.

This multiple time-measurement study has been performed by analysing the computation times obtained during the robustness tests for the three code versions

analysed. Figure 2-21 presents these results, which have been used to obtain the average time reductions with respect to the reference simulator.

Figure 2-21.a shows how, as the complexity of the electrical RS configuration in the robustness test increases, the simulation time rises as well. In the reference code, the traffic scenario leading to the lower number of convergence failures (scenario 1) exhibits the lowest simulation times.

Figure 2-21.b presents the average computation times measured. It must be noted that the average computation times for the robustness test are not the same than those obtained by the Matlab's profiler. The average figure for the refined code before compilation (interpreted Matlab code) is 50.7 s. This represents 23 % computation time reduction with respect to the 65.9 s obtained with the reference code. Then, the code compilation makes the average computation time drop dramatically. The average 1.31 s represent 98 % computation time reduction with respect to the reference simulator.

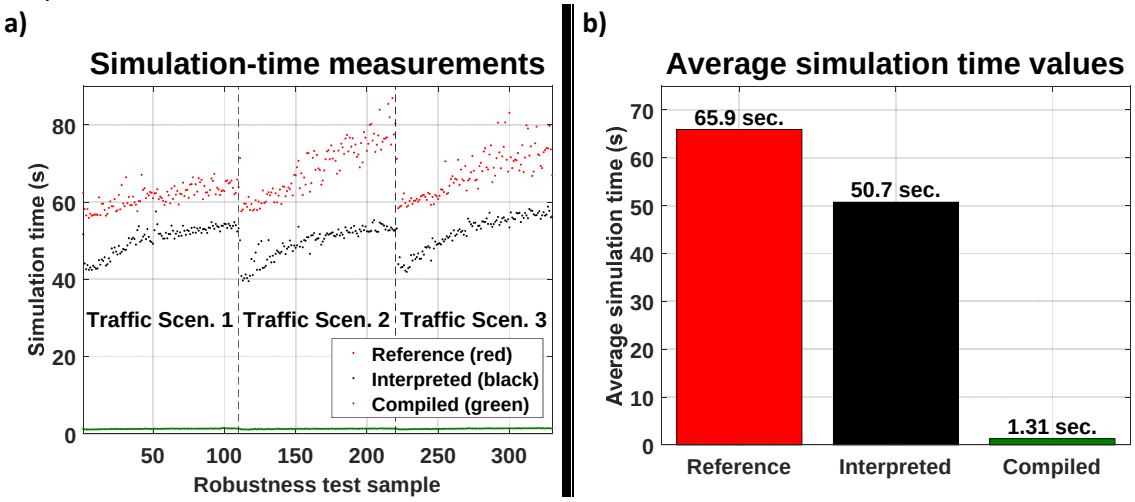

Figure 2-21. Computation times measured during the robustness tests.

The computation time could have been further reduced by the application of paralleling or distributed computation. However, at the moment of the development of this thesis, there were no Matlab licences available to test these techniques.

Nevertheless, some distributed compilation techniques have been applied in Section 6.4.4 for reducing the computation time figures of the infrastructure optimiser presented in the thesis.

2.5. SUMMARY, CONCLUSIONS AND CONTRIBUTIONS

This chapter has been devoted to the description of the electrical multi-train simulator developed in the frame of this thesis. In general, these simulators are key tools to obtain results in MTS infrastructure design and improvement studies.

The presentation of the general structure of an electrical multi-train simulator has been followed by a review of the modelling approaches in the literature for the most relevant elements in the electrical infrastructure of MTSs. The models of the trains, the supply system, SSs and the current trends to improve MTSs (RSs and ESSs) have been reviewed, putting emphasis on the modelling approaches used in this thesis.

Then, the details of the integration of the infrastructure-element models into the electrical multi-train simulator developed in this thesis are given. The approaches to generate the set of electrical circuits to be solved and, especially, the load flow solver are explained with the aim of making it replicable. The strategy followed to find the correct electrical topology of each snapshot represents a novel method which, in addition, covers a part of the electrical railway simulators that is usually omitted in the literature. This system-state search strategy, which implements the topology changes one by one, has proven to be more powerful than other greedier strategies.

Regarding the performance of the simulator, the load flow solver arises as the main concern due to the especial characteristics of the load flow problem. This problem is highly complex, and it is indeed difficult even to find the solution under certain circumstances. In addition, it is the most demanding part of the simulator from the computational burden standpoint. The performance of the simulator has consequently been analysed in terms of robustness and computation time of the load flow solver.

The former consists in the ability to find the solution of the load flows under different and complex load/regeneration profiles and electrical topologies. It has been tackled by the implementation of a robustness test. This test has proven the difficulties to find the solution of all the snapshots when the complexity of the electrical topology of the system increases.

A set of refinements in the load flow solver to enhance the simulator robustness have been presented. Their effectiveness to make it possible to solve all the snapshots in the robustness test has been proved.

Finally, this chapter has analysed the simulator from the computation-time performance standpoint. The most time-consuming parts of the code have been identified and some measures to improve their performance have been implemented. The most relevant conclusion is that the generation of compiled code must be regarded as a fundamental task to boost the computation-time performance of a simulator developed in Matlab language. Nevertheless, there are other concerns to be taken into account, being a refined strategy to access and store data in the hard disk the most relevant one.

Summarising, the most relevant contributions of this chapter are:

- The presentation of a novel strategy to find the electrical structure of DC-railway electrified systems. The combination of a general strategy and a series of mechanisms for difficult snapshots have proven to be highly effective in the solution of complex electrical load flows.
- A review of the computation-time performance of an electrical multi-train simulator developed in Matlab, together with a study on the effectiveness of a series of measurements oriented to improve it.

CHAPTER 3

CASE STUDY AND INTRODUCTORY ANALYSIS

This chapter is devoted to the initial analyses and the description of the main characteristics of MTSs from the energy efficiency standpoint. This will be performed by first describing the case-study line which will be used in the different studies along this thesis (Section 3.1). Then, Section 3.2 performs a comprehensive analysis of the main energy figures in DC-electrified MTSs. After that, Section 3.3 includes a review of some current techniques that may be used to improve MTS energy efficiency. Finally, Section 3.4 presents the main conclusions after the analyses in this chapter.

3.1. THE CASE-STUDY SYSTEM USED IN THE THESIS

There are two different types of line in MTSs: 1) double-track lines between two terminal stations, 2) complex-topology lines.

Lines with two terminals may be operated with homogeneous or different headways, e.g. the headway is shorter in the stretch of the line in the city downtown, which is attained by having trains that only run on this stretch. Circular lines are a particular case of this type of line which do not contain terminal stations.

The complex-topology lines are usually made up of a central corridor and several branches. It is possible to have single-track stretches, more than two tracks in the central corridor, etc. Trains are not forced to stop in all the stations in these lines.

In this thesis, the case-study line used to illustrate its derivations is a double-track line with two terminal stations. In the operation of this line, trains stop at all the stations. The reason for this choice is that this is a very general type of line and operation. Relevant Metro systems as Madrid, Barcelona or Paris use only this type of line and operation.

Nevertheless, it must be noted that the application of the studies in this thesis to different MTS lines would be easy to implement. In the case of circular lines, all the analysis presented in this thesis would be directly applicable. In the case of complex-topology lines, the characteristics of the traffic in these different types of line should be determined and modelled.

The case study used in this thesis is inspired in an actual MTS line in Spain, which is omitted for confidentiality concerns. The presentation of its characteristics has been broken down into infrastructure, rolling stock and operation information.

3.1.1. INFRASTRUCTURE AND ROLLING STOCK

Track characteristics

As already stated, the case study line is a double-track system with two terminal stations. The total length of the line is 19 km, and it is totally underground (tunnel). There are 23 passenger stations, which yields around 860-meter average inter-station distance, which is within the usual range in urban underground systems like the case-study. Table 3-1, which is presented after the description of the electrical SSs, gathers the specific distances between passenger stations.

Figure 3-1 presents the topography of the line, which maximum grade is 40.4 mm. Regarding curves, the minimum radium is 195 m.

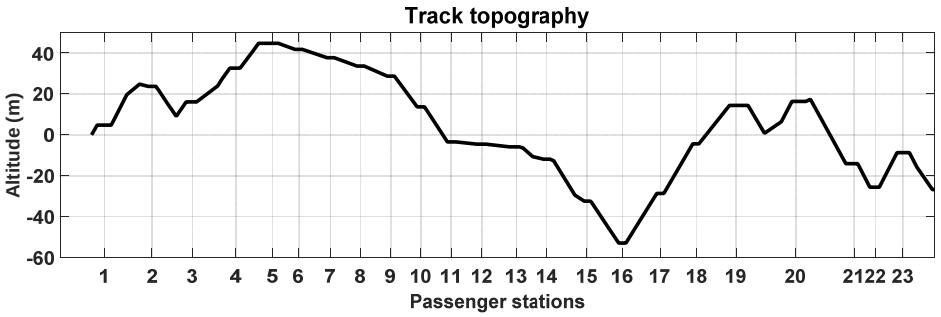

Figure 3-1. Case-study line track topography.

Figure 3-2 presents the track diagram of the line, where the cul-de-sacs at the terminal stations have been simplified. These parts of the line are used to increase the capacity of the line by easing the train manoeuvres required to change the track. In the model included in the case study, these details are omitted. Consequently, the trains that arrive to the final station in a track are placed in the initial station of the other track in the moment required by the train graphic of the line.

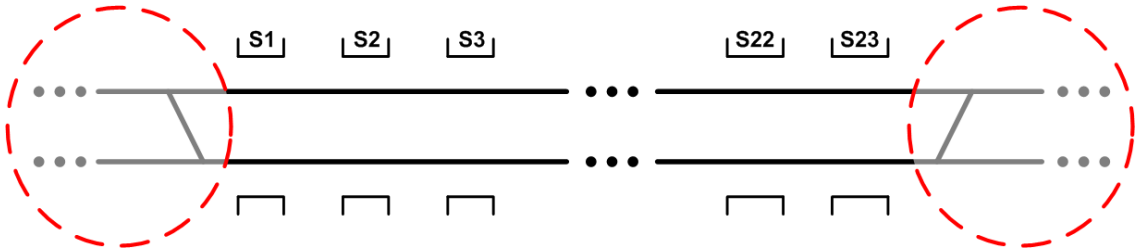

Figure 3-2. Case-study line track diagram.

Rolling stock characteristics

The main characteristics of the rolling stock running on the tracks of the case-study system are:

- **Train composition**: Electrical Multiple Units made up of 8 cars, 5 of which are motor cars. Each motor car contains in turn 2 motors.
- **Train no-load mass:** 190 Tn.
- **Rotative inertia:** 1.9 Tn.
- **Train maximum load:** 90.3 Tn.
- **Train length:** 108.06 m.
- **Running resistance parameters:** These are the coefficients presented in (2.1):
  - A = 1.6052 daN/Tn.
  - B = 0.015 daN-h/Tn-km.
  - C = 0.0002962 daN-h^2/Tn-km^2.
- **Type of braking:** Combination of mechanical and electrical braking.
- **Electrical braking:** Regenerative. Trains feed braking power into the railway line, if possible, after supplying the auxiliary consumption. If the rheostat voltage is reached, the power surplus is sent to rheostats. The rheostat voltage threshold has been set 10 V below the maximum line voltage (710/720 V).
- **Maximum traction power:** 3MW (approx.).
- **Maximum braking power:** 2MW (approx.).
- **Auxiliary consumption:** Although in general this parameter is variable, it has been modelled as a constant 200 kW load (200 kWh/h).

Figure 3-3 shows the equivalent electrical effort curves for the traction and the braking phases of the trains in the case-study, which represent the addition of the effort curves of each motor in the train. These curves, together with the efficiency model described in Section 2.2.1 are used to obtain the electrical power at the pantograph. In the case of the electrical braking curves, they are also useful to determine the blend of electrical and mechanical power. The rule implemented is to use all the available electrical braking and to complement the rest of the braking force required by means of the mechanical braking system.

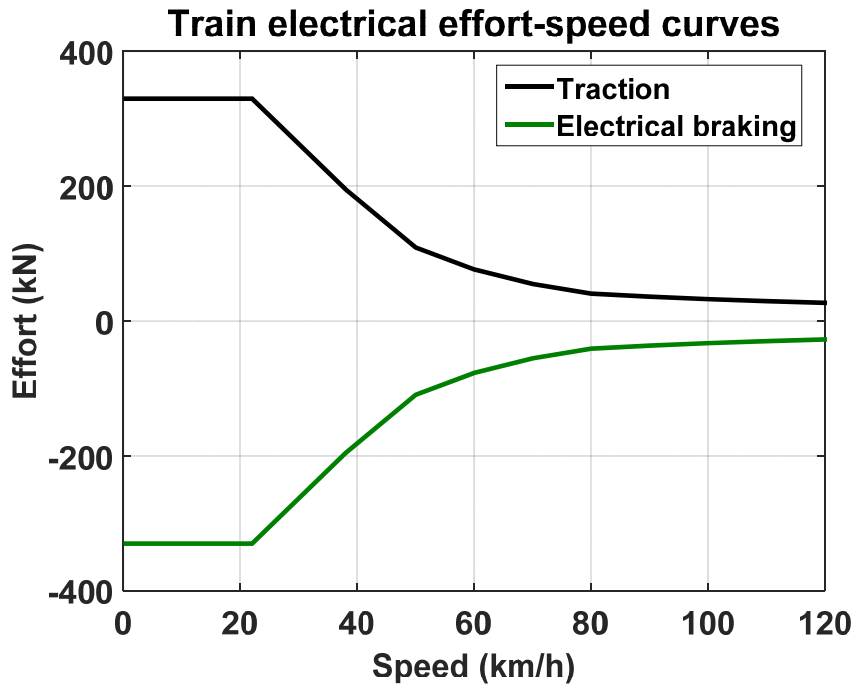

Figure 3-3. Electrical equivalent traction and braking curves of the trains in the case-study system.

Traction substations and passenger stations

There are eleven 600-V traction SSs in the line. All the SSs are connected to a 15 kV node of the utility grid. This node has been modelled to have a finite short-circuit power by adding a low series impedance to the slack node, which represents an infinite network. The value for this impedance given in (Tzeng, Wu 1995) has been selected: 1.2 + j1.8 Ω.

Then, the traction SSs in the case-study system are made up of a transformer and a diode rectifier. This system features six-pulse rectifiers at SSs, which simplifies the transformer secondary windings (only three low voltage AC terminals are required).

Table 3-1 presents the distribution of the passenger stations and the traction SSs along the line, and the main SS electrical characteristics. There are 23 passenger stations, 11 of which contain a traction SS.

All the SSs present 4.8 MVA transformers except SS1, which power rating is 2.4 MVA. In all cases, the short-circuit voltage and power are 9 % and 1 % respectively. SSs are connected to the catenary system by means of two feeders. This leads to a pair of connection points which are separated 0.2 km.

The normalised voltage of the line is 600 V. However, for historical low pantograph voltage problems, the transformer taps are used to set the no-load voltage of the SSs in the line to 640 V.

Table 3-1. Passenger stations and traction SSs in the line.

Passenger station	Position in the line (km)	Traction SS	Installed power (MVA)	Transformer Vsc-Psc (%)	Number of feeders

Passenger station	Position in the line (km)	Traction SS	Installed power (MVA)	Transformer Vsc-Psc (%)	Number of feeders
1	0.3	1	2.4	9-1	2
2	1.4				
3	2.4	2	4.8	9-1	2
4	3.4				
5	4.3				
6	4.9	3	4.8	9-1	2
7	5.7				
8	6.4	4	4.8	9-1	2
9	7.1				
10	7.8	5	4.8	9-1	2
11	8.5				
12	9.3	6	4.8	9-1	2
13	10.1	7	4.8	9-1	2
14	10.8				
15	11.7				
16	12.6	8	4.8	9-1	2
17	13.5				
18	14.4	9	4.8	9-1	2
19	15.3				
20	16.7	10	4.8	9-1	2
21	18.1				
22	18.6				
23	19.3	11	4.8	9-1	2

Figure 3-4 presents the distribution of passenger stations and SSs, together with the topographic characteristics of the line. The latter may have a significant influence in the system energy efficiency, as will be explained in Section 3.1.2.

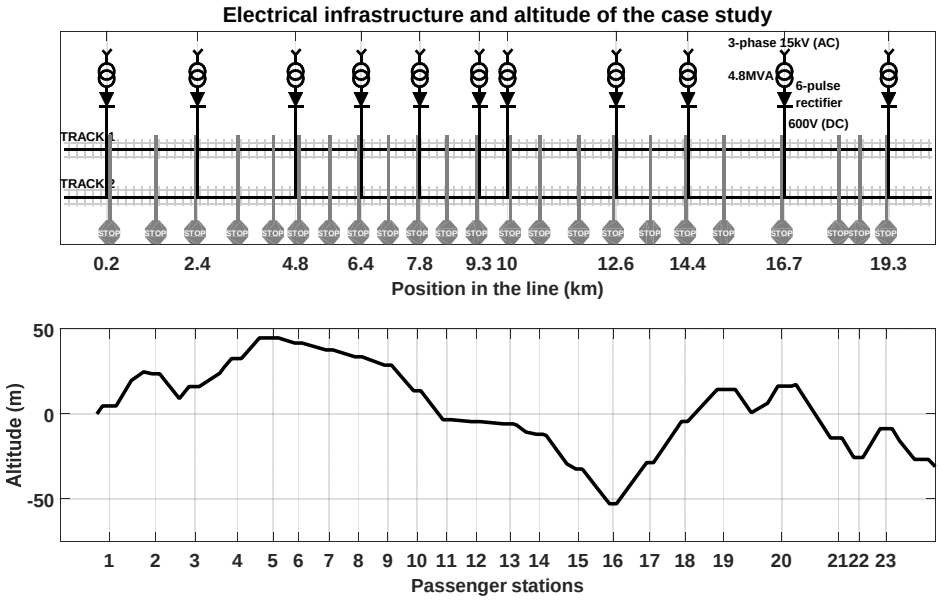

Figure 3-4. Case-study line. Passenger stations, SSs and topography.

Feeder and return circuits

There are two types of catenary systems in the case-study:

- Starting at the beginning of the line, between SS1 and SS2, there is a 1.3 km rigid-catenary stretch. This conductor's resistance equals 11.5 mΩ/km. The supply and return circuits are parallelised every 500 m.
- Then, from that point until the end of the line, the catenary system is made up of a 150-mm^2 copper catenary wire plus two 107-mm^2 copper contact wires. A 30 % wearing coefficient has been applied to contact wires. Therefore, for impedance calculations, the section used for these wires equals 75 mm^2.

Due to low pantograph voltage problems in the line, the latter stretch is reinforced by means of an auxiliary aluminium feeder. This feeder, which is laid in parallel with both tracks, consists of four 645-mm2 wires. A parallelisation point between the feeder and both-track catenary systems takes place every 100 m. Due to this high parallelisation frequency, in practical terms, trains make use of the catenary systems of both tracks. This improves dramatically the train voltage profiles with respect to the habitual approach where tracks are only parallelised at SSs.

For both tracks, traction currents return through both rails, which are isolated from the terrain. These are 54 kg/m rails which resistance per distance unit equals 29 mΩ/km/rail. Rails are only parallelised at SSs.

All the electrical sections in the line are connected (no isolators are open).

With this information, the lumped equivalent resistances, calculated as the addition of the equivalent resistance of the feeder and the return circuits, are:

- 26 mΩ/km for the stretch with rigid catenary system.
- 22.4 mΩ/km for the stretch with conventional catenary plus reinforcement feeder.

3.1.2. OPERATION

The trains in the line feature the Automatic Train Operation (ATO) system. The ATO consists in an automatic guidance system which generates the traction/braking commands for the motors to move the train between stations. This is made observing the maximum speed limits in the line. That leads to a speed profile which determines the energy consumption and the running time at each inter-station stretch. The study of the influence of these speed profiles in the system's efficiency is out of the scope of this thesis.

For this reason, among the several possibilities for these speed profiles (Dominguez, Fernandez et al. 2011), the minimum-running-time one has been used. This option is named the flat-out speed profile, and it has been selected because it renders the maximum running performances. It is, actually the habitual choice in MTS design studies.

The last piece of information required to generate the speed and power profiles is the maximum line speed (70 km/h) and the speed limitations. Figure 3-5 shows the power and speed profiles for each inter-station stretch and track. There is an additional plot which provides information about the track slopes in order to help understand the relations between the power and speed profiles in both tracks.

The speed limitations are not included in the graph for the sake of clarity. Nevertheless, they may be observed in the speed profiles in Figure 3-5 (e.g.: there is a 35 km/h speed limitation in the inter-station stretch 1-2). These are not necessarily the same for both tracks (e.g.: in the inter-station stretch 3-4, there is a 55 km/h limitation only for track 2, which is a downhill stretch).

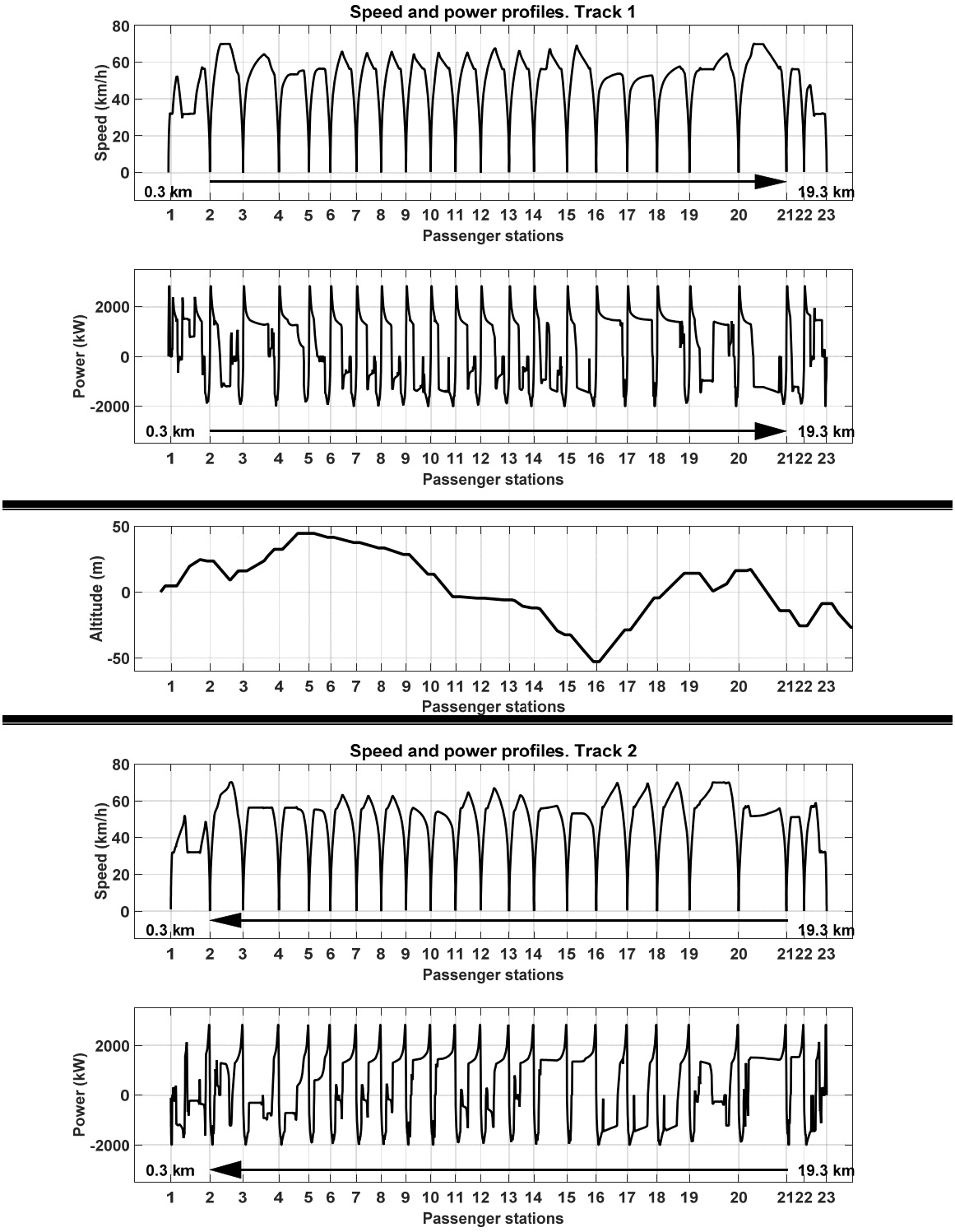

Figure 3-5. Track speed and power profiles in the case study line.

The combination of the power profiles and the SS connection points leads to strong and weak points in the line from the train voltage standpoint. Traction zones around passenger stations with no SS connection are the candidates to exhibit the lowest train voltages.

Figure 3-6 shows the train voltages in both tracks when a single train is running in the system. These results show how passenger stations in the middle of the long stretches between SSs (e.g. stations 4, 15 19, 21) are associated with the weakest zones in the line from the electrical standpoint. Then, in the actual operation of the system (with several trains), the combination of simultaneous motoring phases or the high average loads may make the train voltages reach even lower levels than those presented in Figure 3-6.

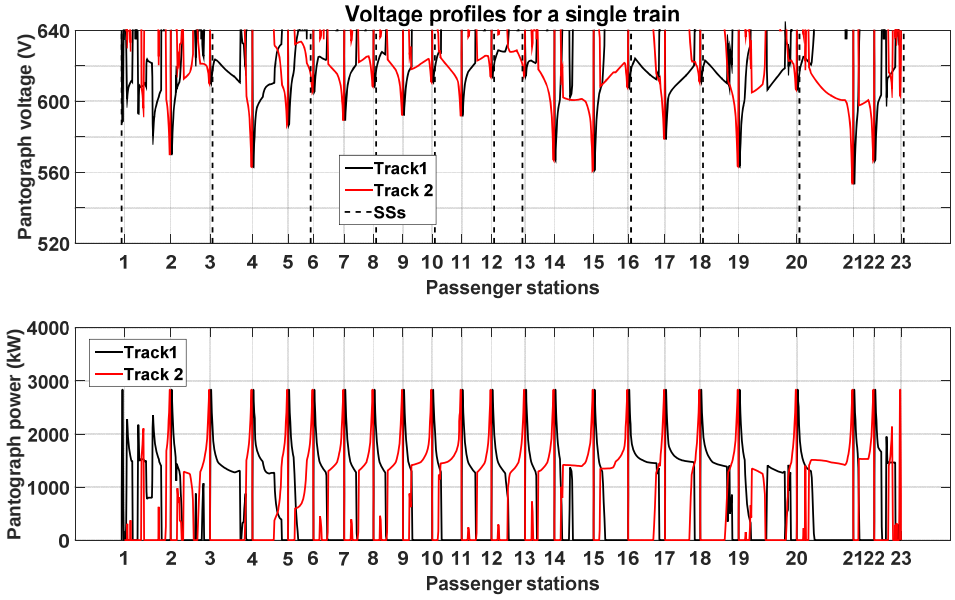

Figure 3-6. Single train voltage profiles for both tracks.

Another factor related to the system operation which has a strong influence in the results is the trains' auxiliary consumption. It must be noted that this consumption is not negligible in MTSs, due to the several systems that consume power on-board the trains (heating, air conditioning, automatisms, etc.). As already stated, the auxiliary consumption has been set to a constant average value of 200 kW (kWh/h). It has not been included in the power profiles shown in Figure 3-5.

Finally, it is obvious that the traffic density in the line influences the behaviour of the MTS from the energy point of view. For the obtainment of the most relevant energy consumption and loss figures in the case-study line, it is necessary to define the traffic in the line.

The traffic density has been expressed by means of the headway, which is defined as the time between two consecutive trains in a line. It is important to note that high traffic-density scenarios correspond to short headways and vice versa.

The classical approach in the infrastructure design studies to generate the traffic in MTSs consists of setting the dwell time at passenger stations to a fixed value, and to force trains at both terminal stations in the line to depart synchronously. Thus, this representation includes no influence of the stochastic conditions in the system. Therefore, the only parameter which changes the system behaviour is the headway

between trains. Under this scheme, the traffic behaviour in the line is periodic: there is a fixed pattern which period equals the headway. Letting the sampling time tend to zero, the use of this approach leads to a set of snapshots which accomplish that every point in the line is visited at least once, but only once. In other words, this fixed dwell time approach implies that in a headway-long time window, the final position of every train in the line coincides with the initial position of the train it is following.

The studies in this chapter are performed with this traffic approach. Then, the traffic model will be revisited in Chapter 4, where the effect of the traffic stochastic parameters on the MTS energy figures will be thoroughly assessed.

Consequently, the analysis of the system behaviour has been performed by simulating a period of time which equals the headway under study. The sampling time has been set to 1 s in all the studies in this thesis.

3.1.3. ENERGY-SAVING DEFINITIONS

The different developments in this thesis are oriented to obtain accurate energy-saving figures. Therefore, it will be required to assess the energy-saving error introduced by the modelling approaches proposed. To tackle this concern, this thesis defines two particular energy-saving accuracy tests: 1) the single RS test, and 2) the multiple RS test.

The single RS test

Provided they are the main current trend to improve MTS energy efficiency for their cost per MW and life cycle characteristics (Gelman 2013, Ibaiondo, Romo 2010), the energy-saving tests are based on the use of RSs. The single RS test consists of trying as many infrastructure improvement configurations as SSs are in the system. Each of these configurations is obtained by installing an RS in one of the available RS locations (SSs). Thus, in the case study in this thesis, 11 configurations will be used to obtain 11 energy-saving values by comparison with the raw system (no RSs installed) consumption.

The single RS test is useful to obtain the precision of the developments in the thesis for each particular available location in the system.

Figure 3-7 presents the power-voltage characteristic of the selected RSs. This curve has been designed to absorb the maximum power regenerated by the trains plus a certain margin at the maximum voltage in the line (720V).

Energy savings are calculated following (3.1). They can be obtained for a single snapshot or for any time period selected.

$$E\_SAVING_i = E\_CONSUMED_{Raw} - (E\_CONSUMED_{RS,i} - E\_RETURNED_{RS,i}) \quad (3.1)$$

Where,

- E_SAVING_i is the energy-saving value obtained when an RS is installed in SS *i*.

- $E\_CONSUMED_{Raw}$ represents the integral over the selected time period of the power delivered by all of the electrical SSs in the raw system (no RSs installed).
- $E\_CONSUMED_{RS,i}$ represents the integral over the selected time period of the power delivered by all of the electrical SSs in the system when it is modified by installing an RS in SS *i*.
- $E\_RETURNED_{RS,i}$ represents the integral over the selected time period of the power returned to the utility grid by the RS installed in SS *i*.

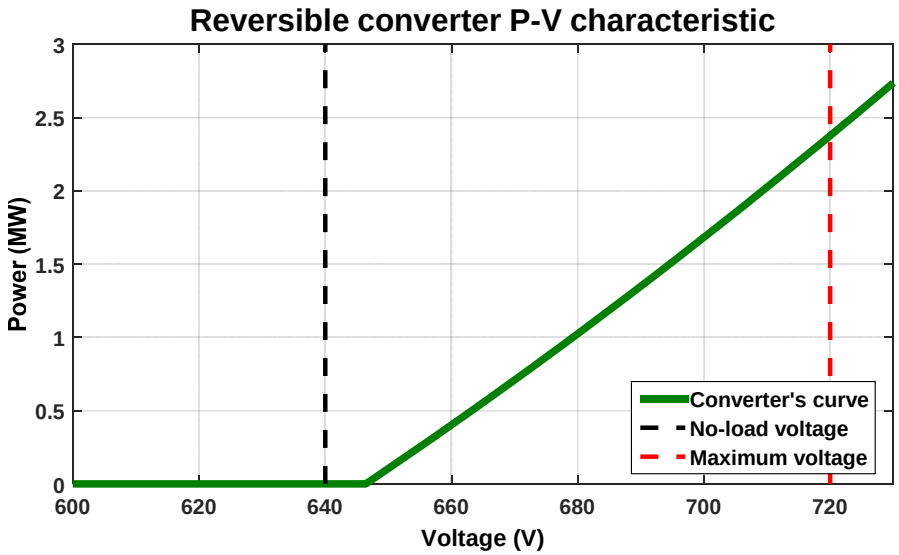

Figure 3-7. Power-voltage curve of the reversible converter used in the study.

With these tools, it is possible to define a validation test for the different analyses in the thesis. The validation test consists of making a comparison between the energy-saving results obtained with a model used as reference, and the results obtained with any of the modelling approaches presented in the thesis. This comparison yields an absolute signed error value which is defined in (3.2).

$$\varepsilon_{COMP} = E_{saving}^{COMP} - E_{saving}^{REF} \tag{3.2}$$

Where,

- E_{saving}^{REF} represents the energy savings used as reference to measure the accuracy of a certain modelling approach in the thesis.
- E_{saving}^{COMP} represents the energy savings obtained with the model that aims to be equivalent to the reference model.
- ε_{COMP} is the absolute error between both models.

Usually, a relative error figure where the absolute error is compared with a certain magnitude will be useful. However, this latter magnitude may differ between the different analyses in the thesis. It will therefore be defined each time relative error figures are presented.

The multiple RS test

The single RS test is useful to scan the available RS locations one by one. However, in general, it will not offer information about the accuracy when the energy savings are close to the maximum achievable savings. The main reason is that in practical terms, it is extremely difficult to remove all the rheostat losses from a single RS location (see Section 3.2.2).

It is therefore useful to have another energy-saving accuracy test that includes more complex infrastructure improvement. The multiple RS test takes advantage of the multiple RS configurations defined in Section 2.4.1 to measure the simulator robustness. Thus, it consists of 11 batches containing 10 infrastructure configuration samples each. Each RS configuration batch is characterised by the number of installed RSs in the system, which has been increased from 1 to 11. The position and size of the RSs have been selected at random. Table 2-2 (pg. 56) shows a selection of samples included in the multiple RS test.

Consequently, the multiple RS test is an extension of the single RS test which contains 110 infrastructure configurations with increasing complexity. The energy saving errors will nevertheless be obtained following (3.2), like for the single RS test.

3.2. ENERGY CONSUMPTION CONCERNS IN MASS TRANSYT SYSTEMS

As in any electric railway system, the supply system of MTSs is connected to the utility grid by means of several SSs placed along the line. These are basically made up of a step-down transformer plus an AC-DC converter.

Provided its robustness and simplicity, in the overwhelming majority of the DC-electrified railway systems, the latter stage of SSs consists in a diode rectifier, i.e. a one-quadrant converter which only allow power to flow from the utility network to the railway system.

This is enough when trains in the system are only designed to draw power from the supply system. However, many trains are nowadays equipped with regenerative braking. This kind of rolling stock is able to convert kinetic energy back into electrical energy during braking. If the intensity of the traffic in a given line is high (peak-hour), power regenerated by a braking train is likely to be absorbed by a powering one. If the traffic density is low, the probability of having no motoring trains nearby when a certain train brakes rises up. When this situation takes place –provided rectifiers do not allow power flows from the railway system to the utility grid– the regenerated power must be burnt in dedicated on-board resistors (rheostats). This is made to prevent the voltage in the feeder line from reaching hazardous levels. Consequently, there are situations where the DC network will be receptive to regenerated power and situations where it will not accept this energy.

This receptivity concept is one of the aspects to take into account in the design of energy-efficient speed profiles (Domínguez, Fernández-Cardador et al. 2010, Domínguez, Fernández-Cardador et al. 2008). Its expression is given in (3.4), after the main energy figures in MTSs have been presented.

3.2.1. ENERGY FLOW AND LOSS ANALYSIS

Figure 3-8 represents the general energy flows in DC-electrified MTSs, including trains that feature regenerative braking. This regenerative energy is fed back into the system and used again by other trains or by braking trains themselves for auxiliary equipment consumption. If trains are not equipped with regenerative braking, the green-coloured energy feedback will not take place, and the whole energy consumed by trains will be delivered by SS rectifiers.

The inputs and outputs regarding the fixed electrical infrastructure have been named with capital letters in Figure 3-8. The energy inputs are: 1) the energy delivered by SSs (RECTIFIED), and 2) the regenerated energy, defined as energy flowing from motors to the electrical side of the system from braking trains (REGENERATED). The energy outputs are: 1) the energy consumed by trains, defined as the CONSUMED BY TRAINS energy (TRAIN hereafter) in the system, which is broken down into traction and auxiliary-equipment energy (TRACTION & AUXILIARY SERVICES); 2) the energy wasted in rheostats when system is not receptive to regenerated energy (RHEOSTAT LOSSES); and 3) the energy losses in conductors (CONDUCTION LOSSES). It must be noted that

there are other outputs inside trains (energy losses), which are a fraction of the TRACTION energy.

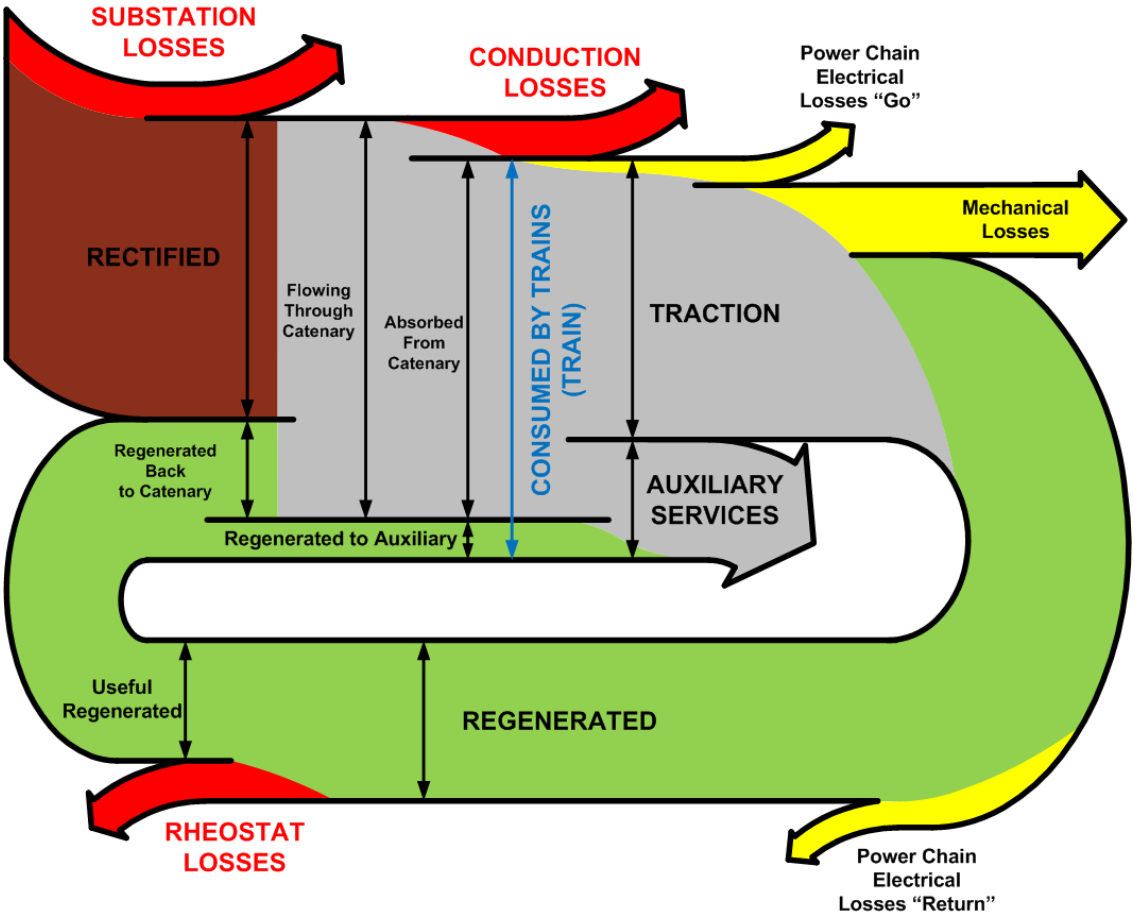

Figure 3-8. DC-electrified MTS Sankey diagram.

The power balance equation for the system determines the relations between these energies, which is given in (3.3). With these energy items, it is possible to define the system receptivity, which expression is given in (3.4).

$$E_{RECTIFIED} + E_{REGENERATED} = E_{TRACTION} + E_{AUXILIARY} + E_{CONDUCTION} + E_{RHEOSTAT} \quad (3.3)$$

$$Receptivity = 1 - \frac{E_{RHEOSTAT}}{E_{REGENERATED}} \quad (3.4)$$

If there are ESSs in the system, the diagram in Figure 3-8 should include a further non-conservative energy loop like the one which represents braking energy. The right-hand side of (3.3) should be complemented by two new terms which account for the amount of energy stored in these systems at the end of the integration period and for losses inside these systems both during the charging and discharging mode. The expression of the energy equation when the system includes ESSs is given in (3.5).

$$\begin{aligned} E_{RECTIFIED} + E_{REGENERATED} \\ = E_{TRACTION} + E_{AUXILIARY} + E_{CONDUCTION} + E_{RHEOSTAT} + E_{LOSS\_ESS} \\ + E_{STORED\_ESS} \end{aligned} \quad (3.5)$$

If there are RSs in the system, the diagram in Figure 3-8 should include an energy flow from the catenary system to the utility grid, with its associated losses. The representations with ESSs and RSs have been omitted for the sake of clarity.

The analysis of Figure 3-8 yields five energy-loss sources in the system, including both the electrical infrastructure and trains:

- **Train power chain losses**: This energy output collects commutation and conduction losses in train converters and motors, and losses in the mechanical transmission. It must be noted that these losses take place both when energy is flowing from the electrical to the mechanical side and vice versa.
  The expression for the calculation of these power losses is given in (2.2) (Section 2.2.1).
- **Mechanical losses**: Mainly losses due to the resistance to train movement ((2.1) in Section 2.2.1) and the fraction of kinetic energy which is dissipated in mechanical braking systems.
- **SS losses**: For each SS, the addition of the losses in the transformer and in the rectifier.
- **Conduction losses:** These are the ohmic losses in conductors. They are proportional to the impedance of conductors and to the square of currents. The expression for the calculation of these losses in an MTS with DC nodes from 1 to N is given in (3.6).

$$P_{CONDUCTION} = \sum_{i=1}^{N-1} \sum_{j>i}^{N} (V_i - V_j)^2 \cdot (-G_{ij}) \tag{3.6}$$

  Where, V_i, V_j are the voltages in nodes *i* and *j*; and G_{ij} represents the element *i*, *j* in the nodal conductance matrix. This matrix defines the electrical conductances between nodes.
- **Rheostat losses**: Energy sent to rheostats when the system is not receptive to regenerated power. It was stated in Section 2.2.1 that when a train's pantograph voltage reaches the rheostat braking threshold, it clamps this voltage. Therefore, the power injected to the catenary system is determined by the rest of elements in the circuit. The expression for the calculation of the rheostat losses in a braking train which regenerates a certain power is given in (3.7).

$$P_{RHEOSTAT} = P_{REGENERATED} - P_{AUXILIARY} - P_{ACCEPTED}; \quad (P_{RHEOSTAT} \geq 0) \tag{3.7}$$

  Where $P_{ACCEPTED}$ represents the amount of regenerated power which is accepted by the system.

The total amount of energy consumed by the system depends on many factors. In underground systems, the maximum line speeds are low in comparison to those of high speed systems, and the number of passenger stations per kilometre is high. In this scenario, factors such as the train weight, the track topography, the speed profiles or the auxiliary equipment consumption become critical issues.

Once all these parameters are defined, the efficiency of the system from the energy standpoint is determined by the five loss sources previously listed. The first and second items in the list represent losses linked to trains. They may be reduced by improving the design of the rolling stock. The third, four and fifth items in the list may be regarded as system losses. They are subject to be reduced, or even minimised, by making the electrification system more efficient. The diagram in Figure 3-8 shows that for a fixed amount of train energy, the system energy consumption becomes minimum when the sum of the system-level losses is minimum and the regenerated energy is maximum.

This thesis focuses on system-level techniques (electrical infrastructure) which aim to reduce conduction and especially rheostat losses. The effect of these techniques on SS losses is indirect, and it tends to be limited. For this reason, and provided this chapter aims to gain insight on the particularities of the energy exchanges inside the MTS, SS losses have not been included in the loss analysis. However, they are, of course, included in the most relevant energy-saving calculations in the rest of chapters. Losses due to the rolling stock design are included in the calculations, but they will not be analysed in depth in this thesis.

The study of the specific figures for the system losses is highly influenced by the average number of trains running on the tracks. It must be noted that this is not a fixed parameter in MTSs, since operators respond to the different affluence of passengers along the day by varying the traffic density. Therefore, the usual approach for the loss study consists of analysing the most relevant system figures for different traffic densities.

To perform this system-loss study, several different headways have been included to carry out a traffic density scan analysis. The dwell times at passenger stations have been set to 30 s, without any stochastic variation.

For their special relevance, two different cases have been analysed in this study: 1) the base case, where trains do not feature any type of electrical braking; and 2) the regenerative train case. This will help assess the importance of this train characteristic from the system energy efficiency standpoint.

Figure 3-9 presents the results of the traffic density scan analysis applied to the case-study system. The energy consumption in SSs (RECTIFIED) and the TRAIN energy have been represented in the left-side graph, whereas the system losses, i.e. conduction and rheostat losses; have been plotted in the right-side graph.

Figure 3-9.a shows a steady decrease in the SS consumption and train energy for increasing headways. Obviously, as the number of trains running on the line increases, more energy is consumed in the SSs. The black curve represents the train energy. It is the same for the base case and for the regenerative train case. It is close to energy in SSs for the base case due to the good energy efficiency in the system. When regenerative braking is introduced, energy in SSs is lower than the train energy, which is due to the fact that a fraction of traction energy is reused in the system.

The curves in this graph are useful to assess the total amount of energy consumed at each traffic density scenario. In addition, the slope of this curve is an interesting magnitude, since it represents the energy-consumption increase associated with a traffic-density increase, i.e. its marginal energy cost.

The analysis of Figure 3-9.b yields some interesting results. First, with regard to conduction losses, it may be observed that they are very high for high traffic densities. Then, as traffic density decreases, conduction losses drop steadily in both cases, presenting a downward trend quite similar to that in SS consumption. They tend to be rather lower than rheostat losses for long headways.

The base case exhibits lower conduction losses than the regenerative train case. This is an interesting result, which means that the average distance between power generation (braking trains and SSs) and power consumption (powering trains) centres in the system decreases when trains are not allowed to regenerate. It may be indeed observed how the two conduction loss curves tend to converge for short headways. In strong networks which are able to drive very high traffic densities, these two curves could intersect each other (López-López, Pecharromán et al. 2014).

Then, with regard to rheostat losses, Figure 3-9.b shows that, of course, they do not take place for the base case. In the regenerative train case, rheostat losses take place from the shortest headway under study. From 4 minute to 8 minute headway, both system losses are in the same range. Then, rheostat losses become dominant with respect to conduction losses for long headways.

There is a singular result for 5 minute headway, which is associated with the particular characteristics of the single traffic scenario studied. This must not be interpreted as a special effect of this particular traffic density. The dependency of the MTS electrical variables on the characteristics of the traffic in the line will be thoroughly studied in Chapter 4.

There are no clear increase or decrease trends in rheostat losses with the headway. However, it must be noted that as the headway is increased, the total amount of regenerated energy decreases steadily. Thus, the constant absolute rheostat loss values express a gradual decrease of system receptivity for long headways.

This may be better observed in the bottom-side graphs: Figure 3-9.c and Figure 3-9.d. These graphs give convenient energy figures, which are made relative to a single train and to a length unit (km). Regarding Figure 3-9.c, it is interesting to note that the train energy is constant for all the headways. The base case consumption figures are the result of the addition of the train energy and the conduction losses represented in Figure 3-9.d. The regenerative-train case exhibits improved relative consumption figures, being the values for short headways clearly lower than the values for the long ones.

The constant absolute rheostat loss values observed in Figure 3-9.b are transformed into a linear-wise increase trend when they are made relative to trains and length, as may be observed in Figure 3-9.d. The shape of this relative rheostat-loss increase

curve is similar to the one obtained for the relative consumption figures, which suggest that the system energy-efficiency is strongly influenced by rheostat losses.

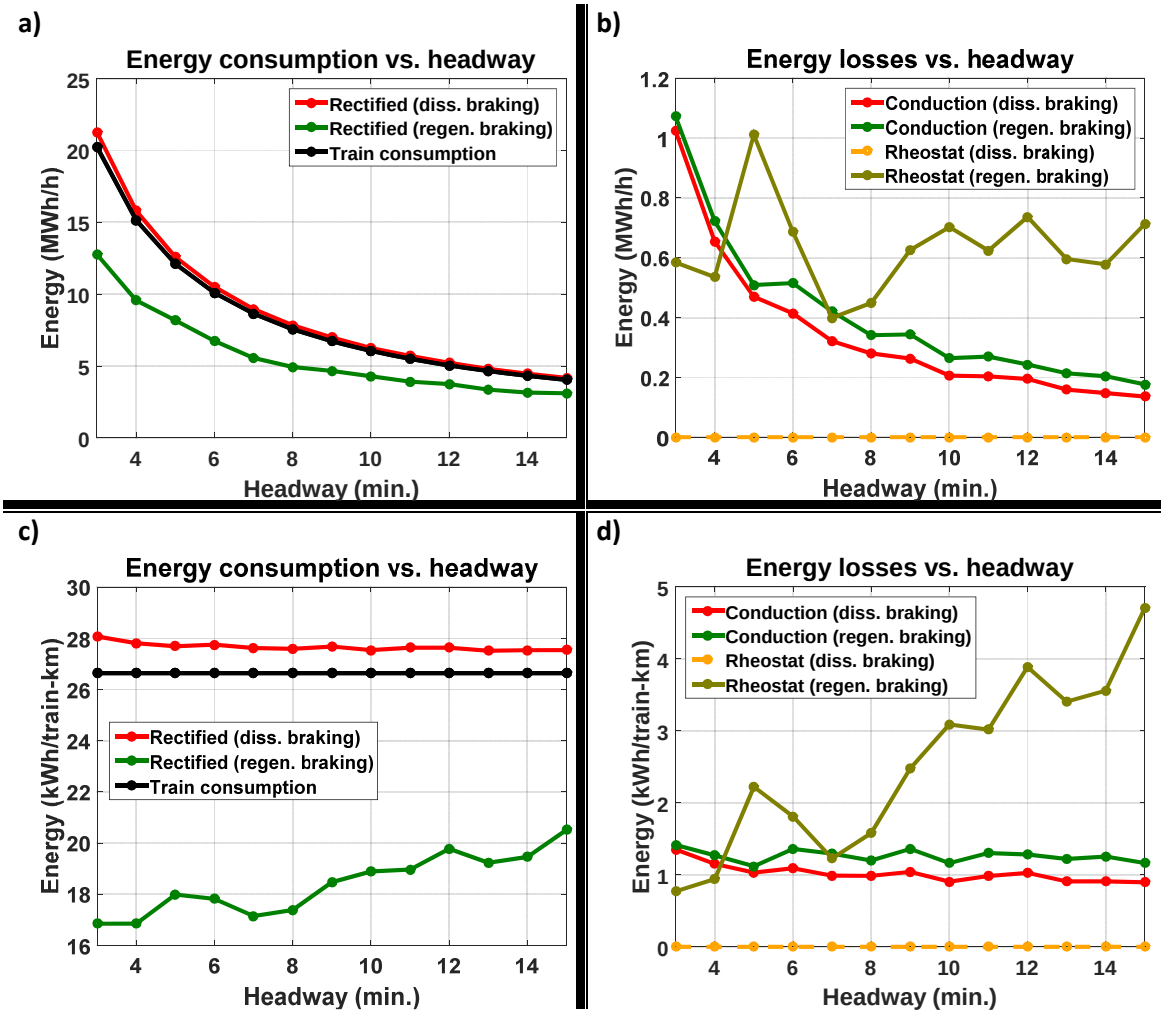

Figure 3-9. Energy figures for different headways.

The relative rheostat-loss linear-wise trend is replicated when receptivity is analysed. Figure 3-10.a shows a large receptivity span between the longest and the shortest headways studied. This is the general situation in DC-electrified railway systems, where the likelihood of having powering trains close to braking trains rises for short operation headways.

Figure 3-10.b confirms the strong correlation between rheostat losses and the relative energy consumption. The Pearson correlation coefficient obtained for these two variables equals -0.9975. With the result of the linear regression presented in Figure 3-10.b, it may be derived that a 0.1 increase in the system receptivity would lead to 1.16 kWh/train-km reduction in the relative energy consumption. This represents 4.3 % of the total train energy.

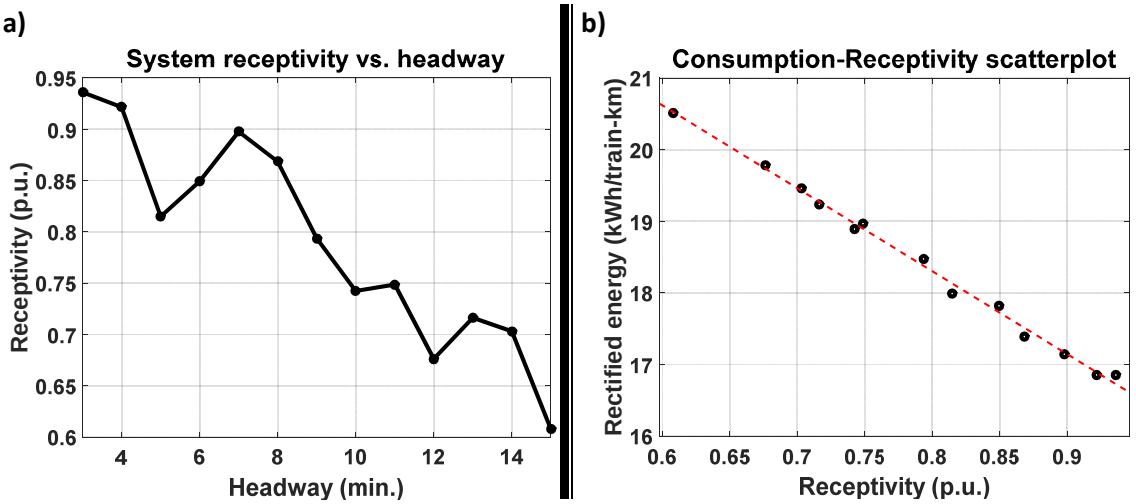

Figure 3-10. System receptivity analysis.

To summarise the results of this headway scan analysis, Table 3-2 presents the main energy figures obtained for a set of equally-spaced headways. The results have been made relative to the train energy per train and kilometre. As observed in Figure 3-9.c (black curve), this energy figure is the same for both type-of-train cases, and it is constant for all the headways. Consequently, as an example to illustrate the way to interpret the results in Table 3-2, the value 0.45 in the row for the regenerated energy in the regenerative-braking case means that trains regenerate 45 % of the energy that they consume for traction and auxiliary-service purposes. This result is the same for all the headways under study.

The most relevant conclusions after inspecting the relative losses presented in Table 3-2 are:

- Regarding the rectified energy, the base case system requires less energy per unit of train energy for long headways (although slightly). The regenerative train case exhibits the opposite trend. This is due to the system receptivity decrease for long headways, which results to be dominant with respect to the conduction loss decrease.
- Due to the cyclic characteristics of the regular traffic in this analysis, the relative energy regeneration is constant. It represents 45 % of the train energy. This figure may be increased by improving the train efficiency and the fraction of regenerative braking in the braking blend. It determines the energy-saving potential derived from regenerative braking.
- In the base case, the conduction losses are lower for long headways than those for short headways. This is an expression of the decrease in the average system load.
- In the regenerative train case, the variation in the system load flow due to the introduction of the braking power makes this relative conduction loss for short headways even smaller.
- The biggest span in the relative losses is observed for the rheostat ones. The amount of energy sent to rheostats during the 3-minute headway operation represents 3 % of the train energy, whereas for the 15-minute case, this figure rises to nearly 20 %.

Table 3-2. Relative energy figures with respect to the train energy.

		3 MIN	7 MIN	11 MIN	15 MIN
RECTIFIED	**BASE**	1.051	1.037	1.037	1.034
	REGEN.	0.631	0.644	0.712	0.77
REGENERATED	**BASE**	0	0	0	0
	REGEN.	0.45	0.45	0.45	0.45
CONDUCTION	**BASE**	0.051	0.037	0.037	0.034
	REGEN.	0.053	0.049	0.049	0.044
RHEOSTAT	**BASE**	0	0	0	0
	REGEN	0.029	0.046	0.113	0.177

To continue with the analysis of the MTS energy efficiency, Figure 3-11 presents the percent reduction in the rectified energy derived from the inclusion of regenerative trains. The results have been made relative to the energy consumption in SSs for the base case. The percent reduction in the SS energy consumption is close to 40 % for short headways. Then, even after a dramatic decrease in the system receptivity, the results for long headways are still higher than 25 %.

Figure 3-11 includes another curve which presents the maximum achievable energy savings. This last result has been obtained by adding the relative rheostat losses to the relative savings. These potential savings would be achieved if the rheostat losses were completely eliminated from the system.

The potential saving curve does not include the increase in the conduction losses derived from the increased average distance between generation and consumption points. It must thus be noted that this maximum energy savings curve is approximated. Nevertheless, the differences in the conduction loss figures for both type-of-train cases have shown to be small, so no large deviations from the potential savings curve are expected.

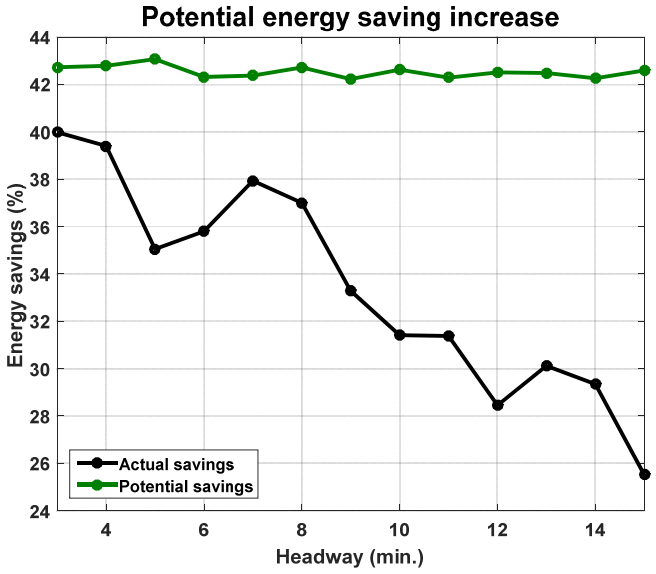

Figure 3-11. Consumption reduction and remaining reduction potential.

After this study on the energy figures in MTSs from the electrical infrastructure standpoint, the main conclusions are:

- With the train electrical-braking curves in this case-study, the energy regenerated by trains accounts for 45 % of the total train energy. This value strongly influences the potential energy savings derived from the inclusion of regenerative braking.
- There is a clear tendency of the system to exhibit high receptivity figures for short headways, and low receptivity values for long headways.
- Regenerative trains change the load flows in the system. Specifically, for the habitual headways and distances between SSs, they increase the average distance between the generation and the consumption points in the system. As a consequence, the conduction losses are increased. However, the results in this study show that the magnitude of this increase is not especially relevant from the energy efficiency standpoint.
- As the traffic density in the line is decreased, the system's ability to absorb regenerative braking drops steadily. If this problem is fixed, the general reduction in the system energy consumption may be extended to nearly the total amount of regenerated energy for all headways.

3.2.2. RHEOSTAT-LOSS REDUCTION MECHANISMS

The results in Section 3.2.1 show that the reduction of rheostat losses plays a pivotal role in the system energy efficiency, especially for long headways.

The origin of rheostat losses is the maximum allowed line voltage. Braking trains usually hit this voltage threshold when there is a lack of power consumption in their environment. The main strategies to reduce the amount of energy sent to rheostats are based on absorbing regenerative power when it is excessive, or increasing the voltage gap for regeneration. More details on this latter strategy will be given in Section 3.3.1 when the effect of the SS no-load voltage on energy consumption is described.

Figure 3-12 illustrates the main rheostat-loss reduction mechanisms that may be identified in a DC-electrified MTS. To assist the presentation of these mechanisms, this study makes use of RSs, which increase receptivity by accepting power flows from the catenary system to the utility grid.

All the three graphs in the figure (a-c) are in turn made up of two graphs. At the top side one, trains are represented by three bars meaning the regenerated power and the rheostat losses before and after introducing an RS into the system (generator criterion). Then, SS power is represented by stems following the load criterion. For each train load-regeneration profile used, only one RS has been placed in the most advantageous position to describe the rheostat reduction process. In the bottom side graph, the variation in the snapshot voltage profile is shown.

Three qualitatively-different rheostat reduction mechanisms may be identified in an MTS:

a) Direct rheostat reduction method without affecting the snapshot load flow. The RS is placed in a branch where no current is flowing. This case is illustrated in Figure 3-12.a. It corresponds to the terminal positions of the line or to any position between two consecutive rheostat braking trains. As far as rheostat losses are not totally eliminated, no variations in the load flow for the rest of the circuit will take place. The energy saving in this case will be the rheostat loss reduction minus the conduction losses and multiplied by the efficiency of the RS converter.

b) Direct rheostat reduction method changing the snapshot load flow. The RS is placed in a power exchange path. This case is illustrated in Figure 3-12.b, where the RS is situated between a rheostat braking train and a motoring train. The absorption of additional braking power at the RS decreases the rheostat losses. However, the voltage reduction at the RS location changes the load flow making SS6 and SS7 to supply more power to the motoring train close to SS7 than in the case without RS. Consequently, a fraction of the RS absorbed energy will not be translated into energy savings.

c) Indirect rheostat-reduction mechanism. The case leading to remarkable rheostat loss decrease and energy savings is shown in Figure 3-12.c. This is an indirect means of reducing rheostat losses: the RS absorbs regenerative power from a train which is not presenting rheostat losses. This changes the snapshot power flow, and will result in a net decrease of the power delivered by SSs only if the power removed by the RS is supplied by a rheostat braking train. It must be noted that for this to take place, it is important that no SSs are delivering power between the RS location and the rheostat braking trains in the original load flow. It can be observed in Figure 3-12.c how SS9, which is in *ON* mode, supplies nearly all the power required from the right side. This makes it very difficult to reduce rheostat losses from this SS to the right. *ON*-mode SSs may be considered as decoupling elements: from them on, no remarkable rheostat loss decrease is expected. This phenomenon implies that it is impossible to eliminate all the rheostat losses in the system from a single RS location.

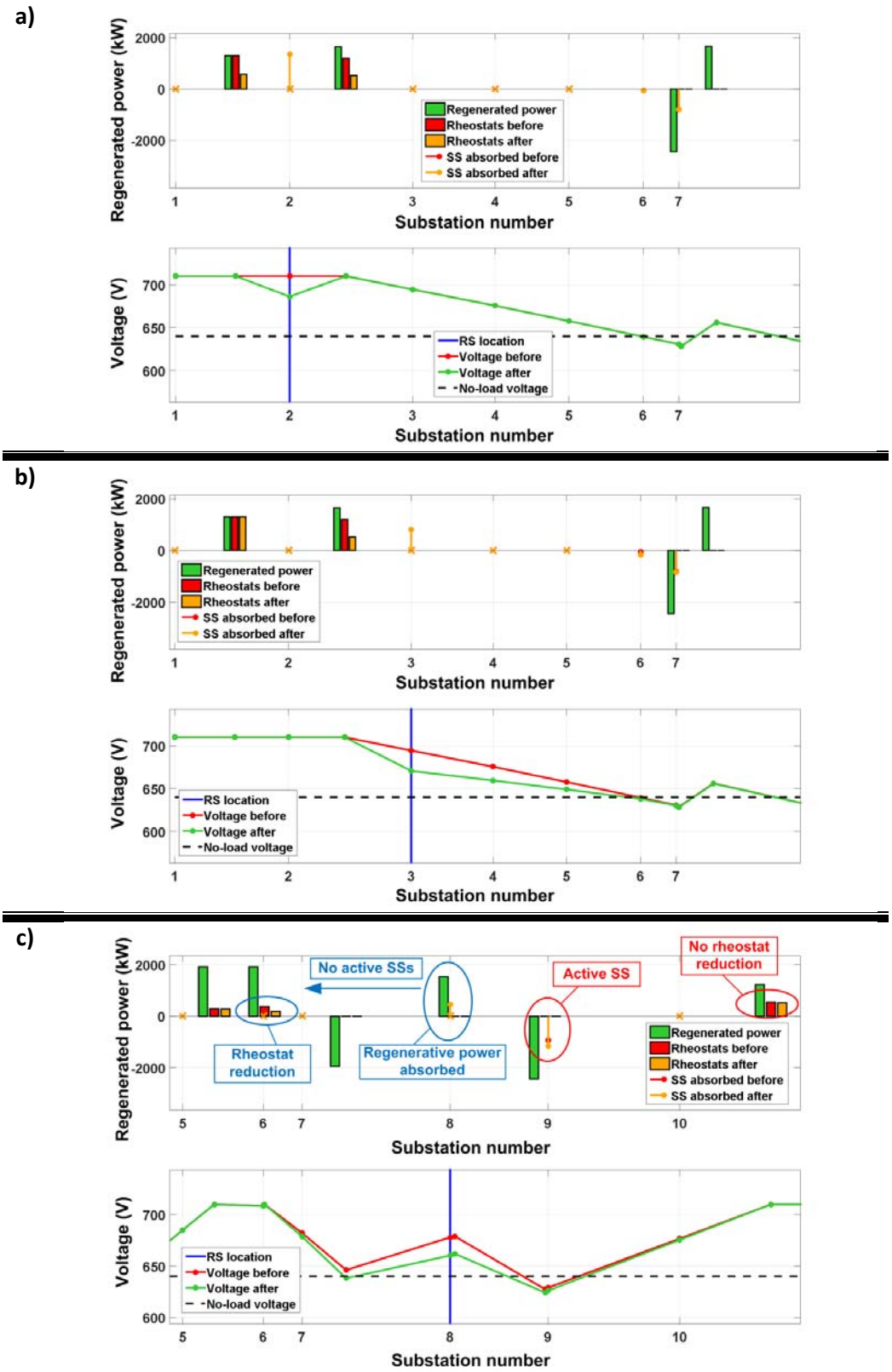

Figure 3-12. Rheostat reduction mechanisms

3.3. INFRASTRUCTURE IMPROVEMENT OPTIONS

Once the study of the MTS energy efficiency has revealed that there is room to improve, it is necessary to define how this energy efficiency improvement may be attained. Nowadays, there are several well known techniques which can be applied to enhance the electrical infrastructure of MTSs. Some of them are mainly oriented to reduce conduction losses, whereas there are other techniques which specifically aim to increase the system receptivity.

This section is devoted to present the most common infrastructure improvement options, making a clear distinction between those ones which may be implemented without incurring a large expense, and those which require a high amount of investment.

3.3.1. LOW-INVESTMENT TECHNIQUES

This group of energy-saving techniques consist of making a more efficient use of the existing infrastructure. They are mainly based on reducing the voltage drops and on the variation of the average train voltages.

The three most common measures are: 1) the electrical segment connection, which makes it possible to parallelise electrical SSs, thus reducing voltage drops; 2) no-load voltage tuning, which affects both conduction and rheostat losses and; 3) SS shutdown, which under low traffic-density conditions may make it possible to increase the energy efficiency.

Whereas the use of the first technique is widespread nowadays, there is little research conducted on the effects of no-load voltage and SS shutdown. The latter is, actually, barely applied. Regarding the no-load voltage tuning, operators tend to fix it to a safe value that make protection triggering for low train voltage unlikely to take place.

Electrical segment connection

For some practical concerns, the operation of MTSs was formerly carried out by implementing an electrical segmentation of the feeder line. With this operation scheme, each SS supplies a single electrical segment. This leads to a radial load flow where trains consume power from a single point.

However, this practice reduces dramatically system receptivity to regenerative braking and leads to a weaker network in train voltage terms. Indeed, the removal of the line segmentation in the actual system represented by the case study led to a notable improvement in the train pantograph voltage profiles of this line.

Nowadays, the overwhelming majority of DC-electrified railway systems are operated without line segmentation. For this reason, the analyses in this thesis do not take into account the effect of line segmentation.

No-load voltage

Once the electrification voltage level is decided, the no-load voltage of SSs may be modified by varying the positions of the transformer taps. Actually, the 600 V case-study line is commonly operated at 640 V no-load voltage.

There are two main implications derived from increasing the SS no-load voltage. On the one hand, it helps to reduce the average currents for a fixed consumed power. Thus, it reduces voltage drops and thus the likelihood of having protection triggering for low train voltage events decreases steadily. This current reduction is, of course, associated with a reduction in the conduction losses. Figure 3-13 depicts the benefits derived from the average line voltage increase associated with higher no-load voltages.

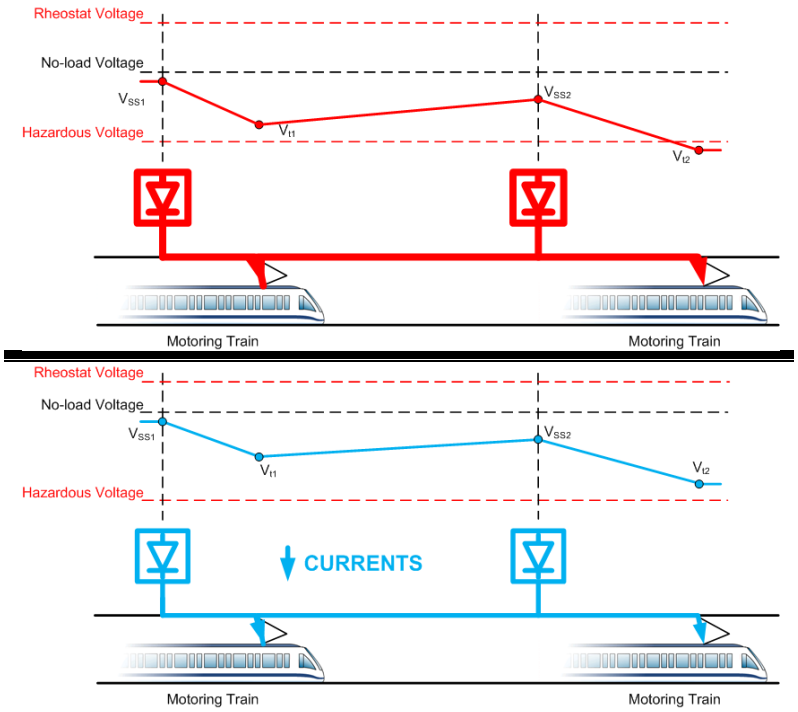

Figure 3-13. High no-load voltage pros.

On the other hand, high no-load voltage operation decreases the voltage gap for trains to regenerate power, i.e., train voltages are closer to the maximum allowed voltage level (720 V in 600 V systems). This brings forward the need for sending energy to rheostats during braking. Figure 3-14 illustrates the receptivity reduction effect of using high no-load voltages. The top-side graph shows a simplified situation with two trains where a braking train regenerates exactly the power consumed by a motoring train plus conduction losses. The no-load voltage is set to a low level that inhibits the activation of the SS between both trains. However, if the no-load voltage is set to a high level, the load flow will change.

The bottom-side graph in Figure 3-14 shows the effect of the no-load voltage increase. Now, the SS between the trains is no longer inhibited, and the power that it supplies will necessarily make the braking train send a fraction of its regenerative power to rheostats. Consequently, it may be derived that in those situations where braking

trains would be able to feed all the motoring trains in the system without rheostat losses, the best option is that SSs do not supply any power. This concept has inspired some energy-saving operation approaches like the SS shutdown, which will be presented in this section.

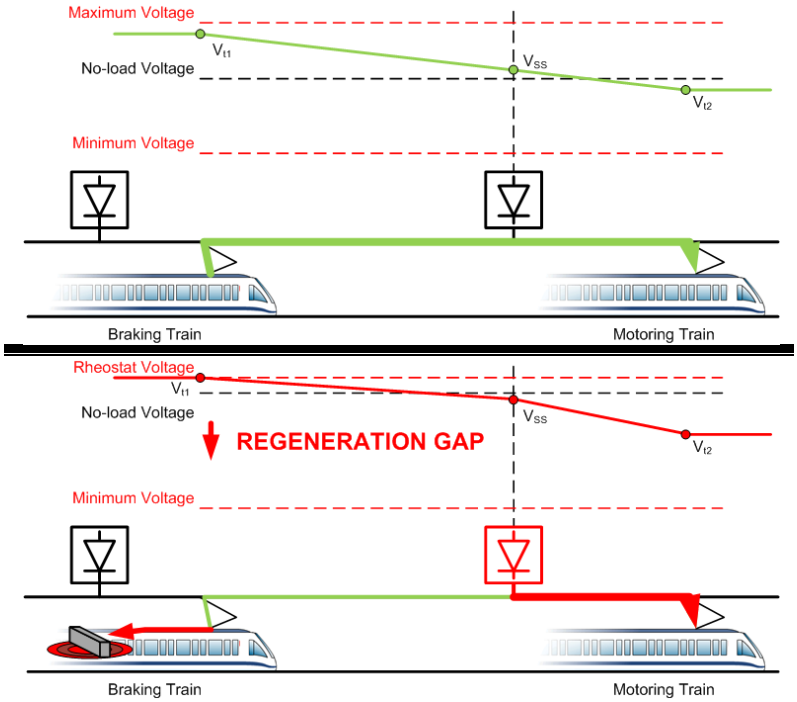

Figure 3-14. High no-load voltage cons.

It should be noted that, following this reasoning, in systems where train voltages remain fairly high in the worst-case traffic scenarios, setting the no-load voltage to values below the nominal voltage may be interesting to increase system receptivity.

Obviously, this technique has very low associated costs. It must indeed be regarded as an efficient operation of the electrical infrastructure. However, the optimum no-load voltage is not straightforward to be determined, since there is a clear trade-off between the safe operation plus conduction loss reduction for high no-load voltages and the receptivity increase for the low ones.

There are few references in the related literature dealing with the effect of the SS no-load voltage on the MTS energy efficiency (López-López, Abrahamsson et al. 2014, Açikbas, Soÿlemez 2010). For this reason, a study of the effect of this parameter, together with a variable no-load voltage approach, has been included in this thesis.

This study consists in an extension of the headway scan analysis in Section 3.2.1. For each headway, the no-load voltage at SSs has been varied from 580 to 690 V with a 10 V step. Then, the effect on the system losses has been measured.

Figure 3-15 shows the evolution of conduction and rheostat losses for four equally-spaced operation headways. The figure also shows the addition of these two variables and the no-load voltage that leads to minimum system losses. It must be noted that maximum energy efficiency corresponds to this minimum system-loss point.

It can be observed how the optimum no-load voltage decreases for long headways. This is due to the smaller influence of conduction losses in these low traffic densities, which makes the reduction in rheostat losses to be dominant.

The optimum no-load voltage point takes place in a relatively flat zone for all the headways. This means that selecting no-load voltages close to the optimum point will not spoil the energy consumption result significantly. However, there is a steep zone for high no-load voltages in all the cases except the 15-minute one. Consequently, it may be deduced that the high no-load voltage operation of the case study system is a disadvantageous approach from the energy efficiency standpoint.

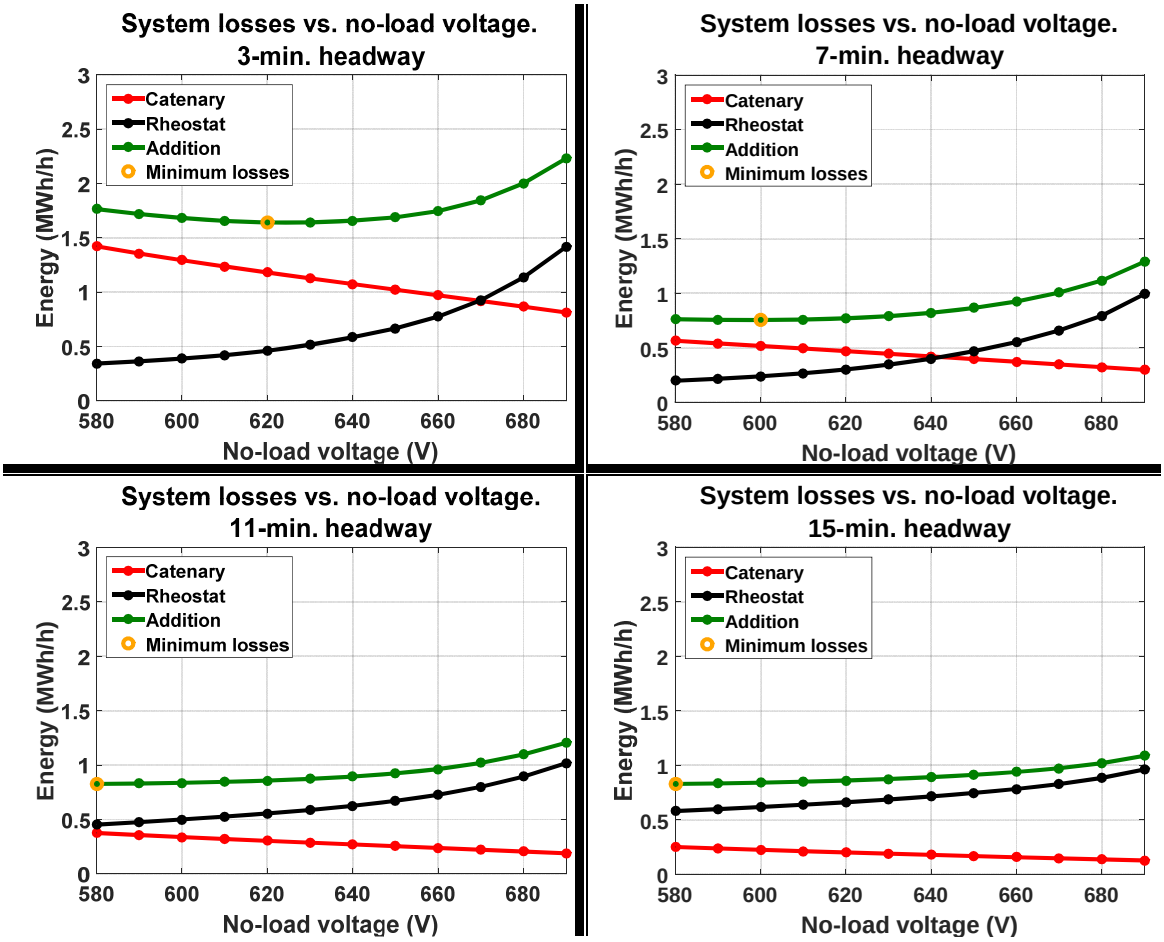

Figure 3-15. Effect of the no load voltage on the system losses.

The relative increase in system losses with respect to the optimum no-load voltage point is shown in Figure 3-16. Only the 3-minute headway case presents a clear increase in system losses for voltages lower than the optimum. Then, the 7-minute headway appears as the case with the highest relative loss increase for high no-load voltages. The 640 V point, which is the one for the actual operation of the system is not a bad solution. However, for all the headways except the 3-minute case, the increase in system losses for this no-load voltage value is close to 10 %.

It must be noted that this latter analysis does not represent a search for the optimum no-load voltage, but an assessment of the way this variable affects the system losses.

From these energy results, a set of optimum no-load voltages can be obtained for the different traffic densities. However, as presented in the bottom-side graph in Figure 3-13, the no-load voltage tuning may lead to hazardous train voltages if it is set to low values. Consequently, the energy consumption study must be complemented with an analysis of the system minimum train voltage.

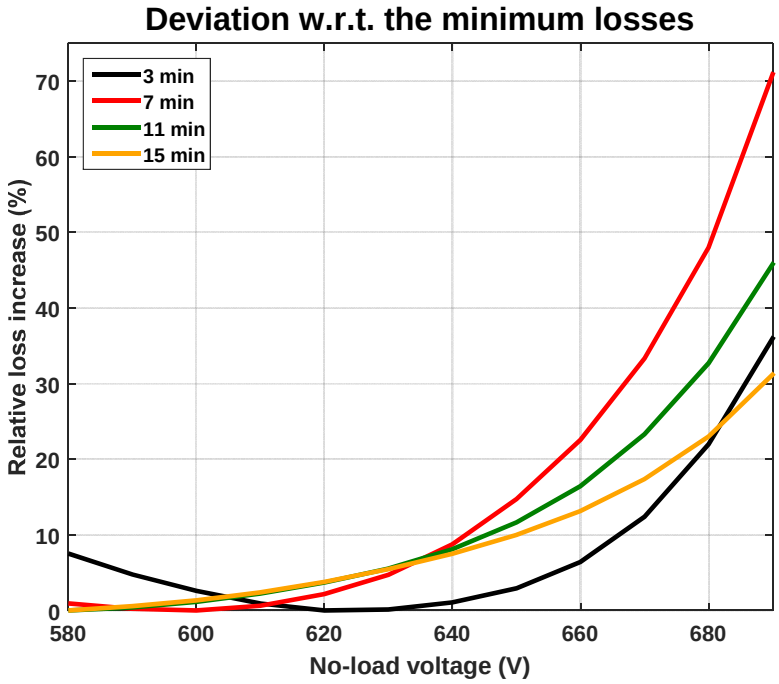

Figure 3-16. System loss increase for different headways and no-load voltages.

The minimum train voltage allowed has been set to 70 % of the nominal voltage of the electrification, i.e. 420 V. It must be noted that the minimum voltage in the applicable normative (EN 50163 2004) is 400 V. However, in informal conversations, MTS operators declare that voltages lower than 70 % of the nominal voltage are regarded as unsafe, and therefore train traction is limited when this threshold is hit. This reinforces the necessity of including voltage in the no-load voltage tuning study, since traction reduction is something to be avoided in MTS operation.

Figure 3-17 shows the results of this minimum voltage analysis. All the no-load voltage configurations for all headways are presented. Configurations which hit the minimum allowed voltage are marked in red. The study has been completed with two additional curves: 1) a curve showing the minimum train voltage for the actual no-load voltage operation of the system (640 V); and 2) a line representing the trend of the average minimum train voltage.

The latter curve shows, as expected, an increase trend of the minimum train voltage as the traffic density is reduced. However, it can be observed how, for instance, the 12-minute case exhibits worse minimum voltage results than the 5-minute case. This result reinforces the idea, presented in Section 3.2.1, that there is a significant effect of the particularities of the traffic used in the MTS study on the results obtained.

The green curve in Figure 3-17 proves that the actual no-load voltage selected for the operation of this system is a safe value from the minimum train-voltage standpoint.

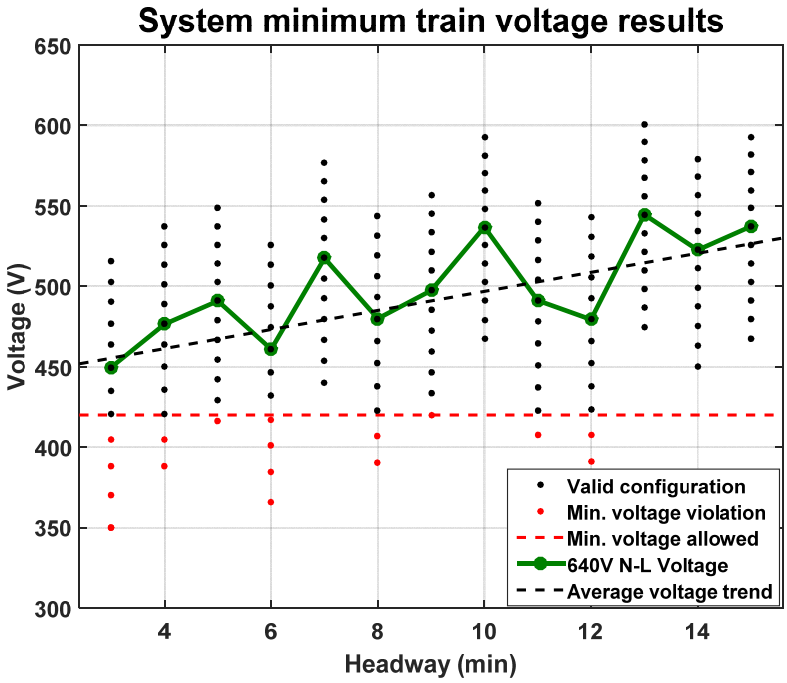

Figure 3-17. System minimum-voltage analysis.

For some traffic densities, the optimum no-load voltage from the system loss standpoint leads to hazardous train voltages. This must be corrected by increasing this optimum voltage to the first value that accomplishes the minimum voltage restriction imposed. Figure 3-18.a shows, in black, the optimum no-load voltages after including the minimum train voltage restriction. In red, the conflictive cases and the no-load voltages when only losses are taken into account.

Then, Figure 3-18.b shows the variation in the deviation from the optimum losses after the inclusion of the minimum voltage analysis. The only changes with respect to the situation before the minimum voltage restrictions are: 1) the no-load voltage for the 11-minute case has been increased to 590, which modifies this curve slightly; and 2) no-load voltages below 620 V for the 3-minute case and 590 V for the 11-minute case are forbidden.

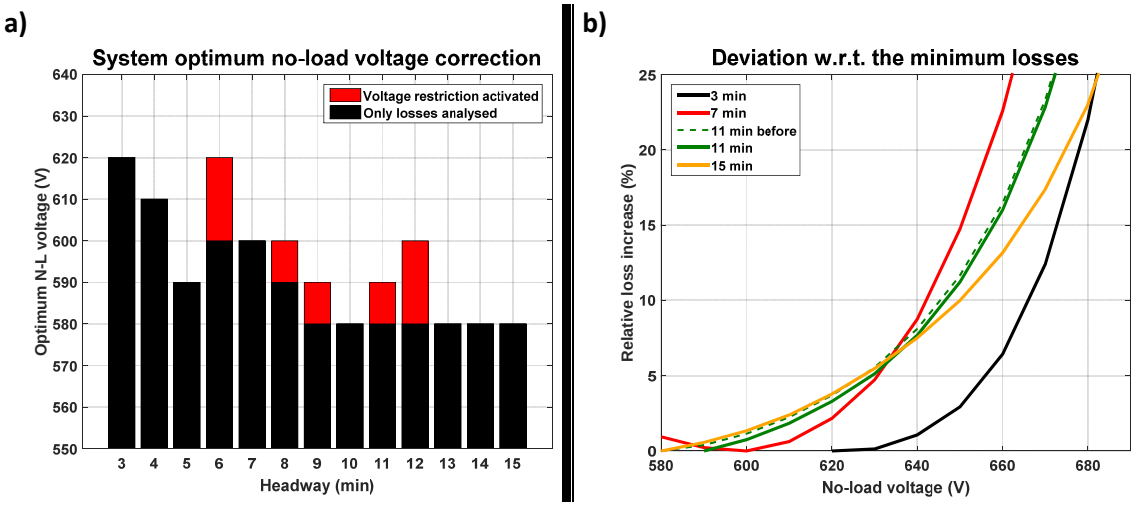

Figure 3-18. Optimum no-load voltage correction after the inclusion of the minimum train voltage restriction & change in the system loss deviation from the optimum point.

Once the results for the different operation headways have been analysed, it is time to present some results on the achievable energy consumption –and so economic– savings. To do that, it is necessary to define some weighting rule between the operation headways to generate a weekly MTS operation table. This will make it possible to obtain annual energy savings by extrapolation.

Since the case-study system is operated at 4-minute headway in the peak time, the 3-minute case has not been included in the analysis. Then, the 7-minute headway has been selected to represent the off-peak operation of the system. Finally, the 15-minute case has been used for the initial and final operation hours. Figure 3-19 presents the specific operation timetable for working and ferial days. This headway distribution leads to the weekly operation hours presented in Table 3-3.

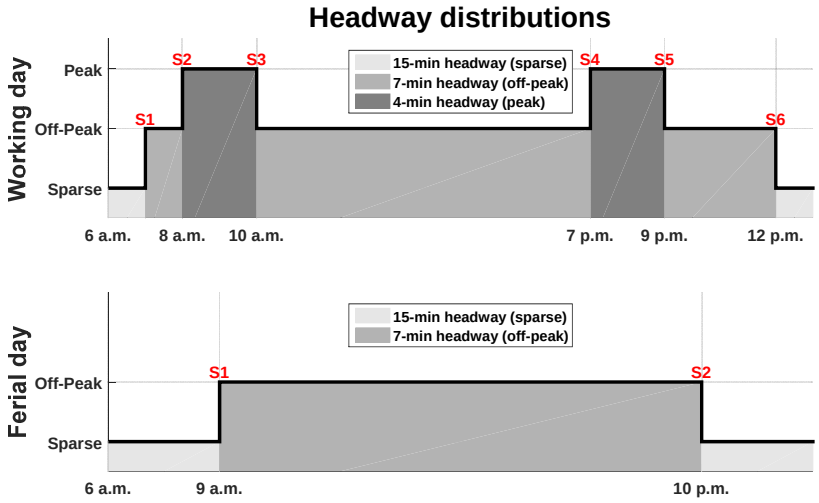

Figure 3-19. Operation timetable for the no-load voltage study.

Table 3-3. Weekly operation hours.

	4 min	7 min	15 min
Weekly operation hours	22	91	20

Two no-load voltage cases have been selected as references to assess the saving results: 1) a high no-load voltage case (680 V) to represent the habitual practice of MTS operators to set high values, especially in systems which exhibit large voltage drops like the case study; 2) the 640 V case, which represents a refined no-load voltage value with good system loss figures and safe minimum voltage values.

Then, this thesis proposes a variable no-load voltage scheme which was presented by the author in (López-López, Abrahamsson et al. 2014). This approach is based on the possibility of remotely varying the no-load voltage by changing the SS transformer tap position. This only requires these tap changers to be remotely commanded.

In order not to lead to an excessive number of tap changes, the switching times have been restricted to 6 events for working days and 2 events for the ferial ones. These switching events are represented in Figure 3-19 (in red). For further information, Table 3-4 includes the list of switching times and the change in the no-load voltage applied.

Table 3-4. List and description of the switching events for working and ferial days.

Working day		
Event	**Voltage before**	**Voltage after**
S1	580 V	600 V
S2	600 V	610 V
S3	610 V	600 V
S4	600 V	610 V
S5	610 V	600 V
S6	600 V	580 V

Ferial day		
Event	**Voltage before**	**Voltage after**
S1	580 V	600 V
S2	600 V	580 V

Table 3-5 presents the annual energy consumption figures for the three no-load voltage schemes analysed. It can be observed that the variable scheme represents the best energy consumption, whereas the 680 V case (reference 1) leads to the highest consumption.

The table is completed with the economic savings and the percent reduction of the total energy consumption with respect to the two references defined. It can be observed that the variable no-load voltage scheme presents 1 % consumption saving with respect to the 640 V case and 5.25 % with respect to reference 1. These figures, taking 0.1 € per kWh as the price for energy, are translated into 42.6 and 222.5 thousand EURO annual savings.

It must be noted that even in case the MTS operator do not regard the possibility of implementing the variable no-load voltage scheme, the study of the effect of the no-load voltage on the system energy consumption may lead to non-negligible energy savings (4.25 %).

Table 3-5. Aggregated energy saving results derived from the variable no-load voltage approach.

	Annual consumption (GWh)	Savings w.r.t. Reference 1		Savings w.r.t. Reference 2	
		k€	%	k€	%
Ref 1	42.35	-	-	-179.8	-4.43
Ref 2	40.56	179.8	4.25	-	-
Variable scheme	40.13	222.5	5.25	42.6	1.05

As will be explained in Chapter 4, the effect of the traffic stochastic variables on the system energy and voltage figures is not negligible. Therefore, the no-load voltage study presented in this section should be complemented by the appropriate analysis of the traffic influence. Specifically, the energy-saving and minimum voltage results must be obtained from the analysis of several traffic scenarios. These scenarios must properly represent a sufficient variety of representative traffic situations.

SS shutdown

As was presented in Figure 3-14, SSs may reduce receptivity if they supply power to feed motoring trains when it is not strictly necessary (the braking trains are able to do it). Therefore, the system receptivity could be increased by adequately turning certain SSs off.

From another perspective, this approach is based on a decrease of the line voltages which effectively increases the voltage gap available for power regeneration.

When the traffic density is high, this technique is not recommendable, since it may lead to low train voltage events. However, in the off-peak hour, this SS shutdown strategy may lead to energy savings without any infrastructure investments.

The specific implementation of this technique consists of switching one or several SSs off in a single event. Then, this set of SSs remains in *OFF* state for a certain period of time (hours), i.e., no complex switching patterns are followed.

The main drawback of shutting SSs down is that it increases the average distance between generation and consumption points, which has been proved in Section 3.2.1 to increase conduction losses. Thus, for the application of this technique, it must be assessed to what extent this loss increase may or not spoil the advantages of the receptivity increase.

3.3.2. HIGH-INVESTMENT TECHNIQUES

This group of energy-saving techniques consists of implementing important changes in the existing infrastructure. These upgrades or reinforcements are usually expensive systems which economic viability must be properly analysed.

Like the low-investment ones, the techniques in this section are mainly based on reducing the voltage drops and in the variation of the average train voltages. This

section performs a review of the most relevant ones which is then complemented by the presentation of some new infrastructure improvement trends.

Electrification voltage level

As the voltage level of the electrification is upgraded, currents in conductors –and so voltage drops– decrease. Whereas the no-load voltage tuning represents a fine adjustment of the supply voltage which requires no infrastructure changes, increasing the electrification standard voltage level leads to large savings which however require deep and expensive changes in the electrical infrastructure. SS transformers, rectifiers and even trains must be changed, which makes this improvement really difficult to justify. For this reason, the nominal voltage level must be taken as a critical decision in the system design stage.

Practical limitations to increase this magnitude are isolation and safety standards, and converter semiconductor technology. The standardized voltage levels for DC electrifications are 600 V, 750 V, 1.2 kV, 1.5 kV and 3 kV.

To illustrate the important effects of increasing the infrastructure nominal voltage level, the scan analysis performed in Section 3.2.1 has been replicated for a 1.5 kV infrastructure. The maximum line voltage rises to 1.8 kV. From the receptivity standpoint, this implies an absolute increase in the regeneration voltage gap which is added to the lower voltage drops for the same transmitted power with respect to the 600-V electrification.

Figure 3-20 presents the new energy figures (it may be interesting to compare them with the results in Figure 3-9). The 1.5 kV infrastructure yields a dramatic decrease in conduction losses. In addition, the voltage drop improvement leads to a large rheostat reduction, which makes it possible to obtain receptivity figures close to 1 for some traffic densities.

Table 3-6, which is analogous to Table 3-2, presents the main energy figures in the system in relation with the train energy. The energy efficiency for the base case is qualitatively increased with respect to the 600-V electrification, with conduction losses below 1 % of the train energy.

Regarding rheostat losses in the regenerative train case, although the receptivity decrease trend is also observed, the minimum receptivity figure is around 9 % for the longest headway (15 minutes). Again, this represents a large reduction in rheostat losses with respect to the 600-V electrification.

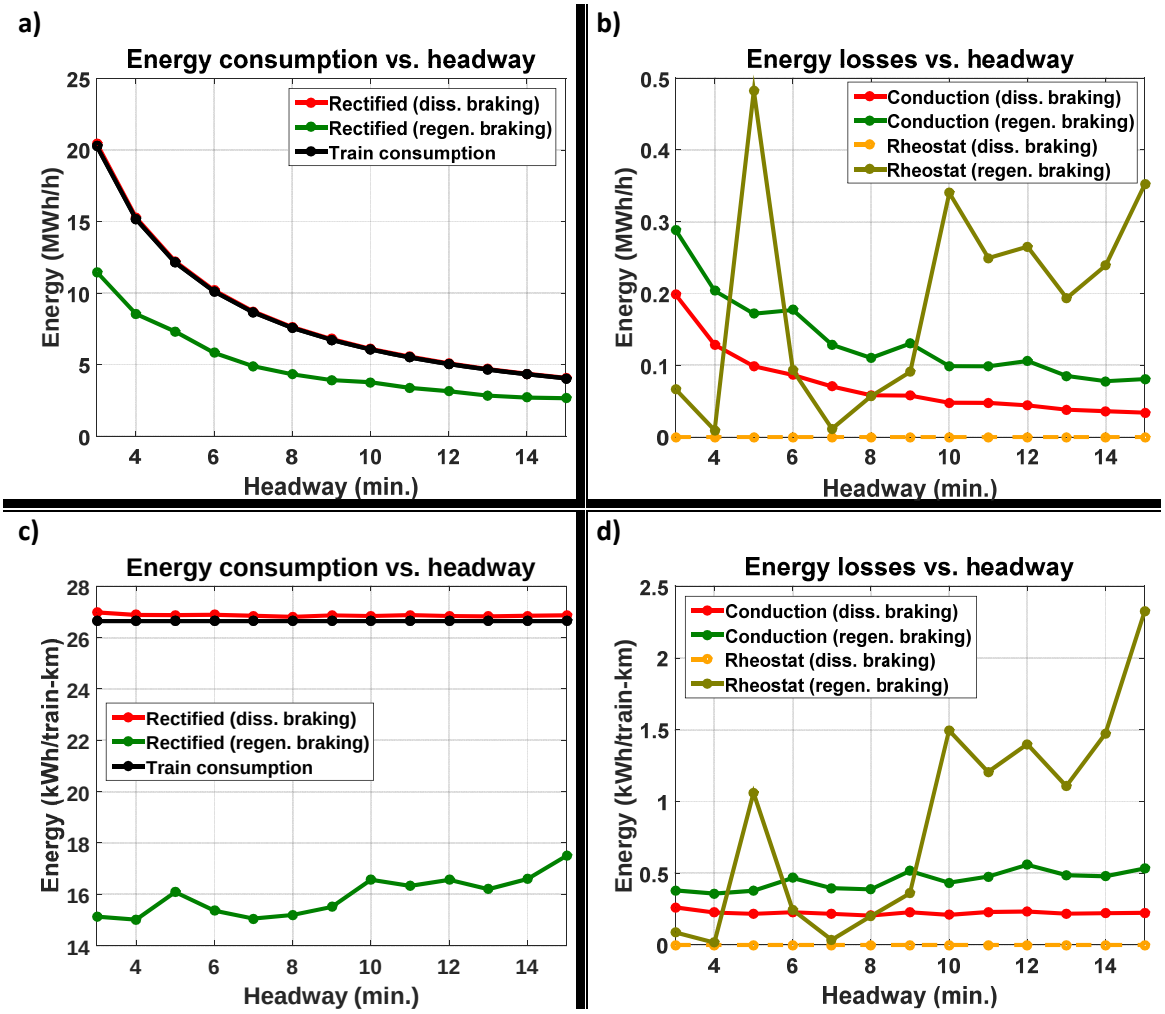

Figure 3-20. Energy figures for different headways. 1.5 kV electrification.

Table 3-6. Relative energy figures with respect to the train energy. 1.5kV electrification.

		3 MIN	7 MIN	11 MIN	15 MIN
RECTIFIED	**BASE**	1.0098	1.0081	1.0086	1.0084
	REGEN.	0.5662	0.5651	0.6126	0.6568
REGENERATED	**BASE**	0	0	0	0
	REGEN.	0.45	0.45	0.45	0.45
CONDUCTION	**BASE**	0.0098	0.0081	0.0086	0.0084
	REGEN.	0.0142	0.0149	0.0179	0.0200
RHEOSTAT	**BASE**	0	0	0	0
	REGEN	0.0033	0.0013	0.0453	0.0872

Therefore, after this analysis of the energy loss improvement associated with a nominal voltage increase, it may be again stated that this system characteristic must be taken as a relevant concern in the design stage.

Conductor impedance

The impedance per kilometre of the feeder system (catenary plus return system) determines the magnitude of the system voltage drops –and hence conduction losses– and the maximum transmittable power for a given distance.

A decrease of the conductor impedance per kilometre will consequently lead to less conduction losses, and it will also increase system receptivity.

The actual impedance value of the feeder system may be reduced with several infrastructure upgrades. Regarding the supply circuit, the conventional catenary conductor section may be increased by installing reinforcement feeders or by replacing it by a rigid catenary system. The latter approach has additional maintenance advantages, but it requires the system to be underground in order not to incur huge expenses. Then, using both rails on the track for the return circuit is also beneficial from the impedance standpoint.

The parallelisation of the supply systems of several parallel tracks is also useful to reduce the net impedance between generation and consumption points. In addition, this measure is less expensive that reinforcement feeders or rigid catenary systems.

However, 1) the addition of reinforcement feeders to the catenary system or 2) the change to rigid catenary system; are expensive infrastructure improvements which in addition force the operators to interrupt the line service.

The case-study catenary system is already upgraded due to its weak train voltage characteristics, as described in Section 3.1.1.

Reversible substations

It is possible to allow power flows from the catenary system to the utility grid by adding a converter to existing SSs. This implies that the cost of the improvement is lower than that of changing the whole SS, and that the infrastructure changes may be implemented without affecting the system operation.

The application of this technique, which is clearly oriented to increase the system receptivity, yields remarkable net energy consumption reductions. However, for this reduction to produce economic savings, it is necessary that the utility grid operator billing scheme takes into account net consumption. In case the local regulations in the region where the MTS is located do not force the utility grid operators to take the returned energy into account, it is difficult to justify the inclusion of RSs from an economic standpoint.

The robustness, useful life, energy efficiency and price per MW of these devices are –currently– clearly better than those for ESS (Gelman 2013). For this reason, and provided in Spain and in most European countries the utility grid operator must pay for returned energy, the studies in this thesis are focused on the effect of RSs on the MTS energy consumption (Chapter 6).

Wayside Energy Storage Systems

These devices are also expected to increase system receptivity, and hence to reduce rheostat losses. The difference with RSs is that they store braking energy when the system is not receptive for later releasing it back to the catenary system when possible. From an energy efficiency standpoint, ESSs present a number of drawbacks if compared with RSs:

- ESS use to exhibit higher losses than RSs, especially when the charge level is low and power is high (see Figure 2-8).
- For the most extended storage technologies, the storage element in the ESS tends to fail after a certain number of charge-discharge cycles. This makes the useful life of these elements to be lower than that of RSs.
- Their storage capacity is finite. When ESSs are full, they are not able to absorb braking power. Therefore, if the charge-discharge processes are not balanced, the receptivity increase effect may be spoiled unless ESSs are over dimensioned. In addition, high storage capabilities often require huge volumes which might not suit the MTS available room.
- For the current state-of-the-art, the price per MW and MWh for these equipments is high. In addition, their power and energy densities are subject to be improved. These reasons make them to be currently less attractive than RSs.

However, ESSs also present some advantages and good characteristics:

- They are an interesting choice –the only choice, indeed– when MTSs are operated in regions where power flows from the railway system to the utility grid are not remunerated.
- They do not require a connection to the utility grid, which allows placing them not only in electrical SSs but in any location with available room in the line (habitually, passenger stations). This makes it possible to implement distributed strategies that can improve the final system receptivity with respect to the RS approach (Takagi 2010).
- The fact that they supply energy to the railway system in the discharge process makes it possible to implement interesting strategies for the system operation like train voltage support and SS peak consumption shaving.
- The intense research on energy storage technology improvement in the frame of the electric car is likely to dramatically reduce the price per MW, MWh and the power and energy densities of these equipments in the coming decades.

Other techniques

Current research efforts into improving DC-railway infrastructure are leading to the proposal of innovative techniques. The study in (Takagi 2012) represents a good example of a rigorous analysis of an innovative technique. This consists of using high-temperature superconducting feeder cables in the electric infrastructure of a DC-electrified MTS. If technical advances on reducing losses in the interconnection points between superconducting and normal cables lead to an economically feasible system, it could be interesting to introduce this technique to assess if it suits the particular system under study.

A similar concept but proposing a HVDC feeder instead of a superconducting feeder is presented in (Abrahamsson, Kjellqvist et al. 2012).

There is also a new research interest devoted to search for synergies between MTSs and electrical vehicles (Falvo, Lamedica et al. 2011)

3.4. SUMMARY, CONCLUSIONS AND CONTRIBUTIONS

This chapter contains the description of the case-study line used in the thesis, and the initial studies to gain insight on the energy concerns in MTSs.

The case-study line used to illustrate its derivations is a double-track line with two terminal stations. The reason for this choice is that this is a very general type of line and operation. Relevant Metro systems as Madrid, Barcelona or Paris use only this type of line and operation.

Nevertheless, it must be noted that the application of the studies in this thesis to different MTS lines would be easy to implement. In the case of circular lines, all the analysis presented in this thesis would be directly applicable. In the case of complex-topology lines, the characteristics of the traffic in these different types of line should be determined and modelled.

These studies have assisted in the comprehension of the problematic to be tackled and in the detection of the potential targets to improve MTS energy efficiency. In addition, it contains the description of the case-study line used in this thesis, and the definition of some test which will be used along the thesis to validate many of the studies presented.

The analysis of the MTS energy figures have identified two sources of losses which may be reduced by the improvement of the electrical infrastructure: 1) conduction losses and 2) rheostat losses.

The study of the energy figures in the case-study line, which is the typical MTS line subject to exhibit poor energy efficiency figures, has yielded some relevant conclusions. First, it has proved that the application of regenerative braking is a very powerful tool to reduce energy consumption in MTSs. Although they tend to produce an increase of conduction losses, especially for medium and long headways, this effect is clearly dominated by the reduction in the energy consumption. This reduction is derived from the reutilisation of a fraction of the kinetic energy of braking trains. The electrical braking curves used in the case study lead to a large reduction in the energy consumption when regenerative energy is received effectively (short headways). The specific figures approach 40 % with respect to the case without regenerative braking in favourable headways, and the worst-case relative reduction is greater than 25 %.

Regarding conduction losses, it has been observed a slight tendency to decrease for long headways in kWh/train-km. When these are the only source of system losses (no regenerative braking is applied), the system exhibits a consequent reduction in the consumption per train and kilometre for long headways due to the decrease in the average line currents.

Then, the analysis of rheostat losses has shown that they are comparable to the conduction losses in kWh/train-km even for short headways. Then, for medium and long headways, they become clearly dominant both in relative and absolute terms. Indeed, the absolute rheostat-loss analysis (kWh/h) has not yielded any clear increase

or decrease trends with the headway. This, together with the steady reduction in the regenerated energy for long headways leads to a continuous increase in the relative rheostat-loss figures with the headway. As a result, the trend in the energy consumption vs. headway when regenerative braking is used is the opposite one: the consumption per train and kilometre is lower for short headways.

The slow conduction-loss increase when large amounts of regenerative energy are injected in the system leads to a high correlation between the system receptivity to regenerative braking and the energy consumption. The linear regression of the receptivity-consumption scatter plot suggests that a 0.1 increase in receptivity would be translated in 1.16 kWh/train-km reduction, which represents 4.3 % of the total train energy. Thus, this implies that it makes full sense to apply techniques which allow improving the system receptivity to regenerative braking.

The mechanisms to increase receptivity (reduce rheostat losses) have been reviewed and classified. They are mainly based on the absorption of the regenerative energy surpluses that leads to rheostat losses. Direct and indirect mechanisms have been observed. In addition, this chapter has identified active SSs as elements which electrically decouple the system from the rheostat-reduction perspective, i.e., from a given RS or ESS location, it is not possible to effectively reduce rheostat losses that take place from an active SS on.

The review of the techniques to improve the MTS infrastructure from an energy-saving perspective makes it possible to divide them into low- and high-investment techniques.

Within the former, this thesis proposes: 1) the electrical segment connection, which is currently implemented in nearly all the DC MTSs, 2) the SS no-load voltage tuning, and 3) the SS shutdown, which is being currently implemented in certain MTSs with promising results.

The SS no-load voltage tuning has been identified as a relevant technique which is not thoroughly covered in the literature, and thus a dedicated study has been included in the chapter. This study uses a conservative no-load voltage scheme as reference, which consists of setting this parameter to a high level in order to prevent protection triggering events from taking place. It has been proved that it is possible to obtain 4.25 % energy consumption reduction with respect to this conservative approach. Then, for the cases where the infrastructure allows performing SS no-load voltage changes during the operation day, a variable no-load voltage scheme has been proposed. This makes it possible to adapt this parameter to the particularities of peak and off-peak operations, which yield 5.25 % reduction with respect to the same reference.

Within the high-investment techniques, the following strategies have been reviewed: 1) the electrification voltage level increase, 2) the conductor impedance decrease, 3) the installation of RSs, 4) the installation of ESSs, and 5) other techniques.

As a prove of the potential of increasing the electrification voltage level, the energy study vs. the headway previously carried out for 600 volts has been replicated. The

results have proven that the effects are notable not only in the reduction of the conduction losses, but also in the increase of receptivity. The latter is derived from the increase of the voltage gap available for energy exchanges between trains, which also allows the no-load voltage tuning to yield net energy benefits. The conclusion is that, in general, the electrification voltage level should be set to the maximum possible during the MTS design stage.

Within the rest of techniques, it has been observed in the literature review that the inclusion of RSs appears as the most convenient technique nowadays to improve MTS electrical infrastructures. For this reason, it has been selected as the key technique in this thesis.

Summarising, the most relevant contributions of this chapter are:

- The comprehensive review of the MTS energy efficiency problem, systematically assessing the relevance of rheostat losses with respect to conduction losses.
- The rheostat-loss reduction mechanisms frame, together with the identification of electrical interferences is a novel approach.
- The no-load voltage study, including the variable no-load voltage scheme. This is a novel scheme proposed in the frame of this thesis.
- The specific figures of the potential savings related with regenerative braking for a particular system as the case-study line. Although there are a number of studies obtaining similar conclusions, the addition of a new significant case study, which may be compared with the rest of cases (e.g. the comparison performed in (Falvo, Sbordone et al. 2014), is a relevant result).

CHAPTER 4

THE TRAFFIC IN MASS TRANSIT SYSTEM INFRASTRUCTURE STUDIES

4.1. INTRODUCTION

As was stated in Section 1.2, the main objective of this thesis consists of finding the way to improve the electrical infrastructure of an actual MTS to make it more energy efficient. Then, it has been proved in Section 3.2 that this infrastructure improvement must be focused on increasing system receptivity, mainly at long operation headways.

Although there are low-investment strategies to increase receptivity, when an MTS exhibit notable receptivity problems, these must be fixed by the addition of devices such as RSs or ESSs. The inclusion of these devices leads to large investments, so their benefits must be properly motivated. Several issues, such as the total number of devices installed, their size, location or control parameters must be properly determined.

Among the different infrastructure and operation characteristics of MTSs, the traffic in the line under study is expected to have a strong influence in the system energy figures. Specifically, it is expected to influence the system receptivity and, in particular, the effectiveness of a given infrastructure improvement configuration to increase the system energy efficiency.

The literature on MTS infrastructure improvements provides a number of studies dealing with the optimal location of RSs or ESSs in a given system. The method used to

obtain the optimal enhancements of electrical infrastructure differs from one study to another. However, to the best of our knowledge, these studies share a common feature: the traffic scenarios used to extract general conclusions are strongly simplified. That means that, although they are rigorous studies, they do not include the traffic variability. Indeed, a single traffic scenario is used in general.

Starting with the works dealing with RSs, (Chang, Wang et al. 1998) proposed a genetic algorithm for optimising RS firing angle. This is one of the first references found on this type of optimisation, and it only uses a time instant with 14 fixed trains. (Hui-Jen, Chao-Shun et al. 2005, Chuang 2005), from the same workgroup, used two different algorithms to obtain optimum RS locations, taking peak and off-peak headways into account. This means a qualitative improvement in the way traffic is tackled. However, dwell time at passenger stations is fixed and a single deterministic traffic scenario for each headway is used to obtain the results. In a more recent work, (Bae 2009) presented a comprehensive study of the way inclusion of RSs in a line affects energy consumption. Although this study takes many factors into account, the traffic input consists of peak and off-peak headways with deterministic traffic parameters. (Fazel, Firouzian et al. 2014) performed a simple study on RS location where only one headway with a single traffic scenario is used.

Among the works which set the scope in ESSs, the work by (Lee, Jung et al. 2013) studies the effects of installing big flywheel ESSs in a Korean line. The study only includes peak-time headway, with fixed dwell time (deterministic). (Xia, Chen et al. 2015, Wang, Yang et al. 2014) are two rigorous studies by the same workgroup devoted to the optimal location and sizing of ESSs. They use three headways with a single traffic scenario per headway.

Although applied to an AC-electrified system, (Abrahamsson, Östlund et al. 2013) represents a fairly good example of an electrical infrastructure optimisation model. This detailed model integrates the electrical and the mechanical parts and makes it possible to study optimal power supply systems. The structure of this model would allow the introduction of stochastic traffic variables, but this study considers a single train.

There is another type of work, which focuses on the study of the optimal control curve of ESSs. (Battistelli, Fantauzzi et al. 2012, Battistelli, Ciccarelli et al. 2009) conducted two studies aimed at determining the optimal control parameters of the DC-DC converter in an ESS; traffic was also simplified. The model presented in the cited articles includes no uncertainties in the traffic. (D'Avanzo, Iannuzzi et al. 2010) analysed the control parameters of an ESS. Several headways are used, but a single deterministic traffic scenario for a scheduled timetable is considered. The study by (Ianuzzi, Ciccarelli et al. 2012) used a simple train load-regeneration profile because its focus is set on the control parameters of the ultracapacitor ESS. However, although it falls outside the scope of the study, the authors explain the importance of taking traffic (timetable) stochastic variables into account. Finally, (Ciccarelli, Del Pizzo et al. 2014) used only two trains in a study on the control strategy of a new storage technology (Lithium-ion EDLCs). The results were then checked in an experimental mock-up.

Table 4-1 summarises this review of the traffic models used in the MTS optimisation studies found in the literature.

Table 4-1. Traffic models in MTS electrical infrastructure optimisation studies.

Optimisation study	Traffic model
(Chang, Wang et al. 1998)	Only one snapshot in the traffic model.
(Hui-Jen, Chao-Shun et al. 2005)	Peak and off-peak headways included. One traffic scenario per headway.
(Chuang 2005)	Peak and off-peak headways included. One traffic scenario per headway.
(Bae 2009)	Peak and off-peak headways included. One traffic scenario per headway.
(Fazel, Firouzian et al. 2014)	Only one headway used. One traffic scenario at this traffic density.
(Lee, Jung et al. 2013)	Only peak-hour headway included. One traffic scenario at this headway.
(Abrahamsson, Östlund et al. 2013)	Only one train running on the tracks.
(Wang, Yang et al. 2014)	Three headways combined. One traffic scenario per headway.
(Xia, Chen et al. 2015)	Three headways combined. One traffic scenario per headway.
(Battistelli, Ciccarelli et al. 2009)	One train per track. One single traffic scenario.
(Battistelli, Fantauzzi et al. 2012)	One train per track. One single traffic scenario.
(D'Avanzo, Iannuzzi et al. 2010)	Timetable operation without deviations from the schedule.
(Ianuzzi, Ciccarelli et al. 2012)	One train per track. One single traffic scenario.
(Ciccarelli, Del Pizzo et al. 2014)	One train per track. One single traffic scenario.

As Table 4-1 illustrates, the habitual traffic input to MTS infrastructure studies is generated by using a constant dwell time at each passenger station, and then including several headways to study the different system operation modes.

In contrast with the references in Table 4-1, (Pilo, Jimenez-Octavio et al. 2011) is the only reference on electrical railway infrastructure studies which attracts attention on the importance of traffic uncertainties in the results obtained. Specifically, this work proposes to use the Montecarlo method to represent the different traffic situations. However, it lacks an assessment on the amount of scenarios to be used in order to increase the result accuracy without an excessive computational burden.

This chapter aims to set the conceptual bases of an extended traffic approach in MTS infrastructure studies. It is started by studying the adequacy of the habitual single-scenario traffic approach (Section 4.2) in general MTS studies. Then, Section 4.3 presents a new traffic approach which includes the random variations of some traffic variables. The habitual single-scenario traffic approach is replaced by a traffic space set which represents the complex energy exchanges between trains in the system and their relative frequencies.

The traffic studies are continued in Section 4.4 by presenting the conceptual frame that makes it possible to use a small-size subset of the total traffic space to generate the traffic input to the MTS infrastructure improvement studies.

Then, Section 4.5 is devoted to present these small-size sets of representative traffic scenarios, and to study the trade-off between the size of the traffic input and the energy saving accuracy.

4.2. ON THE ADEQUACY OF THE SINGLE-SCENARIO TRAFFIC APPROACH

The results in Chapter 3 were obtained by following the habitual procedure in the literature, where a single scenario per headway is included. In this single traffic scenario, the departures are deterministic, and they are fixed to their scheduled times. As stated in Section 3.1.2, this traffic model implies that in the time between two consecutive trains (headway), all the positions in the line are visited once, but only once.

Let us define a system operation sample as an inspection of the system that lasts the time between two consecutive trains, i.e., the headway.

In the actual operation of an MTS, there are several phenomena that make it difficult for trains to meet the scheduled departure times. For this reason, if several operation samples are taken to analyse the system operation, the MTS operator should not expect that these samples follow the characteristics of the scheduled operation.

Figure 4-1 presents some train graphics to illustrate this system operation sampling. Only the positions of trains on track 2 (descending-position trains) have been presented for the sake of clarity. The headway has been set to 11 minutes, so system operation samples last 660 s. Then, the scheduled 30-s dwell time traffic of Chapter 3 (scheduled train graphic) is compared with a more realistic traffic scenario where the departure times have been obtained from a certain probability distribution in dwell times (noisy train graphic). This distribution is centred in 30 s. The figure shows how the 30-s dwell time traffic accomplishes the single-scenario traffic characteristics, whereas the noisy dwell time approach presents a stretch which has been visited by two trains and another one which has not been visited.

On the one hand, if this noisy-dwell-time scenario was used as the only one to obtain energy-saving results, it would bias the conclusions obtained. On the other hand, it must be noted that if the dwell time probability distributions are reliable, the noisy-dwell-time scenario is as likely to take place in the actual operation of the system as the regular dwell time one in a 660-s time window. This concern must therefore be taken into account, and the selection of traffic scenarios must not lack or bias the information about the different zones in the line.

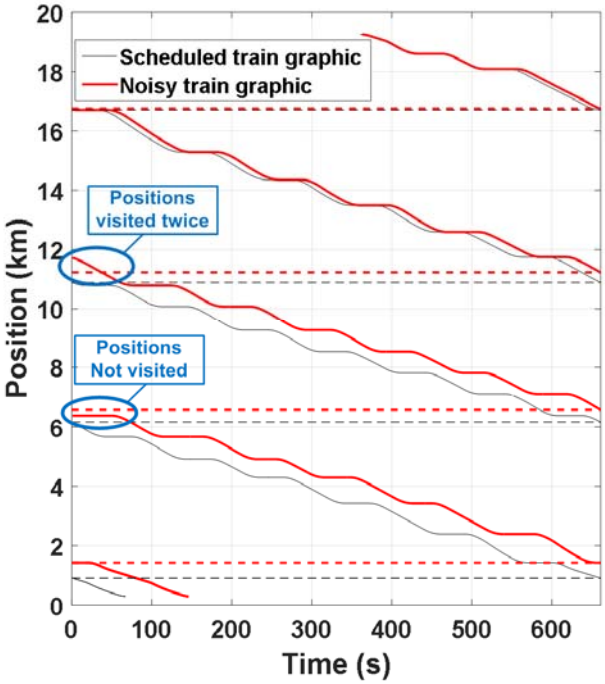

Figure 4-1. Differences between regular and variable-dwell-time traffic examples.

At this point, a question arises: is the constant dwell time traffic approach a good candidate to represent the energy interactions in the system?

The answer to this question will depend on the way in which the change in the relative positions between trains affect the global energy figures of the MTS. Taking a train running on a braking stretch as reference, if the fixed dwell time approach represents recurrent power-regeneration profiles of the rest of trains, it will be a good candidate to express the system receptivity. In case it does not, the energy consumption figures obtained could be inaccurate.

A first exploration of the possible equivalency between the scheduled dwell time traffic and the noisy approach has been made by analysing the rheostat losses around two passenger stations. Figure 4-2 shows the rheostat loss results around stations 7 and 20 for the traffic scenarios presented in Figure 4-1. Trains that approach a station from its left side are increasing their position, and therefore they are on track 1. Consequently, the right side of the station corresponds to the braking stretch in track 2.

It may be observed in Figure 4-2.a that, around station 7, the single-scenario traffic approach leads to greater rheostat losses than the noisy one for both tracks. Then, Figure 4-2.b shows that losses on track 1 for the noisy case are greater than those for the single-scenario one, whereas losses on track 2 present the opposite behaviour. The differences between the results for both traffic cases are not only quantitative: it is possible to have full receptivity with a traffic approach and poor receptivity figures with the other one for the same stretch (e.g. braking stretch in the approach to station 20 on track 1). This notable dispersion in the rheostat loss results suggests that a

single-scenario traffic approach might not be enough to represent the complex energy interactions between trains in DC electrified MTSs.

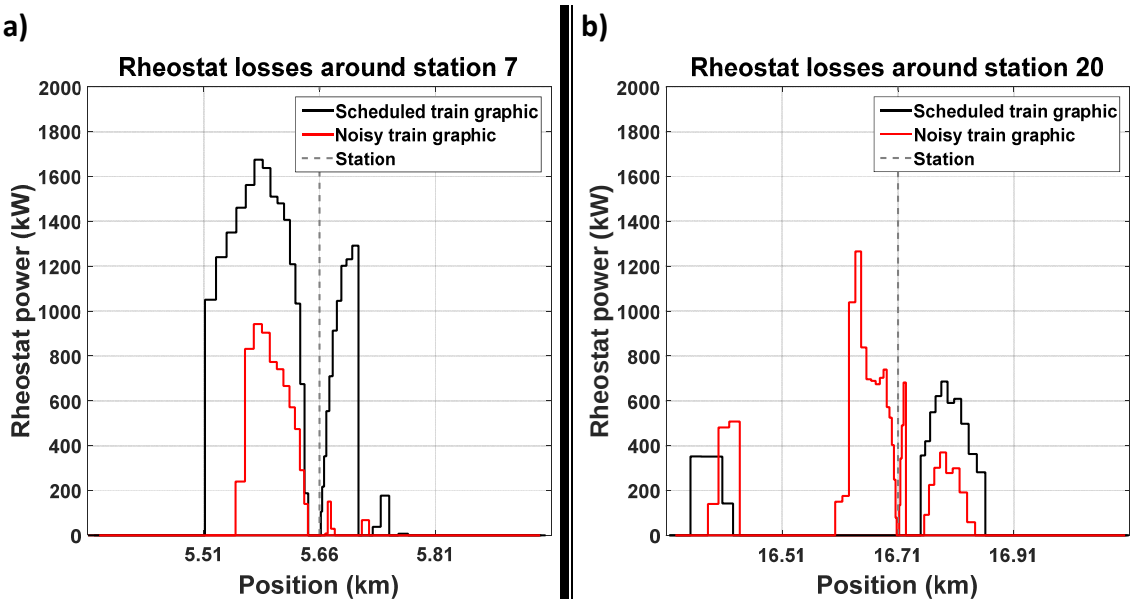

Figure 4-2. Two rheostat loss examples for the regular and variable-dwell-time traffic examples.

Then, the analysis of the adequacy of the single-scenario traffic approach has been continued by exploring the system receptivity figures when noisy dwell times are introduced. This analysis has been performed for all the headways in the traffic density scan performed in Section 3.2.1. 200 operation samples have been generated for each traffic density from a dwell time probability distribution which is centred in the dwell time for the single-scenario traffic approach (30 s). The justification and particularities of this dwell time probability distribution will be given in Section 4.3.1, where the traffic model is presented.

Figure 4-3 shows the sample, average and single-scenario-traffic receptivity results for all the headways under study. Although for some headways the single-scenario-traffic receptivity is close to the average value (e.g. 3, 6 and 10 headways), the results in Figure 4-3 prove that the single-scenario traffic approach does not play the role of an average situation regarding receptivity. Consequently, the use of this single traffic sample for representing the MTS is likely to lead to erroneous conclusions from the energy-saving standpoint.

E.g. Let us take as an example a hypothetical MTS which is only operated at 7-minute headway. Therefore, a simulation study may obtain general energy efficiency results by simulating this traffic density. If the single-scenario traffic approach is used, the results will suggest that the system is highly receptive to regenerated energy, and the achievable energy-saving results will probably be lower than the actual ones.

Even more, the big dispersion in the receptivity values, together with the particularities of the rheostat energy reduction mechanisms presented in Section 3.2.2, make it difficult to stand that a single traffic operation sample –regardless the

set of dwell times used– is enough to obtain accurate energy results for MTSs. This will be studied in Section 4.3.3.

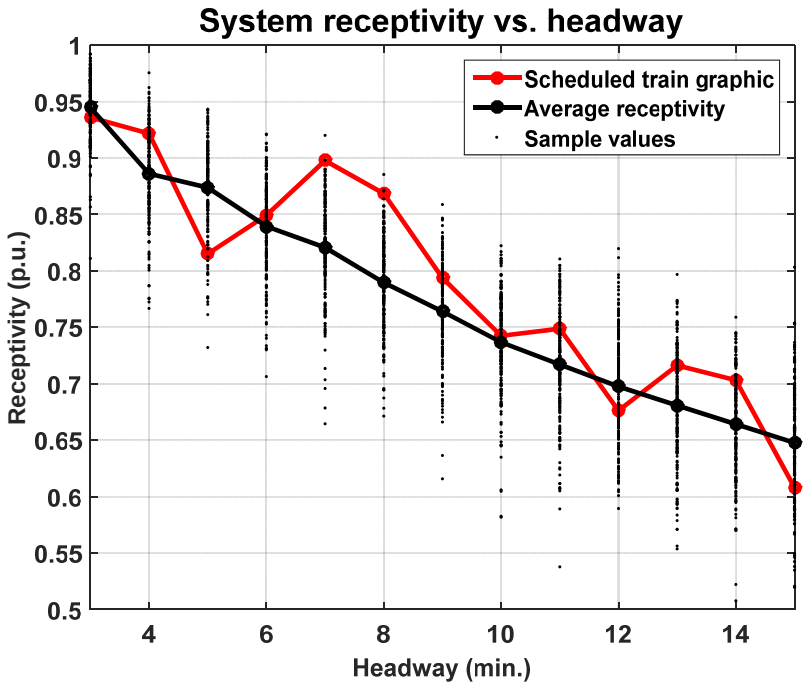

Figure 4-3. Receptivity figures after including stochastic dwell times.

Before accepting the receptivity values in Figure 4-3 as valid and general results, it is necessary to analyse their correlation with the train and regenerated energy sample values (see Figure 3-8 for details on these energy variables). The reason is that, as shown in Figure 4-1, not all the line positions are necessarily visited in a headway-long time window. In addition, there are positions that may be visited more than once. This implies that the sample train and regenerated energies are not constant. Therefore, high sample receptivity values could be in part due to high train energy, low regenerated energy, or both.

To study this concern, Figure 4-4 presents the receptivity scatter plots with respect to the train and regenerated energies for three relevant headways. The simple inspection of the scatter plots suggests that there is no correlation between these energy figures and receptivity. Then, this has been supported by the calculation of the Pearson correlation coefficients for the six cases under study. These values confirm that the receptivity figures are fairly independent from the global system energy values.

It can also be observed in Figure 4-4 that the dispersion in the train and regenerated energy sample values increases for short headways, as a consequence of the smaller sample time window. At this point, it is interesting to note that this dispersion is mainly caused by the variability in dwell times. The variation in other traffic variables like the time shift between departures at terminal stations (defined in Section 4.3.1) would not introduce dispersion in the global energy figures of the system. The reason is that this would not affect the cyclic characteristics of the traffic when dwell time is constant.

The results for the single-scenario traffic approach have been highlighted by using a different colour than that of the rest of samples. It must be noted that, for its cyclic characteristic, the single-scenario traffic approach presents train and regenerated energy figures close to the sample average. Therefore, the 'quasi-outlier' receptivity results that the single-scenario traffic approach exhibits for some traffic densities are not likely to be due to particular train or regenerated amounts of energy.

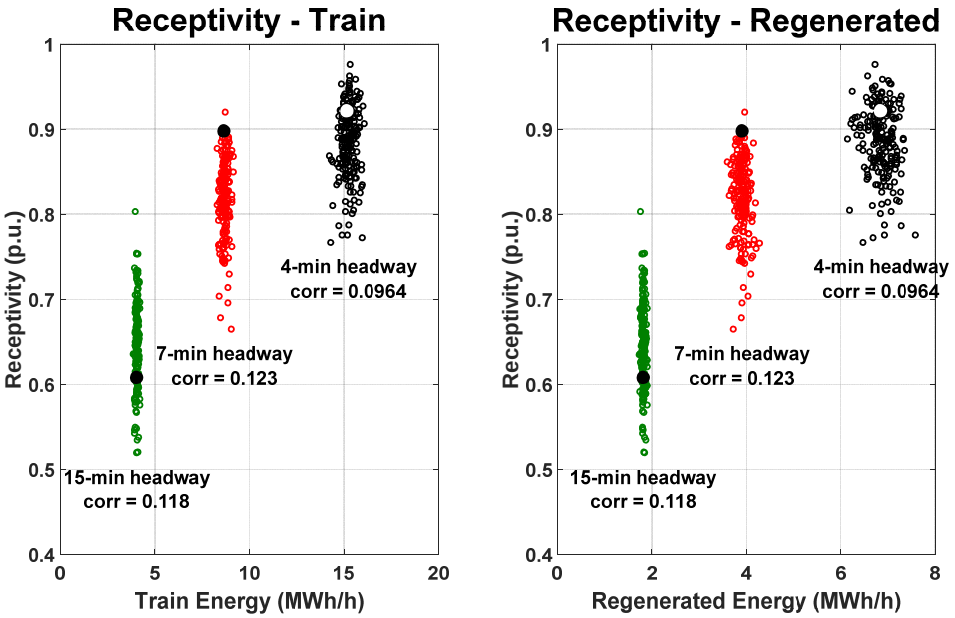

Figure 4-4. Receptivity scatter plots: There is no dependence on the global energy figures.

Prior to the conclusion of this section, it is important to analyse the accuracy of the single-scenario traffic approach from the energy saving perspective. The reason is that, as stated in Section 3.3.2, the inclusion of expensive energy-saving techniques in MTSs must be carefully motivated.

From this standpoint, the main tool to retrieve the economic investment in an infrastructure improvement is the reduction of the energy consumption, which will be translated into a reduction of the energy bill. Therefore, it is extremely important that the infrastructure upgrade studies are able to accurately assess the energy savings derived from the installation of expensive energy-saving devices.

The results presented in Figure 4-3 suggest that the energy saving results with the single-scenario traffic approach are not likely to be similar to those with other traffic samples, nor to the average energy savings. However, to support this hypothesis, the single RS test defined in Section 3.1.2 has been applied to an operation sample following the single-scenario traffic approach and to a different operation sample with noisy dwell time. Then, the results for both samples have been compared. Two different headways have been included into this analysis.

Figure 4-5 presents the energy-saving results obtained by the application of the single RS test. Two traffic samples have been used in order to study whether the results obtained with different traffic samples are similar: 1) the single-scenario traffic sample

and 2) another sample selected at random. These results prove that the dispersion in the energy-saving results from the use of two different operation samples is rather large, both for the 7 and the 15-minute headways. Consequently, it may be derived that the use of a single operation sample in studies which yield investment decisions is likely to lead to inaccurate results.

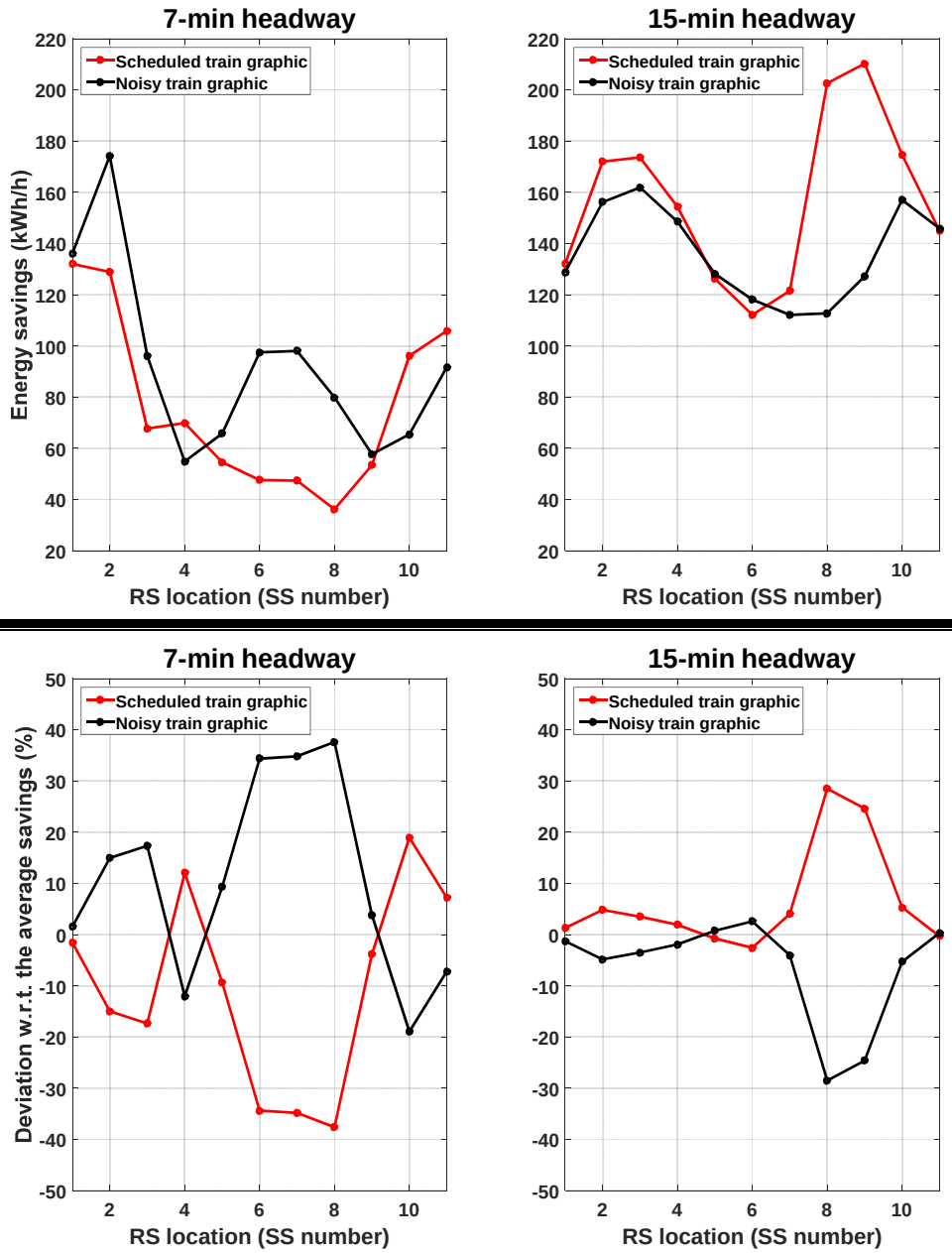

Figure 4-5. Energy-saving figures and discrepancies between two equiprobable traffic cases.

It must be noted that these two operation samples are equiprobable. However, to illustrate the relative error, this analysis makes the hypothesis that for each traffic density, these two samples are the only possible ones in the system operation, with 0.5 probabilities. Under this assumption, the bottom-side graph in Figure 4-5 shows the relative energy saving errors related to the use of a single operation sample. It can be observed that the use of the constant dwell time approach could lead to errors close to 40 % of the actual savings for some RS location. This means a significant lack

of accuracy that must be corrected. After the presentation of the traffic model, Section 4.5 includes a more reliable energy saving error analysis for the single-scenario traffic approach.

To overcome this inaccuracy problem, the rest of this chapter presents a comprehensive study of the traffic and a novel approach for the traffic to be included in infrastructure improvement studies.

4.3. TRAFFIC SPACE ANALYSES

This section aims to properly define the traffic model presented in this thesis. In addition, it obtains the traffic input for the optimisation study presented in Chapter 6. This traffic input will make it possible to obtain accurate energy saving results.

The habitual single-scenario traffic concept, which has been proved to be inaccurate from the energy-saving standpoint in Section 4.2, will be replaced by an extended traffic approach. This new approach makes use of the operation samples presented in Section 4.2, which are included into a set named the traffic space to represent the complex and variant energy exchanges in MTSs.

From this point, the set of operation headways used in the traffic density scan studies will be restricted to three headway samples, used to represent the system operation at peak, off-peak and sparse-traffic hours. The particular headways selected are:

- 4-minute headway for the peak hours, which coincides with the maximum traffic density in the actual operation of the case-study system.
- 7-minute headway to represent the off-peak or the medium traffic density operation. This off-peak operation is important for the system energy figures, since MTS are operated at medium traffic-densities for long periods.
- 15-minute headway for those hours where the traffic in the line is sparse. Habitually, this type of operation takes place at the beginning and end of the daily system operation.

The optimisation study in Chapter 6 will make use of these three headways to compose the MTS operation timetable.

Although the main traffic results will be presented for the three selected headways, the conceptual developments in this chapter will be illustrated with the results for the 7-minute headway.

4.3.1. THE TRAFFIC MODEL

Some of the main system parameters or variables that affect the energy exchanges in MTSs have already been briefly presented in previous sections. However, they are gathered again –and extended– for the traffic model definition to be consistent.

The first aspect to take into account in the traffic model is the correspondence between the track positions in the line and the trains' consumed power. This means that trains usually brake when they approach passenger stations, whereas they consume power when they depart from stations. In addition to these positions, speed limitation points or strong downhill stretches may also lead to train braking; and their opposite points and stretches, to train motoring.

For this reason, the first input to compose the traffic model consists of the trains' speed and power profiles between passenger stations. These profiles define the power consumed and regenerated by trains along their itinerary on each track.

Nowadays, the trend in MTSs is to include Automatic Train Operation (ATO). ATO allows having greater control over speed profiles and thus low consumption driving profiles (eco-driving). ATO line operators usually employ a set of pre-programmed speed profiles with different trip times for each stretch between passenger stations. These trip times usually range from the minimum running time –the so called "flat-out" profile, corresponding to the maximum permitted acceleration and deceleration– to a certain relaxed running time which allows lower consumption. Operators assign one of the available trip times to each train in order to maintain traffic control parameters within range. This thesis uses the flat-out profiles to generate the trains' consumption and regeneration powers along the line. These profiles are frequently used in the MTS design and improvement studies. If there is information about specific profiles used in the system, the application of the concepts presented in this thesis would simply require to properly representing these profiles in the traffic space.

For a given set of trains' speed and power profiles, the energy that trains consume along the tracks is determined by the trains' weights, which in turn depend on their load. This thesis considers that the trains' loads equal the 50 % of the maximum allowed. A possible refinement in this train load model could be used if specific information about the peculiarities in the line were available.

At this point, if the position of a train is known, it is possible to determine the power that it will consume or regenerate (see Figure 3-5 in Section 3.1.2). Now, it is necessary to define the positions and consumed powers of the rest of trains in the system, i.e., the number of trains simultaneously running on the tracks and their positions.

The number of trains is determined by the operation headway. This variable, defined as the distance between two consecutive trains on a track, is usually expressed in time units. It determines the total amount of train energy that will be absorbed by the MTS. However, as was studied in Section 3.2.1, the energy consumption at SSs to supply this train energy will vary depending on the fraction of regenerative energy that is accepted (receptivity).

Just to clarify the implications of the traffic in the system energy figures, it must be noted that the speed profiles determine the zones where power regeneration takes place. Then, the traffic defines whether the regenerated power is absorbed by the system or converted into rheostat losses.

As presented in Section 3.2.1, receptivity tends to be high in average terms when traffic density in the line is high (short headways), whereas it will be likely to decrease for long headways. Nevertheless, for a given headway, there are certain variables related to traffic which may change receptivity and thus affect line energy consumption figures. Given the train running times, in a double-track line with two terminal stations, the main traffic-related variables affecting receptivity are:

- **Dwell times at passenger stations**. Even when the traffic controller allows trains to depart, several circumstances that are commonplace in an MTS (e.g.: an unexpected affluence of passengers) may delay departure time. The work by

(Martínez, Vitoriano et al. 2007) thoroughly studied dwell times in Madrid Metro (Spain). The authors of this study found dwell times at passenger stations - excluding traffic disturbances - to follow log-normal distributions. Figure 4-7.a shows the effect of stochastic dwell times on the 7-minute headway operation of the case study line. The discontinuous curves show the variation of train positions over time for two different samples of the stochastic dwell times generated with 30-second-mean log-normal distributions. It can be observed that the positions where the ascending and descending trains cross each other are strongly affected, as are the load flows in the system.

- **The time shift between the departure times at the two terminal stations**. The operation of double-track lines with two terminal stations is mainly determined by the headway between trains. However, the relative positions between the trains on both tracks are affected by the difference in time between the departures at the two terminal stations. It is graphically illustrated in Figure 4-6. This time shift between tracks influences the positions where trains cross each other, and so the moments (or time intervals) when it is easier for them to exchange power, etc. In the specific operation of an MTS, the nominal value of this variable may be known, so determining the particular train graphic of the line. However, in general, this specific train graphic may be varied by changing the time shift without affecting the service conditions (mainly determined by the headway). Consequently, in the generation of the traffic space to represent the long-term operation of the system, there is no reason to assign a greater probability to a certain time shift than to any other. Hence, it is reasonable to let the time shift between departures follow a uniform distribution from 0 s to the headway. To illustrate this effect in the train graphic, Figure 4-7.b shows a 20-second-time-shift difference in the descending trains. It can be observed that, since the descending trains are delayed, the positions where they cross the ascending trains change.

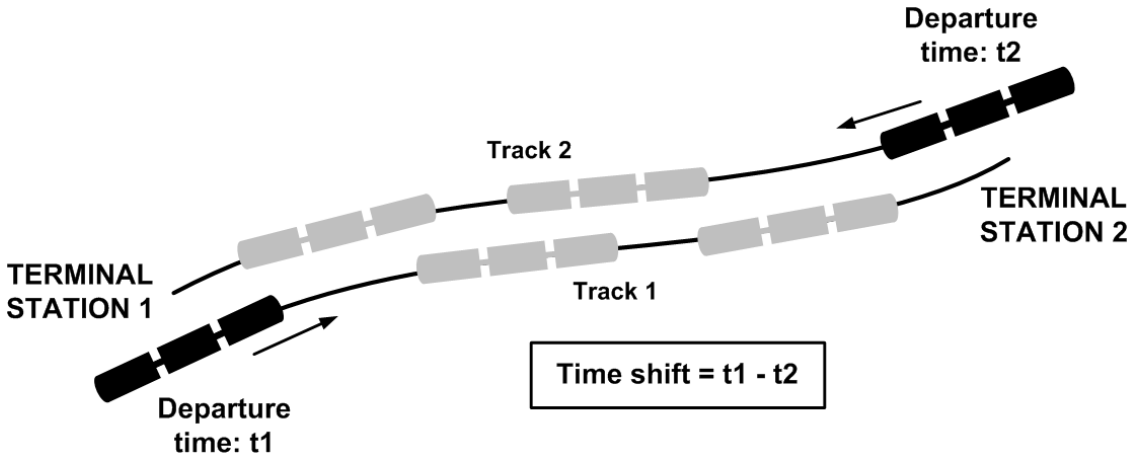

Figure 4-6. Illustration of the time shift between the two terminal stations.

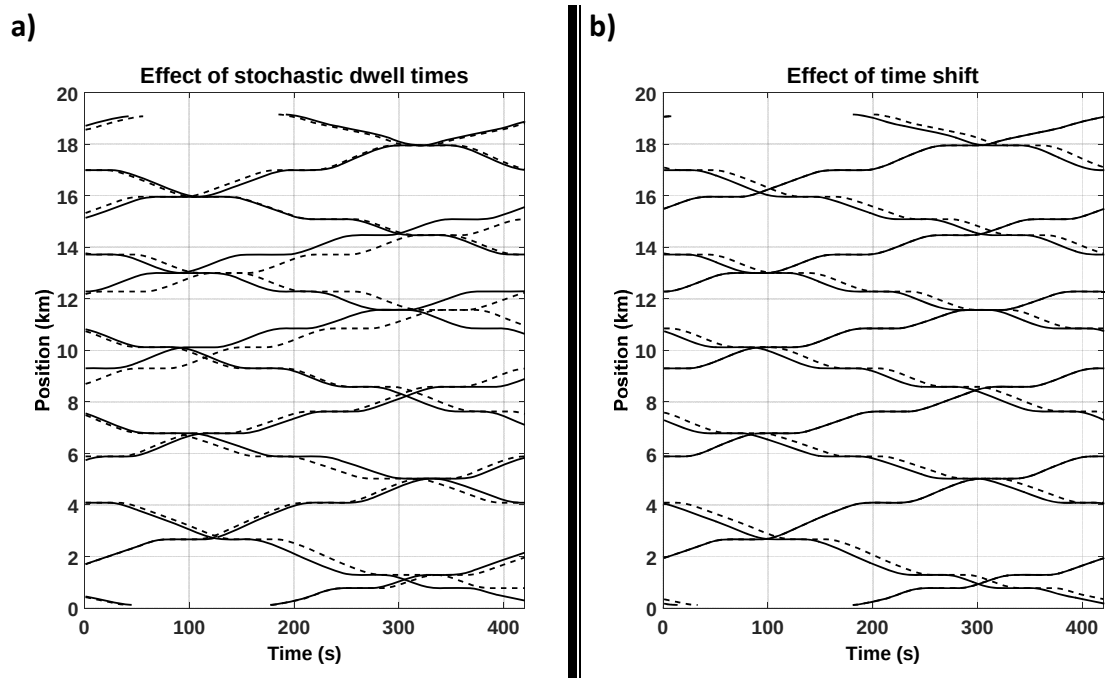

Figure 4-7. Effects of stochastic dwell time and terminal station time shift.

Table 4-2 illustrates the factors included in the traffic model presented in this thesis, which are known to affect the power exchange between trains. In addition, it shows the way they have been modelled in this traffic study.

Table 4-2. Factors included in the traffic model and values used in this study.

Traffic parameter	Model used in the study
Headway	Several. 7-minute headway used for the illustration of the traffic developments in this chapter
Speed profiles from passenger station to passenger station	Flat-out (minimum time) speed profiles.
Dwell times at passenger stations	Log-normal distribution. Mean: 30 s. Std. dev.: 3 s
Time shift between departure times at terminal stations	Uniform distribution from 0 s to the headway

4.3.2. TRAFFIC SPACE GENERATION

This thesis defines the traffic space for a given MTS as a set of operation samples which contains enough information to describe the general energy interactions between trains in the line. Due to the quantitatively difference in the energy figures of the different traffic densities, the total traffic space for the system is broken down into as many traffic spaces as headways are studied.

Each of the operation samples in the traffic space is generated from a particular set of traffic parameters, which may also be named a traffic scenario; i.e., a single operation sample is extracted from each traffic scenario. Provided this latter scenario concept is habitual in studies which deal with stochastic system operation (Baringo, Conejo 2013, Sigrist, Egido et al. 2010, Latorre, Cerisola et al. 2007), this denomination is used for

each sample in the traffic space from here on. Therefore, an operation sample will be referred to as 'traffic scenario sample' or simply 'traffic scenario'.

The traffic scenario concept is a generalisation of the habitual single-scenario traffic approach making the dwell times and time shift between terminal stations non constant. Therefore, the time duration of each scenario is set to the headway in seconds. This coincides with the period of the cyclic interactions between trains in the single-scenario traffic approach. Each traffic scenario is defined by the following parameters: 1) the headway, 2) the dwell times at all stations, and 3) the time shift between departure times at terminal stations in the line.

The process to generate a traffic scenario consists of two steps which are performed by the first stage of the electrical multi-train simulator, presented in Section 2.3.1. The 7-minute headway operation is used to illustrate these steps:

- The first step defines the headway and generates the random values of the traffic stochastic parameters. This requires generating random dwell times for a large-enough set of trains. Following the results from actual measurements by (Martínez, Vitoriano et al. 2007), this thesis uses a log-normal distribution with 30-second mean time and 3-second standard deviation to generate these random dwell times. A lower bound (20 seconds) is set to represent the minimum time below which no train stops are performed in the actual operation of the system. A higher bound (60 seconds) is set to exclude long dwell times which could be regarded as (or lead to) traffic disturbances, which are outside of the scope of this thesis. Then, the time shift value is generated from a random uniform distribution. In the 7-minute headway case, the time shift varies from 0 to 420 seconds.
- The second step composes the traffic resulting from the particular set of traffic parameters generated in the first step. It is in charge of extracting the circuit snapshots, gathering the train positions and power consumptions/regenerations corresponding to 420 seconds (for the 7-minute headway case). The sampling time is set to 1 second, which leads to 420 snapshots per traffic scenario. The first time instant of the time window used to extract the traffic scenario sample is selected so as the traffic in the system is in steady state. This implies that the first trains released on each track have already finished their itineraries, which assures that the number of trains in the system properly represents the operation at this headway.

Once it is clear how to generate traffic scenario samples, it is necessary to decide the number of samples required for the traffic space to represent the general train interactions in the system. The habitual approach in this type of studies consists of increasing the number of samples until the mean and standard deviation of the variables which define the problem are stabilised (Söder, Amelin 2011). For the MTS infrastructure studies, the selected variables are: 1) energy consumption at traction SSs, 2) regenerated energy, 3) rheostat losses and 4) conduction losses.

Figure 4-8 shows the evolution of the mean and standard deviation of the selected energy variables. It may be observed as from around 300 samples all the sample

means and standard deviations are stabilised. Nevertheless, the size of the traffic space has been set to 500 traffic scenario samples, which is regarded as a fair margin.

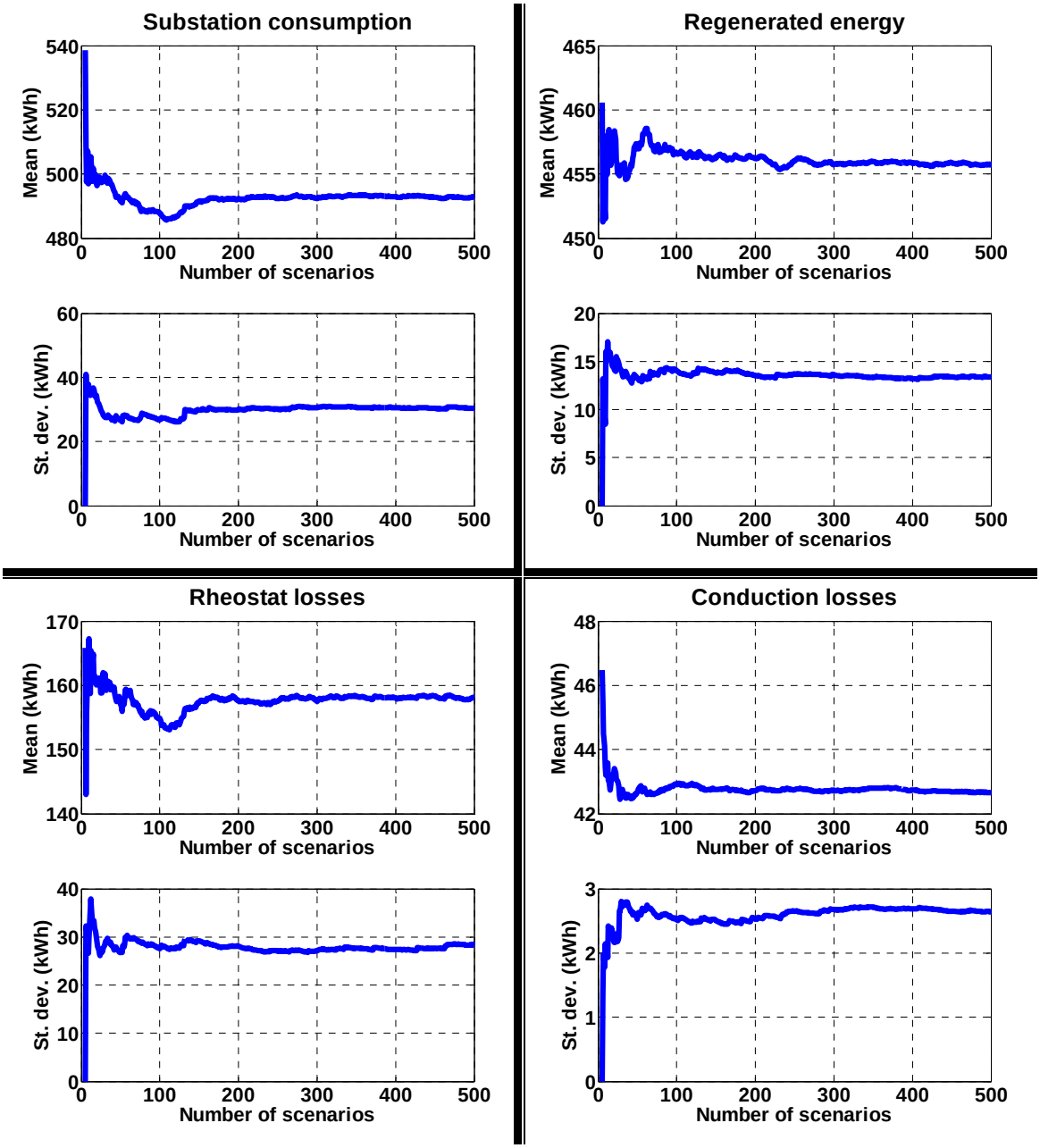

Figure 4-8. Stabilisation of the main energy-related variables as size of the dataset grows.

A clear distinction must be made between the traffic space and the traffic input used in MTS infrastructure improvement studies. The former will be made up of a large number of traffic scenarios. The latter may be a subset of the former, or it could even be made up of traffic scenarios which are not contained in the traffic space. As will be explained in Section 4.3.3, the size of the traffic input is a parameter that may be set to different values depending on the accuracy and computation-time requirements.

Selection of the descriptive statistical variable for the traffic space

In the long-term operation of the system, the economic benefits for an MTS operator resulting from the improvement of the infrastructure will be related to the mean energy-saving values. In this thesis, it is assumed that the mean results obtained with the whole traffic scenario set are able to represent the actual mean energy savings. Thus, this thesis proposes the mean values of the traffic space energy figures as the reference values. The representative traffic scenarios selected to be the traffic input included in MTS infrastructure improvement studies must make it possible to obtain the reference values.

However, mean values are known to lead to a lack of accuracy when the variables under consideration in a simulation-based study follow multimodal distributions or are strongly affected by outliers (Bierlaire 2015). Therefore, energy-saving distributions should be inspected in order to discard these cases.

The required energy-saving figures have been obtained by applying the single RS test defined in Section 3.1.2 to the traffic scenarios in the 7-minute headway traffic space. Figure 4-9 shows the distributions of the energy-saving results for each RS available position (SSs). Figure 4-9.a illustrates how the results for some RS positions are distributed in a normal fashion, whereas for other RS positions the distributions exhibit right-side tails. In any case, it may be stated that all the distributions are unimodal, and therefore the mean and the median values for all cases are expected to be similar.

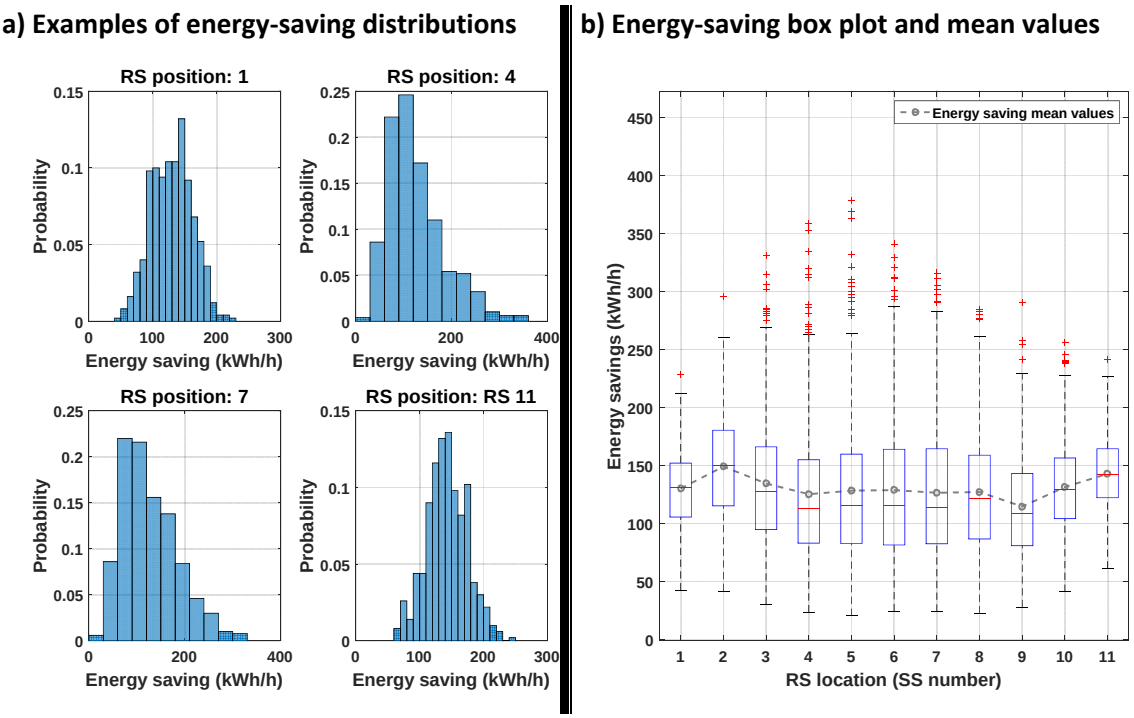

Figure 4-9. Energy-saving statistical figures

Figure 4-9.b supports this result. The mean energy-saving values for each RS position have been added to the energy-saving box plot. Some of the results for several RS positions are interpreted as outliers, but even so, the mean and the median values

remain fairly similar. In addition, all the traffic scenario samples are equiprobable, and there are no unfeasible situations from the traffic regulation standpoint. This implies that there is no reason to exclude extreme energy-saving values from the calculations.

Regarding this, the traffic-space mean energy-saving values represent the average savings that would be obtained in the long-term operation of the system. Consequently, these mean energy-saving values are proposed in order to obtain accurate long-term energy-saving results.

As a conclusion, it may be stated that the set of traffic scenarios used as the input to an MTS infrastructure improvement study must properly represent the mean energy-saving values of the whole traffic space. In the studies in this chapter, the maximum acceptable error has been set to 5% of the mean energy savings.

4.3.3. TRAFFIC-INPUT SIZE CONCERNS

In a case where the number of improvement-configuration options is low, the size of the traffic input to MTS studies will not be a critical concern. However, this is not the habitual situation. In general, the MTS infrastructure optimisation studies have to select a certain improvement configuration in a huge search space, as will be described in Chapter 6. To do that, these studies make use of optimisation algorithms which carry out multiple simulations in order to get good solutions (meta-heuristic, branch and bound, etc.). Large simulation times are likely to make these optimisation problems unmanageable from the computational-burden standpoint. On the other hand, it has already been proved in this chapter that an excessive simplification of the traffic input like the single-scenario traffic approach may lead to significant accuracy problems.

Consequently, a clear trade-off arises between computational burden and accuracy. It is therefore required to study the way to increase accuracy to a certain standard without including an excessive number of traffic scenarios in the traffic input.

This section performs a preliminary analysis on the traffic-input size. To do that, the energy-saving accuracy of some traffic inputs with increasing sizes has been assessed. The single RS test for the whole 7-minute traffic space has been used to obtain the required energy-saving figures.

In this exercise, the traffic-input size has been varied, using the size values contained in (4.1). Then, this analysis assigns, to each traffic-input size, 1000 different combinations of the 500 traffic scenarios in the total 7-minute traffic space. The combinations are obtained at random. E.g.: when the traffic-input size is set to 50 scenarios, 1000 combinations of the 500 scenarios in the total space taken 50 at a time are made.

$$SizeVector = [1 \quad 50{:}50{:}500] \tag{4.1}$$

Finally, the mean energy-saving values for each of these combinations and RS location have been obtained, and the relative errors with respect to the mean energy savings

for the whole traffic space (reference) have been calculated. This will make it possible to assess how frequently a partial selection of the scenarios in the traffic space will allow obtaining the reference energy-saving results.

Figure 4-10 shows the results for a couple of representative RS positions (1 and 7). Both graphs in this figure show a 5 % band around the mean energy-saving and the maximum and minimum mean energy-saving values for the different traffic-input sizes analysed (gray). In addition, the orange curves included represent the way these mean-saving values are distributed. For scale reasons, 100 times the normalised frequency (probability) has been shown. It may be observed that when the amount of scenarios selected is greater than 50, the most probable mean value converges to the mean value for the whole traffic set (130.1 kWh/h for RS1 and 126.5 kWh/h for RS7). Then, from 250-300 scenarios on, even the worst cases are inside the 5% error band. The rest of RS locations follow the same pattern. They have not been represented for the sake of clarity.

To summarise, it may be stated that the mean energy-saving values for a subset in the traffic space will be inside a 5% error band if the number of selected scenarios is greater than 250-300. Unfortunately, this represents a huge number of scenarios. Indeed, it accounts for more than 29 hours at this headway to be simulated in order to obtain accurate results. This situation could perfectly be unmanageable in terms of computing time in an optimisation problem.

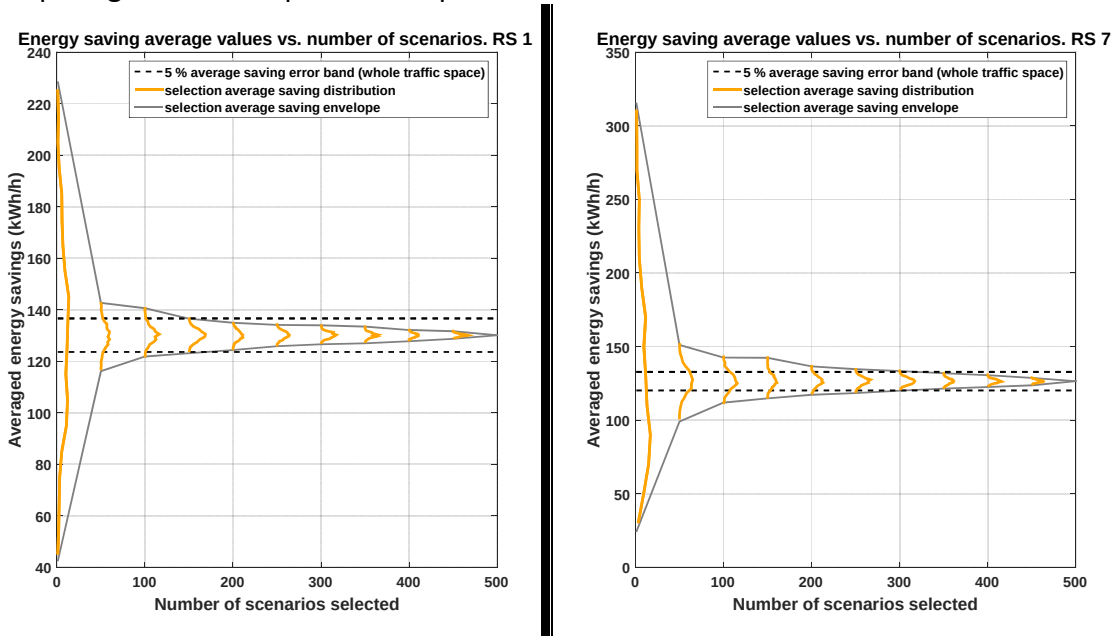

Figure 4-10. Distribution of the average energy-saving values with the size of the representative scenario set.

The general conclusion that may be extracted from this analysis is that the random traffic-scenario selection does not yield acceptable energy-saving accuracy results unless the number of traffic scenarios is set to a large value. It is therefore required to research on a refined method to obtain a better trade-off solution between accuracy and size than the one represented by the random scenario selection or the single-single-scenario traffic approach.

4.4. TRAFFIC-INPUT SIZE REDUCTION

This section aims to reduce the total number of traffic scenarios to represent the total traffic space (representative scenarios). To do that, it performs a proper characterisation of the traffic scenarios in the traffic space. This requires finding the relations between the electrical variables in an MTS and the energy savings resulting from improving the electrical infrastructure. If these relations are identified, it will be possible to have an estimation of the energy-saving accuracy at the moment of the selection of traffic scenarios within the total traffic space.

Therefore, this will make it possible to refine the selection method, obtaining small-size traffic inputs with high accuracy.

4.4.1. ENERGY SAVINGS AND SYSTEM LOSS REDUCTION

As was derived in Section 3.2.1, for the same train energy, the energy savings resulting from the improvement of the MTS electrical infrastructure are a combination of: 1) the reduction of conduction losses and; 2) the reduction of rheostat losses.

Conduction losses will be reduced if the voltages in the line increase, which would make decrease line currents. In addition, changes in load flows due to the inclusion of RSs of ESSs in the system will modify conduction losses as well. The reason is that these devices change the average distance between generation (braking trains and SSs) and consumption (motoring trains) points in the system. Then, rheostat losses will be reduced if the excessive regenerative braking power that provokes them is –at least partially– absorbed.

The relevance of each of these loss sources on the system energy-efficiency improvement has been analysed by searching for significant correlations between savings and loss variations. To do this, the results of the single RS test for all the RS available locations and all the traffic scenarios in the 7-minute headway traffic space have been used. This time, the results have been processed snapshot by snapshot in order to obtain more precise conclusions.

Figure 4-11 shows, respectively, the scatter plots of energy saving versus rheostat-loss reduction and conduction-loss reduction. Each dot in the plot represents the energy savings for a single snapshot. The results suggest that there is a significant correlation between rheostat-loss reduction and energy savings, whereas this correlation does not exist between energy savings and conduction-loss reduction. The Pearson correlation coefficients are 0.998 (high correlation) and -0.334, respectively. Therefore, for the snapshots in these two traffic scenarios, the rheostat-loss reduction effect is dominant in comparison with the conduction-loss reduction effect. It is also important to note that conduction losses may either increase or decrease, being the cases where they increase compensated by a greater decrease in rheostat losses.

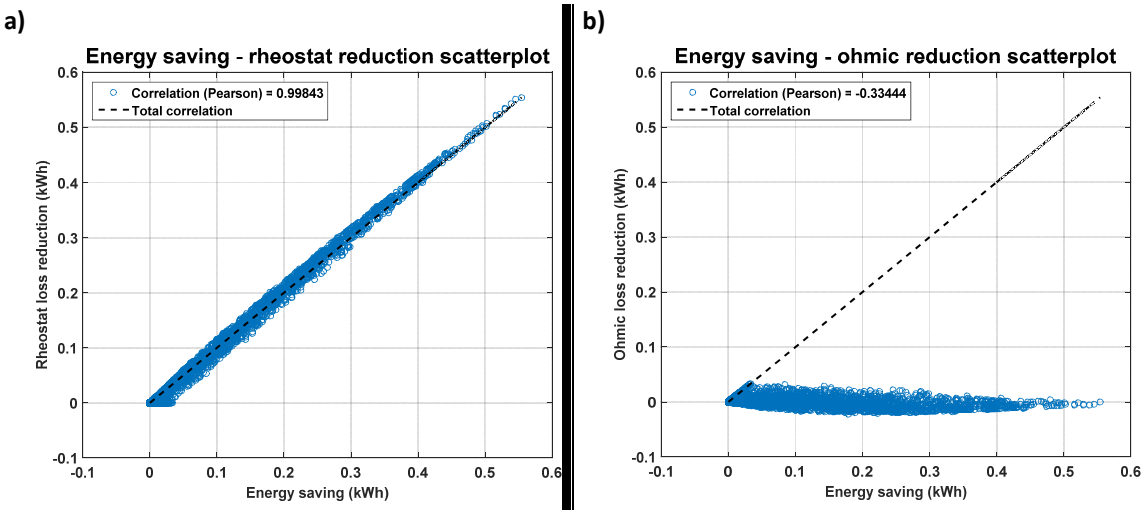

Figure 4-11. Correlation between energy saving and the principal system losses.

On the one hand, it may be stated that the ability to properly represent rheostat-loss reduction arises as a key factor to obtain accurate energy-saving results. However, rheostat-loss reduction is not directly available, it would be necessary to introduce improvements to the system to obtain them. These particular improvements are likely to lead to particular results. It is thus necessary to find a way of properly representing rheostat losses, and not rheostat-loss reductions. Consequently, it may be derived that the traffic input will be likely to exhibit high energy-saving accuracy figures if it includes a proper representation of the rheostat losses.

On the other hand, as was presented in Section 3.2.2, rheostat loss reduction depends on the relative position between rheostat loss trains, RSs, SSs and the rest of trains. Taking a given rheostat loss event in a given position in the line as reference, RSs in some available locations will easily reduce or even remove these losses, whereas RSs in other locations will be unable to absorb any power. This impossibility to reduce rheostat losses from some locations is sometimes due to long distances, and sometimes because of electrical interferences. It is thus important not only to represent rheostat losses in a traffic scenario, but also to include some information about their location and possible electrical interferences.

This means that the global rheostat losses in a traffic scenario will not be enough to represent the energy-saving potential, which depends also on the location of the infrastructure improvement device. Therefore, in order to properly characterise the traffic scenarios, it will be necessary to process rheostat losses by adding some information about where they take place and the traffic in the line.

4.4.2. REPRESENTATION OF THE RHEOSTAT LOSS DISTRIBUTION IN THE LINE

The analysis of the rheostat loss reduction mechanisms presented in Section 3.2.2 yielded three main cases, which were depicted in Figure 3-12:

a) Direct rheostat reduction method without affecting the snapshot load flow. The RS is placed in a branch where no current is flowing. There are no interferences between the RS and the rheostat train.

b) Direct rheostat reduction method changing the snapshot load flow. The RS is placed in a power exchange path. The RS will increase receptivity, but its voltage reduction effect will decrease the amount of energy sent to motoring trains. The amount of energy absorbed by the RS is related with the voltage of the RS location in the raw system (no RSs added).

c) Indirect rheostat-reduction mechanism. In this case, rheostat losses which take place far away from the RS may be reduced. For these events to take place, it is required not to have any active SS between the RS and the rheostat train.

In any of the three mechanisms, it is clear that the addition of an RS in a given location will not modify the load flow, and consequently rheostat losses, unless the voltage in this location before the RS is added (raw system) is greater than the no-load voltage. This implies that even rheostat losses that take place relatively close to a given location may be impossible to remove if there are high consumptions in this zone.

It is thus clear that the casuistic to be covered is very complex, as are the energy interactions between trains in an MTS. The traffic scenarios included in the traffic input must be able not only to represent the global rheostat loss figures, but also their distribution in the line, and how frequently the system is receptive to regenerated energy in each particular stretch in the line.

Following this reasoning, the way to characterise the traffic scenarios for the traffic input selection process must not be based on a single variable, but on a vector of variables which contains as many values as available locations for improvement devices. By doing this, it will be possible to introduce the space distribution of rheostat losses in the traffic scenario characterisation.

Therefore, in the application to the thesis case study, each traffic scenario is characterised by 11 values, corresponding to the 11 available locations for RSs. It must be noted that if ESSs were included in the study, this characterisation vector should be extended to 23 locations for the case study. The processed rheostat variables for each traffic scenario and location are obtained by applying (4.2).

$$PrRh(scen, loc) = \sum_{i=1}^{R} Erh_i \cdot F(drh_i) \; ; \quad F(drh_i) \in [0,1] \;\; \forall \, scen, loc \tag{4.2}$$

Where,

- $scen$ and loc are the traffic scenario and location under study, respectively.
- R is the total number of rheostat-loss events that take place in the scenario $scen$.
- Erh_i is the energy lost in each rheostat-loss event.
- F is the filter function used to process rheostat losses depending on their relative position with respect to the RS location loc and the traffic.

- drh_i is the relative position of the rheostat train with respect to the RS location loc.

Two different filter approaches have been tested in this study. First, a Space Filter Rheostat (SFR) function has been presented. This filter function is based on the evolution of the statistical rheostat reduction ratio with the distance to the RS location.

Second, this study presents a filter function based on the know-how acquired in the rheostat reduction mechanism review. This function filters each rheostat loss event depending on the type of rheostat reduction mechanism detected.

Space Filter Rheostat (SFR) function

The SFR is based on the average rheostat loss reduction as a function of the distance between the RS location and the rheostat train.

To find the evolution of the rheostat reduction with the distance, this study uses the rheostat-loss reduction results obtained from the application of the single RS test to the 7-minute headway traffic space.

The space information has been included by performing a 250-metre segment partition of the case study line. Then, for each RS location, the ratio between the rheostat reduction and the rheostat losses that take place at each segment has been calculated.

After that, the position of each segment is made relative to the corresponding RS location and the results for the 500 traffic scenarios averaged. The result of this exercise is a statistically significant curve representing the way in which rheostats are absorbed as a function of the distance to the RS point and the electrical interferences. Figure 4-12 shows this rheostat reduction curve in green. It may be clearly observed that when rheostat losses take place close to the RS, they are almost fully absorbed, whereas 7 km away from the RS there is practically no reduction, regardless of the amount of rheostat losses.

The shape of the rheostat reduction curve in Figure 4-12 is approximately symmetrical with respect to the RS location. In addition, it is rather similar to that of the frequency filters used to attenuate electronic signals. For this reason, the expression of the SFR function proposed is that of the module of a second order under-damped filter which has been complemented by a couple of ‘high distance’ poles to increase the attenuation for large distances. The SFR function has been refined by setting it to zero when the RS location voltage in the raw load flow is lower than the no-load voltage. The SFR formula is given in (4.3).

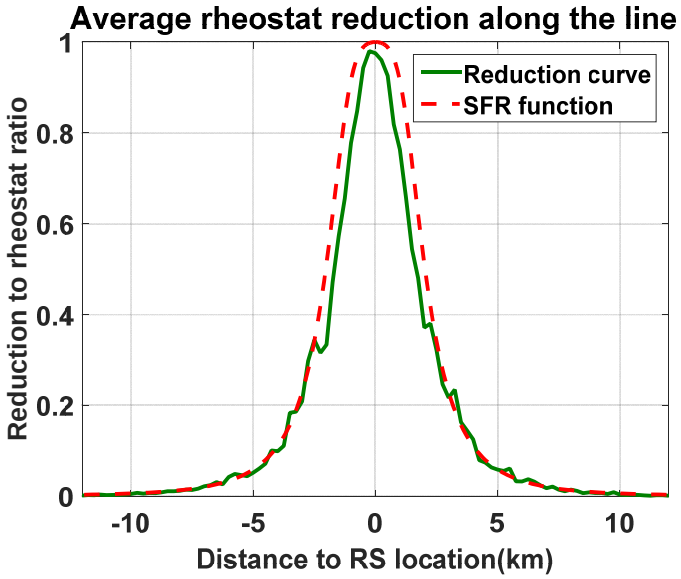

Figure 4-12. Rheostat reduction ratio vs. distance to the RS.

$$SFR(drh_i, V_{loc}) = \begin{cases} 0 & if \quad V_{loc} \leq V_o \\ \dfrac{1}{\left[\left(1 - \dfrac{drh_i^2}{Df^2}\right)^2 + \dfrac{4drh_i^2 Wf^2}{Df^2}\right]\left(1 + \dfrac{drh_i^2}{HDf^2}\right)} & if \quad V_{loc} > V_o \end{cases} \qquad (4.3)$$

Where,

- Df is the filter distance factor, which plays the role of the natural frequency (ω_n) in the under-damped second order filter.
- Wf is a factor to modulate the width of the filter. It is analogous to the damping factor (ζ) in the under-damped second order filter.
- HDf is a high-distance factor, analogous to a couple of high-module real poles.

Table 4-3 presents the particular values used for the SFR parameters. The way in which the SFR curve adjusts the average rheostat reduction ratio is presented in Figure 4-12.

Table 4-3. Particular values for the SFR function parameters.

	Df	***Wf***	***HDf***
Selected values	1.7 km	0.7	5.1 km (3 times *Df*)

The goodness of the SFR approach as a method to characterise the traffic scenarios has been measured by obtaining the Pearson correlation coefficients between the SFR values and the energy savings for each traffic scenario in the traffic space and all the RS location. Figure 4-13 shows these results which are higher than 0.9 (high correlation) except for locations 10 and 11. Nevertheless, the correlation for these two locations is still higher than 0.8.

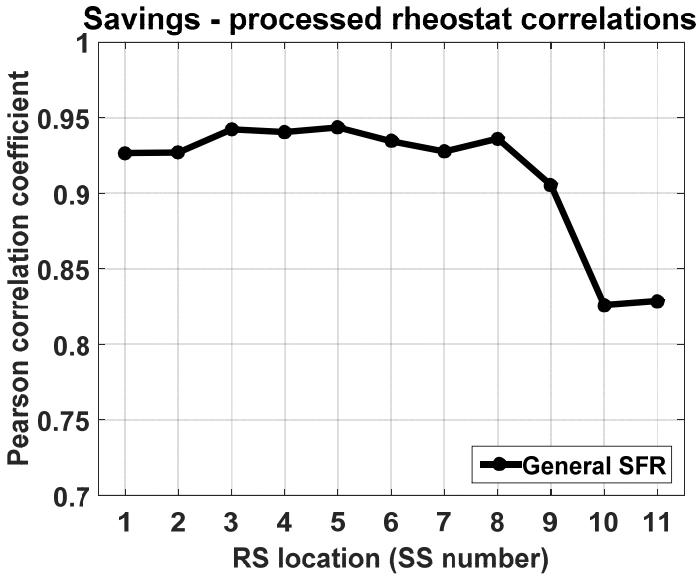

Figure 4-13. saving – processed rheostat correlations. SFR function.

The Experience-Based Filtered Rheostat (EBFR) function

This method is based on the rheostat reduction mechanisms described in Section 3.2.2. Like in the SFR method, the EBFR function assigns a certain fraction of the rheostat losses to each available location in the line. Although is not formally proven to, the EBFR will usually be a higher bound of the rheostat-loss reduction attainable from a given location.

Again, this method filters out all the rheostat loss events for a given location in instants when the voltage value in the raw system load flow is lower than the no-load voltage. This is shown in the preliminary expression of the EBFR function in (4.4).

$$EBFR(Erh_i, drh_i, V_{loc}) = \begin{cases} 0 & if \quad V_{loc} \leq V_o \\ EBFR\_case(Erh_i, drh_i, V_{loc}) & if \quad V_{loc} > V_o \end{cases} \tag{4.4}$$

Then, for these rheostat loss events that coincide with high RS location voltage, the application of the EBFR method requires to detect the type of rheostat reduction mechanism that would take place from the RS location under study to the rheostat loss event. The three main cases have been listed at the beginning of this section.

The expression applied to a rheostat loss event when the case a) is detected is given in (4.5).

$$EBFR\_case(Erh_i, drh_i, V_{loc}) = \frac{\min\left(\frac{V_{Rh}(V_{Rh} - V_{RS})}{R_l d_i}\Delta t, Erh_i\right)}{Erh_i} \tag{4.5}$$

Where,

- V_{Rh} is the rheostat-braking voltage threshold.
- V_{RS} represents an hypothetical voltage in the RS location after the installation of the RS.

- R_l is the impedance of the supply system, in Ω/km.
- Δt is the sampling time used in the traffic scenario generation.

The expression in (4.5) represents a simplification of the power transmission from a V_{Rh}-volt voltage source to another point in the line which voltage is clamped to a certain level. This expression does not aim to be an accurate representation of the actual load flow, but a simplified means to obtain the potential rheostat reduction from the RS location. As can be observed, the EBFR value is limited to the magnitude of the rheostat-loss event and then normalised.

When the case b) is detected, the EBFR is calculated following (4.6).

$$EBFR\_case(Erh_i, drh_i, V_{loc}) = \frac{\min\left(\frac{V_{Rh}(V_{Rh}-V_{RS})}{R_l d_i} \cdot \frac{Vraw_{loc}-V_{RS}}{V_{Rh}-V_{RS}}\Delta t, Erh_i\right)}{Erh_i} \quad (4.6)$$

Where, $Vraw_{loc}$ represents the voltage of the RS location in the raw-system load flow for the raw system.

From the analysis of (4.6), it may be extracted that the EBFR function represents the rheostat reduction when the RS is in a power exchange path by modulating the expression in (4.5) with a coefficient between 0 and 1. This coefficient will naturally tend to 1 when the RS location is close to the rheostat train (the voltage in the raw system is close to the rheostat threshold) and to 0 when it is close to the motoring train (or an active SS). With this modulation, it is possible to obtain an approximate figure of the actual rheostat reduction.

Finally, (4.7) presents the EBFR expression applied when case c) is detected.

$$EBFR\_case(Erh_i, drh_i, V_{loc}) = \frac{\min\left(\frac{V_{BTr}(V_{BTr}-V_{RS})}{R_l d_{BTr}} \cdot \frac{V_{loc}-V_{RS}}{V_{BTr}-V_{RS}}\Delta t, Erh_i\right) \cdot f_{ON\_SS}}{Erh_i} \quad (4.7)$$

Where,

- V_{BTr} is the voltage of the braking train that is causing the high raw-system RS location voltage. It must be noted that in this case, this train is not necessarily in rheostat mode.
- f_{ON_SS} is a binary factor which is set to zero if there is an active (ON) SS between the rheostat train under study and the RS location. This is used to represent the decoupling effect of active SSs that was presented in Section 3.2.2.

The filter expression in (4.7) is applied when there is a motoring train between the rheostat loss train and the RS location. As already stated, the train that provokes a high raw-system RS location voltage is not necessarily in rheostat mode, and so V_{BRt} may be the rheostat threshold voltage or a lower value. When there is an active SS between the rheostat event under study and the RS location, the rheostat reduction is marginal, and the EBFR function has consequently been set to zero.

Table 4-4 presents the particular values used for the EBFR parameters.

Table 4-4. Particular values for the EBFR function parameters.

	V_{Rh}	V_{RS}	R_l
Selected values	710 V	646.4 V (640 V · 1.01)	22.4 mΩ

Figure 4-14 presents the correlations between the EBFR values and the energy savings obtained for each RS location. Figure 4-14.a show that the new correlations represent a notable increase with respect to the SFR function, which has been included in the figure as well. The correlations are greater than 0.9 for all the RS locations. For these improved results, the EBFR function is the one proposed to characterise the traffic scenarios in the traffic space.

Figure 4-14.b presents the extension of the EBFR function correlation results to the three headways included in the analyses of the thesis. The results for 4- and 7-minute headways are very similar, representing high correlation results. The results for the 15-minute headway tend to be worse, but still greater than 0.9 for all the RS locations.

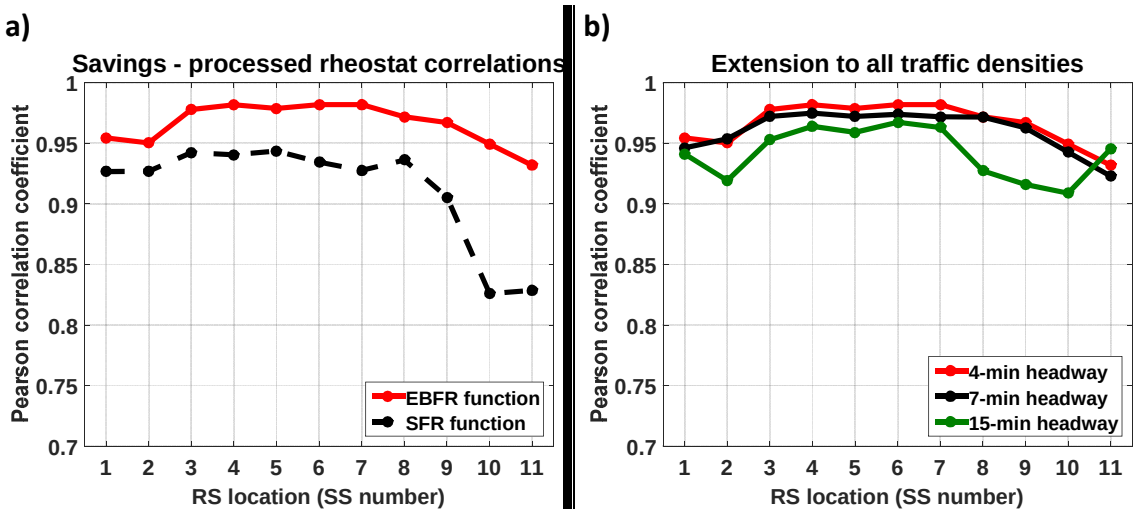

Figure 4-14. Energy saving – processed rheostat correlations. EBFR function.

Based on these high correlation results, this thesis makes the following hypothesis: a good candidate for the traffic input set must be made up of a set of traffic scenarios which average EBFR values are close to the traffic-space average EBFR values for all the locations studied.

The validity of this hypothesis will be studied in Section 4.5, where the EBFR function will be used to guide the traffic input scenario selection.

4.5. REPRESENTATIVE TRAFFIC-SCENARIO SELECTION

This section is devoted to the selection of a set of traffic scenarios which are representative of the complex train energy exchanges expressed in the traffic space. The selection process is based on the EBFR characterisation presented in Section 4.4.2. It aims to reduce the size of the traffic input to the MTS optimisation study in Chapter 6 with respect to the required size for the random traffic scenario selection presented in Section 4.3.3.

The traffic scenario selection itself is preceded by an assessment of the single RS energy-saving errors resulting from the use of the EBFR function.

4.5.1. EBFR BASED SCENARIO SELECTION ACCURACY

This section is in charge of assessing the minimum size of the traffic input to MTS studies required to meet a given accuracy standard. In this thesis, 5 % mean energy saving error has been set as the required traffic-input accuracy.

The MTS-study traffic-input generation proposed in this thesis consists of selecting a subset of the total traffic scenario set. The possible combinations of traffic scenarios depend on the size of the traffic space and the number of traffic scenarios selected, following (4.8).

$$nCOMB_{TS} = \frac{nSAMP_{TS}!}{nSAMP_{TINP}! \cdot (nSAMP_{TS} - nSAMP_{TINP})!} \tag{4.8}$$

Where,

- $nCOMB_{TS}$ is the possible number of combinations.
- $nSAMP_{TS}$ is the number of samples in the total traffic space.
- $nSAMP_{TINP}$ is the number of representative traffic scenarios included in the traffic input to MTS infrastructure studies.

For the traffic space size in this thesis, the possible combinations to obtain the traffic input soar from two-scenario traffic-input-size on. For this reason, the study of the traffic-input size has been based on large sets of randomly selected traffic inputs with increasing size. Specifically, for each traffic-input size, 100000 random traffic scenario combinations have been generated.

A particular traffic scenario selection is classified as a good candidate to represent the traffic space from the energy saving standpoint if its mean EBFR values for all the 11 RS locations in the case-study line are inside a 5 % band around the traffic space mean EBFR values. The 7-minute headway is again used to illustrate the developments.

The first result observed is that for small traffic-input sizes it is very unlikely to obtain good EBFR accuracy for all the RS locations. Figure 4-15 presents the percent of good candidates for the 7-minute headway traffic input. No combinations have met the mean EBFR accuracy standard for all the RS locations until the size of the traffic input has been set to 4 traffic scenarios. From this size on, the number of random

combinations of traffic scenarios that fit the mean EBFR values for all the RS locations rises steadily. Nevertheless, the percentage of good candidates is below 1% until the traffic-input size is set to 14 traffic scenarios.

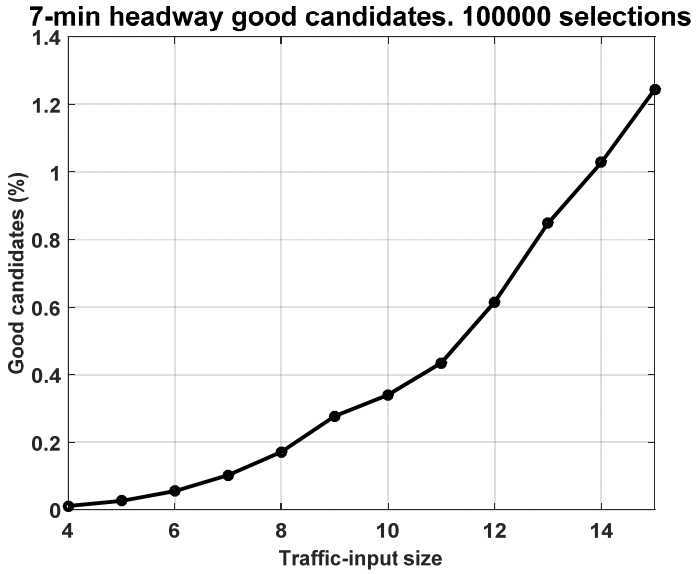

Figure 4-15. Percentage of good traffic input candidates vs. traffic input size.

To continue with the study of the required traffic-input size, the energy-saving accuracy of all the RS locations has been analysed. The energy-saving accuracy evaluation has been restricted to the scenario selections classified as good candidates. The top-side graph of Figure 4-16 shows, in black, the percent of RS locations which energy-saving error with respect to the traffic-space average is lower than 5 %. It can be observed that the percent of samples with good accuracy figures is greater than 90 % of the total number of samples except for the five-traffic-scenario case. However, these results have not been regarded as representative until the number of RS location samples analysed is greater than 1000. The number of samples included in the analysis is presented in the bottom-side graph of Figure 4-16. The required number of samples is attained from the seven-traffic-scenario case on.

The probability for a RS location in a good traffic-space candidate to exhibit acceptable energy-saving figures is greater than 0.95 from the nine-traffic-scenario size on. For all the cases analysed, it may be observed that practically all the RS location which energy-saving accuracy figures do not meet the accuracy standard in the thesis present error figures below 10 %. This result implies that it is very unlikely to have extremely poor accuracy performance if the EBFR traffic characterisation is used to select the representative traffic scenarios to be included in the traffic input to MTS studies.

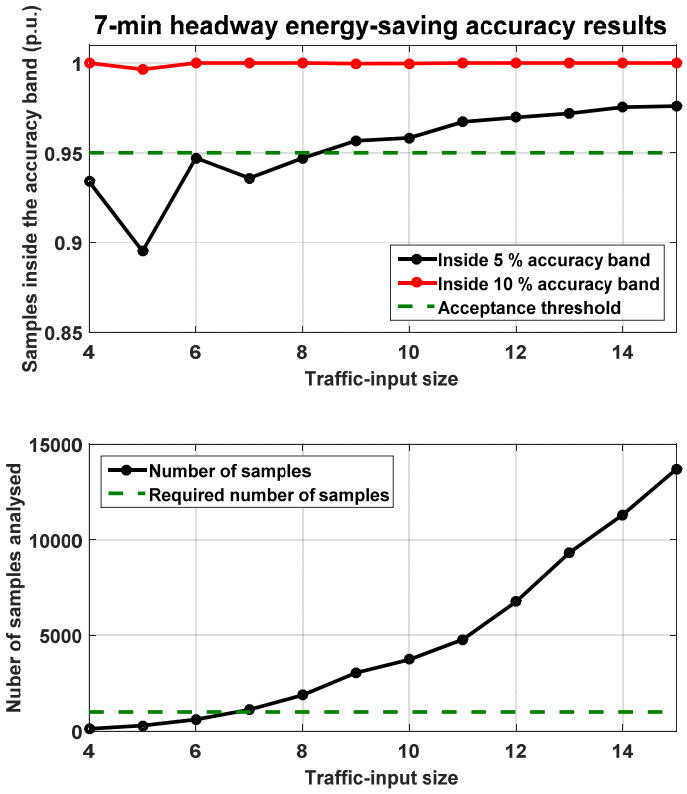

Figure 4-16. Average energy saving accuracy vs. traffic input size.

Finally, Figure 4-17 presents the extension of the energy-saving accuracy results to the 4- and 15-minute headway traffic spaces. The energy-saving accuracy figures are similar to the ones obtained for the 7-minute headway. However, there are several particularities of these two extreme operation headways which are worth to mention:

- In the 4-minute headway case, there are no good candidates for the traffic input until the representative-scenario size is set to 10. Then, the required number of RS location samples is not attained until 18 traffic scenarios are selected. From the 18-traffic-scenario size on, the probability of the RS location energy saving accuracy to be acceptable remains higher than 0.95. For all the good traffic-input candidates found, all the RS location accuracy figures are better than 10 %.
- The 15-minute headway case, the traffic-input size required to obtain the critical number of RS location samples for the results to be significant is reduced to 2 traffic scenarios. Then, from 3 traffic scenarios on, the probability to have good energy saving figures is greater than 0.95. Again, no significant fraction of the RS locations exhibit accuracy figures worse than 10 % when the EBFR function is used to guide the traffic scenario selection process.

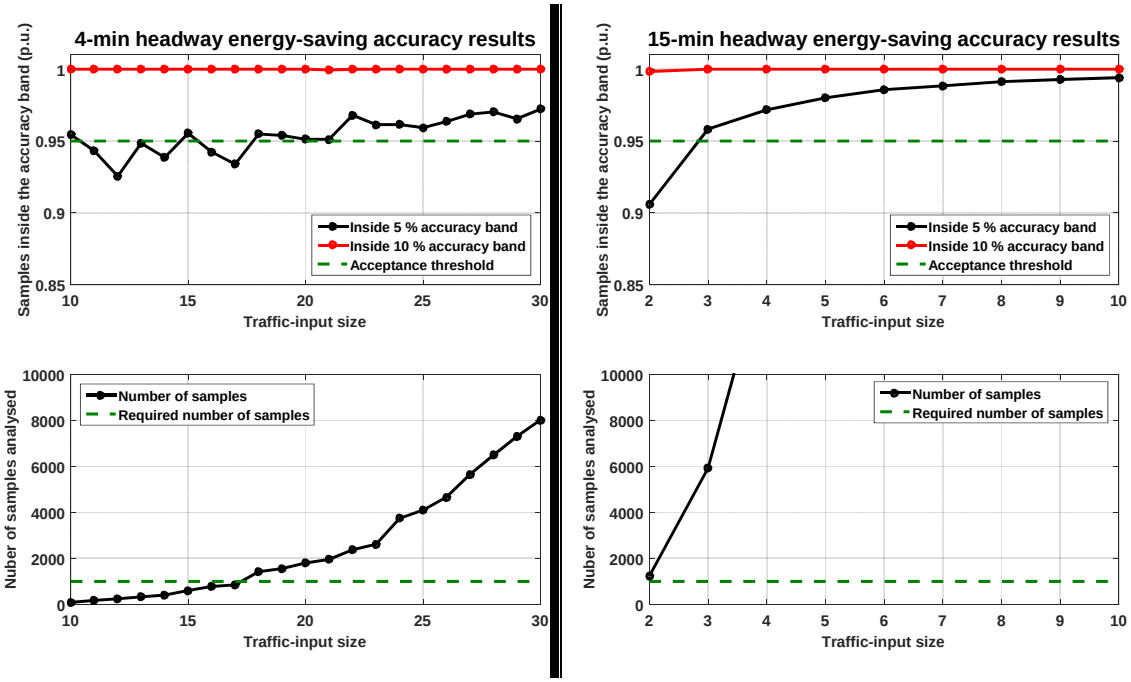

Figure 4-17. Average energy saving accuracy vs. traffic input size.

4.5.2. ASSESSMENT OF THE SELECTED TRAFFIC SCENARIOS

The criterion followed to decide the traffic-input size may be summarised as: the minimum traffic-input size so that the probability for the RS locations to exhibit good energy-saving accuracy figures is greater than 0.95. This leads to traffic-input size 18, 9 and 3 for the 4-, 7- and 15-minute operation headways, respectively.

It was explained is Section 4.2 that in general the scenarios in the traffic space may contain singular characteristics like zones in the line which are not visited by any train or zones which are visited twice. In the method proposed in this thesis, the representative scenarios are forced to properly characterise all the zones of interest in the line, which is attained by combining several scenarios. This approach prevents the representative scenarios from including biased information about the energy exchanges between trains in the line.

It must be noted that the large dispersion in the traffic-input size when this parameter is expressed by the number of traffic scenarios is reduced if the size is measured in number of snapshots, or time. In this case, the total simulation times required to obtain accurate energy saving figures for the operation headways are 72, 63 and 45 minutes, respectively. It may be observed that the higher the traffic density, the larger the required simulation time. This is in line with the expected results, since the complexity of the train energy exchanges in the system depends on the average number of trains.

The energy-saving result accuracy will be measured by applying first the single RS test in order to analyse the goodness of the representative scenarios location by location; and then by applying the multiple RS test to check the accuracy when RSs are located at several locations at a time.

Figure 4-18 presents the energy-saving accuracy results obtained by the application of the single RS test to the 7-minute headway representative scenarios. In addition, it plots the results that would be obtained by implementing the single-scenario traffic approach. It may be observed the notable accuracy increase derived from the application of the representative traffic scenario approach presented in this thesis.

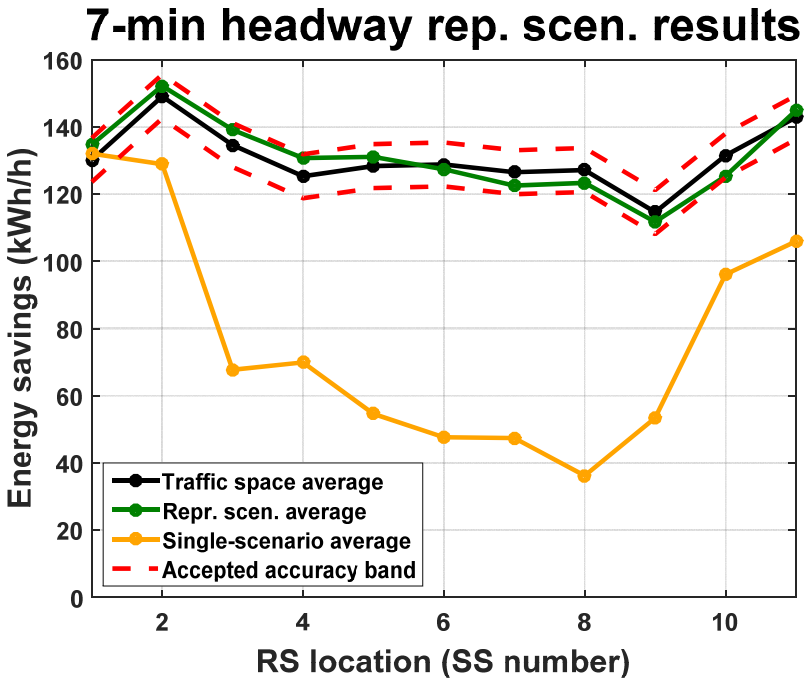

Figure 4-18. Energy saving accuracy figures for the 7-minute headway.

Table 4-5 present the relative accuracy figures for all the RS locations both for the representative-scenario and single-scenario traffic approaches. Percent error results greater than 10 % have been represented in red. It may be observed that all the RS locations exhibit relative errors lower than 5 % for the representative scenario traffic approach. The single-scenario traffic approach may lead to relative errors close to -70 % of the average savings.

Table 4-5. Relative error results for the 7-minute headway traffic space.

RS loc. (SS)	1	2	3	4	5	6	7	8	9	10	11
Rep. Scen. (%)	3.5	2.5	3.5	4.1	2.1	-1.1	-3.1	-2.9	-2.2	-4.7	1.6
Single scen. (%)	1.4	-15.4	-51.1	-42.4	-56.4	-62.1	-60.5	-69.5	-46.8	-27.1	-28.2

Figure 4-19 and Table 4-6 present the extension of the representative traffic scenario results for the 4- and 15-minute headways. Again, all the energy-saving relative errors are lower than 5 %. Regarding the single-scenario traffic approach, it may be observed how it fails to obtain accurate energy-saving results for the 4-minute headway, whereas it obtains better accuracy results for the simpler traffic situations in the 15-minute headway. Nevertheless, for both headways it presents relative energy-saving error figures greater than 10 %.

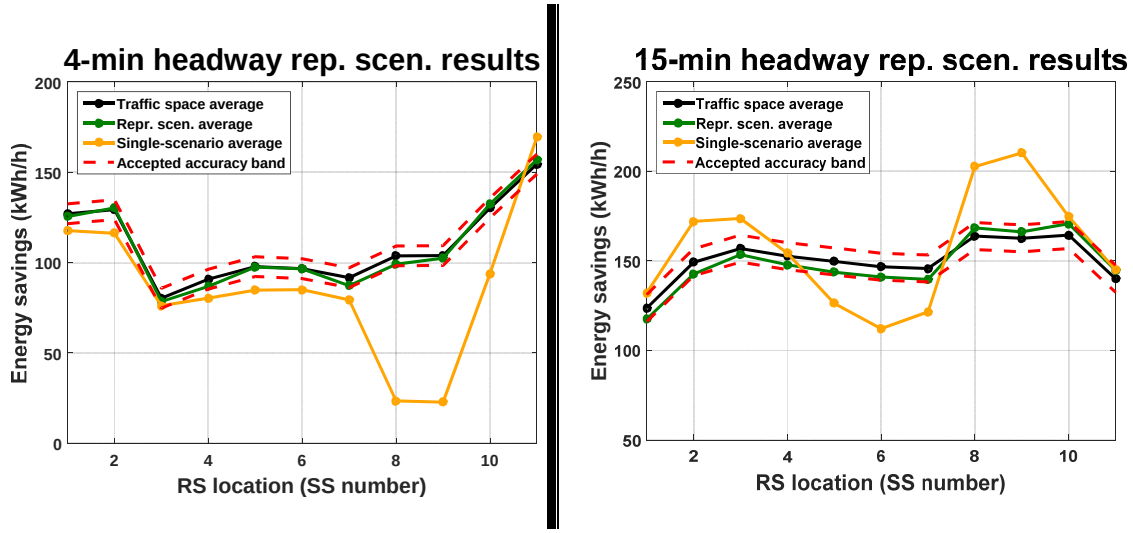

Figure 4-19. Energy saving accuracy figures for the 4- and 15-minute headways.

Table 4-6. Relative error results for the 4- and 15-minute headway traffic spaces.

	RS loc. (SS)	1	2	3	4	5	6	7	8	9	10	11
4 min	Repr (%)	-1.3	0.9	-1.7	-3.7	0.2	-0.1	-4	-4.2	-1.3	-2	2.2
	Single (%)	-8.5	-11.9	-3.8	-9.6	-11.8	-10.6	-11.2	-73.2	-74	-33.1	13.7
15 min	Repr (%)	-4.1	-4.4	-2.2	-3.2	-4	-3.8	-4.1	3	2.4	4.2	3.1
	Single (%)	5.6	15.2	11.1	1.1	-15.6	-23	-16.1	25.8	31.7	6.8	3.3

Once the single RS test has proved that the selected traffic scenarios are able to properly represent all the available RS locations, it is required to assess whether they keep yielding good energy-saving result accuracy when several RSs are installed at a time. This has been evaluated by means of the multiple RS test, defined in Section 3.1.3.

Figure 4-20 presents the energy-saving results obtained in the 110 RS configurations of the multiple RS test for the 7-minute headway case. It represents both the results obtained with the representative scenarios and with the single-scenario traffic approach. It may be observed in the top-side graph that the results obtained with the representative scenarios are close to the reference values (obtained with the whole traffic space). The results from the single-scenario traffic approach differ substantially from the reference values.

The bottom-side graph in Figure 4-20 shows the representative-scenario relative errors. The batch average savings have been used to make the results relative in order not to artificially punish cases with low savings. It must be observed that the accuracy results are inside the accepted tolerance for the representative scenarios. The errors obtained with the single-scenario traffic approach are inside the accepted tolerance band only in one out of the 110 configurations in the multiple RS test. For high energy

savings, it tends to stabilise around 40 % error. It has been proven that the reason for this effect is that the total rheostat-loss values in the particular scenario used in this simplified approach are lower than the average total rheostat-loss values of the whole traffic space.

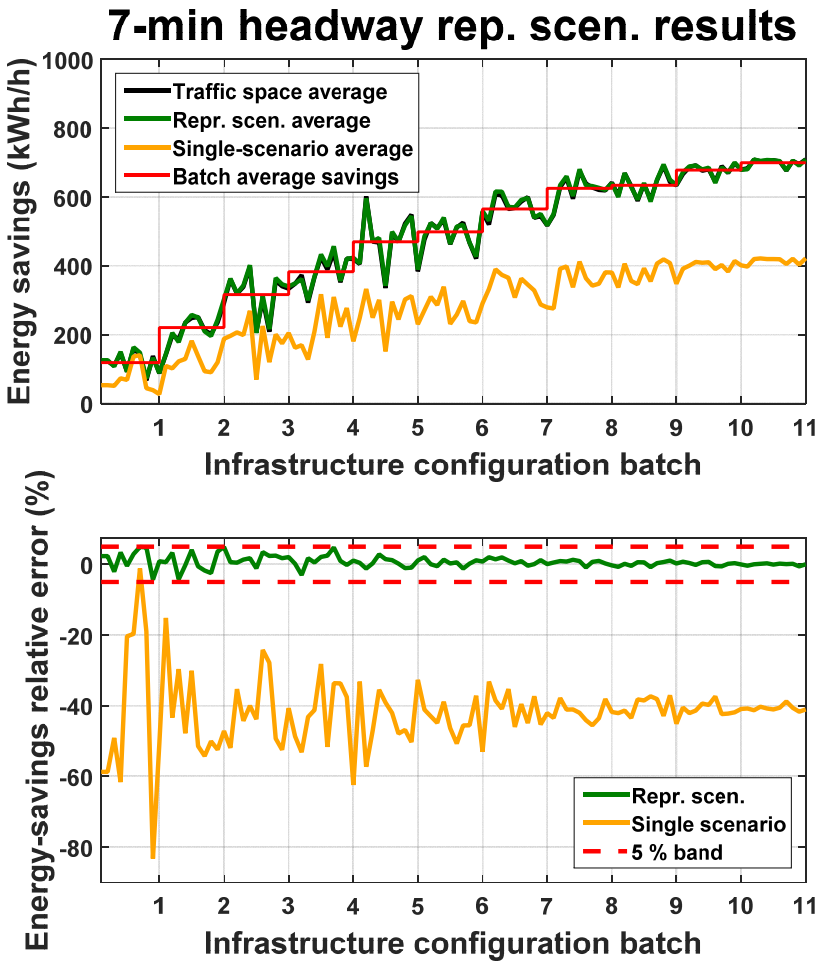

Figure 4-20. Energy saving accuracy figures for the multiple RS test. 7-minute headway.

Figure 4-21 shows the extension of the complex-infrastructure accuracy results for the 4- and 15- minute headways. The results obtained with the representative scenarios are qualitatively better than those yielded by the single-scenario traffic approach. The errors for this latter stabilise in high relative values for large savings which are negative in the 4-minute and positive in the 15-minute headway. Again this is due to a discrepancy in the total rheostat-loss values for the single-scenario traffic approach. These latter results have proven that there is a large uncertainty about the energy-saving results to be obtained with the single-scenario traffic approach. They are always inaccurate, but they may be larger or smaller than the actual reference values.

Regarding the representative-scenario case, a slight negative error is observed for large savings both for 4- and 15-minute headways. This is also due to a –this time slight– total rheostat-loss error discrepancy with respect to the traffic-space average. Thus, it may be extracted that the scenario selection proposed leads indirectly to good

total rheostat-loss values. Nevertheless, this error bias for large savings could be mitigated, or even centred if the total rheostat losses are explicitly forced to be those of the whole traffic space in the scenario selection process.

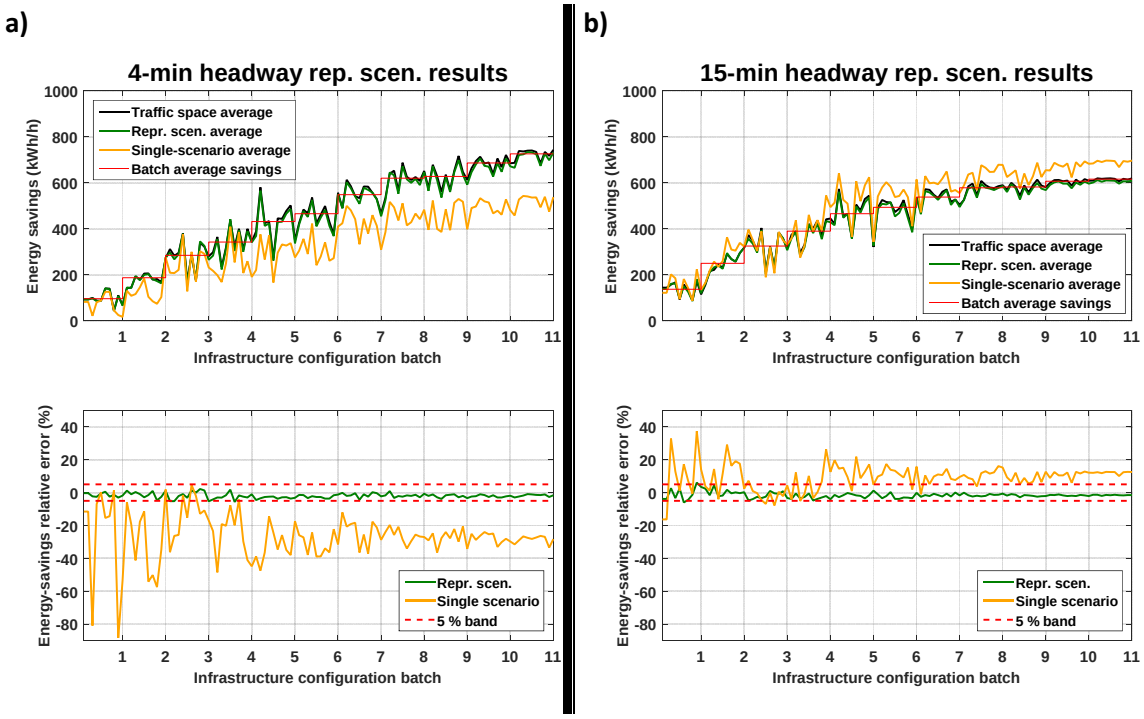

Figure 4-21. Energy saving accuracy figures for the multiple RS test. 4- and 15-minute headways.

The total number of cases out of the ±5 % error band for the representative-scenario case is not zero. The 4-minute headway exhibits 4 cases out of the 110 configurations which are out of the ±5 % error band, with -5.65 % worst-case relative error. The 15-minute case presents 2 cases out of the ±5 % error band, with +6.05% worst case error.

These slightly inaccurate cases are irrelevant enough not to consider them as a precision problem of the method. Nevertheless, this could be improved by including more scenarios in the representative-scenario set.

Figure 4-22 shows the rates of inaccurate cases for the accuracy standard considered. The representative-scenario case exhibit 3.6, 0 and 1.8 % inaccurate cases in the multiple RS case, which represent fairly good precision results. In addition, the worst-case errors are always below ±6.1 %. The single-scenario traffic approach presents poor accuracy results, with inaccuracy rates 93.6, 99.1 and 80 % and relative errors greater than 80 % for some extreme cases.

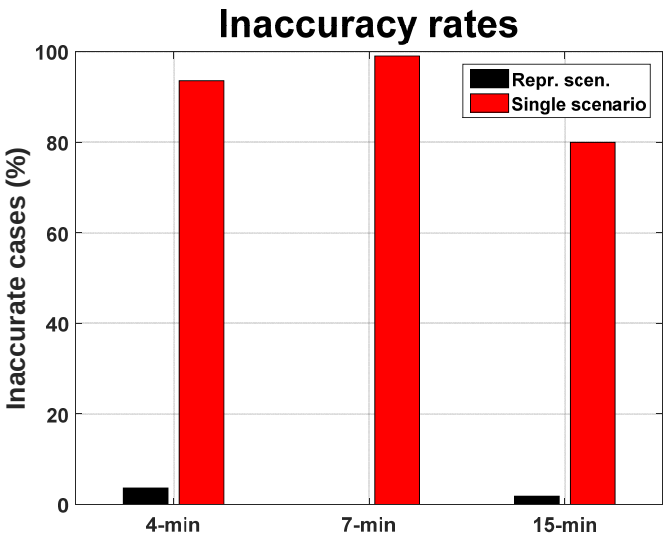

Figure 4-22. Analysis of the number of inaccurate cases in the multiple RS test.

4.6. SUMMARY, CONCLUSIONS AND CONTRIBUTIONS

This chapter has tackled the effects of the most relevant traffic variables on the MTS energy-saving results. In order to motivate the necessity of refining the traffic approach in MTS studies, it has been proven that the usual traffic modelling approach with a single scenario per headway does not cover the complex energy interactions between the trains in an MTS. Specifically, the receptivity figures obtained with this approach are far away from the average receptivity values. Thus, the energy-saving results obtained with the single traffic approach are not similar to those obtained with other traffic scenarios which are as probable to take place in the actual operation of the system as it is. This has been proven by comparison with another traffic scenario selected at random.

To cope with this problem, this chapter develops a detailed traffic model, which is able to represent the recurrent energy exchanges between trains in the case-study line. Under the operation scheme in this thesis, the most relevant traffic variables in double-track lines with two terminals have been identified to be: 1) dwell times at passenger stations, and 2) the time shift between train departure times at terminal stations. The former have been proven in the literature to follow a log-normal probability distribution, whereas it is reasonable to make the latter follow a uniform probability distribution.

The complex energy interactions between trains have been taken into account by the generation of a large number of traffic scenarios, obtained with different samples of the selected traffic variables. This yields a traffic space which consists in a large set of traffic scenarios. The critical mass of traffic scenarios required to represent the traffic in the case-study line has been proven to be around 300 samples. Therefore, three 500-sample traffic spaces have been generated for the different operation headways in the case-study line: peak-hour (4 minutes), off-peak-hour (7 minutes), and sparse traffic (15 minutes).

The mean energy-savings obtained with the whole traffic space have been considered to represent the actual savings that an MTS operator would obtain from the installation of infrastructure improvement techniques. Consequently, if a subset of the traffic space is selected to represent the traffic, its mean savings must be close to the whole-set mean values.

It has been proven that if the traffic representative scenarios are selected at random within the whole traffic space, the required size of the resulting traffic-scenario set would equal 300 samples (more than 29 hours for the 7-minute headway). This size is too large in practical terms.

To overcome this problem, a novel method to reduce the size of the selected set of representative scenarios has been developed. This method is based on the fact that the energy savings derived from improvements of the electrical infrastructure are inextricably linked to the reduction of rheostat losses. Thus, it has been concluded that a proper representation of the traffic must be achieved by a proper characterisation of the amount and location of rheostat losses.

With this basement, two functions that process the rheostat losses to represent the possibility of reducing them from each location in the line have been proposed: 1) the SFR, and 2) the EBFR function.

The latter, which is inspired on the three main rheostat reduction mechanisms defined in Chapter 3, has proven to yield figures which are highly correlated with energy savings for all the locations in the case-study line where it is possible to install RSs. Specifically, the correlation between the EBFR function and energy-savings in the single RS test is greater than 0.9 for all the 11 RS locations in the case-study line.

Consequently, this chapter proposes to obtain reduced-size sets of representative scenarios which are able to represent the energy interactions in the line by imposing their average EBFR values to be close to the whole-traffic-space average EBFR values. This must be fulfilled by all the available RS locations in order not to distort the energy-saving results obtained.

It has been proven that this approach makes it possible to obtain highly accurate energy-saving results both for simple (single RS test) and complex (multiple RS test) infrastructure improvement topologies, with relative errors below 5 %. It has also been observed that the usual single traffic approach in the literature is not able to obtain accurate energy-saving results, exhibiting worst-case relative errors close to 70 %.

Three sets of representative scenarios have been selected. These sets will be used as the traffic input for the MTS infrastructure optimiser developed in this thesis. The specific sizes for these sets are: 18 traffic scenarios for the 4-minute headway, 9 for the 7-minute headway, and 3 for the 15-minute one. These sizes lead to 72, 63 and 45 minutes of operation, respectively. Therefore, larger times are required for these headways where the interactions between trains are more complex (larger number of trains).

Summarising, the most relevant contributions of this chapter are:

- The demonstration that the usual over-simplified traffic modelling approach in the literature (one single scenario per headway) is not detailed enough to represent the complex energy interactions between trains in MTSs.
- The development of a traffic modelling approach for MTS design and improvement studies which includes the most relevant traffic variables.
- The demonstration of the high correlation between rheostat-loss reduction and energy savings.
- The method to characterise the traffic spaces, based on the rheostat-loss reduction mechanisms defined in Chapter 3. The EBFR function also represents a contribution of this thesis aimed to improve the accuracy of MTS design and infrastructure studies without a large increase in the simulation time.
- The method to select a reduce-size set of representative traffic scenarios, which are able to represent with high accuracy the complex energy interactions between trains in MTSs.

CHAPTER 5

TRAFFIC SCENARIO COMPRESSION

5.1. INTRODUCTION

As a result of the traffic analysis in Chapter 4, the number of traffic scenarios to be included in the MTS infrastructure studies has been increased with respect to the single-scenario traffic approach in the literature.

It must be noted that MTS infrastructure optimisation studies are often based on the simulation of the system. When this is the case, the optimiser might require several thousands of simulations under different configurations to converge to a good improvement solution. This usually leads to a heavy computational burden.

To illustrate this fact, let us consider an MTS optimiser which requires 10000 simulations of the system under different configurations to obtain the best possible infrastructure improvement. Let us compare two traffic models, both including 4-, 7- and 15-minute headways: 1) the usual approach in the literature, whit one traffic scenario per headway, and 2) the representative-scenario approach presented in Chapter 4, with 18, 9 and 3 scenarios for the 4-, 7- and 15-minute headways, respectively. Then, regarding the computation times will be obtained from the average results for the compiled simulator obtained in Section 2.4.2, i.e. the simulator takes 1.31 seconds to simulate one 7-minute traffic scenario. This result will be extrapolated to obtain the expected simulation times for the 4- and 15-minute headways: 0.74 and 2.79 seconds, respectively.

Table 5-1 presents the results that would be obtained with each traffic approach in terms of energy-saving error and computation time. On the one hand, the energy-saving accuracy of the usual traffic approach is not acceptable. On the other hand, the representative-scenario approach, which makes it possible to obtain good accuracy figures, exhibits a computation time which is nearly 7 times the one for the usual traffic approach. This makes the optimisation process take more than three days to obtain the results.

Thus, the reduction of the simulation time arises as a critical concern in order to make it possible for the infrastructure optimisers to obtain results in a reasonable time.

Table 5-1. Comparison between the usual and the representative-scenario approaches.

	Single traffic approach	**Representative-scenario approach**
Energy-saving error	>20%	<5%
Computation time	13.4 hours	93.1 hours

The simulation time reduction may be attained following two main strategies: a) reduce the computation time for a single snapshot by refining the load flow solver; b) reduce the number of snapshots to be simulated in a given scenario. The measures implemented to reduce the load-flow-solver simulation time were presented in Section 2.4.2. Then, this chapter is devoted to the study of the possibility of reducing the number of snapshots to be simulated.

The number of snapshots to be simulated is determined by the sampling time used to obtain the electrical snapshots. Most of the MTS electrical simulators and optimisers found in the literature (Chapters 2 and 4) use one-second sampling time to obtain the electrical snapshots to be solved. Thus, assuming that a particular system is operated under three different headways, and that the traffic input contains about one hour of operation per headway, more than 10000 snapshots must be simulated to obtain a single energy consumption result for the system.

There is, of course, a straightforward approach to reduce the number of snapshots to be solved: subsampling. This method makes it possible to steadily reduce the simulation time by simply discarding a subset of snapshots at a regular rate. However, there is a necessary loss of information derived from subsampling that may affect the accuracy of the energy-saving results. It is not clear to what extent the number of snapshots may be reduced without seriously affecting accuracy.

Nevertheless, the one-second sampling time is not a casual selection. In rapid transit systems as MTSs, acceleration and braking phases usually last from 10 to 20 seconds. The overlapping of these acceleration and braking phases determines the absorption of regenerative energy and rheostat losses. This train power phase overlapping is notably affected by the traffic stochastic variables, which may make it follow any complex pattern. Therefore, it does not seem easy to increase the simulation sampling time without a significant decrease in energy-saving accuracy.

To cope with this concern, this thesis proposes a novel method to compress the snapshots in a given traffic scenario. This smart compressor focuses on the most

relevant electrical variables in the system and groups similar snapshots in an initial clustering stage. Then, it searches for an optimised Equivalent Load and regeneration Profile for each cluster (ELP hereafter). The result is an equivalent traffic scenario containing a low number of snapshots which is equivalent to the uncompressed one. The necessary loss of information due to having a low number of samples to represent the traffic scenario is thoroughly reduced compared to the subsampling approach. The energy-saving accuracy is therefore increased.

It must be noted that even those optimisers which do not make use of simulation tools need to represent the traffic as well. The implications of the traffic in the energy figures of the system, presented in Chapter 4, are fully applicable to this kind of optimisers. Indeed, these studies define the electrical equations of the system for a set of time instants, or snapshots. In this case, the compression of snapshots will be translated into a reduction in the number of equations and variables. Consequently, the use of the compressor in this type of studies will also be highly beneficial in terms of computational burden (time to find the solution, computer memory consumption, etc.).

The chapter starts by presenting the conceptual frame that makes it possible the traffic scenario compression, in Section 5.2. Then, Section 5.3 and Section 5.4 explain the particularities of the two stages in the compressor. The representative traffic scenarios of the 7-minute headway traffic space are used to illustrate the derivations. Finally, Section 5.5 presents the traffic scenario compression results.

5.2. TRAFFIC SCENARIO COMPRESSION BACKGROUND

In the derivations in this chapter, a traffic scenario which contains snapshots with the one-second sampling time will be referred to as 'uncompressed scenario'. Obviously, the same traffic scenario, after being processed by the compressor will be named 'compressed scenario'.

The traffic scenario compression method presented in this thesis is based on the equivalency between a single load-regeneration profile (ELP) in the compressed scenario and a set of snapshots in the uncompressed one. The accuracy of this equivalency will be high if the set of snapshots are similar, but it could be poor if the represented snapshots are heterogeneous. In any case, taking into account that the trains are moving loads, it is straightforward to realise that there will be a loss of information as the amount of snapshots represented by a single ELP is increased.

Consequently, it has to be properly assessed which variables must be represented as accurately as possible in the equivalent model. This will in turn depend on which kind of results a particular study focuses on, and will allow having a higher or lower compression of the traffic scenarios. E.g.: The traffic in a study which aims to obtain energy-saving results, where average values play a key role, will be easier to compress without leading to wrong conclusions than the traffic in a study where the maximum power delivered by the SS converters is to be determined.

As stated in Section 1.2, this thesis focuses on energy-saving concerns. Chapter 4 has tackled the energy-saving accuracy problem, which has led to the selection of several traffic scenarios to represent each traffic density in the MTS. Now, the traffic scenario compressor aims to reduce the simulation time required to obtain energy-saving results without notably affecting the accuracy.

Therefore, it is again necessary to base the design of the compression concept on the rheostat reduction mechanisms. An ideal compressor should reduce the number of snapshots to be simulated without introducing a significant distortion in the variables that explain the rheostat loss reduction. Consequently, it is necessary to review the three rheostat-loss reduction mechanisms defined in Section 3.2.2 and to evaluate the important concerns in each of them (see Figure 3-12):

a) Direct rheostat reduction method without affecting the snapshot load flow. The RS is placed in a branch where no current is flowing. The energy saving in this case will be the rheostat loss reduction minus the conduction losses and multiplied by the efficiency of the RS converter. With regard to energy-saving accuracy, an equivalent model for this snapshot should properly represent the distance between the RS and the rheostat braking trains and the amount of rheostat losses.

b) Direct rheostat reduction method changing the snapshot load flow. The RS is placed in a power exchange path. The amount of energy absorbed by the RS depends on its relative position between the rheostat train, the motoring train and other SSs. With respect to this rheostat loss decrease mechanism, it is important to note that a good state variable describing the way power is being exchanged in the line is the line

voltage. Hence, an equivalent model for this type of snapshots should properly represent the position of the rheostat losses, the amount of rheostat losses and the voltage at the RS location.

c) Indirect rheostat-reduction mechanism. With regard to the accuracy of the equivalent model, there are no qualitative differences with the case b). Accurate RS location (SSs) voltages and position-amount of rheostat losses will indirectly lead to a fair representation of braking trains which are not in rheostat mode.

Summarising, for the compressed equivalent traffic scenario to properly obtain energy saving figures, it must reproduce rheostat-loss decrease events. From the analysis of the rheostat reduction mechanisms, it can be stated that the equivalent model will be accurate if it represents properly the positions and rheostat losses of the trains and the SS voltages.

5.2.1. THE COMPRESSION METHOD IN A NUTSHELL

Figure 5-1 shows the flow diagram of the traffic-scenario compressor presented in this thesis. It is essentially carried out in two steps: 1) the uncompressed scenario clustering, and 2) the optimum ELP search.

Uncompressed scenario snapshot clustering

In this first phase, the snapshots in the uncompressed traffic scenario are clustered. The aim of this stage is to group similar snapshots into a single equivalent snapshot or cluster. Those snapshots are solved one by one in the uncompressed scenario, whereas in the compressed scenario, a single execution of the load flow solver will be carried out. Consequently, the computation time will be reduced.

The k-means algorithm has been used to perform this clustering exercise. Since this algorithm requires the number of variables of the input dataset to be constant, an input data pre-processing stage has been included. In this stage, the total set of snapshots is divided into subsets where the number of trains in the line is constant. Then, the most significant electrical variables of these snapshots are collected and some transformations to improve the clustering performance are applied.

Finally, the k-means algorithm is executed and the snapshots are grouped into a given number of clusters. This number of clusters plays a pivotal role in the compression method, and determines the compression ratio (CR). The snapshot clustering process is presented in Section 5.3.

Optimum ELP search

This second phase is in charge of obtaining the ELPs for each particular cluster yielded by the clustering stage. The ELP makes it possible to simulate each equivalent snapshot (cluster) in the compressed scenario. In the simulation of compressed scenarios, each ELP has an associated time which equals the number of snapshots in its cluster times the sample time of the uncompressed scenario.

An evolutionary search method (the Particle Swarm Optimisation (PSO)) has been implemented to obtain the ELPs. After this algorithm finds a good load profile, a rheostat loss correction stage is carried out in order to refine the solution. The two processes in this second stage of the method are described in Section 5.4.

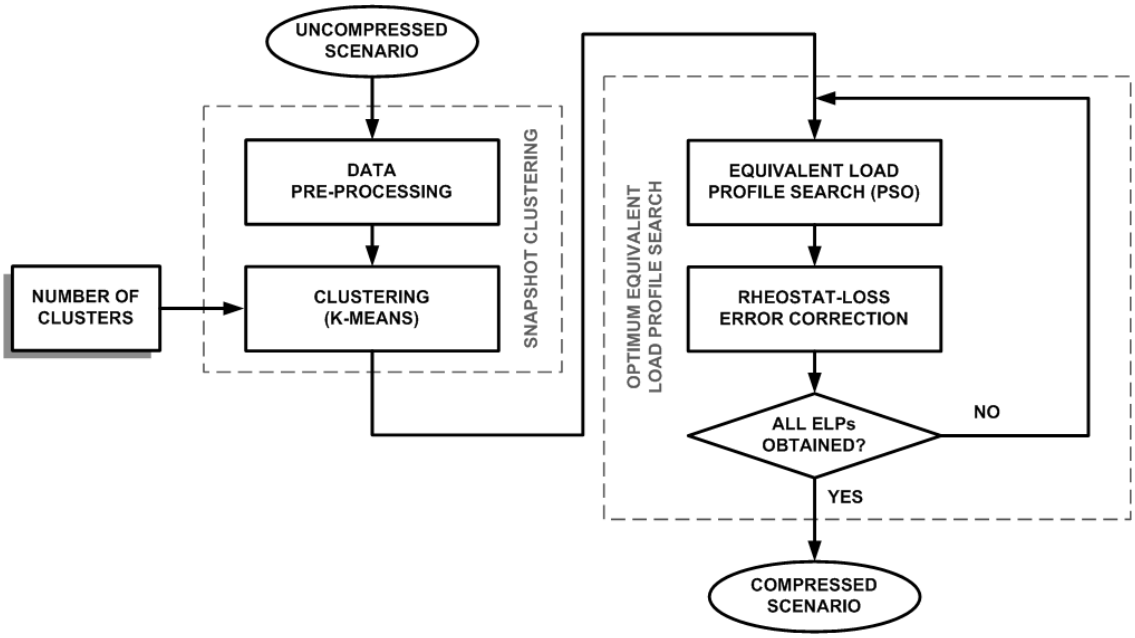

Figure 5-1. Traffic-scenario compression method workflow.

5.3. SCENARIO SNAPSHOT CLUSTERING

In this section, the first step in the compression method is presented. The first traffic scenario included in the 7-minute headway representative-scenario set has been used to illustrate the clustering concept.

In this first phase, the snapshots contained in the traffic scenario to be compressed are grouped following a rheostat-loss (amount and position) and SS voltage similarity criterion. The k-means clustering algorithm has been applied to cluster the snapshots in the traffic scenario.

K-means is a powerful hard-membership clustering algorithm which minimises the distances between the elements included in each cluster to its centre. It is, indeed, a well-known optimisation problem which performs a partition of the input space, defined by a set of variables and a set of samples. Each subset in the partition –a cluster– is in turn defined by the samples it contains and a centre. The elements in a cluster are selected so that they are close to the centre of this cluster and as far as possible to the centres of the rest of clusters in the partition. Further information about this algorithm may be found in the work by (Kanungo, Mount et al. 2002). In this study, the implementation of the k-means algorithm in Matlab has been used.

It is clear that the more similar the snapshots in a cluster are, the more accurate the compression method is. Following the conclusions in Section 5.2, the snapshots grouped in a cluster must be similar in terms of SS voltage, rheostat-loss amount and rheostat loss positions in the line. Therefore, in a first approach, the input variables to be supplied to k-means could be the rheostat power at each train, the positions of the trains and the SS voltages.

Prior to its execution, it must be noted that the k-means algorithm is defined to work with a constant number of variables. However, the number of trains in the system is not necessarily constant between the terminal stations for all the snapshots in the uncompressed traffic scenario (cul-de-sac manoeuvres are not modelled in this study). Thus, it is required to shape the traffic scenario for the k-means algorithm to work properly. This data pre-processing is presented in Section 5.3.1.

5.3.1. DATA PRE-PROCESSING

In this section, a process to transform the variables defining the snapshots is presented. This process both aims to 1) making the samples in the input set meet the format requirements of the k-means algorithm; and 2) easing the clustering process itself.

As previously stated, the variables to be supplied for k-means to cluster the snapshots in a traffic scenario are: train positions, rheostat losses and the SS voltages.

K-means is defined to work with a constant number of variables, whereas the number of trains is not necessarily constant throughout the snapshots in the input space. This could be fixed by inserting fictitious trains in the snapshots that require it. Then, k-

means should naturally separate them from the others. However, that would result in an unnecessary increase in the complexity of the k-means problem. To avoid that, the input samples are pre-clustered, making the number of trains to be explicitly constant for each input subset.

Second, it is important to realise that there are qualitative differences between the elements inside both the rheostat-loss and SS voltage spaces. Regarding the former, if rheostat losses are directly fed into k-means, a sample where rheostat losses for train *k* are zero would be immediately close to another sample where rheostat losses for train k are infinitesimal. These two situations are, however, qualitatively different from an energy saving standpoint. It could be expected that the voltages of the SSs close to train k would be enough to distinguish these two cases regarding the rheostat behaviour. However, it has been found that the final energy-saving result accuracy is improved if an artificial gap is included to separate these qualitatively different samples.

Then, there is an analogous situation when analysing SS voltages: the results have been observed to be better in terms of energy-saving accuracy when a voltage gap is introduced to separate active (*ON* state) from cut-off SSs.

Summarising, this pre-processing stage is made up of two steps:

- Pre-clustering to obtain subsets with constant number of trains.
- Inclusion of gaps to separate qualitatively different situations in the input variables.

The application of the data pre-processing to the traffic scenario used as example leads to two subsets. The first one is made up 267 samples where the number of trains in the system is 11. In the second one, which contains 154 samples, the number of trains in the system equals 12.

5.3.2. SNAPSHOT CLUSTERING

After the data pre-processing, the k-means clustering algorithm is applied to each subset of the input data with constant number of trains. Although this algorithm is very powerful, and it has been intensively used in the literature, it has some weaknesses. The most remarkable one is its tendency to be affected by local minima.

To improve the clustering efficiency of the k-means algorithm, there is a set of parameters that may be tuned. Three are the most important ones, which are given following the notation used in the k-means implementation by Matlab: 1) *distance*, 2) *replicates*, and 3) *start*.

The *distance* parameter represents the measurement used to assess the distances between the elements in the input dataset. The most common distance measurement is the square Euclidean distance. However, for the purposes of the clustering stage in the compressor, it is desired not to include snapshots with qualitatively different values of variables, e.g.: a cluster made up of two snapshots where train *k* presents

rheostat losses only in one of them, will probably lead to poor energy-saving result accuracy in the equivalent compressed model.

Consequently, it is required to make the clustering stage to be reluctant to mix snapshots which are qualitatively different in the same cluster. In addition to the gap inclusion in the data pre-processing, the *correlation* distance has been used. This morphological distance measurement becomes low when all the variables in the snapshots within a cluster are in the same statistical region (quartile, percentile, etc.). Although for the sake of clarity it has not been explicitly shown, it has been checked out that the results with the correlation distance are better than those with the square Euclidean distance in terms of energy-saving result accuracy.

The second parameter –*replicates*– defines the number of times that the algorithm is repeated with a different initial partition. It is used to mitigate the local-minima problems that k-means exhibits, mainly because of its hard membership characteristics. The value selected for this parameter has been tuned empirically.

Third, the *start* parameter defines the way the initial partition is obtained. The options included in the Matlab R2014b implementation of k-means are 'sample', 'uniform', 'cluster' and 'matrix'. In the first one, as many samples as the desired number of clusters are selected at random for the k-means centroid initialisation. The second one differs from the first in that it selects the initial centroids to be uniformly distributed over the input dataset. Then, the third one performs a clustering exercise over the 10% of the samples to select the initial centroids. Finally, for the case some information about the centroids is available, the 'matrix' option allows the user to explicitly introduce the initial centroids.

The clustering stage in the compressor uses the 'sample' as the start parameter choice. The reason is that, in combination with a high number of replicates, it is the best option to reduce the effect of the local minima on the final clustering solution.

Table 5-2 shows, in brief, the k-means parameters selected.

Table 5-2. K-means parameter selection.

	Distance	**Replicates**	**Start**
k-means parameter selection	*Correlation*	25000	*Sample*

Finally, the number of clusters in the traffic scenario partition has to be defined. This is, actually, the most important concern in the clustering stage, since it determines the number of snapshots in the compressed equivalent traffic scenario. Regarding this, the compression ratio (CR) is defined as:

$$CR = \left(1 - \frac{Snapshots\ in\ the\ compressed\ scenario}{Snapshots\ in\ the\ input\ scenario}\right) \cdot 100 \quad (5.1)$$

E.g., applying 90% compression ratio means that a 100-snapshot uncompressed traffic scenario will be expressed by means of only 10 snapshots, with and expected simulation time decrease around 90%. The maximum CR achievable is a-priori unknown, and its associated results must be compared with those of the sub-sampling

method, which appears as a straightforward approach for compressing the traffic-input scenarios.

This section has performed a study to find out the achievable CR. To do that, a CR vector has been defined in (5.2), and the number of clusters requested to the k-means algorithm has been varied accordingly. It must be noted that the same CR is applied to all the subsets defined in the uncompressed scenario after the pre-processing stage.

$$CR_{vec} = [50 \quad 60 \quad 67 \quad 80 \quad 90]\,\% \tag{5.2}$$

The goodness of the clustering results has been measured by using two indexes: 1) the silhouette mean value, and 2) the mean purity of the clusters. The former becomes close to 1 when all the elements in all the clusters are close to their correspondent centroid and far away from the rest of centroids. The latter parameter becomes 1 when all the elements in a cluster are qualitative the same. It has been defined to detect the presence of clusters which present qualitatively different samples regarding variables subject to be pure. E.g.: in the energy-saving case, the trains' rheostat losses (not positions) and SS voltages. An example of an impure cluster is given in Figure 5-2.

Consequently, the individual purity factors are defined for each equivalent train and SS inside a cluster. Then, an average purity factor for the cluster may be easily obtained. These purity factors are defined in (5.3), (5.4), (5.5).

$$PtyT_t^c = \frac{max(nRht_t^c, nNRht_t^c)}{C} \tag{5.3}$$

$$PtySS_a^c = \frac{max(nSS\_ON_a^c, nSS\_OFF_a^c)}{C} \tag{5.4}$$

$$\overline{Pty_c} = \frac{\sum_{t=1}^{NT} PtyT_t^c + \sum_{a=1}^{NSS} PtySS_a^c}{NT + NSS} \tag{5.5}$$

Where,

- $PtyT_t^c$ is the purity factor for the equivalent train *t* in cluster *c*.
- $nRht_t^c$ is the number of samples in cluster *c* where the train represented by *t* presents rheostat losses.
- $nNRht_t^c$ is the number of samples in cluster c where the train represented by t does not represent any rheostat losses.
- C is the number of samples (snapshots) in cluster c, which necessarily coincides with the addition of $nRht_t^c$ and $nNRht_t^c$.
- $PtySS_a^c$ is the purity factor for the SS *a* in cluster *c*.
- $nSS\_ON_a^c$ is the number of samples in cluster *c* where the SS *a* is in ON mode.
- $nSS\_OFF_a^c$ is the number of samples in cluster *c* where the SS *a* is in OFF mode.
- $\overline{Pty_c}$ is the average purity factor associated to cluster *c.*
- NT and NSS are respectively the number of equivalent trains in cluster *c* and the number of SSs in the system.

Before presenting the figures of these two clustering goodness measurements, Figure 5-2 shows two cluster examples. The cluster examples have been extracted from an 80

% CR clustering exercise applied to one of the representative scenarios for the 7-minute headway. The first example belongs to the subset 1 (11 trains), and it contains 8 snapshots (red cluster). The second example belongs to the subset 2 (12 trains), and it contains 9 snapshots.

It may be observed that the clustering algorithm efficiently groups snapshots which contain qualitatively similar information in terms of location and amount of rheostat losses and SS voltages. The SS close to the end of the line (SS 11) would be the only element with purity factor lower than 1, since it contains 1 sample out of 8 in *OFF* state. Since there is an *ON* SS between this impure element (SS10, close to position 17 km) and the rheostat losses (which take place from position 13 km to position 6.3 km) this is not expected to lead to significant energy-saving errors. Nevertheless, the cluster energy-saving errors will be analysed at Section 5.5.

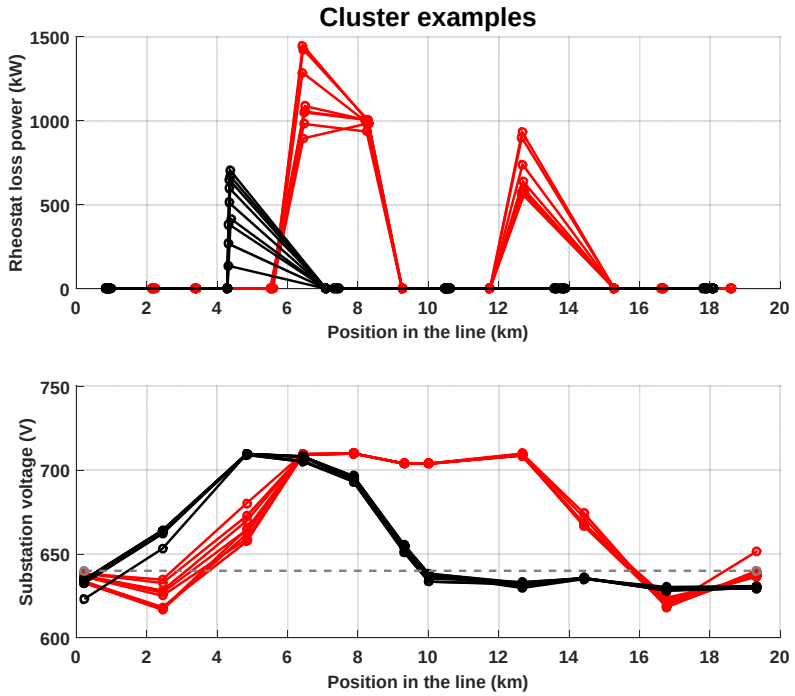

Figure 5-2. Cluster examples after removing the pre-processing gaps.

After this inspection of the clustering results, Figure 5-3 presents the two different measurements of the clustering goodness. Figure 5-3.a shows the silhouette mean results for the different CRs and for both subsets in the traffic scenario. No clear reduction trends with the CR may be observed for the case of the smaller subset (11 trains), whereas the 12-train subset presents a dramatic silhouette average value reduction for the 90 % CR case.

However, the combination of the correlation distance measurement and the gaps to separate qualitatively different situations could distort the silhouette calculations. The reason is that this transformation makes the elements in the input space to intensively populate both endings of the rheostat power and SS voltage distributions, whereas no element is, by definition, in the central zone. Consequently, a snapshot properly

included into a certain cluster may present a low silhouette value because of not being clearly far away from the centroid of another cluster.

To obtain a more reliable measurement of the cluster goodness, the mean purity factors are proposed. In order to have a practical measurement of the cluster purity, the mean purity factors for each particular cluster (defined in (5.5)) have been again averaged to obtain a single purity figure for the subset. These results are presented in Figure 5-3.b. It may now be clearly observed in the graph how the purity figures for both subsets drops steadily as the CR is increased. This result shows how the snapshot clustering finds it difficult to properly partition the traffic space as the number of allowed clusters drops.

On the one hand, it seems clear that the 90% CR case will be problematic due to the high occurrence of impure trains and SSs. On the other hand, the 67% CR case has a mean purity close to the one obtained for the 50% case. The 80% CR case is located in the apparent knee of the purity curves for both subsets. In any case, the results in this step cannot be directly translated into energy-saving accuracy, since it is necessary to have the ELPs for the clusters in order to be able to simulate the compressed scenario. After these ELPs are obtained, it will be possible to compare the results of the compressed scenario with those of the uncompressed one in order to calculate the energy-saving errors.

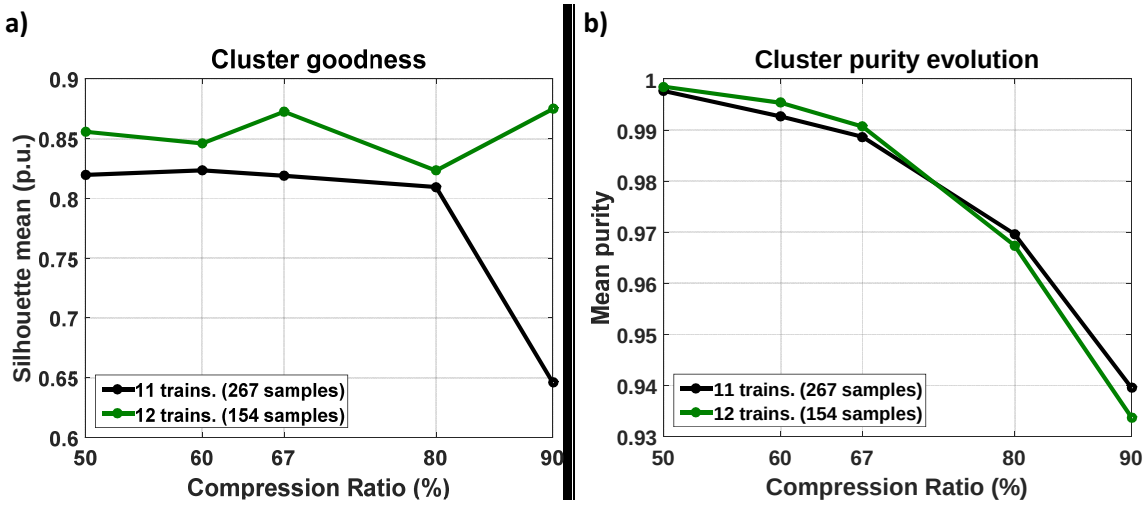

Figure 5-3. Cluster goodness measurements vs. CR for the first traffic scenario.

5.4. OPTIMUM ELP SEARCH

This section is in charge of describing the process to obtain the ELPs for the compressed scenario clusters. The first traffic scenario included in the 7-minute headway representative scenarios has been used again to illustrate the derivations in this section.

The clustering stage outputs a partition of the traffic scenario set. The subsets in this partition contain snapshots which are similar in terms of the k-means variables. However, it is required to have the particular positions and powers of the trains (ELP) representing each cluster in order to make it possible to simulate the compressed equivalent traffic scenario.

A possible approach for obtaining the snapshot ELP could be to average the powers and positions of the trains in this cluster. Unfortunately, averaging is not a powerful approach as the number of snapshots contained in a given cluster grows, especially for the trains' powers. The main reason is that the rheostat and conduction losses do not follow a linear behaviour. Therefore, as the dispersion of the train powers is increased, which happens to take place for high CRs, the rheostat and conduction losses are not properly expressed by averaging. It was derived in Section 5.2, and it has been proven that this results in energy-saving inaccuracy for the equivalent model, especially if rheostat losses are not properly represented.

In order to overcome this problem, this section presents a method to search for the ELP that best represents a given cluster. This is made by varying the powers consumed or regenerated by a set of equivalent trains. The number, positions and boundary powers for these equivalent trains are extracted from the snapshots contained within each particular cluster in the traffic scenario. The number of trains and boundary powers are straightforward to obtain, whereas the trains' positions are set to the central position of all the trains represented by each particular equivalent train.

It must be noted that the position of the equivalent trains could have been varied as well, ranging within the position bounds fixed by the snapshots in the cluster. However, after analysing this possibility, it was concluded that the improvement in the method accuracy would be marginal, and it does not justify the consequent increase in the dimension of the search space and thus in the complexity of the problem.

This novel method is based on an evolutionary algorithm: the Particle Swarm Optimisation (PSO) algorithm. The PSO is the core of the MTS infrastructure optimiser presented in Chapter 6. The optimiser is one of the most relevant developments presented in this thesis. Therefore, in order to make it easier to understand it, the main characteristics of the PSO algorithm have been described in Section 6.2.3 (pg. 185).

Prior to the presentation of the details of the ELP search method, it is important to note that the selection of a metaheuristic algorithm like the PSO is not a casual choice. Before adopting this solution, a non-linear minimisation approach by using the Matlab's function *fmincon* (fmincon 2016) was implemented. However, the

particularities of the problem of finding the rheostat powers of trains makes it difficult for algorithms based on the gradient to obtain good ELP solutions. Specifically, if the initial guess is not set so it presents non-null rheostats in rheostat trains, the application of infinitesimal variations in the trains' powers will yield no sensibility, and the solver will remain in the consequent local minimum. Possible solutions like using larger steps for the numerical calculation of the partial derivatives have not proved to lead to notable improvements in the performances of this approach. Thus, the PSO algorithm, which performs a search from several initial points, arose as a convenient solution to overcome these practical problems.

The ELPs are obtained by varying the positions of the elements in a search population. The positions in the formulation of the PSO method become a vector of powers. Specifically, these are powers of the trains in the snapshots of the cluster represented by each particular ELP. The initial positions of the elements are generated at random inside the feasible region defined by the powers of the trains included in the cluster snapshots. Then, the element positions are varied as a function of the element speeds, which are in turn generated by a combination of the impetus, cognitive and social factors defined in Section 6.2.3.

Table 5-3 shows the particular values used for each parameter and variable defining the PSO behaviour.

Table 5-3. PSO parameter and initial condition selection.

Parameter or initial condition	Selection
Initial position of elements	Randomly distributed over the feasible region without assigning a greater probability to any feasible position
Initial speed of elements	Random initial speed assigned to the power of each train. The maximum module of the initial speed has been set to be lower than 0.7 times the difference between the maximum and the minimum power allowed for this train.
Impetus factor (imp_k)	Following a linear decrease rule so as that it is 1 in the initial iteration and 0.5 in the final one.
Forget coefficients $(c1_k, c2_k)$	Uniformly distributed in the interval [0, 0.5]
Cognitive factor $(fcog)$	0.5
Social factor $(fsoc)$	0.5
Population size (P)	50 times the number of snapshots contained in the cluster.
Maximum number of iterations (I)	100

Once all the PSO parameters have been fixed, the optimisation problem to be solved by means of the PSO is defined in (5.6).

$$\min\left(F_{ELP}(P_1, \dots, P_T, \omega_1, \omega_2, \omega_3)\right)$$

$$s.t. \tag{5.6}$$

$$P_i \leq P_i^{MAX}, \quad \forall\, i = 1, \dots, T, \quad i \in \mathbb{N}$$
$$P_i \geq P_i^{MIN}, \quad \forall\, i = 1, \dots, T, \quad i \in \mathbb{N}$$
$$\omega_i \geq 0, \qquad \forall\ i = 1, 2, 3$$

Where,

- F_{ELP} is the fitness function to be minimised.
- P_i represents the power consumed or regenerated by the ith train in the ELP.
- P_i^{MAX}, P_i^{MIN} are the power bounds for P_i, defined, respectively, by the maximum and minimum power consumed or regenerated by the trains represented by the ith equivalent train (i.e. the trains in the snapshots within the cluster under analysis).
- T is the number of trains in the snapshots contained within the cluster under analysis.
- ω_i are three weighting factors used to modulate the influence of the three main terms of the fitness function. They are defined in (5.7).

Prior to the definition of the fitness function, for the sake of clarity, Figure 5-4 shows the feasible region for the ELP of a cluster containing 8 snapshots. The discontinuous curves represent the load profiles of all the eight snapshots contained within the cluster. The ELP powers must be on the vertical green lines. Thus, the ELP would consist of eleven equivalent trains each of which represents eight train positions and powers. It must be noted that these lines are placed at the central position of the trains it will represent.

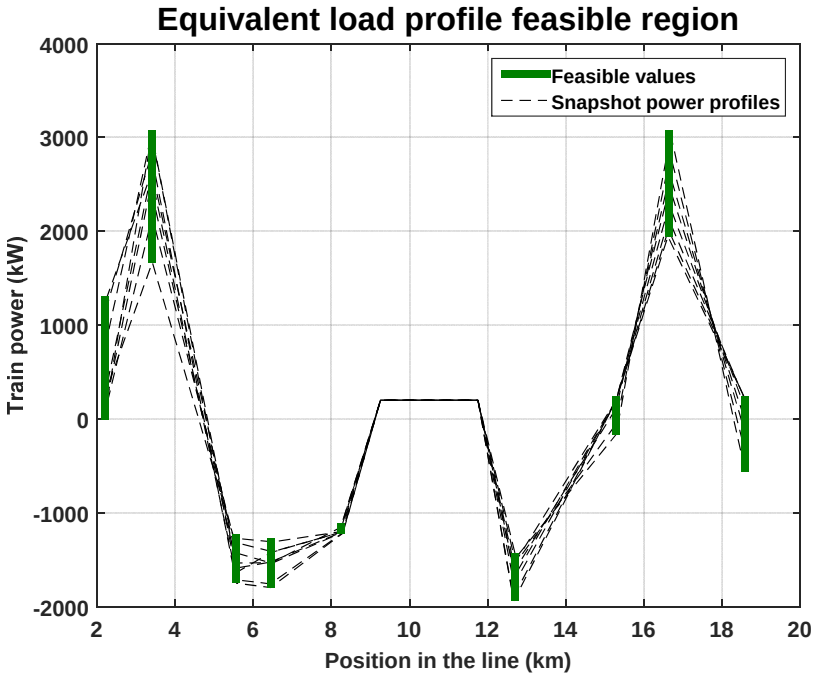

Figure 5-4. Feasible region for the ELP of a paradigmatic cluster.

The requirements that an ELP have to fulfil in order to lead to good energy-saving accuracy results have been explained in Section 5.2. In short, it has to be accurate in terms of the location and amount of rheostat losses and the SS voltages. This has been represented by the fitness function defined in (5.7), which depends on the powers assigned to all the equivalent trains in the ELP. This fitness function makes it possible to find good ELPs by expressing the state of the whole electrical system instead of simply including information about the trains. It has been obtained from a refinement process aimed at optimising the energy-saving result accuracy. As a result of this process, the relation between its terms, rheostat losses and SS voltages is not straightforward; so it is explained hereafter.

$$F_{ELP}(P_1, \dots, P_T) = M \cdot \sum_{i=1}^{T} WRh_i + \omega_1 \cdot \sum_{j \in SS_{OFF}} \left| V_{Ref}^{j} - V_{Eq}^{j} \right| + \omega_2 \cdot \sum_{k \in SS_{ON}} \left| Ess_{Ref}^{k} - Ess_{Eq}^{k} \right| + \omega_3 \cdot \left| Eloss_{Ref} - Eloss_{Eq} \right| \tag{5.7}$$

Where,

- M is a very big number.
- T is the amount of trains in the cluster under analysis.
- WRh stands for *Wrong Rheostats*. It is a Boolean function that expresses if the rheostat losses in a train have been properly identified. It is defined, for each single equivalent train, as:

$$WRh = \begin{cases} 0 & if \quad \left(ERh_{Ref} = 0 \;\&\; ERh_{Eq} = 0\right) \text{ or } \left(ERh_{Ref} > 0 \;\&\; ERh_{Eq} > 0\right) \\ 1 & if \quad \left(ERh_{Ref} = 0 \;\&\; ERh_{Eq} > 0\right) \text{ or } \left(ERh_{Ref} > 0 \;\&\; ERh_{Eq} = 0\right) \end{cases} \tag{5.8}$$

  In this function, ERh_{Ref} represents the reference rheostat-loss value for the train (obtained by averaging the snapshot rheostat losses) and ERh_{Eq}, the rheostat-loss value for the train in the ELP.

- SS_{OFF} is a subset of the SS set which collects those ones which are delivering no power. The mean SS voltage greater than the system no-load voltage has been selected as the criterion to consider that a given SS is in cut-off state. This solves the problem that arises in impure SSs.
- SS_{ON} is the complement of the set SS_{OFF}.
- ω_1, ω_2, and ω_3 are the weighting factors applied to the absolute errors of the SS voltages and conduction losses, respectively.
- V_{Ref}^{j} represents the reference voltage for SS *j*, obtained by averaging the voltage in SS *j* for the snapshots that belong to the cluster under analysis.
- V_{Eq}^{j} is the voltage at SS *j* obtained with the ELP.
- Ess_{Ref}^{k} represents the reference SS energy for SS k, obtained by averaging energy delivered by SS *j* for the snapshots that belong to the cluster under analysis.
- Ess_{Eq}^{k} is the energy delivered by SS *j,* obtained with the ELP.
- $Eloss_{Ref}$ represents the reference conduction losses, i.e., the mean energy losses in conductors for the snapshots that belong to the cluster under analysis.

- $Eloss_{Eq}$ represents the conduction losses obtained with the ELP.

It can be observed by inspection of (5.7) that: 1) this fitness function will make the ELP to represent rheostats only qualitatively, i.e., if possible, it will make all the trains presenting rheostat losses in the cluster snapshots to present rheostat losses in the equivalent model as well, but it will not necessarily be accurate in the amount of rheostat losses; 2) the SS voltage accuracy requirement has been replaced by the delivered energy for the *ON* SSs; 3) ohmic losses have also been represented by an additional term in the fitness function.

The reason for the first is that, once all the trains in rheostat mode are properly represented, the load flow in the electrical system will not be sensitive to changes in the regenerated energy in these trains, and hence in the rheostat losses. Taking this into account, it is straightforward to realise that the rheostat-loss result accuracy may be improved by post-processing the ELP yielded by the PSO. Specifically, the amount of rheostat losses in the equivalent model may be adjusted by varying the regenerated energy in the trains in rheostat mode without changing the load flow in the electrical system, and hence the SSs' voltages. This approach makes it possible to reduce the complexity of the ELP search process. The reason is that in a quantitative rheostat approach, the fitness function would essentially be bi-criterion. That would call for, at least, a complex weight tuning process; or, more generally to a multiple-objective PSO (MOPSO). The rheostat adjustment formula is presented in (5.9). It must be noticed that this rheostat correction method is only applied to those trains which rheostat behaviour has been properly represented by the ELP. Otherwise, this correction mechanism could provoke uncontrolled changes in the load flow, which could perfectly spoil the voltage and delivered power accuracies.

$$P_t^{ELP} = P_t^{PSO} + (PRh_t^{PSO} - PRh_t^{REF}),\ \forall t \in \{1, \dots, T\}/WRh_t = 0 \quad (5.9)$$

Where,

- P_t^{ELP} represents the power for train t in the ELP (the final result).
- P_t^{PSO} represents the power for train t yielded by the PSO algorithm.
- PRh_t^{PSO} represents the rheostat-loss power for train t yielded by the PSO, which may present significant errors for the non-null rheostat trains.
- PRh_t^{REF} represents the mean rheostat-loss power for the trains modelled by the equivalent train t, i.e., the mean rheostat power for train t in the K snapshots contained in the cluster.

The second adaptation of the fitness function consists of using the SS delivered energy instead of the SS voltage, when applicable (on-mode SSs). The reason for this implementation is that in the on SS case, the power delivered by the SSs is highly sensitive to a voltage variation. Hence, the meaning of a voltage error is not symmetric for the on and off SS cases, and a fine weight tuning is necessary. The energy-saving accuracy results after switching the SS voltage to SS energy for the on SS set has shown to be fairly robust to a variation in the weighting factor of this term.

Finally, ohmic losses have been included in the fitness function. This term is somewhat redundant to the delivered energy term, and hence the contribution of this term to the energy-saving results is marginal. Nevertheless, there might be situations where ohmic losses are more important, and hence it could be interesting to explicitly force these losses to be accurately represented.

Figure 5-5 presents some details of the algorithm population size and the search method convergence characteristics. Both graphs in the figure present the results obtained after the application of an 80 % CR to the traffic scenario used as example.

First, Figure 5-5.a shows how the mean fitness values vary with the population size. The mean fitness value stabilises for 75-100 elements per snapshot. The former has been the selected value for the population size. Then, Figure 5-5.b shows the maximum and minimum relative differential variation for the 84 ELPs in the compressed scenario. It can be observed how from 80 iterations on, the fitness value decrease is marginal, which justifies the selected maximum number of iterations. The maximum number of iterations has been set to 100 (see Table 5-3).

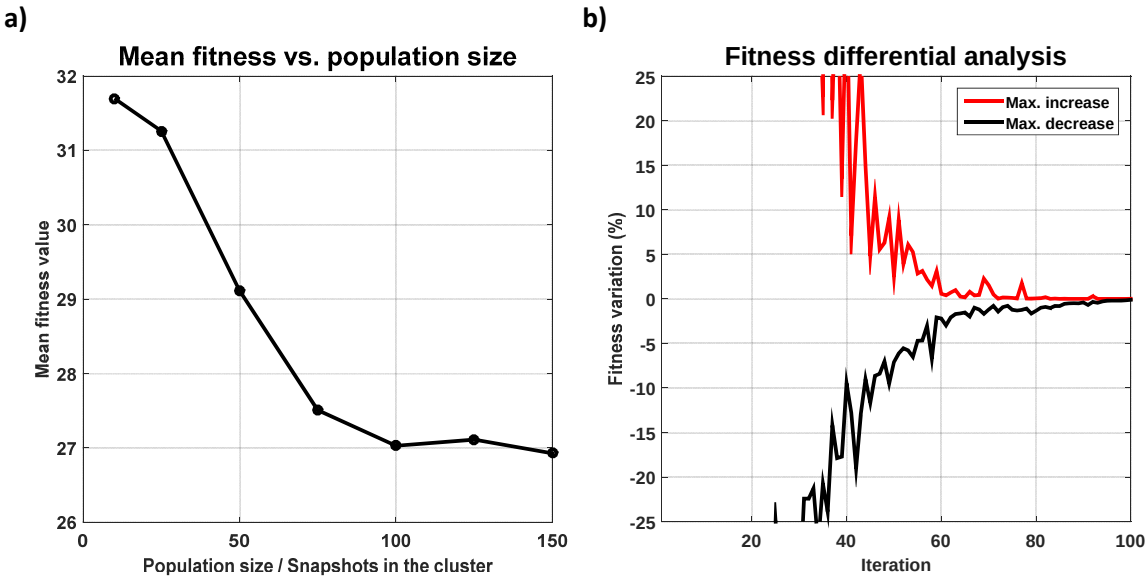

Figure 5-5. Analyses of the PSO population size and convergence.

The accuracy of ELP search stage does not appear as a relevant concern by itself. As has already been mentioned, the key accuracy figures in the study are the energy saving ones, which are presented in Section 5.5. In brief, it must be noted that an impure cluster will lead to difficulties to fit the PSO variables and this will in turn lead to an inaccurate energy saving result.

Nevertheless, Figure 5-6 shows the way the PSO adjusts both the mean SS voltages and the mean rheostat losses for the two cluster examples presented in Section 5.3.2 (Figure 5-2). The PSO precisely adjusts both SS voltages and rheostat losses (the latter is imposed by the method). The only not perfect adjustment is that for SS 11 in the first example (red cluster in Figure 5-2), which happens to be the only impure SS in both cluster examples.

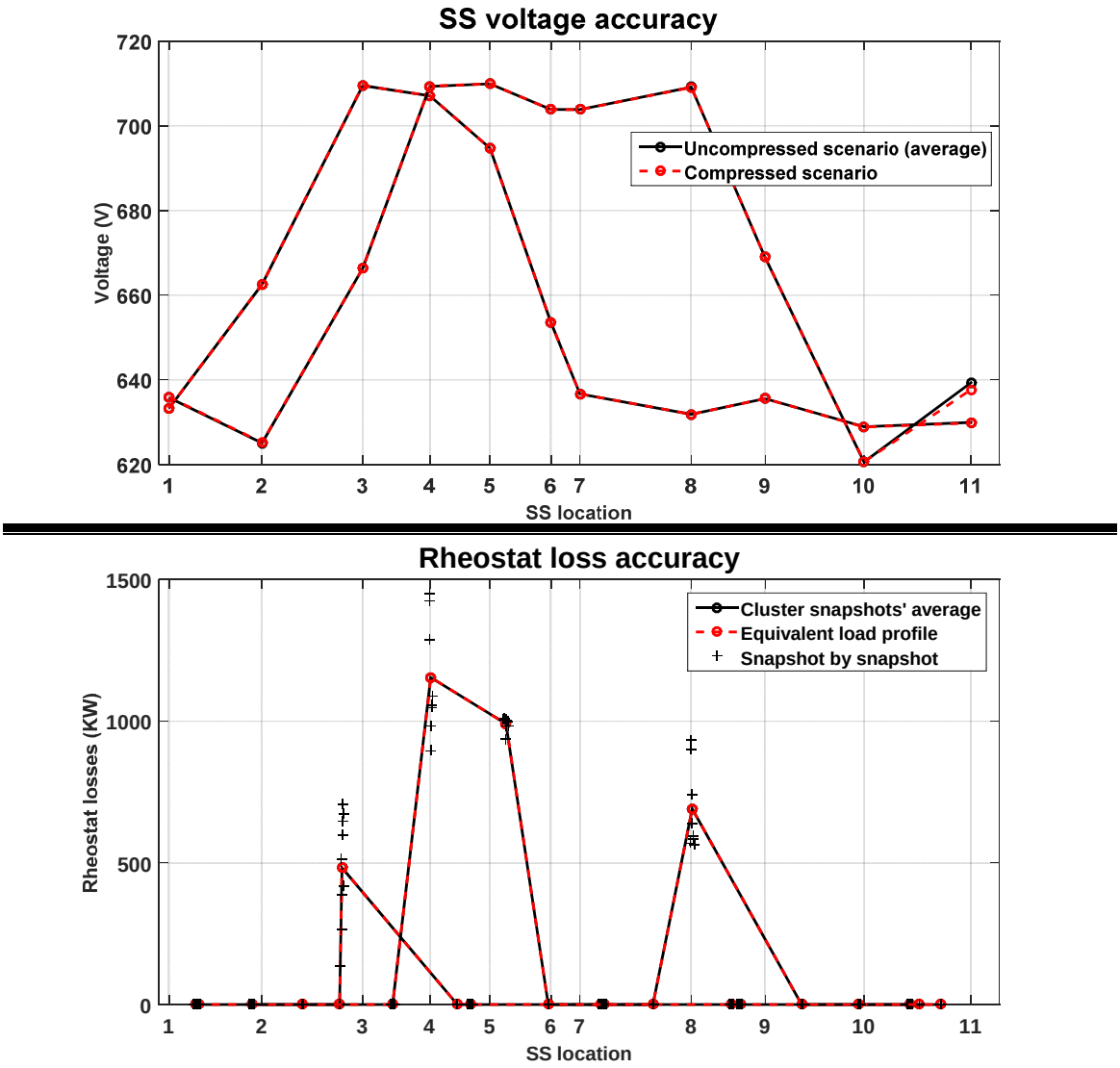

Figure 5-6. SS voltage and rheostat loss adjust example.

5.5. COMPRESSION RATIO EVALUATION AND ACCURACY RESULTS

This section presents the energy-saving accuracy results obtained with the scenario compressor. Prior to the accuracy measurements, the achievable CR has been evaluated. This has been made by applying the variable CRs in CR_{vec} to the first representative traffic scenario for the 7-minute headway traffic space. The 60 % CR has been excluded from the study in order to ease the comparison with the subsampling method. The compressor energy saving accuracy results for the single RS test have been compared with those that would be obtained with the subsampling method. This implies to compare the compressor with a simple snapshot reduction method. It aims to justify the application of a complex number-of-snapshot reduction method like the traffic scenario compression presented in this thesis.

The subsampling method consists of simply selecting one snapshot every subsampling rate, discarding the rest of them (e.g.: selecting one every three snapshots). The selected snapshots play the role of the ELPs in the compression method. It is important to note that the subsampling rate has to be an integer number, and the CR vector defined in (5.2) is equivalent to the subsampling rates: 2, 3, 5 and 10, respectively.

Then, once the minimum CR which meets the accuracy criterion imposed in this study (5% error) has been identified, this CR has been applied to all the 9 traffic scenarios defined in Section 4.5.2 for the 7-minute headway.

Finally, the compression results have been extended to the three operation headways analysed in the thesis and a further validation test with several different infrastructure configurations has been performed to prove the compressor's accuracy.

5.5.1. COMPRESSION RATIO EVALUATION

Figure 5-7 shows the variation in the energy saving accuracy of both the compressor and the subsampling methods as CR is increased. The top side graph in Figure 5-7 shows the maximum and minimum relative errors for both methods. The average savings for the single RS test have been used to make the results relative in order not to artificially punish cases with low savings.

The scenario compressor remains within the allowed error band except for 90 % CR, whereas the subsampling method presents an unacceptable accuracy for 80 % CR. In addition, the maximum error for 67 % CR is close to 5 %.

The compressor accuracy analysis makes use of an additional accuracy index. The reason is that the error index in (3.2) (pg. 77) is the result of the signed addition of the particular error of each ELP. Consequently, a good accuracy result might be the consequence of the compensation of several positive and negative errors. If this situation takes place, albeit accurate, the traffic scenario compressor could not be regarded as a robust method. In order to have an index which shows the worst case deviation from the reference energy saving result, the relative integral absolute error (IAE) is proposed in this study. Its definition is given in (5.10).

$$IAE_{COMP} = \frac{\sum_{h=1}^{H} \left| \left(\sum_{i \in h} E_{saving,i}^{REF} \right) - E_{saving,h}^{COMP} \right|}{E_{saving}^{REF}} \cdot 100 \quad (5.10)$$

Where,

- h, ranging from 1 to H, represents the ELPs in the compressed traffic scenario.
- i has been used to identify the snapshots represented by the ELP h.
- $E_{saving,i}^{REF}$ represents the energy savings for the snapshot i.
- $E_{saving,h}^{COMP}$ represents the energy savings for the ELP h.

Regarding the IAE, the bottom side graph in the Figure 5-7 shows that the scenario compressor leads to a much better approximation of the energy interactions in the uncompressed traffic scenario. Whereas even the minimum IAE in the subsampling case soars from the 67 % CR case, the maximum IAE is lower than 10% of the total savings except for the extreme 90% CR case. This means that the compressor's accuracy is fairly high even for high CRs. It must be noted that an 80 % CR would lead to approximately an 80 % reduction in the simulation time for this traffic scenario.

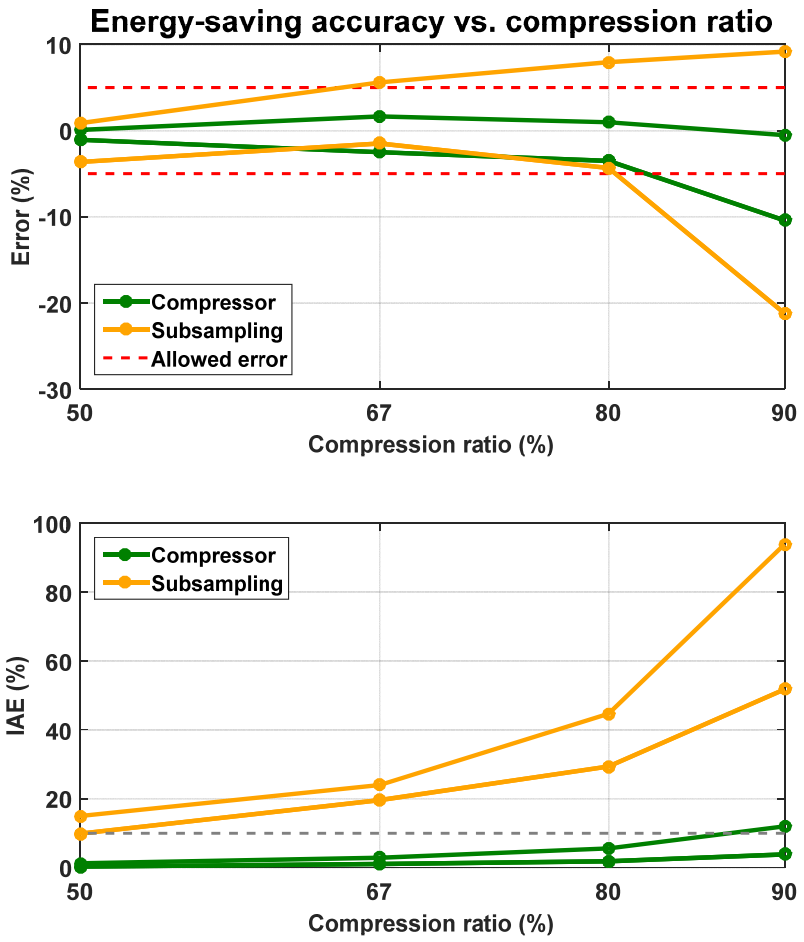

Figure 5-7. Evolution of the energy-saving accuracy figures with the CR.

Regarding the subsampling method, from the signed-error and IAE results for the subsampling method, it may be stated that the sampling time should be limited to 2 seconds in MTS energy-saving studies.

With respect to the compressor, the 80 % CR has shown good accuracy results, and it has therefore been applied to all the representative traffic scenarios in the three operation headways analysed in the thesis.

5.5.2. ENERGY-SAVING ACCURACY EVALUATION

After the variable CR analysis, the 80 % CR has been applied to the nine representative scenarios defined for the 7-minute headway. The results for the subsampling method with the same CR have been included as well.

This second validation stage aims to evaluate the robustness of the compressor to changes in the snapshots contained in the traffic scenario. Figure 5-8 shows these results. The top side graph shows again the maximum and minimum relative errors for both methods. As expected, the subsampling method does not meet the accuracy criterion for any of the traffic scenarios, since 80 % is a too high CR for this method.

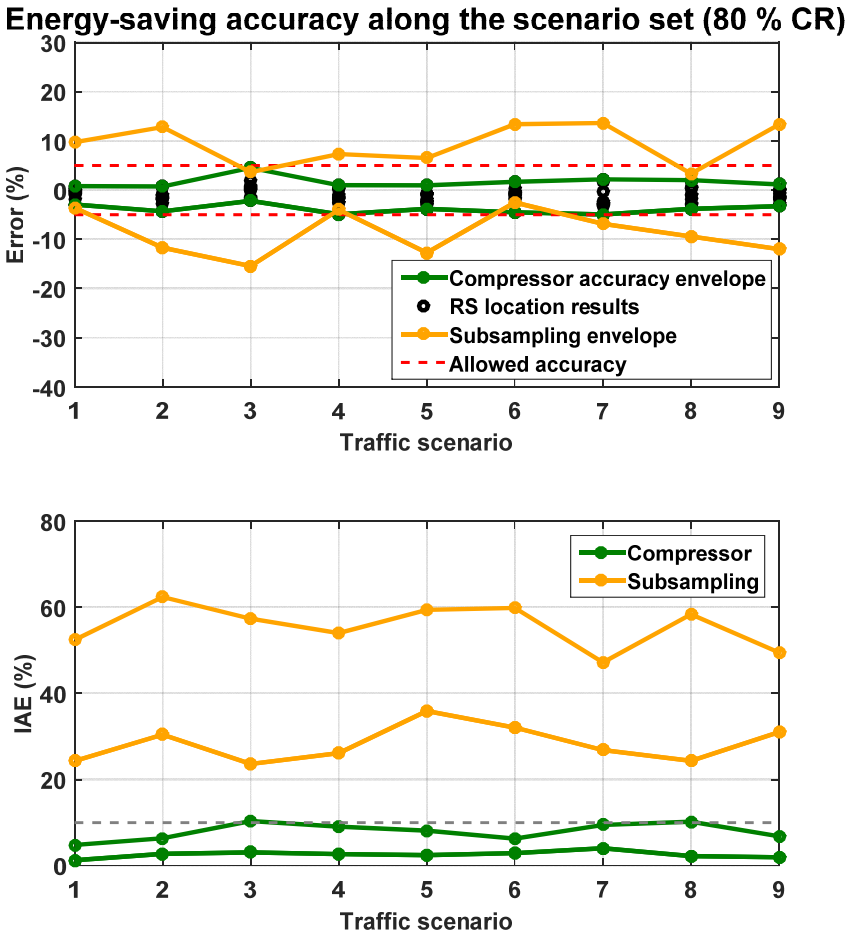

Figure 5-8. Evolution of the energy-saving accuracy figures along the scenario set for a fixed 80% CR.

The compressor is within the accuracy band for all the scenarios, which represents a fairly good robustness result. It has, however, to be pointed out that for some scenarios the worst case error is close to the accepted limit. Nevertheless, the IAE is below 10 % in 7 over the 9 scenarios. The worst IAE error is 10.34 %, in the third scenario.

Figure 5-9 shows the extension of the compressor accuracy results to the 4- and 15-minute headways. The results are qualitatively similar to those for the 7-minute headway. It must be observed that the required precision is attained for all the RS locations in the single RS test. The error dispersion is lower for the 15-minute headway case than for the rest of headways.

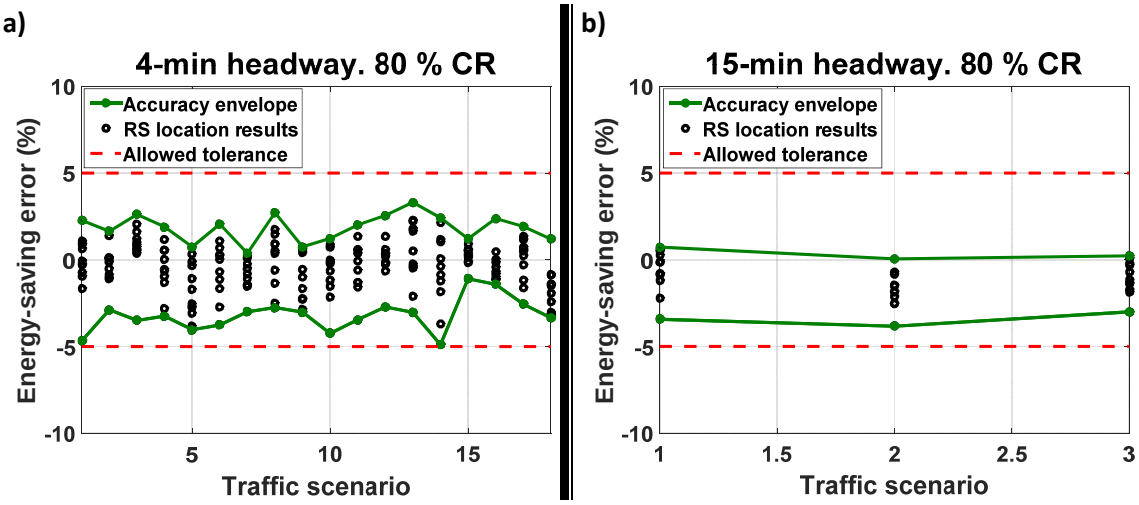

Figure 5-9. Representative-scenario energy-saving accuracy. 4- and 15-minute headways. 80 % CR.

The single RS test is useful for assessing the compressor accuracy. The main reason is that it probes all the available locations independently. However, if the compressed scenarios are used to generate the MTS optimiser traffic input, they must be accurate under highly diverse and complex infrastructure topologies.

To check the compressor accuracy under different infrastructure topologies, this study uses multiple RS test. In this analysis, each headway is represented by the concatenation of all the representative scenarios that it includes, e.g., the 7-minute headway includes nine 7-minute scenarios, so it will be represented by 63 minutes of operation.

Figure 5-10 presents the energy-saving results obtained for the 110 RS configurations in the multiple RS test. It may be observed in the top-side graph that the results obtained with the compressed scenarios are fairly similar to those obtained with the uncompressed one. For high energy-saving figures, a tendency to obtain slightly lower results with the compressed scenarios is observed. It must be noted that this type of biased error: 1) may be compensated by adding a fixed term to the results, and 2) since the energy savings are lower than those for the uncompressed scenario, this will add a margin to the conclusions of the study, i.e., the conclusions with the compressed scenarios will not be excessively optimistic about the installation of expensive devices.

The bottom-side graph in Figure 5-10 shows the compressor relative errors with respect both to the representative scenarios without compression and the whole traffic space. The batch average savings have been used to make the results relative in order not to artificially punish cases with low savings. It must be observed that the accuracy results are inside the accepted tolerance. The errors for high energy savings are around - 2 % both with respect to the representative scenarios and the whole traffic space. This, although biased, represents an excellent accuracy figure.

For lower energy savings, no problems have been found with respect to the representative scenarios. Regarding the error with respect to the whole traffic space, there are four instances out of the 110 cases in the multiple RS test the ± 5 % error band. The worst-case error is nevertheless 5.33 %.

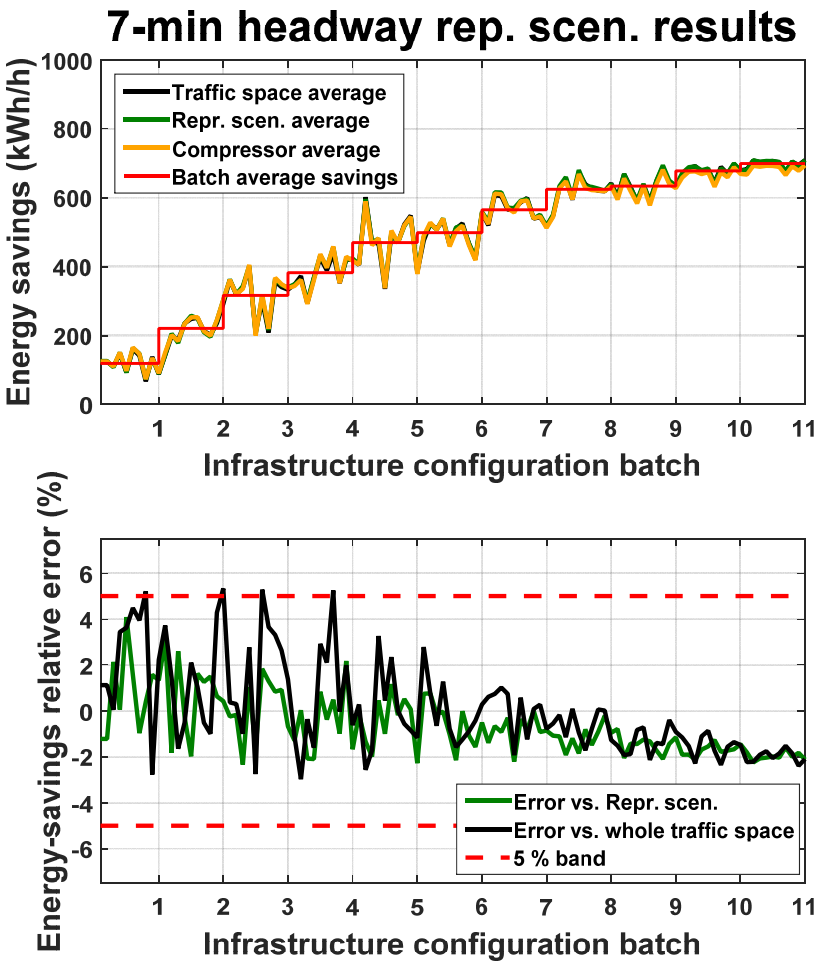

Figure 5-10. Compressor accuracy for multiple infrastructure-improvement configurations. 7-minute headway.

Figure 5-11 shows the extension of the complex-infrastructure accuracy results for the 4- and 15- minute headways. The results are qualitatively similar to those obtained for the 7-minute headway. No anomalous precisions results have been found with respect to the representative scenarios without compression.

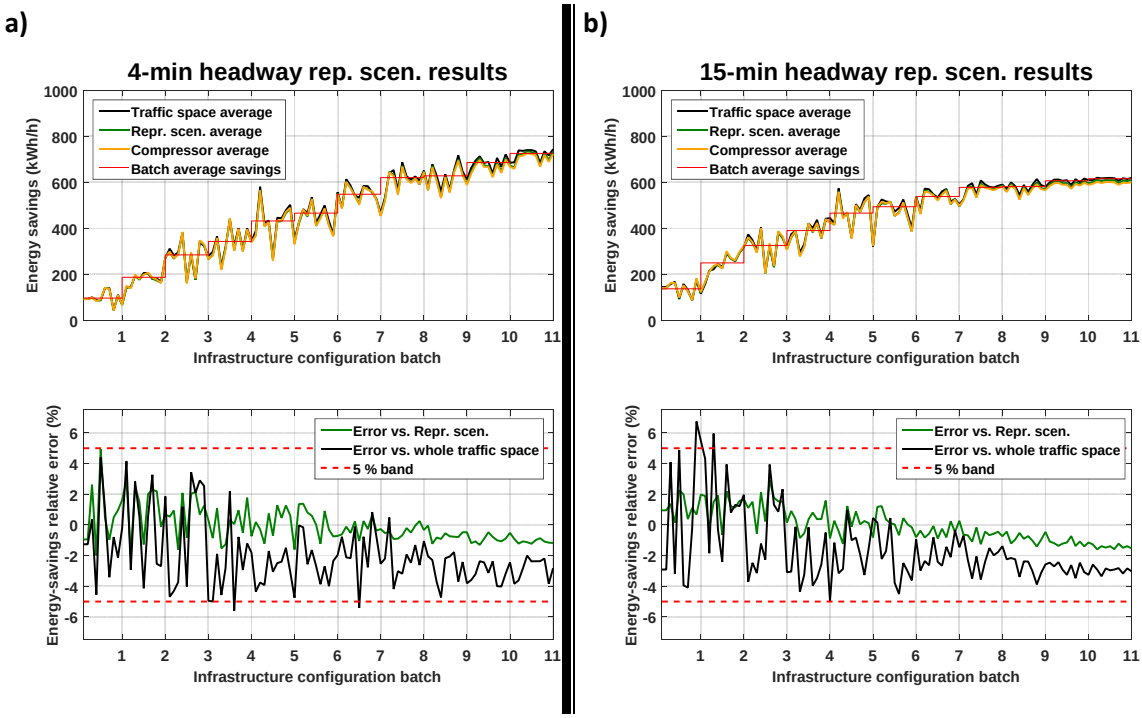

Figure 5-11. Compressor accuracy for multiple infrastructure-improvement configurations. Extension to 4- and 15-minute headways.

Then, with respect to the whole traffic scenario, the 4-minute headway has exhibited two cases which error is lower than -5 %, being -5.6 % the worst-case error. The 15-minute headway exhibits in turn three cases which error is larger than + 5%, being + 6.74 % the worst-case error.

Figure 5-12 shows the rates of inaccurate cases for the accuracy standard considered. The results obtained with the compressor have been compared with those obtained with the uncompressed representative scenarios. It may be observed that the introduction of the compression does not lead to a notable decrease in the accuracy results.

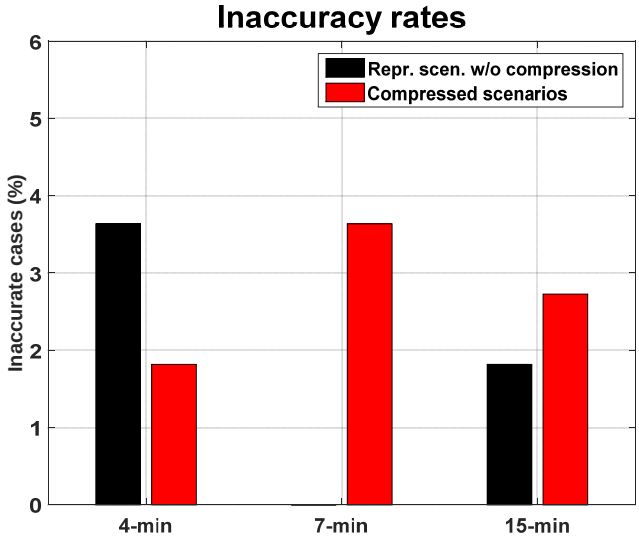

Figure 5-12. Analysis of the number of inaccurate cases in the multiple RS test.

Thus, this low inaccuracy rate, together with the low worst-case relative errors, make it possible to propose the compressed representative scenarios as the input to the MTS infrastructure optimiser that will be presented in Chapter 6.

Back to the example in Section 5.1, now it is possible to include the compressed representative-scenario approach in the comparison. Table 5-4 presents the results obtained with the compressed scenarios. It may be observed that for the same accuracy figures, the computation time is now comparable to that of the usual traffic approach (only 38 % larger). It may hence be stated that the application of the representative-scenario selection, together with the scenario compression, makes it possible to obtain energy-saving results which outperform the usual traffic approach in the literature without an excessive increase in the computation time.

Table 5-4. Comparison between the usual and the representative-scenario approaches.

	Single traffic approach	**Representative-scenario approach**	**Compressed Representative-scenario approach**
Energy-saving error	>20%	<5%	<5%
Computation time	13.4 hours	93.1 hours	18.6 hours

5.5.3. COMPRESSED SCENARIO SIZE CONCERNS

The results in Section 5.5.2 suggest that it could be possible to have worst-case accuracy results out of the accepted error band for a particular traffic scenario. If this takes place, or in case it is necessary to stick to higher accuracy standards, the CR should be relaxed, i.e. more ELPs should be included in the compressed scenario to decrease the energy saving error.

If this is required, a further advantage of the scenario compressor arises: the number of additional ELPs may be increased one by one. It must be noted that this is not possible in a subsampling approach. Figure 5-13 shows the difference in the feasible number of ELPs for both methods. In the 80 % CR case, 84 ELPs are used to represent the 420 snapshots of the uncompressed scenario. If the total error for this CR is not acceptable, the subsampling method would require changing the number of ELPs to 105, whereas with the compressor it would be possible to assess the possibility of using 85 ELPs.

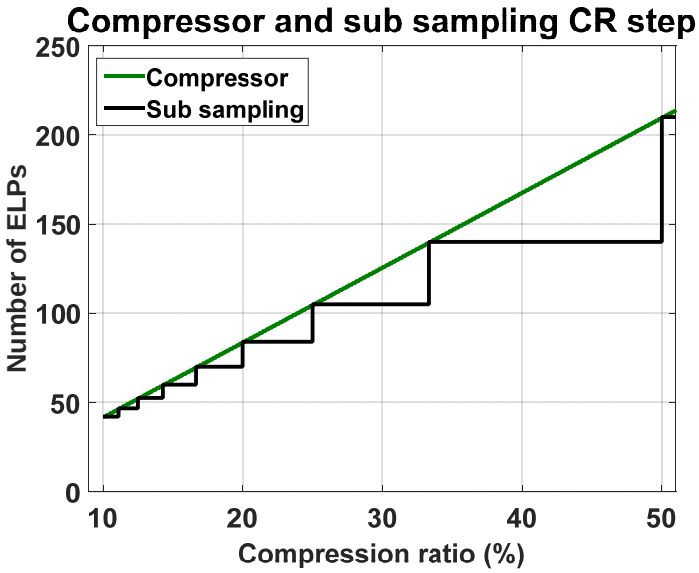

Figure 5-13. CR step size for the compressor and the subsampling methods

From the same perspective, it must be noted that the compressor is suitable to be used in a closed-loop solution to find the minimum number of ELPs required to represent the snapshots in the uncompressed scenario. Figure 5-14 shows a simple closed-loop adjustable CR concept. This simple strategy does not aim to represent a refined closed-loop solution, but to illustrate the potentials of the compression method.

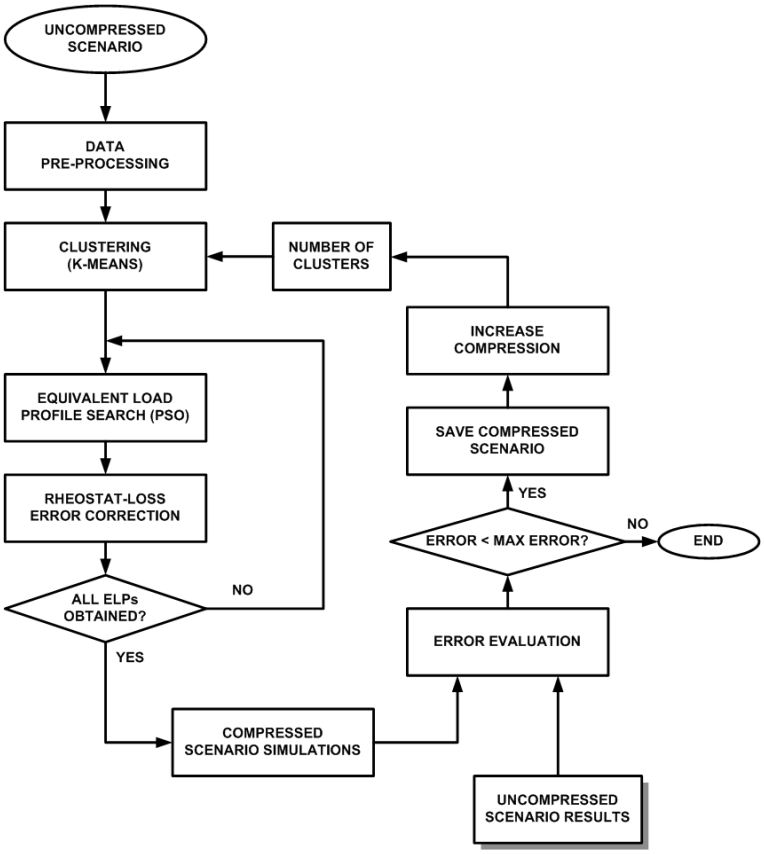

Figure 5-14. Traffic-scenario compression method: adjustable CR approach.

In this compression approach, after the data pre-processing is performed, the clustering process is applied with an initial –high– number of clusters. Then, the ELPs are obtained and the energy-saving accuracy is evaluated following any validation test. If the accuracy standard is fulfilled, the resulting compressed scenario is saved, the number of clusters reduced with a certain step, and the process is repeated. The process ends the first time that the accuracy criterion is not fulfilled.

5.6. SUMMARY, CONCLUSIONS AND CONTRIBUTIONS

This chapter has been devoted to the study of a strategy to reducing the simulation time required to obtain the MTS energy figures under the multiple-scenario traffic approach proposed in Chapter 4. This simulation-time reduction is achieved by means of a traffic-scenario compressor, which is a novel approach in the literature.

In addition, this chapter includes a study which makes it possible to assess to what extent the simulation time may be reduced by simply applying subsampling techniques to the total number of snapshots in the traffic model used.

The review of the rheostat reduction mechanisms has suggested that the obtainment of accurate energy-saving results must be attained by a proper representation of the amount of rheostat losses, their location in the line and the voltage of the RS locations in the system prior to the introduction of improvements.

Taking this into account, this chapter proposes a novel traffic-scenario compression method which obtains an equivalent traffic scenario with a reduced number of snapshots, thus reducing the simulation time. The compressor is performed in two steps: 1) a clustering stage which groups similar snapshots, and 2) a stage in charge of searching for the specific sets of train positions and powers to be simulated.

The compressed traffic-scenarios have proven to lead to a notable increase in the energy-saving result accuracy with respect to the subsampling method. Whereas the subsampling method is out of a 5 % relative-error band for 67 % compression ratio, the proposed compressor is able to obtain accurate results with 80 % compression ratio.

This compression ratio has been proven to be applicable to all the traffic scenarios selected in Chapter 4, for 4-, 7- and 15-minute headways. The accuracy results are good both with respect to the uncompressed representative-scenario average savings and to the whole-traffic-space savings.

In addition, the compressor has exhibited high accuracy values both for the single and multiple RS tests. For this latter test, less than 4 % of the configurations exhibit relative errors out of the 5 % error band, with only 6.74 % worst-case error. It must be noted that this represents a qualitative increase in the energy-saving result accuracy compared to the one obtained with the traffic approach normally used in the literature.

The main contributions of this chapter are:

- The proposal of a novel method to reduce the simulation time required to obtain accurate MTS energy figures. It must be noted that the combination of the compressor and the representative traffic scenario selection represents a qualitative improvement in the energy-saving result accuracy with a limited increase in the associated simulation time. Thus, this contribution will make it possible to implement more complex searches for optimal MTS infrastructure

configurations for the same simulation time, increasing the confidence in the results obtained.

- The review of the connections between the electrical variables in MTSs and energy savings, which has led to proposing rheostat-loss position and amount and SS voltage as the key variables to reduce the number of snapshots to be simulated.
- The use of the subsampling method as a reference to assess the goodness of the compression method has made it possible to conclude that the sampling time in energy-saving studies should not be greater than 2 seconds.

CHAPTER 6

MASS TRANSIT SYSTEM INFRASTRUCTURE OPTIMISATION

6.1. INTRODUCTION

In this chapter, all the studies developed along the thesis are integrated into a MTS electrical infrastructure optimiser. As has been observed in the different analyses in this thesis, it is possible to obtain notable energy consumption reduction in MTSs where rheostat losses take place. Consequently, there are several works in the literature which are devoted to the study of the ways to improve the existing electrical infrastructure of an MTS by including devices to increase its receptivity.

Starting with the works dealing with RSs, (Chang, Wang et al. 1998), proposed a genetic algorithm for optimising RS firing angle. This is one of the first references found on this type of optimisation. Specifically, this work was focused on the benefits of load sharing between the SSs in the system, which was presented as a trade-off problem with respect to energy saving. It used a genetic algorithm (GA) to obtain the optimal firing angles in a pre-defined set of RSs for different relative weights between load sharing and energy savings.

(Hui-Jen, Chao-Shun et al. 2005), proposed a GA to obtain the optimum RS location in an MTS. The inclusion of RS cost analysis allowed this optimiser to suggest the installation of RSs in 4 out of the 12 SSs in an MTS line in Taiwan. This work represents a fairly rigorous study. However, the parameterisation of the search method is

omitted. Therefore, it is not clear to what extent it arrives to global optimum or nearly optimum solutions. The same authors improved the search method in (Chuang 2005) by combining the GA with the Immune Algorithm. The main advantages of this evolutionary method, which is inspired in the response of the immune system to the presence of antigens (antibodies), are related with the exploration-exploitation trade-off in the search process. However, the authors did not show any details of the method parameterisation or its search behaviour. The size of the RS to install was not tackled in any of these two RS location studies.

It is important to remark that the exploration-exploitation trade-off is well known to be one of the most important concerns in metaheuristic search methods (Eiben, Shippers 1998, Renders, Flasse 1996), and thus, it must be properly tackled.

In a more recent work, (Bae 2009) presented another study of the way inclusion of RSs in a line affects energy consumption. Although the quality standard of this study is high, the search method implemented is over-simplified. The size of the RSs is not included, and the number of RS to be installed is initialised to the maximum available locations (SSs) and decreased two-by-two. The optimum number of RSs is not motivated by the analysis of the investment feasibility.

(Fazel, Firouzian et al. 2014) represents a recent work on RS location. The traffic assumptions in this work are too simple, and so is the case-study line implemented. There is not a formal search-method presented and no economic concerns are included.

Among the works which set the scope in wayside ESSs, the work by (Lee, Jung et al. 2013) studied the effects of installing big flywheel ESSs in a Korean line. There is no formal search method in the study. The ESSs were installed at all the SSs and then the economic savings derived from energy consumption and peak-power reduction were assessed. However, it is not clear whether the huge investment derived from the installation of 7 ESS will be somehow retrieved within the useful life of these equipments.

(Wang, Yang et al. 2014) presented a more rigorous study on the MTS infrastructure improvement. Super-capacitor ESSs were proposed as the technology to install. The authors proposed a search method which consists in an enhancement of the GA by the inclusion of simulated annealing. The study included cost analysis to justify the investment decisions. Both energy savings and voltage concerns were included in the fitness function defined. Thus, this is a rigorous work. However, it uses cost per MWh which are far lower than the typical ESS costs. In addition, it does not show any results justifying that the solution obtained is clearly better than other ones. The work by (Xia, Chen et al. 2015), from the same workgroup, is fairly similar to the previous one, but including the ESS energy management. The search method is a GA without improvements. The work is again comprehensive and rigorous, but it presents the same weaknesses as the previous one.

All the studies previously analysed are performed by means of electrical multi-train simulators.

There is another type of work, which focuses on the study of the optimal control curve of wayside ESSs with different storage technologies (Ciccarelli, Del Pizzo et al. 2014, Battistelli, Fantauzzi et al. 2012, Ianuzzi, Ciccarelli et al. 2012, D'Avanzo, Iannuzzi et al. 2010, Battistelli, Ciccarelli et al. 2009). These studies are conducted by means of formal optimisation models. Consequently, they must solve the highly non-linear and non-convex load flow problem simultaneously to the optimisation of the infrastructure. They implement several traffic simplifications which do not allow assessing whether these optimisations models would be able to tackle complex MTS lines with different headways and traffic scenarios.

It must be concluded after this review that the location of devices devoted to increase receptivity in MTSs is a topic to be further developed. Although there are several references tackling this concern, there are still many issues to be dealt with in the MTS electrical infrastructure optimisation problem. Regarding the receptivity improvement technology, it may be observed that there are several examples of studies dealing with RSs and other ones devoted to the study of ESSs. However, as explained in Section 3.3.2, the current state-of-the-art in RS and ESS manufacturing makes it difficult to justify the installation of the latter technique. For this reason, this thesis is focused on the installation of RSs.

This chapter presents the MTS optimisation solution proposed in this thesis. In Section 6.2, the main characteristics of this optimiser are described. Then, Section 6.3 performs an analysis of the search space which aims to make it possible to assess the goodness of the solutions proposed by the optimiser. Section 6.4 presents the parameterisation of the optimiser and the results obtained. The most relevant computational concerns and the measures taken to reduce optimisation times are also included in this section. Finally, Section 6.5 presents the main conclusions drawn from the studies in this chapter.

6.2. OPTIMISER DESCRIPTION

The possibility of implementing a formal mathematical optimisation model was explored in (López López, Pecharromán et al. 2012). The particularities of the electrical system in DC-electrified MTS make the more general formulation of this problem become a Mixed Integer Non Linear Problem (MINLP) with several different binary variables. In the first approach to the problem modelling, some simplifications were introduced to assess the behaviour of the model from a simpler to a more complex approach. Specifically, a linear approximation of the power equations of the load flow was carried out, and a mock-up system made up of just a few SSs, trains and snapshots was used to test the model. Although this simple model performed correctly, the generalisation of the model to the case study system in this thesis never found correct solutions. This MILP formulation is basically affected by the huge amount of binary variables and equations that the computer has to handle simultaneously. This model makes the model unmanageable, especially from the computer memory standpoint. A refinement in the use of binary variables could play a pivotal role in the improvement of the computational behaviour of this model.

This modelling experience reinforced the idea of dealing with the highly complex and non linear MTS infrastructure optimisation problem in a simulator based approach. Figure 6-1 shows a block diagram of the MTS electrical infrastructure optimiser proposed in this thesis. Its fundamental parts are the electrical multi-train simulator (developed in Chapter 2) and an algorithm that performs the search for the best possible infrastructure improvement. Both have been included in the Infrastructure Optimiser block in Figure 6-1.

This algorithm and the simulator are used in a master-slave fashion: the master (algorithm) decides which changes in the infrastructure must be applied in the search for the optimum infrastructure. The change decisions are taken by analysing the energy saving results obtained with the simulator (slave). The search method, based on the PSO algorithm, is thoroughly described in Section 6.2.3.

The accuracy and significance of the energy saving results obtained with the simulator are inextricably linked to the representativeness of the traffic scenarios used in the study. This has been proved in Chapter 4, where the trains' power and speed profiles have been combined with the main stochastic and deterministic traffic variables to generate a minimum-size set of representative traffic scenarios. This, together with the traffic scenario compressor developed in Chapter 5, is represented in Figure 6-1 inside the traffic generator block. The use of the traffic scenario compressor makes it possible to have a dramatic decrease in the simulation time, but it can be disabled if necessary. The combination of the different traffic headways tackled in Chapters 4 – 5 to generate the traffic scenario set is described in Section 6.2.1.

In general, an optimisation algorithm is in charge of minimising a given function, subject to a set of restrictions. In the MTS infrastructure optimisation problem tackled in this thesis, the main restrictions are:

- Technical restrictions, e.g.: the available space for a certain device in a SS's facilities may limit the maximum power of the RS.

- Layout restrictions, e.g.: the absence of a link to the utility grid makes impossible to place RSs in passenger stations, whereas an ESS is only subject to room restrictions.

Finally, it has to be taken into account that the cost of placing devices to increase receptivity in an MTS is rather high. In addition, if no terms representing costs are included in the evaluation of the best infrastructure improvement, the solution could be unbounded, i.e., place infinitely large RSs in all the available locations; regardless the fact that the improvement of the optimiser fitness function would be marginal from a given point.

As a conclusion, it is required to carry out some economical assessment of the investment required to improve the infrastructure. The details on the way the economic concerns have been tackled in this thesis are given in Section 6.2.2.

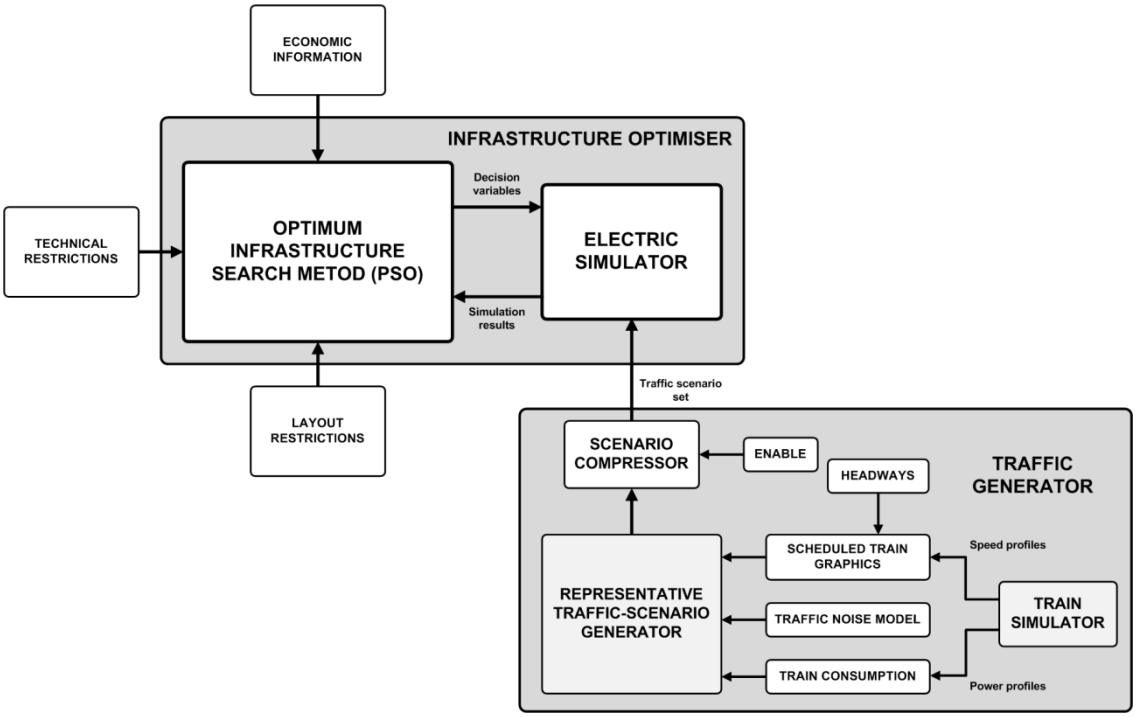

Figure 6-1. Infrastructure optimiser concept.

6.2.1. TRAFFIC SCENARIOS

The importance of the traffic input for the accuracy of the MTS infrastructure optimisation results has been proved in Chapter 4. In that chapter, it was shown that for each headway under study, it is important to include several traffic scenarios in order to properly represent the energy interactions between trains.

The studies devoted to the traffic input in Chapters 4 and 5 have taken three traffic headways into account. These three headways are used in this chapter as the tools to represent the main traffic patterns in the operation of an MTS. Two qualitatively different kinds of operation days have been included into the traffic input to the simulator: 1) Working days, and 2) Ferial days.

In the working days, MTSs are generally used by thousands of people to make it to their working places. That usually leads to a well known user affluence pattern, which consists of two peaks of affluence separated in time around eight hours. The MTS operator must use a higher number of trains to satisfy this peak-hour demand. Then, during the major part of the rest of the day, the system is operated to satisfy the off-peak demand conditions. In this operation headway, the number of trains is decreased, but the headway between trains remains in relatively medium conditions. Finally, in the beginning and the end of the operation hours, the user affluence reaches its minimum values. The MTS operator takes advantage of this situation to softly release or retrieve the trains rolling on the line tracks in an operational mode that has been named sparse mode in this thesis.

During the ferial days, the user affluence peaks related with workers do not generally take place. MTS operators tend to satisfy the lower demand with a lower number of trains. Therefore, this kind of days may be represented with the off-peak and sparse traffic modes.

Figure 6-2 presents the headway distributions defined for the working and the ferial days. For the former, two peak-hour intervals represent the two periods with very high user affluence. Both peak-hour intervals last for two hours. The first begins at 8 a.m., whereas the second starts at 7 p.m. Then, two hours of sparse traffic have been included at the beginning and the end of this type of operation day. The rest of hours of the working days are operated at the off-peak headway.

For the ferial days, the sparse traffic intervals at the beginning and at the end of the operational hours have been extended to three hours. The MTS is operated at the off-peak headway during the rest of the ferial day.

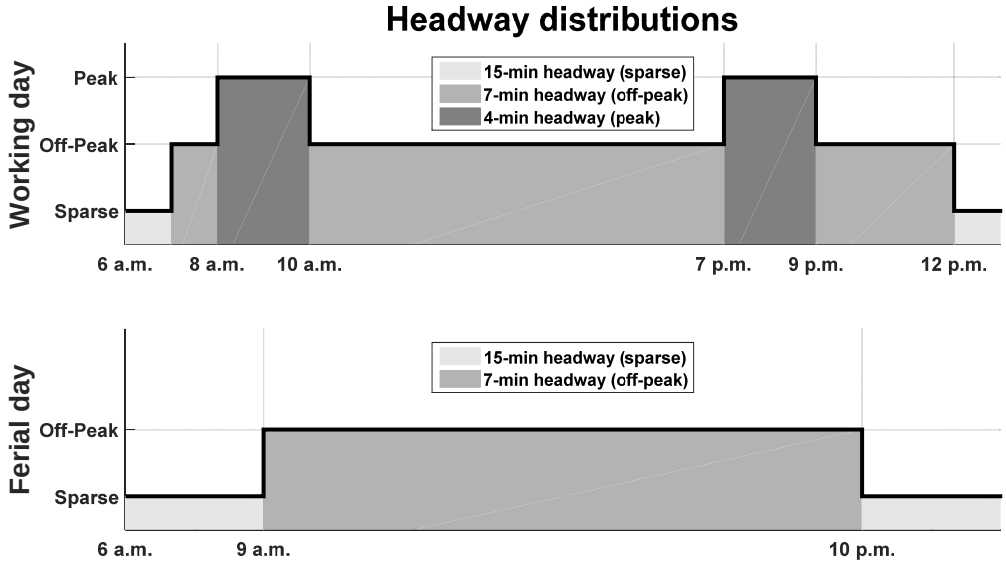

Figure 6-2. Headway distributions for working and ferial days.

Table 6-1 shows the total number of hours of operation for each traffic mode and type of operational day. In an additional column, the total number of hours per week is accounted. This data will be used to obtain the annual energy figures by extrapolation.

Table 6-1. Daily and weekly number of operation hours assigned to each traffic headway.

	Working day	**Ferial day**	**Weekly total**
Sparse headway (hours)	2	6	22
Off-peak headway (hours)	13	13	91
Peak headway (hours)	4	0	20

The traffic representation in this thesis includes the main traffic pattern in the operation of an MTS. It is clear that in the actual operation of a line, there may be many particular circumstances. The MTS operator has the task of finding a good trade-off solution between the user's satisfaction and the operational expenses (mainly the energy and personnel bills). That could lead to a more complex traffic pattern with more than three different headways.

However, that does not imply that the results obtained in this thesis are not general. The application of the optimisation methodology presented in this thesis to another MTS line with more detailed information about the traffic, would just require defining the particularised train timetables and training graphics.

6.2.2. ECONOMIC CONCERNS

In general, the inclusion of RSs in an MTS with significant rheostat losses will lead to energy savings. In addition, as the number of RSs and their sizes are increased, the energy efficiency of the system will be increased as well. However, this energy efficiency increase will probably be marginal from a given number of RSs installed on. Consequently, in order to discard expensive solutions which are not necessary, it is required to include the costs related to the installation of RSs in the investment decision process.

In most MTSs, the prices of the few installed ESSs and RSs are secret. This is the particular case for the Spanish MTSs. However, it is well known that the inclusion of a converter in a diode SS to make it a RS is relatively expensive. The work by (Gelman 2013) brings some light on the prices of the converters used in RSs. This study, carried out by a power converter manufacturer, in addition to emphasize the big difference in price which currently exist between storage and reversible solutions, states that the price per MW in reversible converters may vary from around 100 and 200 thousand dollars.

This data, which is only referred to the cost of the reversible converter itself, has been complemented in this thesis by a fixed cost in order to represent the different works required to install and have the equipment functioning in an actual MTS. The RS pricing rule is presented in (6.1).

$$C_{RS} = C_{Fixed} + \alpha_{PWR} \cdot P_{SS} \tag{6.1}$$

Where,

- C_{Fixed}, is the fixed cost for a SS. It represents the costs related with personnel, the works to install the SS, etc. In this study, the fixed cost parameter has been set to 250k€.
- α_{PWR}, is a coefficient that represents the cost per installed MW. The cost per MW has been set to 150 k€/MW.
- P_{RS}, represents the RS size (installed power).

Under this pricing rule, a 2 MW RS will cost 5.5 million euro. This final price per MW has been confirmed as a sensible price in informal conversations with members of the staff of a Spanish MTS operator. Taking this into account, the total investment for a hypothetical infrastructure upgrade made up of four 2 MW RSs would equal 2.2 million euro. This amount represents a large cash outflow for a MTS operator company, and its profitability has to be properly motivated.

The future events derived from the installation of RSs that will make the investment profitable have a special nature: they are not cash inflows but operation cost savings. Specifically, the energy bill will be reduced in accordance to the operation energy savings.

Therefore, both a rule to calculate the annual energy savings and an energy price are required. The energy savings derived from the installation of RSs have been intensively studied along the thesis, since they have been used to define the accuracy of both the representative scenarios and the traffic scenario compressor. Their expression is given in (3.2) (pg. 77). Then, the energy price used in this study is 0.1 €/kWh.

With these tools, it is only necessary to define an investment profitability criterion in order to be able to assess whether it is worth to apply a given infrastructure improvement or not. Classical examples of investment assessment are the Retrieve of Investment (ROI) and the Net Present Value (NPV). The latter is known to present some advantages with respect to the former (Christen, Ohler 2002), and has been used in studies aimed at justifying the investment on railway infrastructures (de Rus, Nombela 2007). For these reasons, the NPV has been selected as the investment profitability criterion in this thesis. Its definition is given in (6.2).

$$NPV = \sum_{t=1}^{T} \frac{ES_t}{(1+r)^t} - C_0 \tag{6.2}$$

Where,

- ES_t, represents the total economic savings for the period t. In the general NPV formula, this is usually represented by the cash inflow, but in this case it is more accurate to deal with earnings in terms of saved money.
- r, equals the discount rate. This is used to represent factors as the investment risk or the attractiveness of having the money in financial investment products. Under the current financial market conditions, the 5 % discount rate used in this thesis

may be regarded as a conservative rate from the investment standpoint (i.e., it will make the NPV results to be somewhat pessimistic about the investment).

- T, represents the total number of periods taken into account in the NPV calculation. This value must be linked to the life expectancy of the installed equipments. RSs are well known to be robust devices which may perfectly last for 20 years. However, only 10 years have been included in the NPV calculations in this thesis in order to avoid excessively optimistic investment profitability assessments.
- C_0, equals the investment costs, which are obtained by using (6.1).

Finally, the rule used to decide whether an investment is profitable or not is based on the NPV sign. If the NPV value for a given infrastructure improvement is positive, the investment will be regarded as profitable, whereas configurations with negative NPV will be discarded (non profitable).

6.2.3. SEARCH METHOD

As stated at the beginning of this section, the application of classical optimisation methods to the MTS electrical infrastructure optimisation problem is not convenient. The main reasons are the high complexity of the problem (discrete, non-linear, non-convex, etc.) and its large size in terms of number of variables and equations for usual MTS lines.

Consequently, metaheuristic methods arise as good candidates to tackle this optimisation problem. Among the different options within these methods (heuristic search, simulated annealing, etc.) this thesis has selected an evolutionary computation method for its good characteristics.

Specifically, a swarm intelligence method has been used: the PSO method, presented by (J. Kennedy, R. Eberhart 1995). The reasons for the selection of this method are basically: 1) the PSO is well known to find optimum or nearly optimum solutions for complex problems in a fast and efficient way (Domínguez, Fernández-Cardador et al. 2014b, Sharafi, ELMekkawy 2014, Eberhart, Shi 2001). It has been, indeed, used in the traffic scenario compressor presented in Chapter 5 with satisfactory results. 2) The PSO dynamics are rather intuitive, and the sensitivity of the results to its parameters' tuning makes it a powerful search tool.

The search dynamics of the PSO are inspired on the way swarms of bees or birds, or school of fishes forage for resources in a restricted environment. Therefore, it is a population based algorithm which assigns a given speed to each element in a multi-dimensional search space in order to minimise a certain fitness function. For each iteration and element in the total population, the speed is made up of three factors:

- The impetus factor or the speed of the element itself in the previous iteration. This factor is especially useful in the first iterations of the PSO in order to enhance the exploration features of the algorithm. With a high impetus factor in the first iterations, the elements in the population will tend to significantly change their

positions, increasing the probability of exploring the best zones in the search space.

- The cognitive factor, which represents the knowledge of the element about the search space. This factor is used to attract each element in the population to its best position.
- The social factor, which models the communications between the members of the swarm. This factor is included to attract all the elements of the population to the position of the element with the best associated fitness value.

These three factors are weighted and combined to move the elements into the search space along the algorithm iterations. The expressions of the position and speed for the element *k* at the iteration *i* are given by (6.3) and (6.4).

$$p_k^i = p_k^{i-1} + v_k^i \tag{6.3}$$

$$v_k^i = imp_k \cdot v_k^{i-1} + c1_k^i \cdot fcog \cdot \left(p_k^{best} - p_k^{i-1}\right) + c2_k^i \cdot fsoc \cdot \left(p^{BEST} - p_k^{i-1}\right) \tag{6.4}$$

Where,

- p_k^i, v_k^i are the position and speed for the element *k* at iteration *i*.
- imp_k is the impetus factor for the iteration k.
- $c1_k^i$, $c2_k^i$ are two random forget coefficients for the cognitive and social speed factors.
- $fcog$, $fsoc$ are the cognitive and social factors.
- p_k^{best}, p^{BEST} are, respectively, the position with the best fitness value for the element k and the position with the best fitness value among all the elements in the swarm. Obviously, both coincide for these elements standing in the global best positions.

Some worth-to-comment implications of the parameters and variables to modulate the speed are:

- It must be noticed that the position for *i* = 1 requires initial position and speed to be defined. The initial speed might also be null, but in this thesis the elements in the swarm have been given a non-zero initial speed in order to enhance the search space exploration.
- The impetus factor could be constant along the iterations, but allowing it to be variable renders greater control over the algorithm convergence and the exploration-exploitation balance. It must be noticed that in the constant impetus factor case, this has to be strictly lower than 1 for the speeds of the elements in the swarm to be attenuated as the PSO algorithm evolves. Making it variable allows both to have a greater excitation level in the first steps of the algorithm (thus promoting the exploration of the search space) and to have small movements in the environment of the best solution in the last steps of the algorithm (thus promoting the exploitation of the hyper-volume around the best element).
- The forget coefficients range from zero to one. They are used to further enhance the exploration features of the algorithm. These random forget coefficients play a

fundamental role at the final iterations, where the swarm movements would otherwise be dominated by the social and cognitive factors. This mechanism is similar to the mutation mechanism in the well known genetic algorithm.

To conclude the PSO parameterisation, it is required to select values for both the size of the population and the number of iterations. The former parameter should be increased when the complexity of the search space is high. The latter should be limited to a large-enough value in order to prevent the method from being terminated before it has attained convergence. The particular values selected for the PSO parameters will be presented and justified in Section 6.4.

Once the PSO method and its main parameters have been introduced, it is time to describe the application of this method to the MTS infrastructure improvement problem.

The motivation to improve the infrastructure of an existing MTS is the potential to reduce its energy consumption when there are low receptivity situations. The start point is the case-study system, with 11 diode SSs that cannot feed regenerative power surpluses back to the utility grid. The improvement solution selected in this thesis consists of adding a reversible converter in parallel with the main diode converter. This additional converter is only in charge of allowing reverse power flows. The set of diode and reversible converter is what has been called along the thesis RS.

It was studied in Chapter 4 that the area of influence of each of these RSs is limited. It seems clear that two RS located in distant locations will not have strong interferences. However, when the number of RSs in the system is increased, it is not clear to what extent two neighbour RSs may interfere with each other.

Taking this into account, the main goal of the optimiser may be defined as the search for the optimum total number of RSs to install in the system, in which locations they should be installed, and their sizes in terms of maximum power.

The approach used to model this optimisation problem is based on the definition of RS objects, which are assigned in a given number to the elements in the swarm. RS objects are dynamic objects defined by two variables: position and size. As a result, each element in the swarm is made up of a vector of RS objects, which positions and sizes change from iteration to iteration depending on the element RS speed vector. The concatenation of the variables of these RSs leads to a state matrix for each element.

Table 6-2 presents the state matrix of the k^{th} element in the swarm during iteration *i*. This generic element contains N RS objects which movements are independent. This number of RS objects in the elements in the swarm determines the maximum number of RSs than can be installed in the system. It may be changed from execution to execution of the optimiser. However, once fixed, it is the same for all the elements in the swarm and during all the iterations.

When the locations and sizes of the RSs for iteration *i* are calculated, this state matrix is interpreted as a certain infrastructure improvement, as will be explained later in this section.

Table 6-2. Structure for the state matrix of element k in iteration i.

	RS1	**RS2**	**...**	**RSN**
Position	$pos_{k,1}^{i}$	$pos_{k,2}^{i}$	...	$pos_{k,N}^{i}$
Size	$sz_{k,1}^{i}$	$sz_{k,2}^{i}$	...	$sz_{k,N}^{i}$

The content of the state matrix in Table 6-2 is obtained from the previous state (iteration *i-1*), the element and global bests and the RS speeds following (6.5) and (6.6).

$$pos_{k,n}^{i} = pos_{k,n}^{i-1} + Vpos_{k,n}^{i}$$
$$sz_{k,n}^{i} = sz_{k,n}^{i-1} + Vsz_{k,n}^{i} \tag{6.5}$$

$$\begin{aligned} Vpos_{k,n}^{i} = {} & imp_{pos}^{i} \cdot Vpos_{k,n}^{i-1} + c1pos_{k,n}^{i} \cdot fcog_{pos} \cdot \left(pos_{k,n}^{best} - pos_{k,n}^{i-1}\right) + c2pos_{k,n}^{i} \\ & \cdot fsoc_{pos} \cdot \left(pos_{n}^{BEST} - pos_{k,n}^{i-1}\right) \\ Vsz_{k,n}^{i} = {} & imp_{sz}^{i} \cdot Vsz_{k,n}^{i-1} + c1sz_{k,n}^{i} \cdot fcog_{sz} \cdot \left(sz_{k,n}^{best} - sz_{k,n}^{i-1}\right) + c2sz_{k,n}^{i} \cdot fsoc_{sz} \\ & \cdot \left(sz_{n}^{BEST} - sz_{k,n}^{i-1}\right) \end{aligned} \tag{6.6}$$

The elements in (6.5) and (6.6) are nothing but the generalisation of the components in (6.3) and (6.4). However, the following differences, which result from the application of the general PSO formulation to the particularities of the MTS optimisation problem, must be taken into account:

- Both the initial positions and sizes and their respective initial speeds are defined at random within the limits set by the corresponding restrictions.
- The position impetus factor in (6.6) is the same for all the elements (and therefore for all the RS objects inside it) in iteration *i*. This is also applicable for the size impetus factor. Both impetus factors are, however, independent from each other.
- The forget factors (*c1* and *c2*) are obtained from a random uniform distribution from 0 to 1 for each particular RS object in the swarm.
- Positions are real numbers bounded to the beginning and end of the line.
- Sizes are real numbers bounded to the minimum and maximum RS size respectively.

Once the evolution of the element states has been presented, it is necessary to define a rule to transform an element state matrix into a specific infrastructure upgrade configuration. Before the particularities of this transformation rule are described, Figure 6-3 presents a graphical example of this transformation from the element state matrix to a particular RS configuration. In the upper graph, a certain set of positions and sizes for one 3-RS-object element in a simplified 5-SS infrastructure leads to the installation of three RSs. The position and size speeds in this hypothetical iteration are also presented. As a result of these speeds, the lower graph shows the new positions

of the RS objects. RS1 and RS2 have been forced to enter the area of influence of SS1 to illustrate the RS combination mechanism featured by the optimiser.

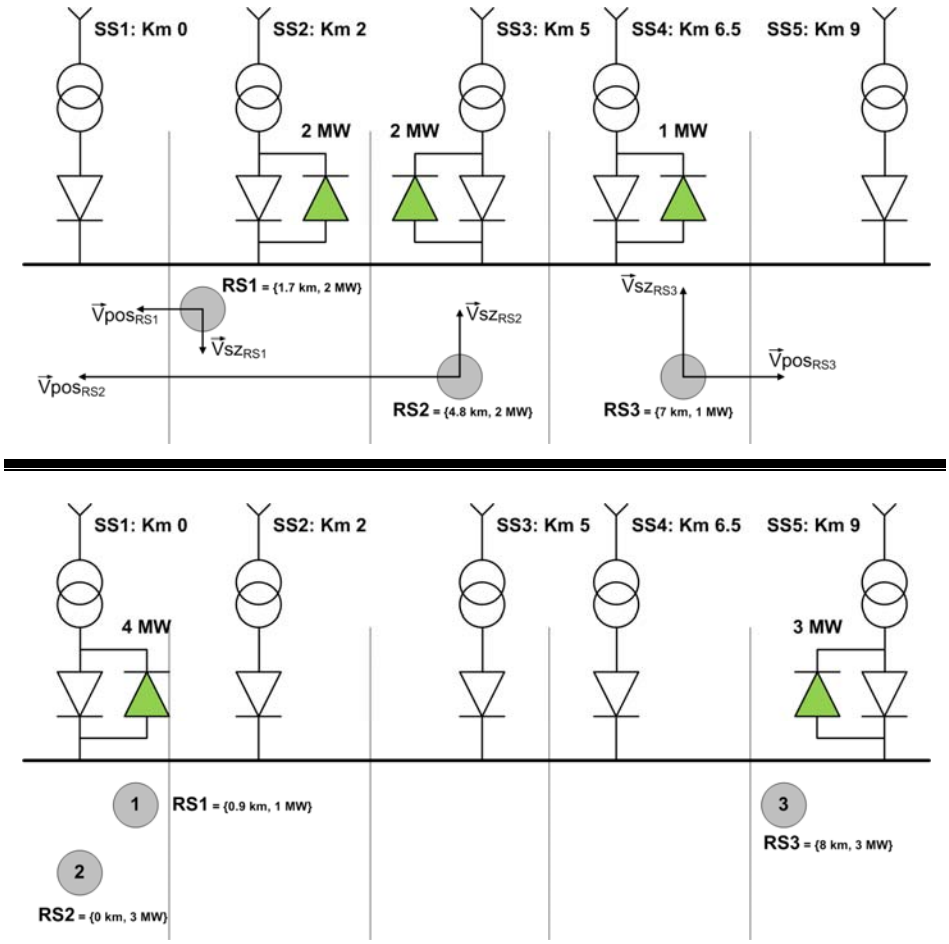

Figure 6-3. PSO algorithm RS placement dynamics.

It has been stated in Section 6.2 that RSs may only be located in electrical SSs, which provide a connection to the utility grid. Consequently, the real position values of all the RS objects have to be somehow transformed to meet the SS location vector (6.8). To do that, a RS placement rule has been defined in (6.7).

"For each element in the swarm and iteration, a RS is placed in a given location in the SS location vector only if at least one RS object is inside its area of influence" (6.7)

The area of influence of each SS is defined in (6.9).

$$SS_{VEC} = \{SS_1, \dots, SS_{11}\} \quad (6.8)$$

$$AoI_{SSi} = \begin{cases} \left({}^{(SS_{i-1} + SS_i)}/_{2}, {}^{(SS_i + SS_{i+1})}/_{2} \right) & if \quad i > 1 \,\&\, i < 11 \\ \left(SS_1, {}^{(SS_1 + SS_2)}/_{2} \right) & if \quad i = 1 \\ \left({}^{(SS_{10} + SS_{11})}/_{2}, SS_{11} \right) & if \quad i > 11 \end{cases} \tag{6.9}$$

Where,

- SS_{VEC} is the SS location vector, that has been particularised for the 11 SSs in the case-study system. SS_i is expressed in km.
- AoI_{SSi} is the area of influence of SS *i*.

Two main implications of the RS placement rule must be highlighted:

- The maximum number of RS installed in the system is fixed by the number of RS objects in the element (top-side graph in Figure 6-3).
- It is explicitly allowed to have more than one RS object in the area of influence of the same SS. That means that the optimiser lets the number of RS installed in the system be lower than the number of RS objects (bottom-side graph in Figure 6-3). It will be discussed later in this section that it would even be possible to have a configuration analogous to the base case, regardless the number of RS objects in the elements.

Regarding the RS size, although this variable is not discrete by nature, it must be noted that in practice, the reversible converter manufacturers will not serve a continuous range of sizes. The converter power will be mainly limited by the maximum currents in its high and low voltage sides. In order to represent this fact in the optimiser, the values of the RS object sizes have also been restricted to a discrete set of values in a size vector (6.10).

$$SIZE_{VEC} = \{0, 0.7, 1, 2, 3, 4, 5\}\ [MW] \tag{6.10}$$

Consequently, although the RS object size values are continuous, in the translation from the element state matrix to the particular RS configuration, they are changed to the closest value in the size vector. Since this vector is bounded, this represents an indirect bound of the RS size. It can be observed in (6.10) that the minimum size is zero. Allowing the size of the RSs to be zero is a useful means to remove RSs which associated energy saving is marginal.

To conclude the presentation of the transformation from the element state matrix to a particular RS configuration, since it is permitted to have several RS objects inside the area of influence of a given SS, it is required to define the way the size of the RSs is computed when these events take place. Although the half addition of the sizes was also considered, due to the improved behaviour of the optimiser, the size of the resultant RS when several RS objects are in the area of influence of a certain SS has

been computed as the addition of all these RS object sizes. An example of RS object combination is given in the bottom-side graph in Figure 6-3. It must be noted that if all the sizes of the RS objects in an element equal zero, no RS will be installed in the system.

Once the optimiser dynamics definitions have been made, it is possible to formulate the general expression of the optimisation problem to be solved (6.11).

$$\max\left(F(pos_1, sz_1, \dots, pos_N, sz_N)\right)$$

$$s.t.$$

$$\begin{aligned} pos_i &\leq \max(SS_{VEC}), \quad \forall RS\ objects\ (1\ to\ N) \\ pos_i &\geq \min(SS_{VEC}), \quad \forall RS\ objects\ (1\ to\ N) \\ sz_i &\leq \max(SIZE_{VEC}), \quad \forall RS\ objects\ (1\ to\ N) \\ sz_i &\geq \min(SIZE_{VEC}), \quad \forall RS\ objects\ (1\ to\ N) \end{aligned} \tag{6.11}$$

The formulation is expressed as a maximisation problem because the fitness function, *F*, represents the energy savings as a function of the RS object characteristics, which are indeed the decision variables of the optimiser. Its expression is given in (6.12).

$$F(pos_1, sz_1, \dots, pos_N, sz_N) = \begin{cases} E\_SS_{Raw}^{WEEK} - E\_SS_{Elem}^{WEEK}(pos_1, sz_1, \dots, pos_N, sz_N) & if \quad NPV_{Elem} \geq 0 \\ -\infty & if \quad NPV_{Elem} < 0 \end{cases} \tag{6.12}$$

Where,

- $E\_SS_{Raw}^{WEEK}$, is the addition of the weekly energy consumption in all the electrical SSs in the base-case system (without any added RSs).
- $E\_SS_{Elem}^{WEEK}$, which depends on the decision variables of the optimiser, is the addition of the weekly energy consumption in all the electrical SSs for the improved infrastructure configuration expressed by the element under evaluation.
- NPV_{Elem}, is the NPV of the element under evaluation, which of course depends on the weekly energy savings and the cost of the set of installed RSs.

When the element NPV is positive, the fitness function consists in the weekly energy savings derived from the infrastructure improvement. The weekly savings are obtained by composing the headway results following the information in Table 6-1. The weekly energy consumption formula for the base case is given in (6.13). The formula for the improved infrastructure case is analogous, and has been omitted for the sake of simplicity. The annual energy savings, required for the NPV calculation in (6.2), are obtained by extrapolation of the weekly energy savings to the 52 weeks in a year (6.14).

$$E\_SS_{Raw}^{WEEK} = \sum_{h=1}^{Hdw} \left(OpH_h^{WORK} + OpH_h^{FERIAL}\right) \cdot \frac{\sum_{\text{repr}}^{\text{ReprH}_h} E\_SS_{repr}^{h}}{ReprH_h \cdot ScenDur_h} \tag{6.13}$$

Where,

- Hdw is the total number of operation headways included in the study.

- $E\_SS_{repr}^{h}$ is the addition of the energy consumption at all the electrical SSs during the representative scenario $repr$, included in the operation headway *h*.
- $ReprH_h$ is the number of representative scenarios for the operation headway *h*.
- $ScenDur_h$ is the duration (in hours) of the representative scenarios for the operation headway *h*.
- OpH_h^{WORK} is the total number of hours per week assigned to the operation headway *h* on working days.
- OpH_h^{FERIAL} is the total number of hours per week assigned to the operation headway *h* on ferial days.

$$ES_t = 52 \cdot \left(E\_SS_{Raw}^{WEEK} - E\_SS_{Elem}^{WEEK}\right) \tag{6.14}$$

The discontinuity in the fitness function introduced by setting to minus infinity the value of these elements with negative NPV allows defining the optimiser's objective: to minimise the energy consumption for the same service parameters subject to having a profitable investment.

In this point, it has to be remarked that other fitness functions are also possible. For instance, an MTS operator could be interested in the maximisation of the investment NPV. However, this will in general lead to sub optimum solutions from the system energy efficiency standpoint (see Figure 6-6 in Section 6.3.1), which has indeed been defined to be the objective of this thesis. In addition, it must be noted that this latter fitness function, which is continuous, is softer from the search-complexity standpoint. This alternative fitness function, which would also have to be maximised is presented in (6.15).

$$F\_alt(pos_1, sz_1, \dots, pos_N, sz_N) = NPV(pos_1, sz_1, \dots, pos_N, sz_N) \tag{6.15}$$

Regarding the way the position and size bound restrictions have been tackled, it has to be noted that when any of the variables of the RS objects go beyond the imposed limits, this variable must be saturated. Then, there are two options for its associated speed: 1) take no action on it; 2) set it to zero. The second option has proved to lead to a better behaviour of the optimiser, and thus, it is the one implemented. It must be taken into account that cancelling the speed of a state variable which is saturated will not make it remain static. In the following iterations, the element and the global bests will determine its speed which will be, in general, non null. This mechanism is analogous to the anti-windup mechanism usually implemented in PID control systems to enhance their dynamic response.

At this point, both the optimisation problem and the method to find the optimum solution are defined. Now, it is only required to define the particular strategies implemented to find the optimum infrastructure upgrade configuration for the MTS case study. Two different strategies have been implemented.

General Search for the Optimum RS Configuration

This represents the general search for the optimum configuration without any additional restrictions. In this approach, the values of the RS objects in the elements of the swarm are independent from each other.

Without the profitability concern introduced by the NPV, the problem would not be easy to bind. Once all the rheostat losses are eliminated, all the configurations would be similar, and only the difference in the rest of system losses would determine the difference in the energy savings. The problem could be tackled by increasing the number of RS objects in the elements of the swarm one by one. Then, an analysis of the energy saving knee in the optimum configurations could make it possible to find a trade-off solution between energy savings and costs.

However, once the economic assessment of the infrastructure upgrade is introduced in the fitness function, the ideal strategy to find the global optimum consists of setting the number of RS objects in the elements of the swarm to the number of electrical SSs in the system. For the case study, if a configuration with 11 RSs is not worth to be installed, the RS objects in the elements will be naturally combined to find cheaper solution with still good energy saving figures.

Consequently, in this general search strategy, 11 RS objects are included in all the elements of the swarm, and the PSO method is executed with no additional restrictions.

Since under certain circumstances the method may converge before the iteration limit has been reached, an early stopping criterion has been defined in this general search strategy. Specifically, the method is stopped if the best fitness value in the swarm is the same during ten iterations.

Two-Stage Search for the Optimum RS Configuration

In practical terms, a RS configuration made up of RSs with several different sizes may be a problem for the MTS operation in terms of maintainability, cost of the works, etc. In order to tackle this hypothetical customer request, a two-stage search strategy is proposed in this thesis.

This strategy consists of carrying out a first search where the sizes of all the RS objects inside each element in the swarm are forced to be the same. This is named the homogeneous size restriction, expressed in (6.16), which is added to the optimisation problem defined in (6.11). Then, there is a second search stage where the PSO method is executed exactly in the same mode than for the general search strategy. This second stage aims to assess the possible energy efficiency improvement that may be achieved by relaxing the homogeneous size restriction.

$$sz_1 = sz_2 = \cdots = sz_N \tag{6.16}$$

In the practical implementation of the PSO method, the size variables of all the RS objects in each element are treated as a single size, with a single speed. The RS combination rule is, of course, modified by the application of (6.16): if more than one RS objects fall within the area of influence of a certain SS, their sizes are not added.

With this implementation, the PSO will converge to an optimum infrastructure upgrade configuration with a single RS size. This search is actually carried out in a subset of the general search space.

Once this first stage has been executed, it is possible to find the global optimum for the general search space by relaxing the homogeneous size restriction. It must be realised that the result of the first stage represents a very good starting point for the second stage, so there is no need to spread the elements in the swarm across the search space. For the same reasons, since this second stage will be mainly devoted to exploration concerns, the initial speeds in this second stage should ideally be reduced.

The same early stopping criterion than the one defined for the general search strategy has been applied to the two stages in this two-stage search approach.

6.3. SEARCH SPACE ANALYSES

After the presentation of the optimiser method, this section is devoted to the analysis of the solution space where this optimiser will look for the best infrastructure upgrade solutions: the search space.

The size of the converters (MW) has been defined to be a discrete variable. Two different search spaces will be analysed: 1) the solution space where all the RSs added to the system have the same size; 2) the solution space where the size of each RSs is independent from the size of the rest of RSs. The reason for the analysis of the former search space is that MTS operators may find it more convenient for the maintainability of the system to have homogeneous SSs in the system. The latter search space represents a general exploration of the general upgrade solutions in order to analyse to what extent it could be justified to have heterogeneous SSs in the system.

6.3.1. HOMOGENEOUS RS SIZE SEARCH SPACE

This section analyses the possible infrastructure upgrade configurations which consist of installing a certain number of RSs in the line with the same size. To start this study, the general solution set has been broken down into subsets which contain samples with equal number of installed RSs. Figure 6-4 shows the size of each of these subsets for a given RS size. The number of elements belonging to each subset is given by (6.17).

$$SubsetSize = \frac{NSS!}{NRS! \cdot (NSS - NRS)!} \tag{6.17}$$

Where,

- NSS represents the total number of SSs in the line.
- NRS represents the total number of RSs installed.

The total number of combinations for a given RS size (all the subsets) is 2048, and the subsets where RSs are placed in half the available SSs (5 & 6) are the ones with the higher number of combinations. This search space is then replicated for the six RS sizes taken into account in this study, making the number of possible combinations to be studied increase to 12283.

Even when all the sizes are included, it must be stated that the size of the search space when the size of the RSs is forced to be homogeneous is perfectly suitable for an exhaustive evaluation of the whole space. I.e., for this number of available locations, it would not be necessary to run the search method. It would be simpler to simulate all the possible combinations. Nevertheless, it must be taken into account that when the number of available locations to install infrastructure upgrade devices rises up, the number of possible combinations diverges. Actually, if every passenger station in the line was suitable to install a certain device (which could be the case of ESSs), the total number of possible combinations would be increased to 50331643. In this case, it would definitely be worth to run the PSO search method proposed in this thesis.

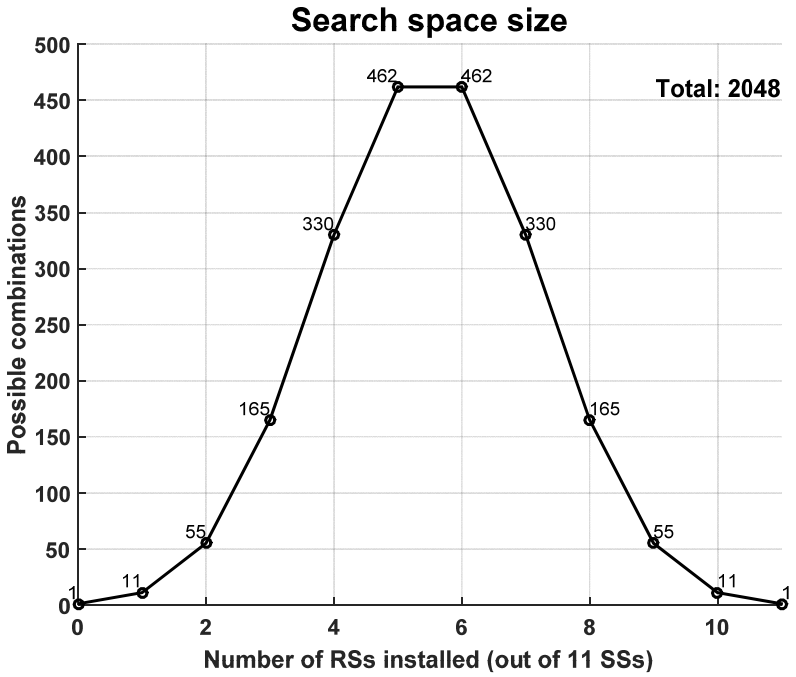

Figure 6-4. Search space size when a single reversible converter size is allowed.

In order to find out about the characteristics of the search space, the exhaustive simulation of all the possible location and size combinations has been carried out. Figure 6-5 (left side) shows the optimal curves regarding the energy saving results for each subset in the whole search space and RS size. Then, the right-side graph in Figure 6-5 includes the best and worst energy saving curves for the 2-MW RS case. This has been added to show the importance of properly placing the RSs, especially in these subsets with higher number of possible combinations. The rest of worst-case curves follow a similar trend. They have not been represented for the sake of clarity.

This figure can be regarded as the representation of a 3-D energy saving surface where the third axis is the RS size. Hence, the curves could be regarded as the projections of the intersection of the energy-saving surface with constant RS-size planes. Taking this into account, energy-saving vs. RS power curves, included in profile planes, can be read in the figure as well.

The inspection of the curves in Figure 6-5 yields the following results:

- 0.7 and 1 MW converters do not perform well in this system. The energy savings are increased steadily as the number of RSs grows, but the rest of curves seem to belong to a better cluster.
- This is actually the second important conclusion to be extracted from the figure: from 2 MW converters on, the increase in energy savings flattens out. This effect is more accentuated from 3 MW converters on, but the knee in these energy-saving vs. converter power curves takes clearly place for the 2 MW case.
- Disregarding the 0.7 and 1 MW cases, three different zones are observed in the energy-saving vs. installed RSs curves. In the first one, corresponding to a low number of RSs, the inclusion of a further RS in the system leads to a quasi linear increase in the energy saving figures. Then, there is an intermediate zone, from 4

to 7-8 RSs where the slope of the curves is decreased, but there is still an improvement of the energy saving figures associated with the addition of a further RS. Finally, there is third zone where the curves flatten out. In this zone, the inclusion of a sufficient number of big RSs to the system has made the rheostat losses to become marginal.

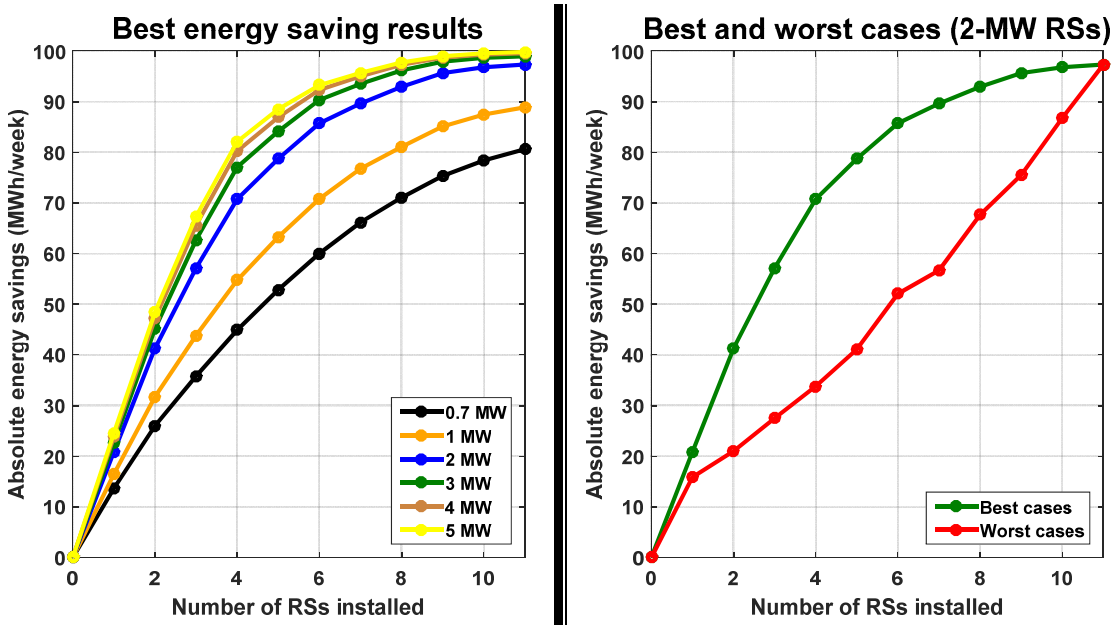

Figure 6-5. Energy savings for the best RS location when the allowed number of RSs and their sizes are varied.

The results in Figure 6-5 suggest that there will be a number and size of RS from where the economic index used to decide the profitability of the investment (NPV) will drop. It looks clear that if a 7 x 3-MW infrastructure upgrade has a low NPV, the same configuration with 4-MW converters will not be profitable. There must be a relation between the knees in the curves in Figure 6-5 and the last profitable configurations, but it is not straightforward to deduce which configuration represents the global optimum without calculating the particular NPV values.

In Section 6.2.3, the fitness function has been defined as the energy savings when the NPV value is positive, and minus infinity for those elements with negative NPV (non profitable investment). In order to analyse the configuration with the greatest energy saving result in the profitable region, Figure 6-6 represents the NPV vs. energy savings for the elements represented in Figure 6-5. Since its results are not relevant, the 0.7 MW case has been removed from the representation. The energy savings for the elements with negative NPV have not been set to minus infinity, but the negative NPV region has been represented in red. For constant RS size curve, the number of RS installed corresponds to the number of elements between the point under analysis and the origin of the plane (including this point).

The results in Figure 6-6 make it clear that it is not only important to decide how many RSs to install, but also their sizes. The analysis of the constant number of RS curves

shows that the maximum NPV always coincides with the 2-MW configuration, whereas the maximum energy savings are obtained when 5-MW RSs are installed.

On the one hand, the bigger price of these big converters makes its associated curve (yellow) to enter the non profitable region soon (3 RSs). On the other hand, it can be observed that the low energy saving performance of the 1-MW RSs is partially compensated in terms of NPV by their lower price.

For the fitness function defined in (6.12), the global optimum for the whole search space takes place when 6 2-MW RSs are installed in the line. The case with 5 3-MW RSs presents a nearly zero NPV with big but lower energy savings, and the NPV and energy saving results for the 8 x 1 MW and 4 x 4 MW cases are very similar.

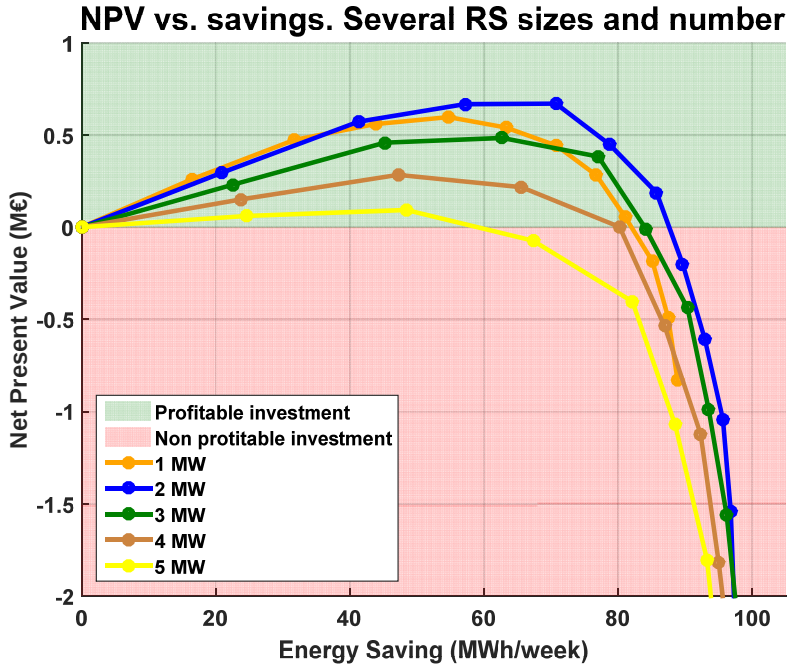

Figure 6-6. NPV – energy savings evolution for the best RS location when the allowed number of RSs and their sizes are varied.

To conclude this section, it is important to remark that the relative position between the RSs in the line is as important as their size and number. It can be observed in Figure 6-5 that the energy saving result can be thoroughly reduced if the RSs are not properly located. Figure 6-7 shows the best 6 x 2 MW configuration, which has been proved to be the global optimum for this search space. Thus, the PSO method must converge to this configuration when it is run under the homogeneous RS size restriction.

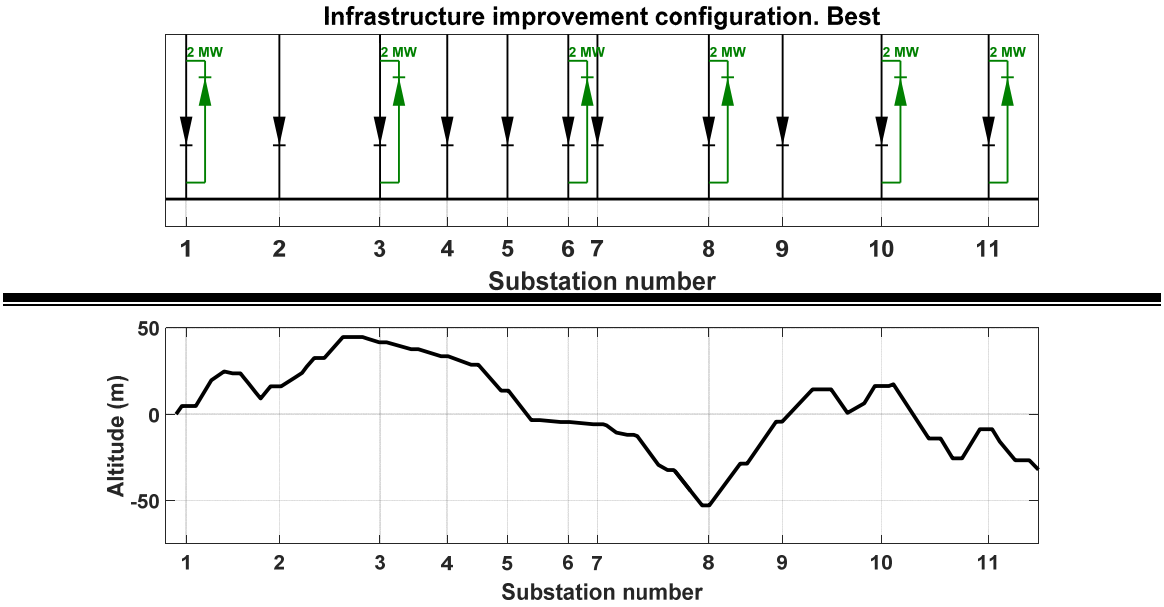

Figure 6-7. Optimum RS placement configuration when a single RS size is allowed.

6.3.2. ON THE POSSIBILITY OF TRIVIALLY OBTAINING THE OPTIMUM RS CONFIGURATION

It has been discussed in Chapter 3 that the relation between the passenger stations and the track altitude profile affects the amount of regenerated energy in certain zones, and that may lead to hot rheostat-loss zones in the system. It could consequently be argued that it is not necessary to carry out a comprehensive study of the system in order to decide the best locations where to include RSs.

This Section elaborates on the possibility of obtaining the optimum infrastructure upgrade in a trivial manner. In the first step of this analysis, it has been measured the frequency at which each available location in the line (SS) has been included in an optimum (or quasi optimum) infrastructure upgrade configuration. To do it, this study focuses on the search space depicted in Figure 6-4. Each RS location has been assigned a frequency value accounting the ratio between the times it has been included in an optimum configuration and the total number of configurations under study. Three different cases which analyse the 3, 4 and 5 best RS configurations in terms of energy savings have been defined. This has been included in this study to prevent it from obtaining noisy results.

Figure 6-8 shows the frequency results for each SS and the line altitude profile. The most significant findings have been marked in the figure. Specifically, all the SSs which frequency is greater than 0.4 are close to passenger stations in valleys. It can also be observed that the line endings reinforce this tendency to be included in the best configuration. This is due to the lower receptivity in line endings, linked to the lower average number of neighbouring trains when trains approach the terminal stations. This effect can be clearly observed if SSs 8 and 11 are analysed at a time: SS 11's frequency is much higher, whereas its topographic characteristics are similar to those of SS 8.

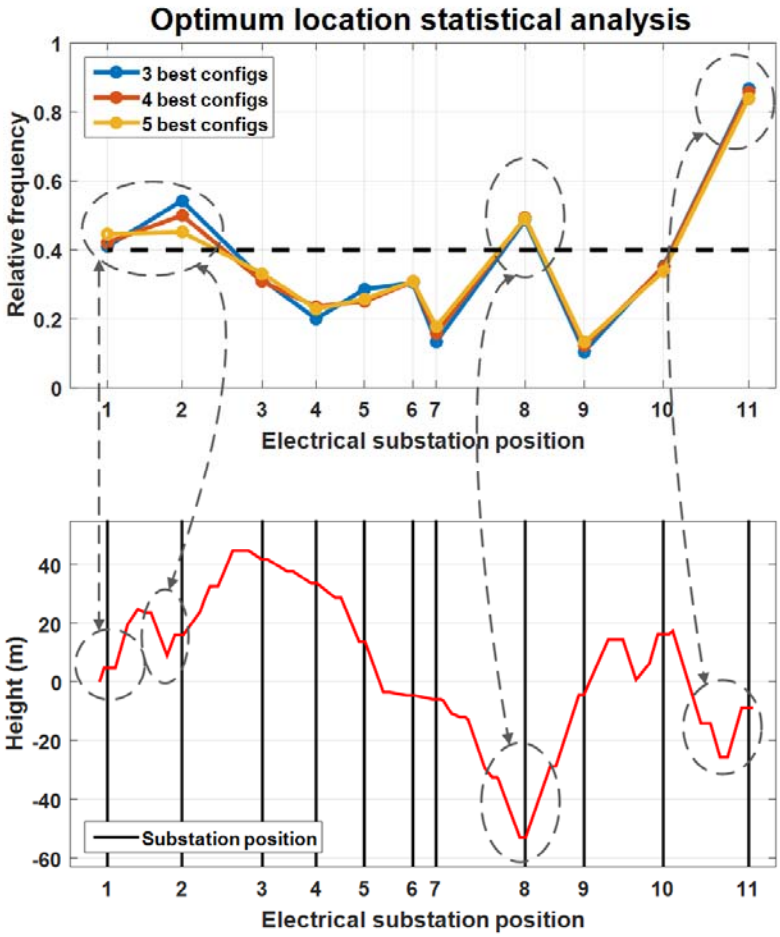

Figure 6-8. Optimum location frequency vs. line height profile.

After this brief inspection of the best infrastructure upgrade configurations, it could be argued that if the line altitude profile is known, it is not essential to perform a comprehensive study to decide where to place RSs. SSs close to passenger stations located at valleys and terminal SSs arise as good candidates. However, when the number of RSs installed in the line rises up, it becomes more difficult to select the best set of locations.

To explore the possibility of trivially finding the global best, let us suppose that an expert in MTS energy concerns decides to install RSs in the four advantageous locations marked in Figure 6-8: SS 1, 2, 8 and 11. In order to make a better comparison, let us suppose that this expert has somehow deduced that the best configuration contains not four but six RSs, and that their ideal size is 2 MW. Consequently, the expert must decide where to install these two extra RSs, and it seems logical to place them in the gap without RSs between SS2 and SS8. Figure 6-9 shows the specific layout of the probable expert choice for the improved infrastructure configuration. The extra RSs have been represented in orange. Then,

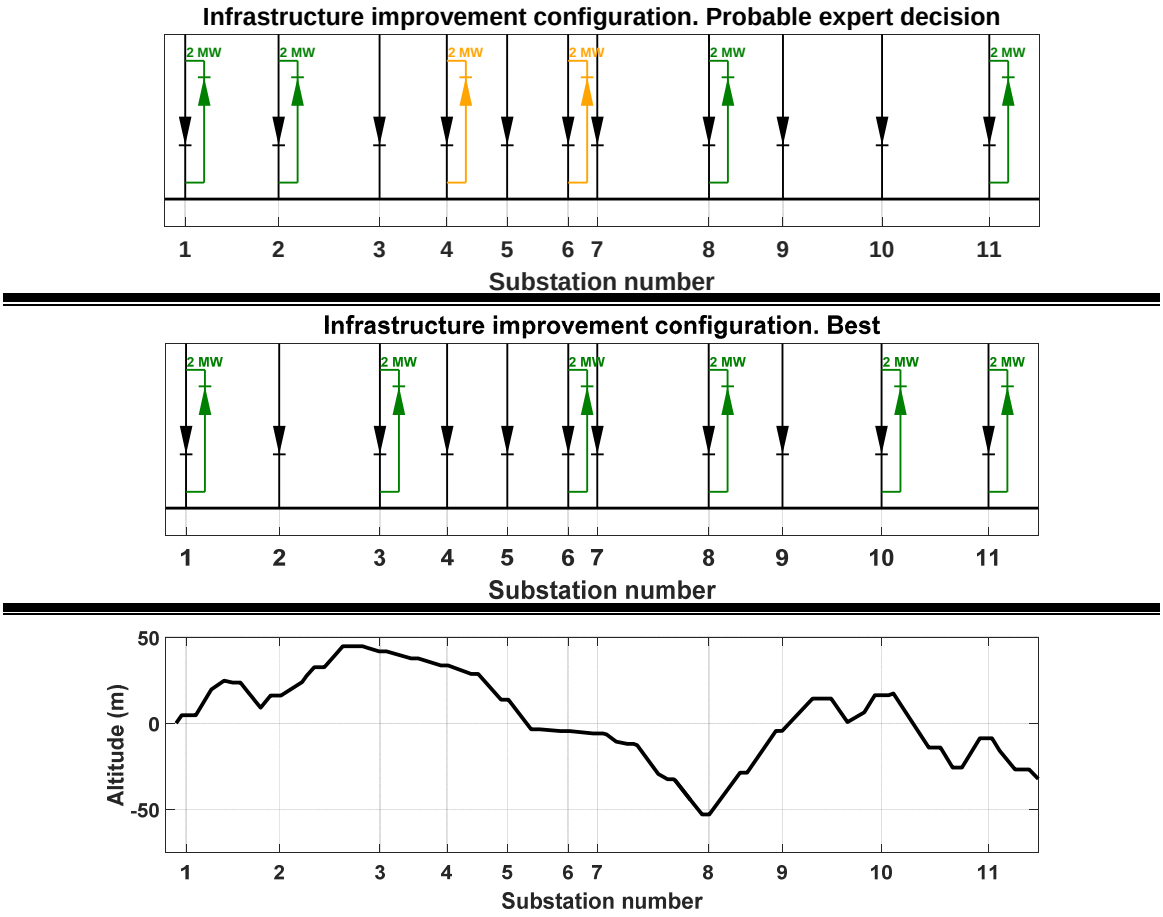

Figure 6-9. Specific RS layout for the best configuration and the probable expert decision.

Figure 6-9 also shows the best configuration when six 2-MW RSs are installed in the system. It may be observed that both configurations are similar, but there are differences. For instance, SS2 is not in the optimum configuration, whereas SS10 – which in principle is not an optimum location regarding the topography– appears in this optimum layout. In the same line, the optimum configuration includes SS3, which has a very low associated frequency.

Figure 6-10 shows a detail of the results of the 462 combinations for six 2-MW RSs in the Energy savings – NPV plane. The results for the best configuration and the probable expert choice have been highlighted. It may be observed that the probable expert decision is the 29th location, with energy savings clearly worse than the best configuration's. The resulting NPV for the expert choice is close to suggest that the investment would be infeasible.

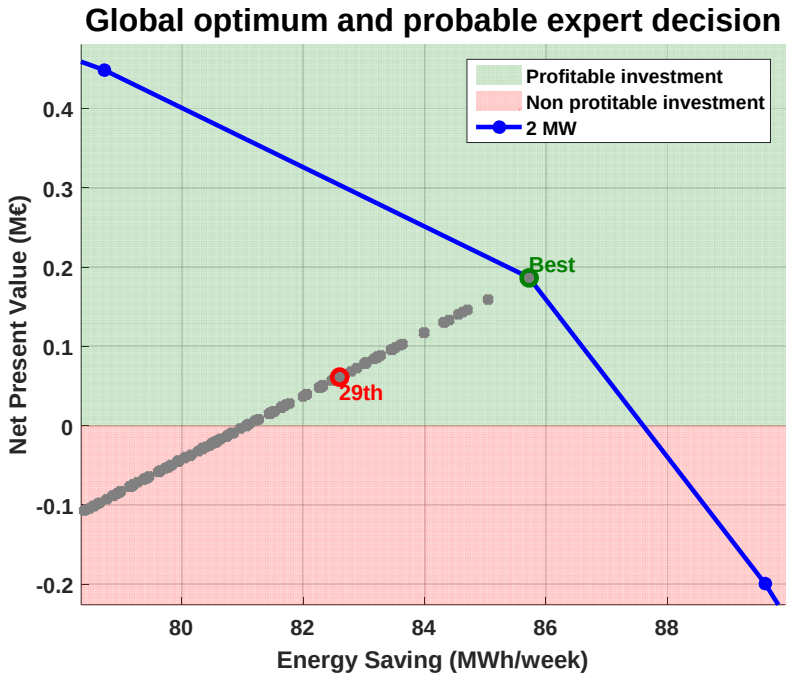

Figure 6-10. NPVs for the best configuration and the probable expert choice. Six 2-MW RSs installed.

To summarise this section, it can be stated that when a single RS is to be installed in a system, it could be easy to (at least) avoid a wrong location. However, in systems where it is worth to install several RSs, the number of possible configurations rises up. If this takes place, the task to identify the best RS configuration by simple inspection of the line may turn out to be impossible. In addition, it has to be taken into account that if RSs sizes or control curves are not forced to be homogeneous, the search space size soars dramatically, and the global optimum identification will consequently become more difficult. This relaxed constraints search space is analysed in Section 6.3.3.

6.3.3. GENERAL HETEROGENEOUS RS SIZE SEARCH SPACE

This section analyses the characteristics of the search space when the homogeneous RS size restriction is relaxed. The general solution set has been broken down into subsets which contain samples with equal number of installed RSs. Figure 6-11 shows the size of each of these subsets, and the total number of possible combinations. The number of elements belonging to each subset is given by (6.18).

$$SubsetSize_2 = \frac{NSS!}{NRS! \cdot (NSS - NRS)!} \cdot {N_{sizes}}^{NRS} \tag{6.18}$$

Where,

- NSS represents the total number of SSs in the line.
- NRS represents the total number of RSs installed.
- N_{sizes} represents the number of discrete RS sizes selected.

The size of the general search space is qualitatively greater than the one with homogeneous RS size. It must be taken into account that the accurate evaluation of

the fitness value for a single RS configuration requires the simulation of around three hours of operation of the system at different traffic densities. Although it depends on the machine where this simulation is carried out, 10 seconds can be taken as a fair value for simulation time required to evaluate the fitness of a single configuration. With this simulation time, the exhaustive simulation of all the possible combinations would take around 230000 days. Hence, it can be stated that the exhaustive simulation of all the possible infrastructure upgrade configurations is unmanageable. The use of a search method like the PSO method presented in this thesis arises as a good solution to find the best RS configuration for the system.

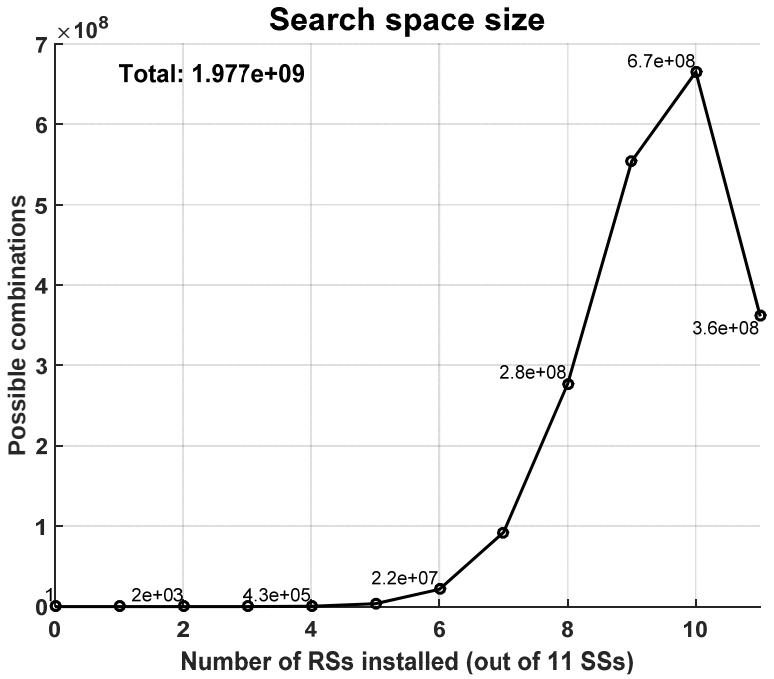

Figure 6-11. Search space size when 6 different reversible converter sizes are allowed.

Regarding the global optimum for this search space, the results shown in Figure 6-6 and Figure 6-10 suggest that it will be in the environment of the best 6 x 2 MW configuration. It is clear that more expensive configurations will generally increase energy savings. However, they will also induce a decreasing effect in the NPV value which will occasionally make it go to the non-profitable region. Consequently, the analysis of this environment oriented to search for the global optimum element requires searching for more expensive infrastructure upgrade configurations until the NPV value goes below zero.

Figure 6-12 shows the results of this search exercise. It consists of upgrading first one 3 MW RS to the best 6 x 2 MW configurations; then two 3 MW RSs, and so on. Each single 6 x 2 MW configuration generates six 5 x 2 MW + 1 x 3 MW configurations, fifteen 4 x 2MW + 2 x 3 MW configurations, etc.

These configurations appear grouped below the 6 x 2 MW case, but some elements lead to greater energy saving results than those of the global optimum in Section 6.3.1. The specific results show that no 4 x 2 MW + 2 x 3 MW configurations present a

positive NPV value. Consequently, the global optimum is in the 5 x 2 MW + 1 x 3 MW curve.

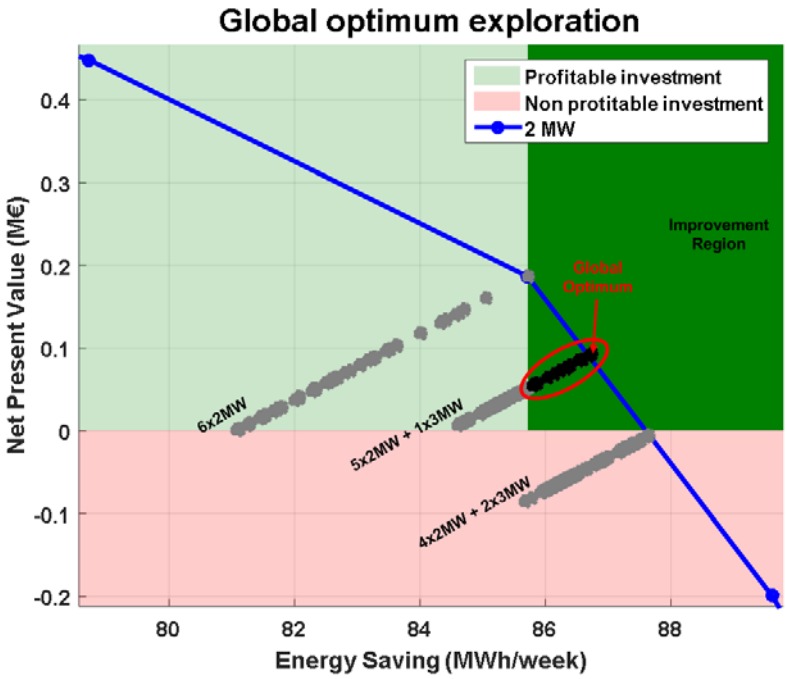

Figure 6-12. Exploration of the global optimum region.

Figure 6-13 presents the particular configuration in the 5 x 2 MW + 1 x 3 MW group that leads to the global optimum. Section 6.4.2 shows a clear tendency of the optimiser to obtain this point from different independent initial conditions. This fact strengthens the validity of regarding the configuration in Figure 6-13 as the global optimum in this complex solution space.

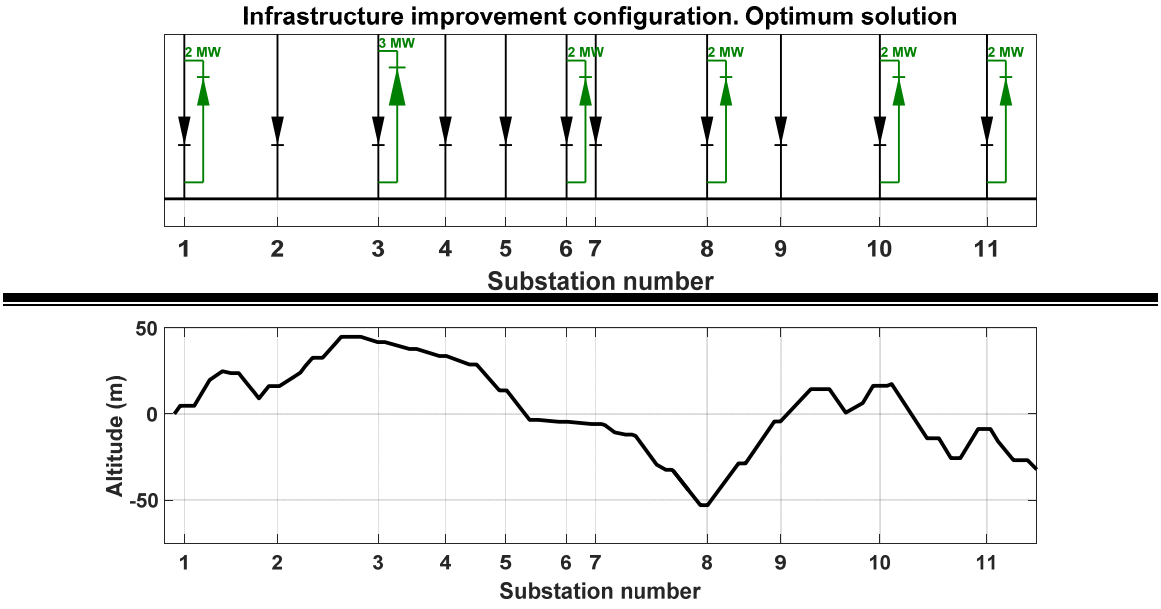

Figure 6-13. Global optimum RS placement configuration.

6.4. OPTIMISATION RESULTS

This section analyses the performance of the optimiser. In addition, this section assesses the correct values for the parameters that affect the behaviour of the PSO method, both in terms of accuracy and convergence.

6.4.1. OPTIMISER PARAMETER SELECTION

Section 6.2.3 has presented the main factors in the PSO method used in the thesis. The set of values for these parameters must be selected in order to have a good trade-off solution between exploration and exploitation of the search space. Given the nature of the PSO algorithm, the first iterations in the optimum search process should be designed to have high speeds, and so to allow the elements to have big movements regardless they move from their own best position, which is still not reliable. For the same reason, from a given iteration, the speed of the elements must be decreased in order to restrict the element to move in the surroundings of the best position, which represents the exploitation of the best region.

The way these parameters affect exploration and exploitation is fairly complex, and therefore, their values have been selected experimentally. It has to be taken into account that although they are not a formal optimum set of parameters, they have proved to converge to a good solution from different initial conditions. For the sake of clarity, the iterations followed to decide these values have been omitted. Table 6-3 collects the results of the PSO algorithm parameter tuning process.

Table 6-3. Optimiser parameter and initial condition selection.

Parameter or initial condition	Selection
Initialisation of elements	Eleven SS objects with random position and size are assigned to each element in the population. Consequently, the infrastructure configuration corresponding to each element may have from no installed RSs to eleven 5 MW RSs with equal probability.
Initial speed of elements. Position	The initial speed for the position of the RS objects ranges, in absolute terms, from 0 to half the length of the line. Then, the sign may be positive or negative with equal probability. Thus, an RS object initially placed in one of the edges of the line might only be displaced until the middle of the line.
Initial speed of elements. Size	The module of the initial speed for the size of the RS objects ranges from 0 to the maximum power. The sign may be positive or negative with equal probability. Consequently, an RS object with zero power may become a 5 MW RS in the following iteration.
Impetus factor (imp_k). *Position.*	Following a linear decrease rule from 0.95 in the initial iteration to 0.9 in the final one. These values have been tuned experimentally to find a good trade off solution between exploration and exploitation of the search space. It must be taken into account that the method can be interrupted before the final programmed iteration is

Parameter or initial condition	Selection
	reached, but this does not affect the impetus factor reduction trend.
Impetus factor (imp_k). Size.	Following a linear decrease rule from 0.97 in the initial iteration to 0.95 in the final one. These values have been tuned experimentally to find a good trade-off solution between exploration and exploitation of the search space. It must be taken into account that the method can be interrupted before the final programmed iteration is reached, but this does not affect the impetus factor reduction trend.
Forget coefficients ($c1_k, c2_k$). *Position and size.*	Uniformly distributed in the interval [0, 1]. The same forget coefficients have shown to perform correctly for both the position and the size of the RS objects.
Cognitive factor ($fcog$). *Position and size.*	0.5. The same cognitive factor has shown to perform correctly for both the position and the size of the RS objects.
Social factor ($fsoc$). *Position and size.*	0.5. The same social factor has shown to perform correctly for both the position and the size of the RS objects.
Population size (P)	100
Maximum number of iterations (I)	100

Regarding the elements' speed, the parameters in Table 6-3 must allow a soft speed reduction trend which leads to high speeds in the first iterations and low speeds in the final iterations in order to find convergence. Figure 6-14 presents the speed results for 10 executions of the method for the general search space (Section 6.3.3). The top side graph represents the position speed results (module) of the elements in the population, whereas the bottom side graph shows the size speed results (module). Both graphs in Figure 6-14 plot the speed of the fastest (maximum) and the slowest (minimum) RS object inside each element; and mean element speeds.

In both speed graphs, it can be observed how the mean and maximum speed values present a unique increasing zone around iteration 5, which is related to the fact that they have both a high impetus and they have moved far away from their particular and global best locations. Then, there is a clear speed reduction trend. In the final iterations, the mean and the minimum speed values become similar, but there are still some elements moving at higher speeds, what represents a marginal exploration of the search space that does not represent any problem regarding the swarm's global best.

These speed results match the regular patterns to be searched in this kind of optimisers, but they still need the support of the accuracy results that will be presented in Section 6.4.2 and, marginally, in the following discussion about the population size.

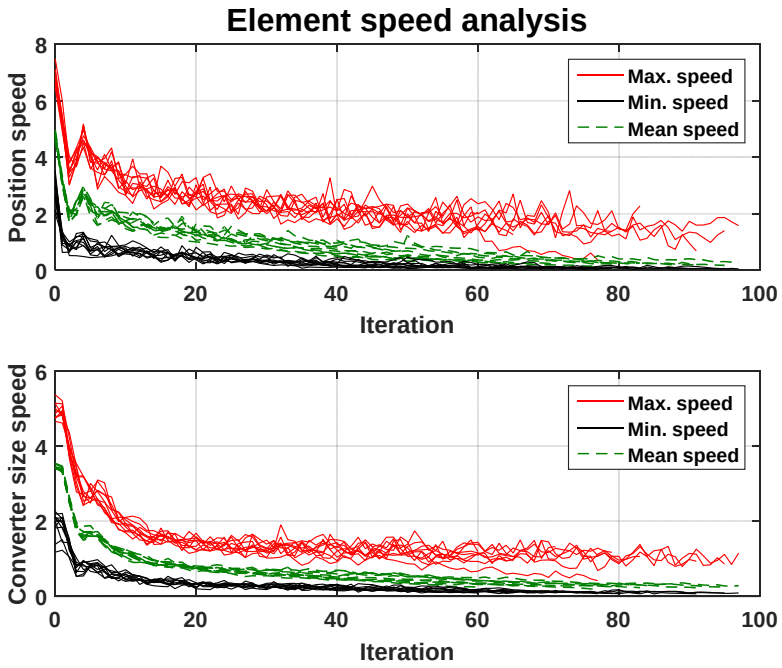

Figure 6-14. Evolution of the population element speeds (10 executions).

After the element speed analysis, it is important to determine the population size. When the search space size is as big as the one in this thesis, it is not enough to tune the parameters that allow the algorithm to have good dynamics. It is also important to generate a big-enough set of elements in the population in order to make it possible to find the global optimum.

In this thesis, the population size has been selected following an experimental approach. This has consisted of increasing the number of elements in the population until a given accuracy standard has been reached. In order to have reliable results, ten executions of the optimiser have been carried out for each population size.

The specific population values have been [25, 50 and 100], and the percentage of executions which fitness value differs less than 5 % with the global optimum fitness value have been used as the accuracy index (good solution frequency).

Figure 6-15 shows the evolution of the good solution frequency with the population size. Only 1 over 10 executions is inside the accepted error band when the population size is made up of 25 elements. It can therefore be stated that this population size is not enough for the PSO to obtain good solutions. When the population size is increased to 50 elements, the accuracy frequency rises to 60 %, which although being higher is still not enough. All the PSO executions lead to accurate enough results when the population size is set to 100 elements. This has consequently been selected as the ideal population size, as presented in Table 6-3.

Finally, a good PSO parameter selection requires the method not to be prematurely stopped. This means that the best fitness must be properly stabilised when the algorithm is stopped. The elements speed results in Figure 6-14 suggest that the

swarm is reasonably stabilised in all the executions, but this has to be further analysed.

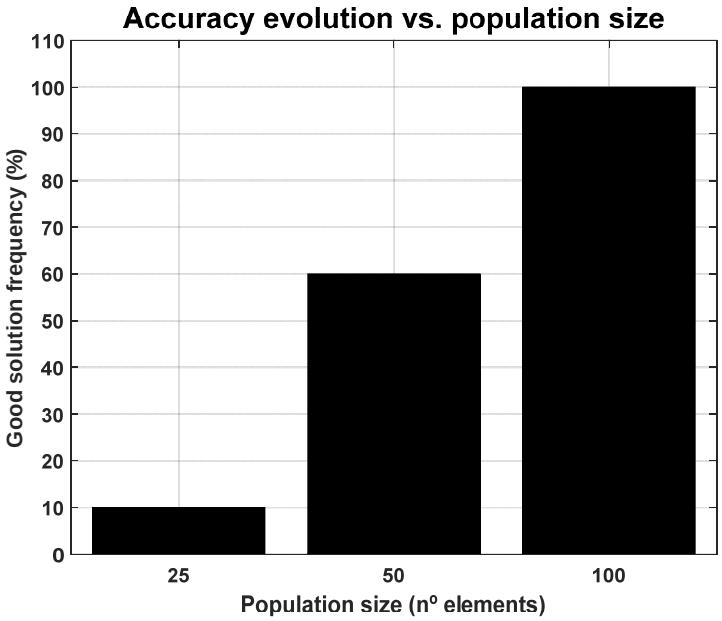

Figure 6-15. Analysis of the population size.

For the optimisation problem tacked in this thesis, the stopping criterion has been set to having 10 iterations with the same best fitness function in a row. Figure 6-16 presents the evolution of the best fitness value for ten executions of the PSO algorithm. The number of iterations has always been lower than 100. Thus, this value (100) has been selected as the maximum number of iterations allowed.

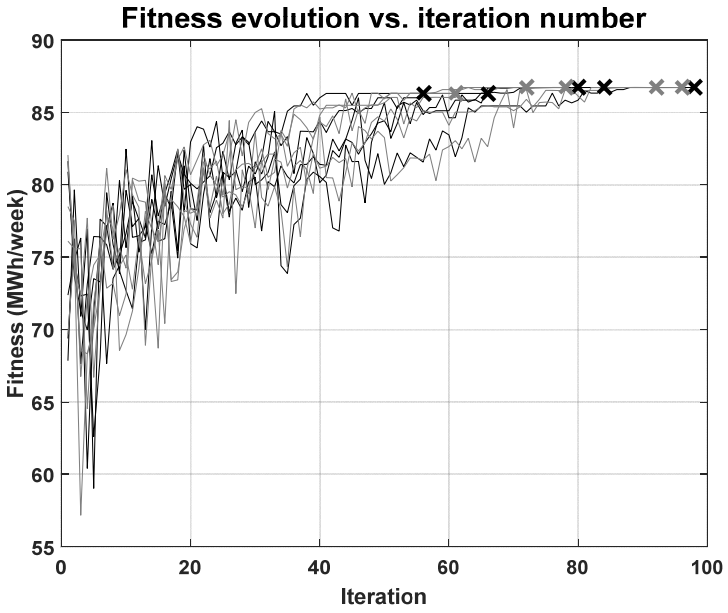

Figure 6-16. Stabilisation of the fitness value (10 executions).

6.4.2. GENERAL SEARCH OPTIMISER RESULTS

This section performs a more formal analysis of the optimiser results, which have been partially shown in the parameter selection discussion in Section 6.4.1.

The fact that the PSO method has been initialised to a random set of element positions and speeds makes it necessary to introduce several executions of the optimiser in the result analysis. This makes it possible to discard the possibility of having good accuracy results produced by a favourable set of initial positions and speeds.

The high complexity of the search problem, presented in Section 6.3.3, has made the population size of the swarm grow. In addition, the complex energy interactions in MTSs have led to the necessity of simulating a long-enough execution time in order to have general energy saving results. The search method execution time is therefore rather high. As a result, since it is not easy to obtain thousands of execution samples, ten executions have been selected as a reasonable number to discard potential malfunctions of the method. The reader is invited to visit Section 6.4.4 to find a deeper analysis of the computational concerns of the PSO method execution.

Figure 6-17 shows the final fitness value and the number of iterations taken to get this result. The optimiser obtains the global optimum solution 7 times over 10 executions. The rest of times, it gets to a sub-optimum solution which represents the second best fitness value in the search space. As it is represented in the figure, the difference between the global optimum and this sub-optimum solution is less than 1% of the total savings. Thus, it can be stated that the results obtained by the optimiser are fairly good.

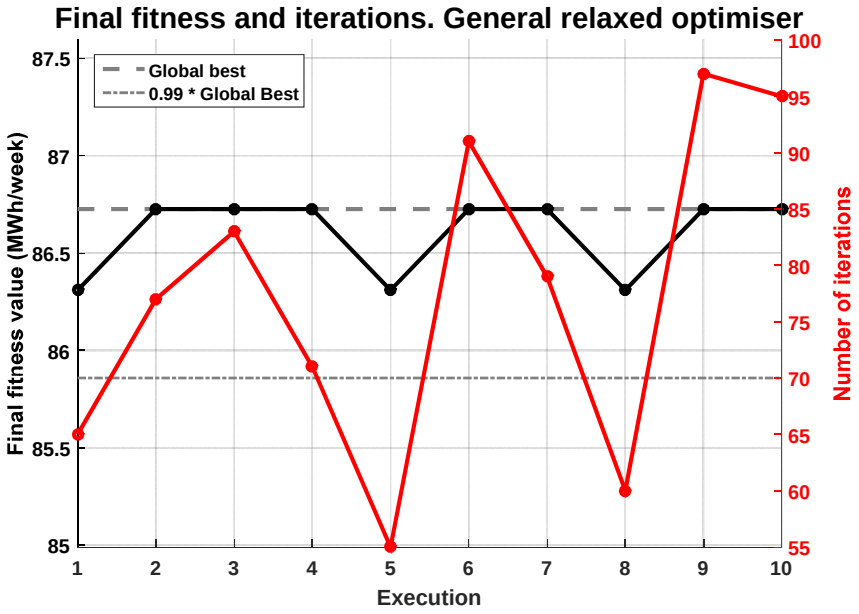

Figure 6-17. Relaxed optimiser results for 10 executions.

Regarding the number of iterations, Figure 6-17 shows that the executions that obtain the sub-optimum solution take less iterations than those that obtain the global optimum. Again, since the alternative solution is as good as the global optimum, this local minimum effect has not been interpreted as a problem.

Figure 6-18 shows these two infrastructure upgrade configurations obtained by the optimiser. Obviously, the global optimum coincides with the configuration presented in Figure 6-13. It has been replicated here to make it more comfortable to compare both solutions. The second best solution is a variation of the third best configuration in the 6 x 2 MW group. This implies that there are configurations that, even being slightly worse than others, have more energy saving potential when the installed power is increased.

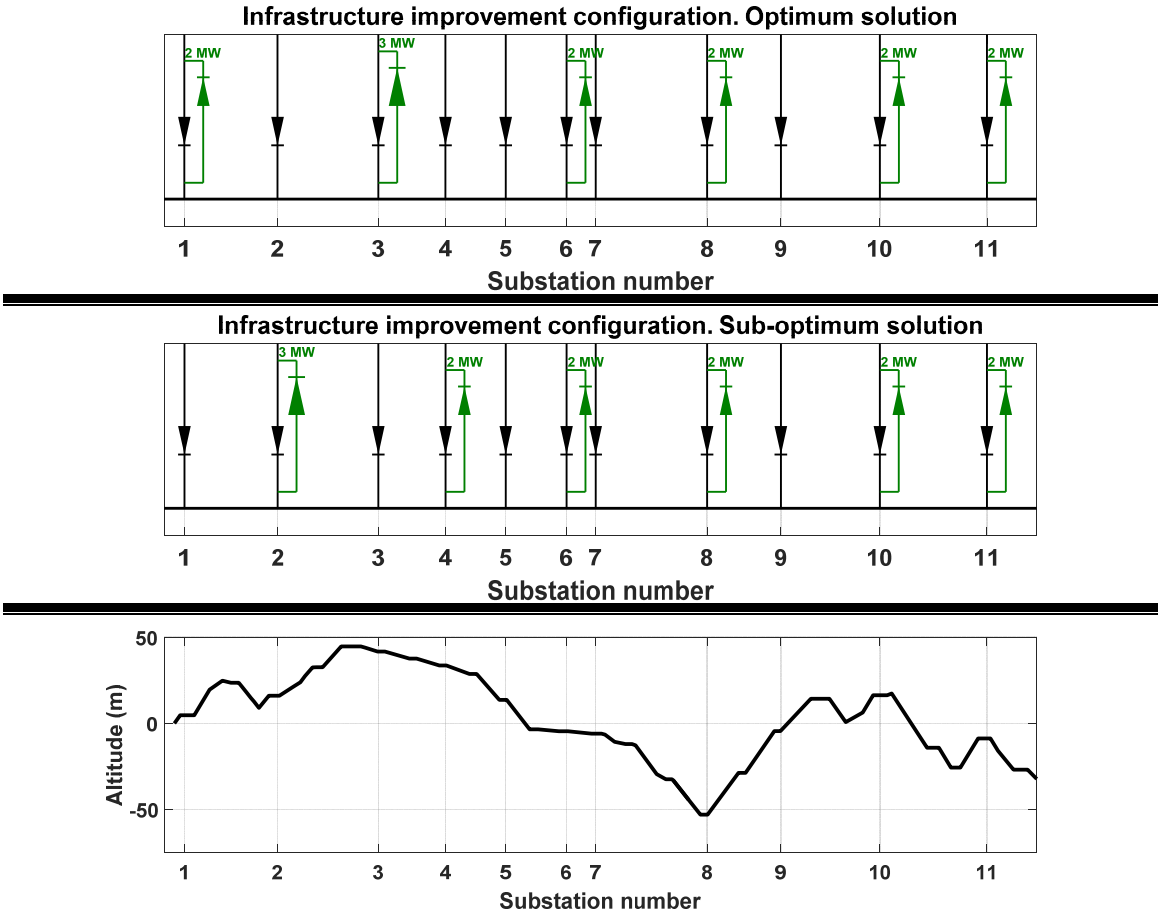

Figure 6-18. Solutions obtained by the optimiser.

6.4.3. TWO-STAGE OPTIMISER APPROACH RESULTS

This alternative two-stage approach has been introduced in Section 6.2.3. It presents the advantage of offering both a solution with a single type of installed RSs and the best possible infrastructure upgrade solution by simply executing the optimiser twice.

Figure 6-19 shows the results of the first stage, where the homogeneous RS size restriction is active. The search space for this stage is the one presented in Section 6.3.1, and therefore, the global optimum is the one presented in Figure 6-7. The

optimiser is executed again ten times in order to prevent the results presented to be affected by particular initial states. The set of PSO parameters used in the executions is the one presented in Table 6-3.

The complexity of the search space is lower than the one for the general search space. Thus, the optimiser reaches the global optimum 100 % of the times. The only remarkable situation is that occurred in the third execution, where the maximum number of iterations is hit. However, the solution proposed by the optimiser is the best possible. The reason for the maximum number of iterations to be hit is a slight movement of the global best element from its position that has taken place a few times during this execution. That could be fixed by tuning the impetus envelope, so a stronger speed reduction is imposed. However, the correct behaviour of the optimiser in the rest of executions suggests that the PSO parameters are well tuned.

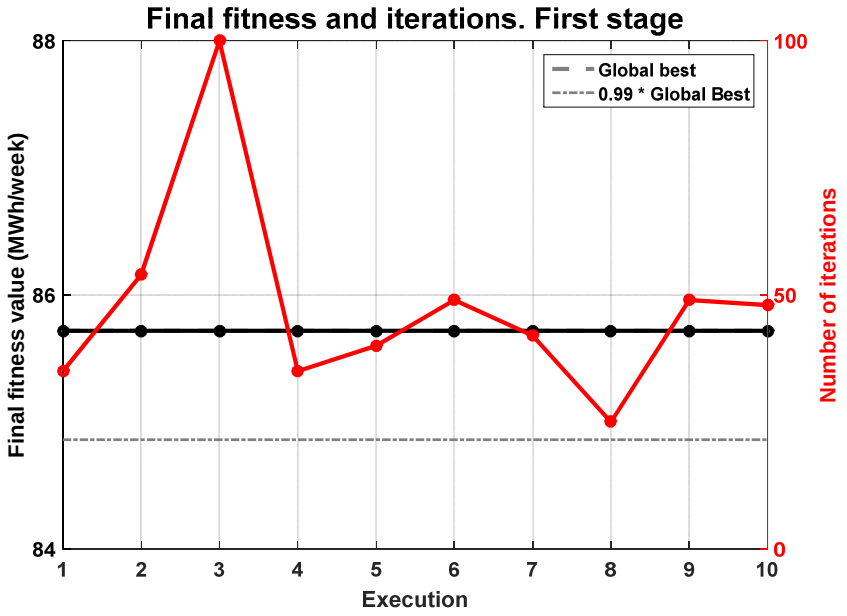

Figure 6-19. Two-stage optimiser results for 10 executions. First stage: a single converter size is allowed.

Figure 6-20 presents the results obtained by the second stage in this approach. The only changes with respect to the rest of executions of the optimiser are: 1) the initial position of the elements in the population is the solution obtained by the first stage; 2) the maximum speed has been reduced both for element positions and sizes. The former has been restricted, in module, to a 10 % of the total length of the line. The latter has been reduced to half the total swing between the maximum and the minimum allowed size.

The optimiser exhibits a good behaviour in moving from the global best in the homogeneous RS size search space to the global best in the general search space. Only one execution over ten fails to converge to the global optimum. The solution is again the sub-optimum solution found by the general optimiser in Section 6.4.2. The optimiser could have been forced to keep the RS location configuration obtained in the first stage in order to prevent it from moving to a sub-optimum solution. However, the fact that the global best in the general search space is a size upgrade of the global

best of the homogeneous RS search space is a particular feature of this problem. The optimiser's ability of moving from this position is essential to guarantee a proper exploration of the search space; regardless it could obtain a sub-optimum solution. In any case, it must be taken into account that the sub-optimum solution 1) is only obtained once over ten executions and; 2) it is nearly as good as the global best configuration, with a difference in the fitness value lower than 1 %.

Regarding the number of iterations used to obtain the solution by this second stage, it is worth to mention that in all the cases it is below half the maximum number of iterations allowed, which may be regarded as a good convergence behaviour.

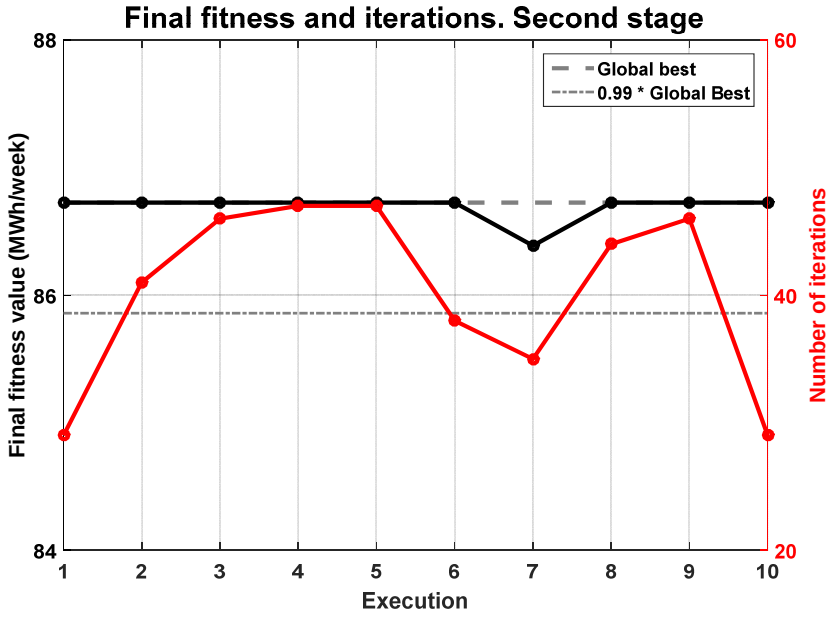

Figure 6-20. Two-stage optimiser results for 10 executions. Second stage: converter size is relaxed.

6.4.4. COMPUTATIONAL CONCERNS

The computational burden of MTS simulators is an important concern. In the case of the optimiser presented in this thesis, the traffic input has been treated in a rigorous way. This has led to an increase in the number of scenarios to be simulated to obtain the energy saving related to each infrastructure configuration.

In order to mitigate this computation time increase, Chapter 5 has presented a traffic scenario compressor that allows reducing the simulation time with a limited effect on the method's accuracy. Figure 6-21 presents the simulation times for 20 elements in the swarm with and without the traffic scenario compressor. Although there is a steady decrease in the simulation time when the compressor is activated, the simulation time for a single element in the swarm still takes around 7.82 seconds.

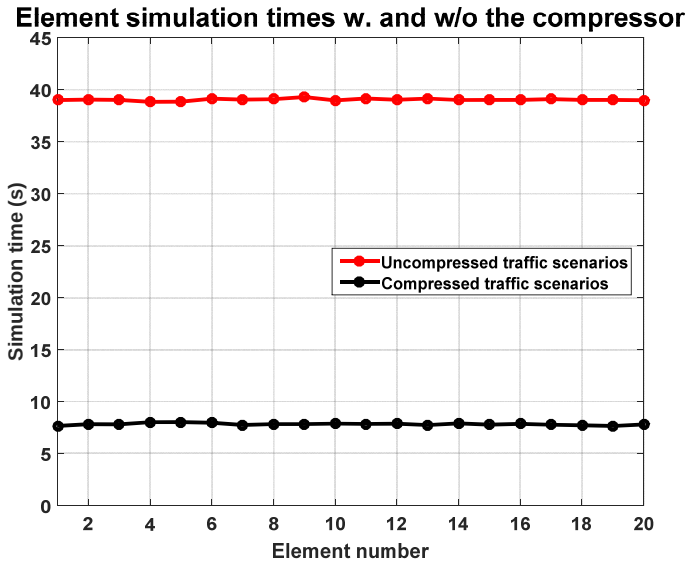

Figure 6-21. Element simulation times with and without traffic compression.

With these figures, the optimiser execution time for 100 elements and 100 iterations would be 0.9 days (7.82 average seconds per element). This does not represent a problem if a single execution of the method is required to obtain the results, since the method is executed off-line. However, the PSO parameter tuning stage requires the method to be run several times to assure a correct trade-off between exploration and exploitation of the search space is attained.

Nowadays, there are several options to reduce this computation time. First, the simulation method has to be refined. The several actions carried out to refine the electrical multi-train simulator used in this thesis have been exposed in Chapter 2. Then, once the simulation procedure has been reviewed, a big time reduction potential may be obtained by parallelising the computation thread.

There are two main parallelisation trends. If a simulation task allows doing it, it may be broken down into several independent sub-tasks. Then: 1) these portions can be sent to different processing units inside a single machine; 2) if there are several machines available in a computer network, the sub-tasks may be sent to different computers in the network. Although both approaches are qualitatively similar, they are substantial quantitative differences between them. The former approach is commonly referred to as parallel computing, whereas the latter approach is known as distributed computing.

The PSO method is rather friendly from a parallelisation standpoint. The only moment where there are some data required is in the moment of updating the elements' positions from iteration to iteration. Then, the simulations required to obtain the fitness values of the elements in the swarm for a given iteration are completely independent.

In this thesis, in the moment of the obtainment of the optimiser results, there was no Matlab parallel computing licence available. Consequently, the parallel computing approach consisted of using different instances of the Matlab application in the same computer. However, this approach is not as fine as the "worker" approach in the

Parallel Computing Toolbox of Matlab. Noticeable interferences have been observed between the Matlab application instances within the same computer. In addition, the memory consumption in this approach is not optimised at all, and the increase in utilised memory as several instances are open is linear.

As a result, since there are several machines in the Institute for Research in Technology (IIT, from its Spanish initials) network with computing power available, distributed computed arose as a good solution to steadily decrease the optimiser simulation time. In the following, these computers in the network with available computing power will be called Distributed Resources (DRs). Figure 6-22 shows the workflow of the code developed to coordinate the obtainment of the PSO element fitness values in an environment with DRs. This code is divided into two programs. The first one is the master program. It is in charge of assigning the elements in the swarm to the available DRs, sending the simulation orders, measuring the simulation times and coordinating the result collection. Its workflow is presented in the left graph in Figure 6-22. Then, the right side graph shows the workflow of the slave programs. For the distributed method to work, each DR is required to have a program running, which interprets the orders of the master program and generates the provisional result files with the appropriate format.

The first task of the DR coordinator is to check how many machines are available to carry out the optimiser execution. This task is performed only once, at the beginning of the optimiser execution. Thus, if additional machines become available during the PSO execution, they are ignored.

Then, the PSO initialisation task is followed by the DR simulation time equaliser. This equaliser distributes the elements in the swarm to the DRs based on their element simulation time. In this first execution of the equaliser, theses simulation times are estimations entered by the user.

After this, the method enters the PSO iteration loop. The simulation instructions are generated and sent to a dedicated shared folder in each DR. Then, the machine where the coordinator is run (local machine, LM) would be in idle state until the DRs finished their simulations. In order to improve the computation performance of the optimiser, a mechanism to treat the LM as a further DR has been implemented. If this is enabled, the LM performs its assigned simulations before the iteration results are harvested.

In its following task, the coordinator enters a polling phase where it harvests the DR iteration results, including the simulation time measurements, when they are available.

Then, the coordinator performs all the tasks required for the PSO method evolution. Mainly, it moves the element positions and sizes, applies restrictions and updates element speeds.

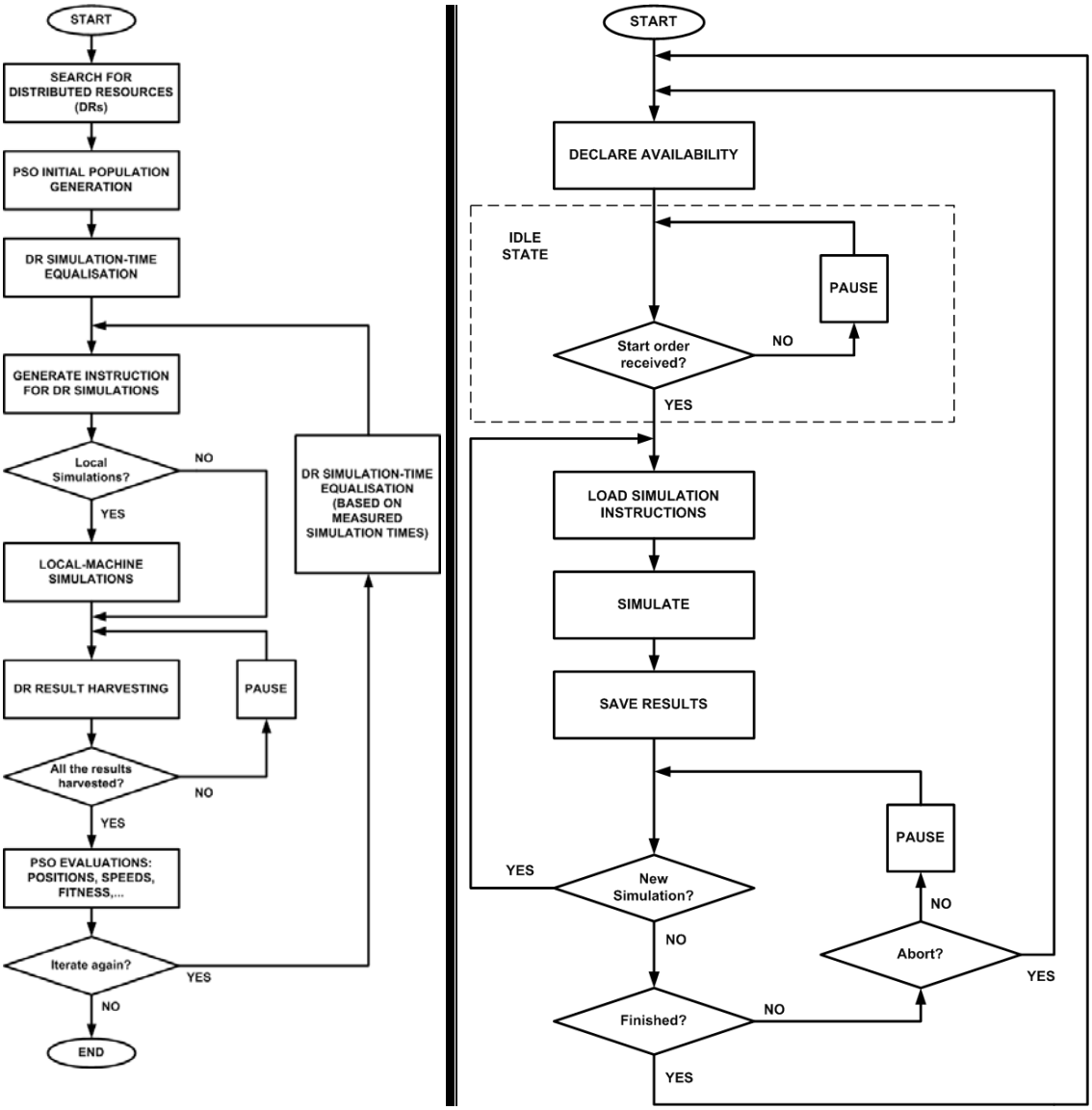

Figure 6-22. Distributed computation workflows.

Before executing the next iteration of the PSO loop, the DR simulation time equaliser is executed again. Now, the time measurements are reliable, and the equaliser makes it possible to assign the swarm elements to the DR so as the iteration time is minimised.

Regarding the code running in each DR, it is a simple program in charge of carrying out the distributed simulations. When it is started, or when the PSO execution is finished, it is in charge of declaring the availability of this DR. Then, it enters an idle state while it waits for the start order.

When this order is received, the slave program reads the simulation instructions, performs the simulations, and saves the results. Then, it waits for the order to perform the simulations of the following iteration unless the last one has already been carried out. In this case, it declares availability and waits for the start order. An early abort mechanism has been implemented to allow the coordinated interruption of the distributed PSO.

Table 6-4 presents the list of machines with available computing power in the network. The first one is the LM where the PSO method has been executed. There is a list of researcher's working stations kindly lent by a group of colleagues, and a server facility of the IIT. Table 6-5 shows the characteristics of each type of machine. In the case of the server, the extended RAM capacity made it possible to run up to 10 Matlab applications in parallel. The simulation time per element in the server machine is increased when more than a single instance of the Matlab application is run at a time. However, this figure is stabilised at around twice the single-running-Matlab simulation time from four Matlab instances on. Taking this result into account, the limiting resource is the RAM memory. The server is able to host 10 DRs at a time.

Table 6-4. List of DRs for the distributed PSO method.

MACHINE NAME	MACHINE TYPE	AVAILABLE RESOURCES
IIT-ALLOPEZ (LM)	Working station	1
quadiit3	Server	10
IIT-AFRODRIGUEZ	Working station	1
IIT-WCARVAJAL	Working station	1
IIT-EPJIMENEZ	Working station	1
IIT-JCROMERO	Working station	1
IIT-ACONCHADO	Working station	1

Table 6-5. Characteristics of the different machine types.

MACHINE TYPE	PROCESSOR	INSTALLED RAM	SYSTEM TYPE
Working station	Intel(R) Core(TM) i7-2600 CPU @ 3.4 GHz	8 GB	64 bits
Server	Intel(R) Xeon(R) CPU E5520 @ 2.27 GHz	32 GB	Microsoft Windows Server 2003 R2 Enterprise x64 Edition

Figure 6-23 shows the simulation times per iteration for the 10 executions of the optimiser in the general search approach. This simulation time is defined as the simulation time of the slowest DR. In 5 over 10 executions there were 16 DRs available (the LM, 10 DRs in the server and 5 additional working stations). In the rest of executions, there was an additional DR. Since the DRs in the server are the slowest ones, and they exhibit approximately the same element simulation time (20 seconds) they become the bottleneck of the simulator. That means that the total iteration time for 17 DRs is the same in practical terms than the one for 16 DRs because in both cases there is a DR in the server with 4 elements assigned. That leads to around 80 seconds of average iteration time for the optimiser.

It can be clearly observed how the iteration time is decreased after the first iteration. This is the effect of the DR simulation time equalisation with real time measurements.

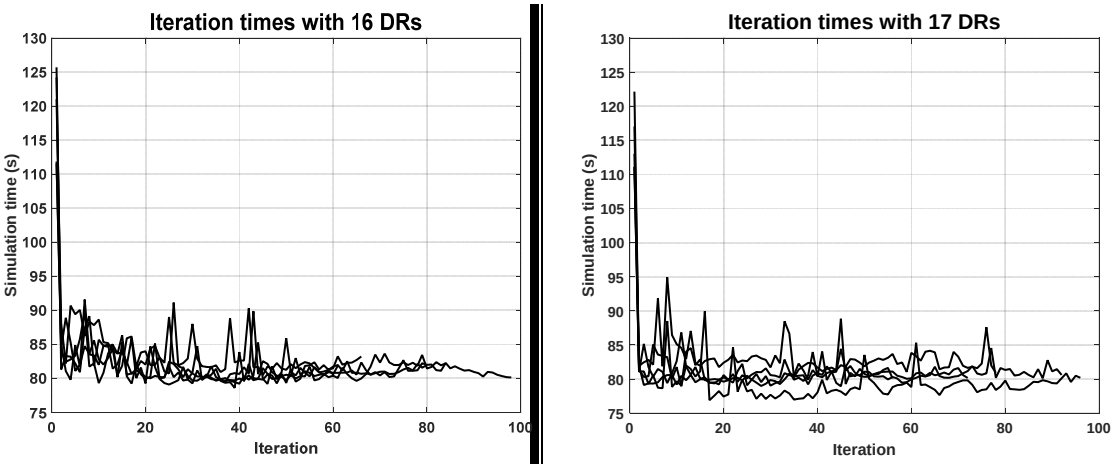

Figure 6-23. Evolution of the iteration simulation time.

These iteration times represent a dramatic reduction in the simulation time per element in comparison with the serial computation case. Figure 6-24 present the average simulation time per element for the distributed PSO method and the percent time reduction with respect to the estimated serial computation time. The simulation time per element for the serial computation time has been set to 7.82, as presented in Figure 6-21.

The average simulation time per element has been dramatically reduced. The upper graph in Figure 6-24 shows an average simulation time around 0.82 seconds. The percent time reduction with respect to the serial computation case is close to 90 %, which represents a qualitative improvement in the optimisation time. The total time for the distributed optimiser swings from 1.29 to 2.23 hours, depending on the moment in which the early stopping criterion is activated. The 2.23-hour long execution corresponds to a case where 97 iterations were made. Therefore, it is close to the worst case execution time for the distributed optimiser.

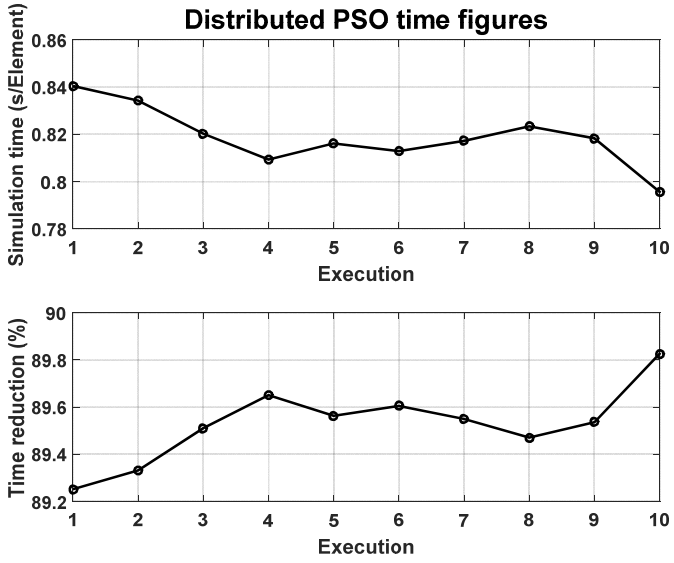

Figure 6-24. Element average simulation time and time reduction.

6.5. SUMMARY, CONCLUSIONS AND CONTRIBUTIONS

This chapter has presented the MTS electrical infrastructure optimiser proposed in this thesis. The optimiser has incorporated all the know-how generated along the thesis: the understanding of the system losses, their relevance and the possible ways to reduce them, the use of representative traffic scenarios which are then compressed to decrease the simulation time, etc.

The compressed representative traffic scenarios for 4-, 7- and 15-minute headways are used as the traffic input to the optimiser. Each one of these headways has a certain weight in hours per week, which is obtained from the headway distributions for working and ferial days. The specific values are 20, 91 and 22 hours per week, respectively. They allow obtaining the annual energy consumption, and therefore the consumption reduction by comparison of two infrastructure configurations.

This chapter has included an economic model of the RS cost in order to evaluate the feasibility of the investment in their installation. This has been obtained as the combination of a fixed term and a variable term which depends on the RS size, in MW. Once this cost is defined, it is compared to the economic savings derived from the reduction in the system energy consumption. The feasibility of the investment is finally obtained by application of the NPV.

With these tools, it is possible to define the optimisation method presented in this chapter, which is devoted to the obtainment of optimal MTS infrastructure improvements. The optimiser is based on the PSO method. Specifically, it defines elements which in turn contain a number of RS objects. The RS objects are defined by their position in the line and their size. These elements, together with some combination rules, endow the optimiser with the ability to find optimum infrastructure configurations regardless the best number of RSs to install.

The optimiser has been defined to work with two search strategies, which are aimed at proving its versatility to adapt to different requirements. The first one is unconstrained, whereas the second one is carried out in two stages, with a first stage where the size of the RSs installed is constrained to be homogeneous.

Prior to the results of the optimiser's search for optimal infrastructures, this chapter has included several studies on the search spaces resulting from the application of infrastructure improvements to the case-study line. It has been proved that the search space for the unconstrained strategy consists in a complex search space where the exhaustive simulation of all the infrastructure possibilities is unfeasible.

In addition, this chapter has proven that the optimum number, size and location of RSs cannot be obtained from the simple inspection of the topography or from the operator experience. Similar RS topologies have shown to lead to notably different energy-saving results.

Regarding the optimiser behaviour, this chapter has presented a PSO parameter tuning analysis which makes it possible to obtain a good trade-off solution between

exploration and exploitation of the search space. The required population size and maximum number of iterations have also been studied and the selected parameters justified.

As a result of the proper PSO parameterisation and the suitability of the method to this problem, the optimiser has exhibited fairly good results. Specifically, for the general search strategy it has proven to obtain the global optimum 70 % of the times it is executed. In the rest of execution, it obtains a sub-optimum configuration which energy-saving result is only 0.5 % lower than the global optimum's.

In the two-stage search strategy, the first stage obtains the global optimum 100 % of times, as expected in this simpler search space. Then, the second stage obtains the global optimum in the general search space 90 % of the times it is executed. The rest of times, it obtains the same sub-optimum infrastructure than the general search strategy.

Finally, this chapter proposes a distributed computation approach to boost the computation-time efficiency of the PSO. The distributed-computation strategy is enhanced by a time equaliser that optimises the share of elements to simulate between the distributed resources, making it possible to adapt to changes in their simulation times measured. The use of 16-17 machines has proven to reduce the optimisation time 89.5 % in average.

The main contributions of this chapter are:

- The presentation of a novel MTS infrastructure optimisation method that applies the PSO algorithm to this problem.
- The demonstration of the difficulties associated to finding optimum –or even good– infrastructure improvements with straightforward methods.
- The PSO parameter tuning. It is important to note that it may be extrapolated to other search methods because it is based on the deep knowledge of the system form the energy-saving perspective. It makes it possible to obtain a good trade-off solution between exploration and exploitation of the search space.
- The presentation of the distributed computation strategy as a tool to boost the optimisation times of population-based search methods.

CHAPTER 7

CONCLUSIONS AND CONTRIBUTIONS

7.1. CONCLUSIONS AND CONTRIBUTIONS

This section collects the main conclusions drawn along the thesis. They are arranged following the main sections in this document.

MTS simulation

The presentation of the general structure of an electrical multi-train simulator has been followed by a review of the modelling approaches in the literature for the most relevant elements in the electrical infrastructure of MTSs. The models of the trains, the supply system, SSs and the current trends to improve MTSs (RSs and ESSs) have been reviewed, putting emphasis on the modelling approaches used in this thesis.

Then, the details of the integration of the infrastructure-element models into the electrical multi-train simulator developed in this thesis are given. The approaches to generate the set of electrical circuits to be solved and, especially, the load flow solver are explained with the aim of making it replicable. The strategy followed to find the correct electrical topology of each snapshot represents a novel method which, in addition, covers a part of the electrical railway simulators that is usually omitted in the literature. This system-state search strategy, which implements the topology changes one by one, has proven to be more powerful than other greedier strategies.

Regarding the performance of the simulator, the load flow solver arises as the main concern due to the especial characteristics of the load flow problem. This problem is highly complex, and it is indeed difficult even to find the solution under certain circumstances. In addition, it is the most demanding part of the simulator from the computational burden standpoint. The performance of the simulator has consequently been analysed in terms of robustness and computation time of the load flow solver.

The former consists in the ability to find the solution of the load flows under different and complex load/regeneration profiles and electrical topologies. It has been tackled by the implementation of a robustness test. This test has proven the difficulties to find the solution of all the snapshots when the complexity of the electrical topology of the system increases.

A set of refinements in the load flow solver to enhance the simulator robustness have been presented. Their effectiveness to make it possible to solve all the snapshots in the robustness test has been proved.

The most time-consuming parts of the code have been identified and some measures to improve their performance have been implemented. The most relevant conclusion is that the generation of compiled code must be regarded as a fundamental task to boost the computation-time performance of a simulator developed in Matlab language. Nevertheless, there are other concerns to be taken into account, being a refined strategy to access and store data in the hard disk the most relevant one.

Summarising, the most relevant contributions in this area are:

- The presentation of a novel strategy to find the electrical structure of DC-railway electrified systems. The combination of a general strategy and a series of mechanisms for difficult snapshots have proven to be highly effective in the solution of complex electrical load flows.
- A review of the computation-time performance of an electrical multi-train simulator developed in Matlab, together with a study on the effectiveness of a series of measurements oriented to improve it.

Case-study and preliminary analysis

The case-study line used to illustrate its derivations is a double-track line with two terminal stations. The reason for this choice is that this is a very general type of line and operation. Relevant Metro systems as Madrid, Barcelona or Paris use only this type of line and operation.

Nevertheless, it must be noted that the application of the studies in this thesis to different MTS lines would be easy to implement. In the case of circular lines, all the analysis presented in this thesis would be directly applicable. In the case of complex-topology lines, the characteristics of the traffic in these different types of line should be determined and modelled.

The analysis of the MTS energy figures have identified two sources of losses which may be reduced by the improvement of the electrical infrastructure: 1) conduction losses and 2) rheostat losses.

The study of the energy figures in the case-study line, which is the typical MTS line subject to exhibit poor energy efficiency figures, has yielded some relevant conclusions. First, it has proved that the application of regenerative braking is a very powerful tool to reduce energy consumption in MTSs. Although they tend to produce an increase of conduction losses, especially for medium and long headways, this effect is clearly dominated by the reduction in the energy consumption. This reduction is derived from the reutilisation of a fraction of the kinetic energy of braking trains. The electrical braking curves used in the case study lead to a large reduction in the energy consumption when regenerative energy is received effectively (short headways). The specific figures approach 40 % with respect to the case without regenerative braking in favourable headways, and the worst-case relative reduction is greater than 25 %.

Regarding conduction losses, it has been observed a slight tendency to decrease for long headways in kWh/train-km. When these are the only source of system losses (no regenerative braking is applied), the system exhibits a consequent reduction in the consumption per train and kilometre for long headways due to the decrease in the average line currents.

Then, the analysis of rheostat losses has shown that they are comparable to the conduction losses in kWh/train-km even for short headways. Then, for medium and long headways, they become clearly dominant both in relative and absolute terms. Indeed, the absolute rheostat-loss analysis (kWh/h) has not yielded any clear increase or decrease trends with the headway. This, together with the steady reduction in the regenerated energy for long headways leads to a continuous increase in the relative rheostat-loss figures with the headway. As a result, the trend in the energy consumption vs. headway when regenerative braking is used is the opposite one: the consumption per train and kilometre is lower for short headways.

The slow conduction-loss increase when large amounts of regenerative energy are injected in the system leads to a high correlation between the system receptivity to regenerative braking and the energy consumption. The linear regression of the receptivity-consumption scatter plot suggests that a 0.1 increase in receptivity would be translated in 1.16 kWh/train-km reduction, which represents 4.3 % of the total train energy. Thus, this implies that it makes full sense to apply techniques which allow improving the system receptivity to regenerative braking.

The mechanisms to increase receptivity (reduce rheostat losses) have been reviewed and classified. They are mainly based on the absorption of the regenerative energy surpluses that leads to rheostat losses. Direct and indirect mechanisms have been observed. In addition, the thesis has identified active SSs as elements which electrically decouple the system from the rheostat-reduction perspective, i.e., from a given RS or ESS location, it is not possible to effectively reduce rheostat losses that take place from an active SS on.

The review of the techniques to improve the MTS infrastructure from an energy-saving perspective makes it possible to divide them into low- and high-investment techniques.

Within the former, this thesis proposes: 1) the electrical segment connection, which is currently implemented in nearly all the DC MTSs, 2) the SS no-load voltage tuning, and 3) the SS shutdown, which is being currently implemented in certain MTSs with promising results.

The SS no-load voltage tuning has been identified as a relevant technique which is not thoroughly covered in the literature, and thus a dedicated study has been included in the thesis. This study uses a conservative no-load voltage scheme as reference, which consists of setting this parameter to a high level in order to prevent protection triggering events from taking place. It has been proved that it is possible to obtain 4.25 % energy consumption reduction with respect to this conservative approach. Then, for the cases where the infrastructure allows performing SS no-load voltage changes during the operation day, a variable no-load voltage scheme has been proposed. This makes it possible to adapt this parameter to the particularities of peak and off-peak operations, which yield 5.25 % reduction with respect to the same reference.

Within the high-investment techniques, the following strategies have been reviewed: 1) the electrification voltage level increase, 2) the conductor impedance decrease, 3) the installation of RSs, 4) the installation of ESSs, and 5) other techniques.

As a prove of the potential of increasing the electrification voltage level, the energy study vs. the headway previously carried out for 600 volts has been replicated. The results have proven that the effects are notable not only on the reduction of the conduction losses, but also on the increase of receptivity. The latter is derived from the increase of the voltage gap available for energy exchanges between trains, which also allows the no-load voltage tuning to yield net energy benefits. The conclusion is that, in general, the electrification voltage level should be set to the maximum possible during the MTS design stage.

Within the rest of techniques, it has been observed in the literature review that the inclusion of RSs appears as the most convenient technique nowadays to improve MTS electrical infrastructures. For this reason, it has been selected as the key technique in this thesis.

Summarising, the most relevant contributions from these studies are:

- The comprehensive review of the MTS energy efficiency problem, systematically assessing the relevance of rheostat losses with respect to conduction losses.
- The rheostat-loss reduction mechanisms frame, together with the identification of electrical interferences is a novel approach.
- The no-load voltage study, including the variable no-load voltage scheme. This is a novel scheme proposed in the frame of this thesis.
- The specific figures of the potential savings related with regenerative braking for a particular system as the case-study line. Although there are a number of studies

obtaining similar conclusions, the addition of a new significant case study, which may be compared with the rest of cases, is a relevant result.

The traffic in MTSs

In order to motivate the necessity of refining the traffic approach in MTS studies, it has been proven that the usual traffic modelling approach with a single scenario per headway does not cover the complex energy interactions between the trains in an MTS. Specifically, the receptivity figures obtained with this approach are far away from the average receptivity values. Thus, the energy-saving results obtained with the single traffic approach are not similar to those obtained with other traffic scenarios which are as probable to take place in the actual operation of the system as it is. This has been proven by comparison with another traffic scenario selected at random.

To cope with this problem, this thesis develops a detailed traffic model, which is able to represent the recurrent energy exchanges between trains in the case-study line. Under the operation scheme in this thesis, the most relevant traffic variables in double-track lines with two terminals have been identified to be: 1) dwell times at passenger stations, and 2) the time shift between train departure times at terminal stations. The former have been proven in the literature to follow a log-normal probability distribution, whereas it is reasonable to make the latter follow a uniform probability distribution.

The complex energy interactions between trains have been taken into account by the generation of a large number of traffic scenarios, obtained with different samples of the selected traffic variables. This yields a traffic space which consists in a large set of traffic scenarios. The critical mass of traffic scenarios required to represent the traffic in the case-study line has been proven to be around 300 samples. Therefore, three 500-sample traffic spaces have been generated for the different operation headways in the case-study line: peak-hour (4 minutes), off-peak-hour (7 minutes), and sparse traffic (15 minutes).

The mean energy-savings obtained with the whole traffic space have been considered to represent the actual savings that an MTS operator would obtain from the installation of infrastructure improvement techniques. Consequently, if a subset of the traffic space is selected to represent the traffic, its mean savings must be close to the whole-set mean values.

It has been proven that if the traffic representative scenarios are selected at random within the whole traffic space, the required size of the resulting traffic-scenario set would equal 300 samples (more than 29 hours for the 7-minute headway). This size is too large in practical terms.

To overcome this problem, a novel method to reduce the size of the selected set of representative scenarios has been developed. This method is based on the fact that the energy savings derived from improvements of the electrical infrastructure are inextricably linked to the reduction of rheostat losses. Thus, it has been concluded

that a proper representation of the traffic must be achieved by a proper characterisation of the amount and location of rheostat losses.

With this basement, two functions that process the rheostat losses to represent the possibility of reducing them from each location in the line have been proposed: 1) the SFR, and 2) the EBFR function.

The latter, which is inspired on the three main rheostat reduction mechanisms defined in Chapter 3, has proven to yield figures which are highly correlated with energy savings for all the locations in the case-study line where it is possible to install RSs. Specifically, the correlation between the EBFR function and energy-savings in the single RS test is greater than 0.9 for all the 11 RS locations in the case-study line.

Consequently, the thesis proposes to obtain reduced-size sets of representative scenarios which are able to represent the energy interactions in the line by imposing their average EBFR values to be close to the whole-traffic-space average EBFR values. This must be fulfilled by all the available RS locations in order not to distort the energy-saving results obtained.

It has been proven that this approach makes it possible to obtain highly accurate energy-saving results both for simple (single RS test) and complex (multiple RS test) infrastructure improvement topologies, with relative errors below 5 %. It has also been observed that the usual single traffic approach in the literature is not able to obtain accurate energy-saving results, exhibiting worst-case relative errors close to 70 %.

Three sets of representative scenarios have been selected. These sets will be used as the traffic input for the MTS infrastructure optimiser developed in this thesis. The specific sizes for these sets are: 18 traffic scenarios for the 4-minute headway, 9 for the 7-minute headway, and 3 for the 15-minute one. These sizes lead to 72, 63 and 45 minutes of operation, respectively. Therefore, larger times are required for these headways where the interactions between trains are more complex (larger number of trains).

Summarising, the most relevant contributions in this section are:

- The demonstration that the usual over-simplified traffic modelling approach in the literature (one single scenario per headway) is not detailed enough to represent the complex energy interactions between trains in MTSs.
- The development of a traffic modelling approach for MTS design and improvement studies which includes the most relevant traffic variables.
- The demonstration of the high correlation between rheostat-loss reduction and energy savings.
- The method to characterise the traffic spaces, based on the rheostat-loss reduction mechanisms defined in Chapter 3. The EBFR function also represents a contribution of this thesis aimed to improve the accuracy of MTS design and infrastructure studies without a large increase in the simulation time.

- The method to select a reduce-size set of representative traffic scenarios, which are able to represent with high accuracy the complex energy interactions between trains in MTSs.

Traffic-scenario compression

The review of the rheostat reduction mechanisms has suggested that the obtainment of accurate energy-saving results must be attained by a proper representation of the amount of rheostat losses, their location in the line and the voltage of the RS locations in the system prior to the introduction of improvements.

Taking this into account, this thesis proposes a novel traffic-scenario compression method which obtains an equivalent traffic scenario with a reduced number of snapshots, thus reducing the simulation time. The compressor is performed in two steps: 1) a clustering stage which groups similar snapshots, and 2) a stage in charge of searching for the specific sets of train positions and powers to be simulated.

The compressed traffic-scenarios have proven to lead to a notable increase in the energy-saving result accuracy with respect to the subsampling method. Whereas the subsampling method is out of a 5 % relative-error band for 67 % compression ratio, the proposed compressor is able to obtain accurate results with 80 % compression ratio.

This compression ratio has been proven to be applicable to all the traffic scenarios selected in Chapter 4, for 4-, 7- and 15-minute headways. The accuracy results are good both with respect to the uncompressed representative-scenario average savings and to the whole-traffic-space savings.

In addition, the compressor has exhibited high accuracy values both for the single and multiple RS tests. For this latter test, less than 4 % of the configurations exhibit relative errors out of the 5 % error band, with only 6.74 % worst-case error. It must be noted that this represents a qualitative increase in the energy-saving result accuracy compared to the one obtained with the traffic approach normally used in the literature.

The main contributions drawn from the scenario compressor studies are:

- The proposal of a novel method to reduce the simulation time required to obtain accurate MTS energy figures. It must be noted that the combination of the compressor and the representative traffic scenario selection represents a qualitative improvement in the energy-saving result accuracy with a limited increase in the associated simulation time. Thus, this contribution will make it possible to implement more complex searches for optimal MTS infrastructure configurations for the same simulation time, increasing the confidence in the results obtained.
- The review of the connections between the electrical variables in MTSs and energy savings, which has led to proposing rheostat-loss position and amount and SS voltage as the key variables to reduce the number of snapshots to be simulated.

- The use of the subsampling method as a reference to assess the goodness of the compression method has made it possible to conclude that the sampling time in energy-saving studies should not be greater than 2 seconds.

MTS infrastructure optimiser

The compressed representative traffic scenarios for 4-, 7- and 15-minute headways are used as the traffic input to the optimiser. Each one of these headways has a certain weight in hours per week, which is obtained from the headway distributions for working and ferial days. The specific values are 20, 91 and 22 hours per week, respectively. They allow obtaining the annual energy consumption, and therefore the consumption reduction by comparison of two infrastructure configurations.

The optimiser includes an economic model of the RS cost in order to evaluate the feasibility of the investment in their installation. This has been obtained as the combination of a fixed term and a variable term which depends on the RS size, in MW. Once this cost is defined, it is compared to the economic savings derived from the reduction in the system energy consumption. The feasibility of the investment is finally obtained by application of the NPV.

With these tools, it is possible to define the optimisation method presented in this thesis, which is devoted to the obtainment of optimal MTS infrastructure improvements. The optimiser is based on the PSO method. Specifically, it defines elements which in turn contain a number of RS objects. The RS objects are defined by their position in the line and their size. These elements, together with some combination rules, endow the optimiser with the ability to find optimum infrastructure configurations regardless the best number of RSs to install.

The optimiser has been defined to work with two search strategies, which are aimed at proving its versatility to adapt to different requirements. The first one is unconstrained, whereas the second one is carried out in two stages, with a first stage where the size of the RSs installed is constrained to be homogeneous.

Prior to the results of the optimiser's search for optimal infrastructures, the thesis has included several studies on the search spaces resulting from the application of infrastructure improvements to the case-study line. It has been proved that the search space for the unconstrained strategy consists in a complex search space where the exhaustive simulation of all the infrastructure possibilities is unfeasible.

In addition, this thesis has proven that the optimum number, size and location of RSs cannot be obtained from the simple inspection of the topography or from the operator experience. Similar RS topologies have shown to lead to notably different energy-saving results.

Regarding the optimiser behaviour, this thesis has presented a PSO parameter tuning analysis which makes it possible to obtain a good trade-off solution between exploration and exploitation of the search space. The required population size and maximum number of iterations have also been studied and the selected parameters justified.

As a result of the proper PSO parameterisation and the suitability of the method to this problem, the optimiser has exhibited fairly good results. Specifically, for the general search strategy it has proven to obtain the global optimum 70 % of the times it is executed. In the rest of execution, it obtains a sub-optimum configuration which energy-saving result is only 0.5 % lower than the global optimum's.

In the two-stage search strategy, the first stage obtains the global optimum 100 % of times, as expected in this simpler search space. Then, the second stage obtains the global optimum in the general search space 90 % of the times it is executed. The rest of times, it obtains the same sub-optimum infrastructure than the general search strategy.

Finally, this thesis proposes a distributed computation approach to boost the computation-time efficiency of the PSO. The distributed-computation strategy is enhanced by a time equaliser that optimises the share of elements to simulate between the distributed resources, making it possible to adapt to changes in their simulation times measured. The use of 16-17 machines has proven to reduce the optimisation time 89.5 % in average.

The main contributions in the MTS electrical optimisation area are:

- The presentation of a novel MTS infrastructure optimisation method that applies the PSO algorithm to this problem.
- The demonstration of the difficulties associated to finding optimum –or even good– infrastructure improvements with straightforward methods.
- The PSO parameter tuning. It is important to note that it may be extrapolated to other search methods because it is based on the deep knowledge of the system form the energy-saving perspective. It makes it possible to obtain a good trade-off solution between exploration and exploitation of the search space.
- The presentation of the distributed computation strategy as a tool to boost the optimisation times of population-based search methods.

7.2. PUBLICATIONS

The studies carried out in the frame of this thesis have yielded a series of publications in Journals and Conferences. Specifically:

JCR Journals

LÓPEZ-LÓPEZ, A.J., PECHARROMÁN, R.R., FERNÁNDEZ-CARDADOR, A. and CUCALA, A.P., [Under review]. Improving the traffic model to be used in the optimisation of mass transit system electrical infrastructure. *International Journal of Electrical Power & Energy Systems*.

Falvo, M.C., Sbordone, D., Fernández-Cardador, A., Cucala, A.P., Pecharromán, R.R., López-López, A.J. 2014. Energy savings in metro-transit systems: a comparison between operational Italian and Spanish lines. *Proceedings of the Institution of Mechanical Engineers, Part F: Journal of Rail and Rapid Transit*. 230 (2), 345-359.

López-López, A.J., Pecharromán, R.R., Fernández-Cardador, A., Cucala, A.P. 2014. Assessment of energy-saving techniques in direct-current-electrified mass transit systems. *Transportation Research Part C - Emerging Technologies*. 38, 85-100.

Other Journals

Pecharromán, R.R., López-López, A.J., Cucala, A.P., Fernández-Cardador, A. 2014. Riding the rails to DC power efficiency: energy efficiency in dc-electrified metropolitan railways. *IEEE Electrification Magazine*. 2 (3), 32-38.

López-López, A.J., Pecharromán, R.R., Cucala, A.P., Fernández-Cardador, A. 2013. Aprovechamiento de la energía procedente del frenado regenerativo en ferrocarriles metropolitanos. *Anales de Mecánica y Electricidad*. XC (III), 12-18.

Congress presentations

López-López, A.J., Abrahamsson, L., Pecharromán, R.R., Fernández-Cardador, A., Cucala, A.P., Östlund, S., Söder, L., "A variable no-load voltage scheme for improving energy efficiency in DC- electrified mass transit systems", *ASME/IEEE 2014 Joint Rail Conference - JRC 2014*. Colorado Springs, CO, USA, April 2-4, 2014.

López-López, A.J., Pecharromán, R.R., J.A. García Matos, Fernández-Cardador, A., Cucala, A.P., "Optimal deployment of energy storage systems in a DC-electrified railway system", *13th International conference on design and operation in railway engineering 2012 - COMPRAIL 2012*. ISBN: 978-1-84564-616-5, pp. 603-614, New Forest, UK, September 11-13, 2012.

Pilo, E., Jiménez-Octavio, J.R., Pecharromán, R.R., López-López, A.J., "Stochastic traffic generator for Monte Carlo load flow simulation", *15th International Conference on Computational Methods and Experimental Measurements - CMEM 2011*. pp. 659-669, New Forest, UK, 31 May - 02 June, 2011.

López-López, A.J., Pecharromán, R.R., Pilo, E., Cucala, A.P., Fernández-Cardador, A., "Analysis of energy-saving strategies in railway power supply systems", *9th World Congress on Railway Research - WCRR 2011*. Lille, France, 22-26 May, 2011.

Pilo, E., Pecharromán, R.R., López-López, A.J., "Stochastic traffic generator for Montecarlo load flow simulation", *12th International Conference on Computer System Design and Operation in the Railway and other Transit Systems. COMPRAIL 2010*. Beijing, China, 31 August - 02 September, 2010.

Books and book chapters

López-López, A.J., Pecharromán, R.R., García-Matos, J.A., Fernández-Cardador, A., Cucala, A.P., "Optimal deployment of energy storage systems in a DC-electrified railway system", en *Computers in railways XIII. Computer system design and operation in the railway and other transit systems. WIT Transactions on the built environment, 127*. Eds Brebbia, C. A. [et al]. Ed. WIT Press. Southampton, UK, 2012.

Pilo, E., Jiménez-Octavio, J.R., Pecharromán, R.R., López-López, A.J., "Stochastic traffic generator for Monte Carlo load flow simulation", en *Computational methods and experimental measurements XV. WIT Transactions on modelling and simulation, 51*. Eds Carlomagno, G. M.; Brebbia, C. A. Ed. WIT Press. Southampton, UK, 2011.

7.3. FUTURE WORK

This section proposes some recommendations to continue with the studies presented in this thesis. They are arranged following the main sections in this document.

MTS simulation

The main recommendation for the electrical multi-train simulator developed in this thesis is to evaluate the possibility of implementing parallel computing techniques in order to solve several snapshots simultaneously. It is important to note that this technique is clearly applicable when the elements in the system have no memory. In case there are elements with memory (mainly ESSs), i.e., it is necessary to know previous states of the system to solve the current state, parallel computing must be avoided or carefully implemented.

Traffic models

Although the traffic model included in the thesis makes it possible to obtain general conclusion, it could be interesting to include some variants and to perform a series of studies on this concern:

- The inclusion of eco-driving profiles in the traffic model. It would be interesting to study the way in which these speed and power profiles may change the main conclusions obtained with the current approach. This means to study the robustness of the traffic model to changes in the system operation.
- The extension of the traffic model to complex-topology MTSs. This type of line, which are operated following a rigid timetable, and where it is possible to have train services which do not visit all the passenger stations, require some slight modifications of the current traffic model.
- The inclusion of some noise to the speed and power profiles. This means to include perturbed traffic conditions into the traffic input to the MTS optimiser. This task would also require assessing the proportion of the total operation time which is performed in perturbed traffic conditions.

Traffic-scenario compressor

If ESSs are included in the system, the current version of the scenario compressor could lead to some errors in the evaluation of the optimum ESS size. The main reason is that to boost the scenario compression, it is allowed to group snapshots regardless time concerns, i.e., it is not possible to group snapshots which take place in different time instants. Thus, it would be necessary to adapt the compressor to the specific characteristics of ESSs. In particular, it is necessary to impose time continuity in the clustering stage. Although this measure will limit the maximum CR achievable, it is necessary when the charge-discharge processes of ESS are to be optimised.

In addition, it is also possible to improve the compressor, both for RSs and ESSs, by smartly splitting conflictive (impure) clusters. Thus, the accuracy of the compressor could be quantitatively increased by clearly identifying the clusters which have a greater impact on the energy-saving error. The subdivision of only these conflictive clusters would have a limited impact on the final CR.

Optimiser

The main recommendations to improve the MTS infrastructure optimiser are:

- To include dynamic RS control curves in the optimisation process.
- Although the required investment would be difficult to justify, it could be interesting to optimise the location, and size (in this case power and energy size) of ESSs. The inclusion of these devices implies several potential benefits that should be addressed:
    - The possibility to install devices both in traction SSs and in passenger stations, which would allow the operator to implement distributed receptivity-increase strategies.
    - The possibility to reduce the energy bill in case it has terms related to the traction SS peak power, which is decreased when ESSs are installed. In addition, the benefits derived from the improvement of the train-voltage profiles could be assessed.

References

ABRAHAMSSON, L., KJELLQVIST, T. and ÖSTLUND, S., 2012. High-voltage DC-feeder solution for electric railways. *IET Power Electronics,* **5**(9), pp. 1776-1784.

ABRAHAMSSON, L., ÖSTLUND, S., SCHÜTTE, T. and SÖDER, L., 2013. An electromechanical moving load fixed node position and fixed node number railway power supply systems optimization. *Transportation Research, Part C: Emerging Technologies,* **30**, pp. 23-40.

ABRAHAMSSON, L. and SÖDER, L., 2011. Fast Estimation of Relations Between Aggregated Train Power System Data and Traffic Performance. *IEEE Transactions on Vehicular Technology,* **60**(1), pp. 16-29.

AÇIKBAS, S. and SOŸLEMEZ, M.T., 2010. The effects of no-load voltage level of traction power supplies on energy consumption of a mass rail transit system, *IET Conference on Railway Traction Systems (RTS 2010)*, 13-15 April 2010, IET, pp. 1-5.

ARBOLEYA, P., COTO, M., GONZÁLEZ-MORÁN, C. and ARREGUI, R., 2014. On board accumulator model for power flow studies in DC traction networks. *Electric Power Systems Research,* **116**, pp. 266-275.

ARBOLEYA, P., DIAZ, G. and COTO, M., 2012. Unified AC/DC Power Flow for Traction Systems: A New Concept. *IEEE Transactions on Vehicular Technology,* **61**(6), pp. 2421-2430.

ARRILLAGA, J. and WATSON, N.R., 2001. *Computer Modelling of Electrical Power Systems.* Second edn. Chichester, England: John Wiley & Sons, Ltd.

BAE, C.H., 2009. A simulation study of installation locations and capacity of regenerative absorption inverters in DC 1500 V electric railways system. *Simulation Modelling Practice and Theory,* **17**(5), pp. 829-838.

BARINGO, L. and CONEJO, A.J., 2013. Correlated wind-power production and electric load scenarios for investment decisions. *Applied Energy,* **101**, pp. 475-482.

BARRERO, R., MIERLO, J. and TACKOEN, X., 2008. Energy savings in public transport. *IEEE Vehicular Technology Magazine,* **3**(3), pp. 26-36.

BARRERO, R., TACKOEN, X. and VAN MIERLO, J., 2008a. Improving energy efficiency in public transport: stationary supercapacitor based energy storage systems for a metro network, *2008 IEEE Vehicle Power and Propulsion Conference (VPPC)*, 3/5 September 2008a, IEEE, pp. 1-8.

BARRERO, R., TACKOEN, X. and VAN MIERLO, J., 2008b. Quasi-static simulation method for evaluation of energy consumption in hybrid light rail vehicles, *2008 IEEE Vehicle Power and Propulsion Conference (VPPC)*, 3-5 September 2008b, IEEE, pp. 1-7.

BATTISTELLI, L., CICCARELLI, F., LAURIA, D. and PROTO, D., 2009. Optimal design of DC electrified railway stationary storage system, *International Conference on Clean Electrical Power (ICCEP)*, 9-11 June 2009, IEEE, pp. 739-745.

BATTISTELLI, L., FANTAUZZI, M., IANNUZZI, D. and LAURIA, D., 2012. Energy management of electrified mass transit systems with Energy Storage devices, *Power Electronics, Electrical Drives, Automation and Motion (SPEEDAM), 2012 International Symposium on*, 20-22 June 2012, IEEE, pp. 1172-1177.

BIERLAIRE, M., 2015. Simulation and optimization: A short review. *Transportation Research: Part C,* **55**, pp. 4-13.

BOMBARDIER, 2009-last update, FLEXX Eco Bogie. Available: http://www.bombardier.com/en/transportation/products-services/technology-solutions/eco4-technologies/flexx-eco-bogie.html [02/25, 2016].

BRENNA, M. and FOIADELLI, F., 2010. Sensitivity Analysis of the Constructive Parameters for the 2 × 25-kV High-Speed Railway Lines Planning. *IEEE Transactions on Power Delivery,* **25**(3), pp. 1923-1931.

BRUNEKREEF, B. and FORSBERG, B., 2005. Epidemiological evidence of effects of coarse airborne particles on health. *The European respiratory journal : official journal of the European Society for Clinical Respiratory Physiology,* **26**, pp. 309-318.

BRUNEKREEF, B. and HOLGATE, S.T., 2002. Air pollution and health. *The Lancet,* **360**(9341), pp. 1233-1242.

CAF, 2016. *http://www.caf.es/en/ecocaf/nuevas-soluciones/tranvia-acr.php*.

CAI, Y., IRVING, M.R. and CASE, S.H., 1995a. Iterative techniques for the solution of complex DC-rail-traction systems including regenerative braking. *IEE Proceedings-Generation, Transmission and Distribution,* **142**(5), pp. 445-452.

CAI, Y., IRVING, M.R. and CASE, S.H., 1995b. Modelling and numerical solution of multibranched DC rail traction power systems. *IEE Proceedings-Electric Power Applications,* **142**(5), pp. 323-328.

CARVAJAL-CARREÑO, W., CUCALA, A.P. and FERNÁNDEZ-CARDADOR, A., 2014. Optimal design of energy-efficient ATO CBTC driving for metro lines based on NSGA-II with fuzzy parameters. *Engineering Applications of Artificial Intelligence,* **36**, pp. 164-177.

CHANG, C.S., WANG, W., LIEW, A.C. and WEN, F.S., 1998. Bicriterion optimisation for traction substations in mass rapid transit systems using genetic algorithm. *IEE Proceedings - Electric Power Applications,* **145**(1), pp. 49-56.

CHRISTEN, T. and OHLER, C., 2002. Optimizing energy storage devices using Ragone plots. *Journal of Power Sources,* **110**(1), pp. 107-116.

CHUANG, H.J., 2005. Optimisation of inverter placement for mass rapid transit systems by immune algorithm. *IEE Proceedings -- Electric Power Applications,* **152**(1), pp. 61-71.

CHYMERA, M.Z., RENFREW, A.C., BARNES, M. and HOLDEN, J., 2010. Modeling Electrified Transit Systems. *IEEE Transactions on Vehicular Technology,* **59**(6), pp. 2748-2756.

CICCARELLI, F., DEL PIZZO, A. and IANNUZZI, D., 2014. Improvement of Energy Efficiency in Light Railway Vehicles Based on Power Management Control of Wayside Lithium-Ion Capacitor Storage. *IEEE Transactions on Power Electronics,* **29**(1), pp. 275-286.

COTO, M., ARBOLEYA, P. and GONZALEZ-MORAN, C., 2013. Optimization approach to unified AC/DC power flow applied to traction systems with catenary voltage constraints. *International Journal of Electrical Power & Energy Systems,* **53**(0), pp. 434-441.

D'AVANZO, S., IANNUZZI, D., MUROLO, F., RIZZO, R. and TRICOLI, P., 2010. A Sample Application of Supercapacitor Storage Systems for Suburban Transit, *Electrical Systems for Aircraft, Railway and Ship Propulsion (ESARS)*, 19-21 October 2010, IEEE, pp. 1-7.

DE RUS, G. and NOMBELA, G., 2007. Is Investment in High Speed Rail Socially Profitable? *Journal of Transport Economics and Policy,* **41**(1), pp. 3-23.

DEL TORO GARCIA, X., RONCERO-SANCHEZ, P., PARRENO, A. and FELIU, V., 2010. Ultracapacitor-based Storage: Modelling, Power Conversion and Energy Considerations, *International Symposium on Industrial Electronics (ISIE 2010)*, 4-7 July 2010, IEEE, pp. 2493-2498.

DESTRAZ, B., BARRADE, P., RUFER, A. and KLOHR, M., 2007. Study and simulation of the energy balance of an urban transportation network, *European Conference on Power Electronics and Applications*, 2-5 September 2007, IEEE, pp. 1-10.

DOMINGUEZ, M., 2013. *Conducción eficiente de trenes metropolitanos con ATO*, Comillas Pontifical University, Madrid, Spain. In Spanish.

DOMÍNGUEZ, M., FERNÁNDEZ-CARDADOR, A., CUCALA, A.P., GONSALVES, T. and FERNÁNDEZ, A., 2014a. Multi objective particle swarm optimization algorithm for the design of efficient ATO speed profiles in metro lines. *Engineering Applications of Artificial Intelligence,* **29**, pp. 43-53.

DOMINGUEZ, M., FERNANDEZ, A., CUCALA, A.P. and LUKASZEWICZ, P., 2011. Optimal design of metro automatic train operation speed profiles for reducing energy consumption. *Proceedings of the Institution of Mechanical Engineers, Part F (Journal of Rail and Rapid Transit),* **225**, pp. 463-473.

DOMÍNGUEZ, M., FERNÁNDEZ-CARDADOR, A., CUCALA, P. and BLANQUER, J., 2010. Efficient design of ATO speed profiles with on board energy storage devices. *WIT Transactions on The Built Environment,* **114**, pp. 509-520.

DOMÍNGUEZ, M., FERNÁNDEZ-CARDADOR, A., CUCALA, P. and PÉREZ-CAYUELA, L., 2008. Computer-aided design of ATO speed commands according to energy consumption criteria. *WIT Transactions on The Built Environment,* **103**, pp. 183-192.

DOMÍNGUEZ, M., FERNANDEZ-CARDADOR, A., CUCALA, A.P. and PECHARROMAN, R.R., 2012. Energy Savings in Metropolitan Railway Substations Through Regenerative Energy Recovery and Optimal Design of ATO Speed Profiles. *IEEE Transactions on Automation Science and Engineering,* **9**(3), pp. 496-504.

DOMÍNGUEZ, M., FERNÁNDEZ-CARDADOR, A., CUCALA, A.P., GONSALVES, T. and FERNÁNDEZ, A., 2014b. Multi objective particle swarm optimization algorithm for the design of efficient ATO speed profiles in metro lines. *Engineering Applications of Artificial Intelligence,* **29**, pp. 43-53.

EBERHART, R. and SHI, Y., 2001. Particle swarm optimization: developments, applications and resources, *Proceedings of the 2001 Congress on Evolutionary Computation*, 27-30, May 2001, IEEE, pp. 81-86 vol. 1.

EIBEN, A.E. and SHIPPERS, C.A., 1998. On Evolutionary Exploration and Exploitation. *Fundamenta Informaticae,* **35**(1-4), pp. 35-50.

EN 50163, 2004. *European Standard. Railway Applications - Supply voltages of traction systems.*

EN 50388, 2012. *European Standard. Railway Applications - Power supply and rolling stock - Technical criteria for the coordination between power supply (substation) and rolling stock to achieve interoperability.*

FALVO, M.C., LAMEDICA, R., BARTONI, R. and MARANZANO, G., 2011. Energy management in metro-transit systems: An innovative proposal toward an integrated and sustainable urban mobility system including plug-in electric vehicles. *Electric Power Systems Research,* **81**(12), pp. 2127-2138.

FALVO, M.C., SBORDONE, D., FERNÁNDEZ-CARDADOR, A., CUCALA, A.P., PECHARROMÁN, R.R. and LÓPEZ-LÓPEZ, A., 2014. Energy savings in metro-transit systems: A comparison between operational Italian and Spanish lines. *Proceedings of the Institution of Mechanical Engineers, Part F: Journal of Rail and Rapid Transit,* **230**(2), pp. 345-359.

FAZEL, S.S., FIROUZIAN, S. and SHANDIZ, B.B., 2014. Energy-Efficient Emplacement of Reversible DC Traction Power Substations in Urban Rail Transport through Regenerative Energy Recovery. *International Journal of Railway Research,* **1**(2), pp. 11-22.

FERNÁNDEZ-CARDADOR, A. and CUCALA, P., 2010. Energy efficiency in high speed train operation. *European Rail Review,* **4**, pp. 46-50.

FMINCON, 2016-last update, fmincon: Find minimum of constrained nonlinear multivariable function. Available: http://www.mathworks.com/help/optim/ug/fmincon.html [02/25, 2016].

FRANCIS, 2015. *Encyclical Letter Laudato Si' of the Holy Father Francis On Care For Our Common Home.* Vatican Press.

FUNAKI, T., 2010. Evaluating Energy Storage Efficiency by Modeling the Voltage and Temperature Dependency in EDLC Electrical Characteristics. *IEEE Transactions on Power Electronics,* **25**(5), pp. 1231-1239.

GANE, C. and SARSON, T., 1979. *Structured Systems Analysis: Tools and Techniques.* Prentice Hall.

GELMAN, V., 2013. Energy Storage That May Be Too Good to Be True: Comparison Between Wayside Storage and Reversible Thyristor Controlled Rectifiers for Heavy Rail. *Vehicular Technology Magazine, IEEE,* **8**(4), pp. 70-80.

GONZÁLEZ-GIL, A., PALACIN, R., BATTY, P. and POWELL, J.P., 2014. A systems approach to reduce urban rail energy consumption. *Energy Conversion and Management,* **80**, pp. 509-524.

GOODMAN, C.J., SIU, L.K. and HO, T.K., 1998. A review of simulation models for railway systems, *International Conference on Developments in Mass Transit Systems*, 20-23 April 1998, IEEE, pp. 80-85.

GRAINGER, J.J. and STEVENSON, W.D., 1994. *Power system analysis.* McGraw-Hill.

GUNSELMANN, W., 2005. Technologies for increased energy efficiency in railway systems, *2005 IEEE 11th European Conference on Power Electronics and Applications*, 11-14 September 2005, IEEE, pp. 1-10.

HUI-JEN, C., CHAO-SHUN, C., CHIA-HUNG, L. and SHI-HONG, C., 2005. Optimization of inverter placement for mass rapid transit systems using genetic algorithm, *Transmission and Distribution Conference and Exhibition: Asia and Pacific, 2005 IEEE/PES* 2005, pp. 1-6.

IANUZZI, D., CICCARELLI, F. and LAURIA, D., 2012. Stationary ultracapacitors storage device for improving energy saving and voltage profile of light transportation networks. *Transportation Research, Part C: Emerging Technologies,* **21**, pp. 321-337.

IBAIONDO, H. and ROMO, A., 2010. Kinetic energy recovery on railway systems with feedback to the grid, *Power Electronics and Motion Control Conference (EPE/PEMC), 2010 14th International* 2010, pp. T9-94-T9-97.

IPCC, 2014. *Climate Change 2014: Synthesis Report. Contribution of Working Groups I, II and III to the Fifth Assessment Report of the Intergovernmental Panel on Climate Change [Core Writing Team, R.K. Pachauri and L.A. Meyer (eds.)].* IPCC. Geneva, Switzerland: 151 pp.

J. KENNEDY and R. EBERHART, 1995. Particle swarm optimization, *Neural Networks, 1995. Proceedings., IEEE International Conference on* 1995, pp. 1942-1948 vol.4.

KANUNGO, T., MOUNT, D.M., NETANYAHU, N.S., PIATKO, C.D., SILVERMAN, R. and WU, A.Y., 2002. An Efficient k-Means Clustering Algorithm: Analysis and Implementation. *IEEE Transactions on Pattern Analysis & Machine Intelligence,* **24**(7), pp. 881.

KENWORTHY, J., 2013. Decoupling Urban Car Use and Metropolitan GDP Growth. *World Transport Policy and Practice,* **19**(4), pp. 8-21.

KO, H., KOSEKI, T. and MIYATAKE, M., 2005. Numerical Study on Dynamic Programming Applied to Optimization of Running Profile of a Train. *IEEJ Transactions on Industry Applications,* **125**(12), pp. 1084-1092.

KONDO, K., 2010. Recent Energy Saving Technologies on Railway Traction Systems. *IEEJ Transactions on Electrical and Electronic Engineering,* **5**(3), pp. 298-303.

KONISHI, T., MORIMOTO, H., AIHARA, T. and TSUTAKAWA, M., 2010. Fixed Energy Storage Technology Applied for DC Electrified Railway. *IEEJ Transactions on Electrical and Electronic Engineering,* **5**(3), pp. 270-277.

KOSEKI, T., 2010. Technologies for Saving Energy in Railway Operation: General Discussion on Energy Issues Concerning Railway Technology. *IEEJ Transactions on Electrical and Electronic Engineering,* **5**(3), pp. 285-290.

LAFOZ, M., UGENA, D., VAZQUEZ, C., TORAL, F., GARCIA-TABARES, L. and LUCAS, J., 2005. A 200 kVA prototype of kinetic energy storage system based on switched reluctance machine technology, *2005 IEEE 11th European Conference on Power Electronics and Applications*, 11-14 Sept. 2005, IEEE, pp. 1-8.

LATORRE, J.M., CERISOLA, S. and RAMOS, A., 2007. Clustering algorithms for scenario tree reduction: Application to natural hydro inflows. *European Journal of Operational Research,* **181**(3), pp. 1339-1353.

LEE, H.M., OH, S.C., LEE, C.M. and KIM, G.D., 2008. Factory test for development of energy storage system, *2008 International Conference on Control, Automation and Systems (ICCAS)*, 14-17 October 2008, IEEE, pp. 1495-1498.

LEE, H., JUNG, S., CHO, Y., YOON, D. and JANG, G., 2013. Peak power reduction and energy efficiency improvement with the superconducting flywheel energy storage in electric railway system. *Physica C: Superconductivity,* **494**(0), pp. 246-249.

LIN, W. and SHEU, J., 2011. Optimization of Train Regulation and Energy Usage of Metro Lines Using an Adaptive-Optimal-Control Algorithm. *IEEE Transactions on Automation Science & Engineering,* **8**(4), pp. 855-864.

LÓPEZ LÓPEZ, A.J., PECHARROMÁN, R.R., GARCÍA-MATOS, J.A., FERNÁNDEZ-CARDADOR, A. and CUCALA, A.P., 2012. Optimal deployment of energy storage systems in a DC-electrified railway system. *Computers in Railways XIII. WIT Press,* **127**, pp. 603-614.

LÓPEZ-LÓPEZ, ÁJ., PECHARROMÁN, R.R., FERNÁNDEZ-CARDADOR, A. and CUCALA, A.P., 2014. Assessment of energy-saving techniques in direct-current-electrified mass transit systems. *Transportation Research: Part C,* **38**, pp. 85-100.

LÓPEZ-LÓPEZ, ÁJ., ABRAHAMSSON, L., PECHARROMÁN, R.R., FERNÁNDEZ-CARDADOR, A., CUCALA, A.P., ÖSTLUND, S. and SÖDER, L., 2014. A Variable No-Load Voltage

Scheme for Improving Energy Efficiency in DC-Electrified Mass Transit Systems, *ASME-IEEE Joint Rail Conference (JRC)*, April 2-4 2014, ASME-IEEE, pp. 1-7.

LUKASZEWICZ, P., 2001. *Energy Consumption and Running Time for Trains*, Div. Railway Technology. Royal Institute of Technology, Stockholm, Sweden.

MARISCOTTI, A., 2003. Distribution of the Traction Return Current in AC and DC Electric Railway Systems. *IEEE Transactions on Power Delivery,* **18**(4), pp. 1422-1432.

MARISCOTTI, A., POZZOBON, P. and VANTI, M., 2007. Simplified Modeling of 2 × 25-kV AT Railway System for the Solution of Low Frequency and Large-Scale Problems. *IEEE Transactions on Power Delivery,* **22**(1), pp. 296-301.

MARTÍNEZ, I., VITORIANO, B., FERNANDEZ-CARDADOR, A. and CUCALA, A.P., 2007. Statistical dwell time model for metro lines. *WIT Transactions on The Built Environment,* **96**, pp. 1-10.

MELLITT, B., GOODMAN, C.J. and ARTHURTON, R.I.M., 1978. Simulator for studying operational and power-supply conditions in rapid-transit railways. *Proceedings of the Institution of Electrical Engineers,* **125**(4), pp. 298-303.

MILLER, K.A., 2007. Long-term exposure to air pollution and incidence of cardiovascular events in women. *The New England journal of medicine,* **356**, pp. 447-458.

MILLS, N.L., DONALDSON, K., HADOKE, P.W., BOON, N.A., MACNEE, W., CASSEE, F.R., SANDSTROM, T., BLOMBERG, A. and NEWBY, D.E., 2009. Adverse cardiovascular effects of air pollution. *Nat Clin Pract Cardiovasc Med,* **6**(1), pp. 36-44.

MIYATAKE, M. and KO, H., 2007. Numerical analyses of minimum energy operation of multiple trains under DC power feeding circuit, *European Conference on Power Electronics and Applications*, 2-5 September 2007, IEEE, pp. 1-10.

MIYATAKE, M., HAGA, H. and SUZUKI, S., 2009. Optimal speed control of a train with On-board energy storage for minimum energy consumption in catenary free operation, *13th European Conference on Power Electronics and Applications (EPE '09)*, 8-10 September 2009, IEEE, pp. 1-9.

MIYATAKE, M. and KO, H., 2010. Optimization of Train Speed Profile for Minimum Energy Consumption. *IEEJ Transactions on Electrical and Electronic Engineering,* **5**(3), pp. 263-269.

NAGAOKA, N., OUE, H., SADAKIYO, M., MORI, N., AMETANI, A., UMEDA, S. and ISHII, J., 2006. Power compensator using lithium-ion battery for DC railway and its simulation by EMTP, *VTC 2006-Spring.2006 IEEE 63rd Vehicular Technology Conference*, 7-10 May 2006, IEEE, pp. 3021-3025.

NASRI, A., MOGHADAM, M.F. and MOKHTARI, H., 2010. Timetable optimization for maximum usage of regenerative energy of braking in electrical railway systems, *International Symposium on Power Electronics Electrical Drives Automation and Motion (SPEEDAM)*, 14-16 June 2010, IEEE, pp. 1218-1221.

ÖSTLUND, S., 2012. *Electric Railway Traction.* Stockholm, Sweden: Royal Institute of Technology.

PENA-ALCARAZ, M., FERNÁNDEZ-CARDADOR, A., CUCALA, A.P., RAMOS, A. and PECHARROMÁN, R.R., 2012. Optimal underground timetable design based on power flow for maximizing the use of regenerative-braking energy. *Proceedings of the Institution of Mechanical Engineers, Part F: Journal of Rail and Rapid Transit,* **226**(4), pp. 397-408.

PETERSON, E.B., SCHLEICH, J. and DUSCHA, V., 2011. Environmental and economic effects of the Copenhagen pledges and more ambitious emission reduction targets. *Energy Policy,* **39**(6), pp. 3697-3708.

PILO, E., JIMENEZ-OCTAVIO, J., PECHARROMÁN, R.R. and LÓPEZ LÓPEZ, A.J., 2011. Stochastic traffic generator for Montecarlo load flow simulation. *WIT Transactions on Modelling and Simulation,* **51**, pp. 659-11.

PILO, E., ROUCO, L., FERNANDEZ, A. and ABRAHAMSSON, L., 2012. A monovoltage equivalent model of bi-voltage autotransformer-based electrical systems in railways. *IEEE Transactions on Power Delivery,* **27**(2), pp. 699-708.

PILO, E., ROUCO, L., FERNANDEZ, A. and HERNANDEZ-VELILLA, A., 2000. A simulation tool for the design of the electrical supply system of high-speed railway lines, *2000 Power Engineering Society Summer Meeting (Cat. No.00CH37134)*, 16-20 July 2000, IEEE Power Eng. Soc., pp. 1053-1058 vol. 2.

PIRES, C.L., NABETA, S.I. and CARDOSO, J.R., 2009. DC traction load flow including AC distribution network. *IET Electric Power Applications,* **3**(4), pp. 289-297.

PIRES, C.L., NABETA, S.I. and CARDOSO, J.R., 2007. ICCG method applied to solve DC traction load flow including earthing models. *IET Electric Power Applications,* **1**(2), pp. 193-198.

POPE CA, I., 2004. Cardiovascular mortality and long-term exposure to particulate air pollution: epidemiological evidence of general pathophysiological pathways of disease. *Circulation,* **109**, pp. 71-77.

PROFILLIDIS, V.A., 2006. *Railway Management and Engineering.* Third edn. Ashgate Publishing Limited.

RENDERS, J.M. and FLASSE, S.P., 1996. Hybrid methods using genetic algorithms for global optimization. *IEEE Transactions on Systems, Man, and Cybernetics, Part B (Cybernetics),* **26**(2), pp. 243-258.

ROCKSTRÖM, J., STEFFEN, W., NOONE, K., PERSSON, A., CHAPIN, F.S., LAMBIN, E.F., LENTON, T.M., SCHEFFER, M., FOLKE, C., SCHELLNHUBER, H.J., NYKVIST, B., DE WIT, C.A., HUGHES, T., VAN, D.L., RODHE, H., SORLIN, S., SNYDER, P.K., COSTANZA, R., SVEDIN, U., FALKENMARK, M., KARLBERG, L., CORELL, R.W., FABRY, V.J., HANSEN, J., WALKER, B., LIVERMAN, D., RICHARDSON, K., CRUTZEN, P. and FOLEY, J.A., 2009. A safe operating space for humanity. *Nature,* **461**(7263), pp. 472-475.

RUFER, A., HOTELLIER, D. and BARRADE, P., 2004. A supercapacitor-based energy storage substation for voltage compensation in weak transportation networks. *IEEE Transactions on Power Delivery,* **19**(2), pp. 629-636.

SCHAFER, A. and VICTOR, D.G., 2000. The future mobility of the world population. *Transportation Research Part A: Policy and Practice,* **34**(3), pp. 171-205.

SEGUIER, G. and LABRIQUE, F., 1993. *Power Electronic Converters. AC/DC Conversion.* English edn. Springer-Verlag Berlin Heidelberg.

SHARAFI, M. and ELMEKKAWY, T.Y., 2014. Multi-objective optimal design of hybrid renewable energy systems using PSO-simulation based approach. *Renewable Energy,* **68**, pp. 67-79.

SHEU, J. and LIN, W., 2012. Energy-Saving Automatic Train Regulation Using Dual Heuristic Programming. *IEEE Transactions on Vehicular Technology,* **61**(4), pp. 1503-1514.

SICRE, C., CUCALA, P., FERNÁNDEZ-CARDADOR, A., JIMÉNEZ, J.A., RIBERA, I. and SERRANO, A., 2010. A method to optimise train energy consumption combining manual energy efficient driving and scheduling. *WIT Transactions on The Built Environment,* **114**, pp. 549-560.

SICRE, C., CUCALA, A.P., FERNÁNDEZ, A. and LUKASZEWICZ, P., 2012. Modeling and optimizing energy-efficient manual driving on high-speed lines. *IEEJ Transactions on Electrical and Electronic Engineering,* **7**(6), pp. 633-640.

SIEMENS, 2009. *Sitras SES. Energy Storage System for Mass Transit Systems.* available at: https://w3.usa.siemens.com/mobility/us/Documents/en/rail-solutions/railway-electrification/dc-traction-power-supply/sitras-ses2-en.pdf.

SIGRIST, L., EGIDO, I., SÁNCHEZ-ÚBEDA, E.F. and ROUCO, L., 2010. Representative Operating and Contingency Scenarios for the Design of UFLS Schemes. *IEEE Transactions on Power Systems,* **25**(2), pp. 906-913.

SIMS, R., SCHAEFFER, R., CREUTZIG, F., CRUZ-NÚÑEZ, X., D'AGOSTO, M., DIMITRIU, D., FIGUEROA MEZA, M.J., FULTON, L., KOBAYASHI, S., LAH, O., MCKINNON, A., NEWMAN,

P., OUYANG, M., SCHAUER, J.J., SPERLING, D. and TIWARI, G., 2014. Transport. In: O. EDENHOFER, R. PICHS-MADRUGA, Y. SOKONA, E. FARAHANI, S. KADNER, K. SEYBOTH, A. ADLER, I. BAUM, S. BRUNNER, P. EICKEMEIER, B. KRIEMANN, J. SAVOLAINEN, S. SCHLÖMER, C. VON STECHOW, T. ZWICKEL and J.C. MINX, eds, *Climate Change 2014: Mitigation of Climate Change. Contribution of Working Group III to the Fifth Assessment Report of the Intergovernmental Panel on Climate Change.* Cambridge, United Kingdom and New York, NY, USA: Cambridge University Press, pp. 599-670.

SÖDER, L. and AMELIN, M., 2011. Simulation of Electricity Markets. In: L. SÖDER and M. AMELIN, eds, *Efficient Operation and Planning of Power Systems.* Eleventh edn. Stockholm: Royal Institute of Technology. Electric Power Systems, pp. 83-154.

STEFFEN, W., RICHARDSON, K., ROCKSTRÖM, J., CORNELL, S.E., FETZER, I., BENNETT, E.M., BIGGS, R., CARPENTER, S.R., DE VRIES, W., DE WIT, C.A., FOLKE, C., GERTEN, D., HEINKE, J., MACE, G.M., PERSSON, L.M., RAMANATHAN, V., REYERS, B. and SÖRLIN, S., 2015. Planetary boundaries: Guiding human development on a changing planet. *Science,* **347**(6223), pp. 1259855-1-1259855-10.

TAKAGI, R., 2012. Preliminary evaluation of the energy-saving effects of the introduction of superconducting cables in the power feeding network for DC electric railways using the multi-train power network simulator. *IET Electrical Systems in Transportation,* **2**(3), pp. 103-109.

TAKAGI, R., 2010. Energy Saving Techniques for the Power Feeding Network of Electric Railways. *IEEJ Transactions on Electrical and Electronic Engineering,* **5**(3), pp. 312-316.

TALUKDAR, S.N. and KOO, R.L., 1977. The analysis of electrified ground transportation networks. *IEEE Transactions on Power Apparatus and Systems,* **PAS-96**(1), pp. 240-247.

TYLAVSKY, D.J. and TRUTT, F.C., 1983. The Newton-Raphson load flow applied to AC/DC systems with commutation impedance. *IEEE Transactions on Industry Applications,* **IA-19**(6), pp. 940-948.

TZENG, Y.S., WU, R.N. and CHEN, N., 1998. Electric network solutions of DC transit systems with inverting substations. *IEEE Transactions on Vehicular Technology,* **47**(4), pp. 1405-1412.

TZENG, Y.S. and WU, R.N., 1995. A detailed R-L fed bridge converter model for power flow studies in industrial AC/DC power systems. *IEEE Transactions on Industrial Electronics,* **42**(5), pp. 531-538.

UMEDA, S., NOBUHARA, T., NAGAOKA, N. and AMETANI, A., 2011. Field Tests of a Power Storage System with a Li-ion Battery for a DC Railway Feeding System. *Science and Engineering Review of Doshisha University,* **52**(3), pp. 163-170.

UNFCCC, 2015. *United Nations Framework Convention on Climate Change. Adoption of the Paris Agreement.* L.9, Rev.1 edn. Paris: FCCC.

WANG, B., YANG, Z., LIN, F. and ZHAO, W., 2014. An Improved Genetic Algorithm for Optimal Stationary Energy Storage System Locating and Sizing. *Energies,* **7**(10), pp. 6434.

WHO, 2014-last update, Burden of disease from Ambient Air Pollution for 2012. Available: http://www.who.int/phe/health_topics/outdoorair/databases/AAP_BoD_results_March2014.pdf [02/21, 2016].

XIA, H., CHEN, H., YANG, Z., LIN, F. and WANG, B., 2015. Optimal Energy Management, Location and Size for Stationary Energy Storage System in a Metro Line Based on Genetic Algorithm. *Energies,* **8**(10), pp. 11618-11640.

YANG, X., CHEN, A., LI, X., NING, B. and TANG, T., 2015. An energy-efficient scheduling approach to improve the utilization of regenerative energy for metro systems. *Transportation Research: Part C,* **57**, pp. 13-29.

YU, J.G. and GOODMAN, C.J., 1990. Modelling of rail potential rise and leakage current in DC rail transit systems, *IEE Colloquium on Stray Current Effects of DC Railways and Tramways (Digest No.129)*, 11 October 1990, IEE, pp. 2/2/1-2/2/6.